

Microperimetry and Multimodal Retinal Imaging

Edoardo Midena
Editor

 Springer

Microperimetry and Multimodal Retinal Imaging

Edoardo Midena
Editor

Microperimetry and Multimodal Retinal Imaging

 Springer

Editor

Edoardo Midena
Department of Ophthalmology
University of Padova
Padova
Italy

ISBN 978-3-642-40299-9 ISBN 978-3-642-40300-2 (eBook)
DOI 10.1007/978-3-642-40300-2
Springer Heidelberg New York Dordrecht London

Library of Congress Control Number: 2013955617

© Springer-Verlag Berlin Heidelberg 2014

This work is subject to copyright. All rights are reserved by the Publisher, whether the whole or part of the material is concerned, specifically the rights of translation, reprinting, reuse of illustrations, recitation, broadcasting, reproduction on microfilms or in any other physical way, and transmission or information storage and retrieval, electronic adaptation, computer software, or by similar or dissimilar methodology now known or hereafter developed. Exempted from this legal reservation are brief excerpts in connection with reviews or scholarly analysis or material supplied specifically for the purpose of being entered and executed on a computer system, for exclusive use by the purchaser of the work. Duplication of this publication or parts thereof is permitted only under the provisions of the Copyright Law of the Publisher's location, in its current version, and permission for use must always be obtained from Springer. Permissions for use may be obtained through RightsLink at the Copyright Clearance Center. Violations are liable to prosecution under the respective Copyright Law.

The use of general descriptive names, registered names, trademarks, service marks, etc. in this publication does not imply, even in the absence of a specific statement, that such names are exempt from the relevant protective laws and regulations and therefore free for general use.

While the advice and information in this book are believed to be true and accurate at the date of publication, neither the authors nor the editors nor the publisher can accept any legal responsibility for any errors or omissions that may be made. The publisher makes no warranty, express or implied, with respect to the material contained herein.

Printed on acid-free paper

Springer is part of Springer Science+Business Media (www.springer.com)

Foreword

We are fortunate in living in a period of rapidly advancing technology in medicine. The pharmacologic, surgical, and diagnostic advances throughout medicine over the last three decades have served to improve not only the quality of life but also the duration of life for millions of individuals throughout the world. No one area of advancement takes credit for the advancing benefits offered by the medical community to our patients without acknowledging the contributions of the other areas of research and advancement.

An understanding of the diagnostic technology that has occurred in ophthalmology over a little more than a decade and half is summarized, analyzed, and explained in this beautifully developed textbook edited by Edoardo Midena. Dr. Midena, a world's authority in multimodal retinal imaging, has put together a list of who's who in imaging technology in the area of retinal and vitreous disorders. He has carefully orchestrated some of the world's finest ophthalmologists and developed a score, which, when taken in its entirety, is a magnificent work of art. His textbook *Microperimetry and Multimodal Retinal Imaging* allows the reader an opportunity of understanding the basic physiology of many of the technologies now developed and being developed in the area of the posterior segment of the eye. Each author has been given an opportunity of expressing his or her expertise in carefully edited and well-written text. Dr. Midena has then organized these individual pieces into a beautiful symphony of intelligence that is easy to read and understand.

It is said that the sum is often greater than the individual pieces, and Dr. Midena, in this beautifully organized text, shows that while each individual contribution is superb, the final cumulative result is a magnificent textbook that will serve for many years as the go-to text on Microperimetry and Posterior Segment Retinal Imaging.

Philadelphia, Pennsylvania, USA

Alexander J. Brucker, MD

Preface

The progress in retinal disorders depends on a comprehensive pathophysiologic interpretation (up to the genetic level), a complete and correct diagnosis, and the possibility to cure the disease. Recently, the rapid and significant progress in retinal diagnostic technologies has dramatically and positively modified our approach to retinal disorders; a sort of mini revolution which allows us to obtain, mostly non-invasively, a large amount of information about the morphology and function of the retina. What was lacking was a sort of “holistic” approach allowing us to integrate all information to obtain the real retina scenario of each individual patient in the context of clinical practice. This book represents the first initiative to overcome this limitation and offers a way to integrate function and morphology of the retina. The visual function side is mainly represented, besides visual acuity, by microperimetry, a technique which deserves strong attention because it offers unparalleled data on the reality of an individual’s vision. The analysis of retina fixation data, obtained by microperimetry, is, for example, instrumental to have a real representation of reading capacity and offers a large contribution in visual rehabilitation. The overlapping of point-by-point retinal threshold onto autofluorescence images and OCT is invaluable in detecting disease progression, and contributes to quantify the effects of any new therapy (even previously unknown side effects). Because the quality of life highly depends on the quality of vision, the multimodal integrated diagnostic approach to retinal diseases is also instrumental to this objective.

I am deeply indebted to all contributors, whose efforts to report the best of their research and daily clinical data in multimodal imaging of retinal diseases was essential to the preparation of this book. They have been enthusiastic of the project since its beginning, and their individual contribution represents the state of the art of microperimetry and multimodal retinal imaging.

I have to thank Simonetta, Mattia and Giulia (my beloved family) whose support has been continuous and strong in any moment of my life. Without them even this project was impossible to be realized.

Padova, Italy

Edoardo Midena

Contents

Part I Microperimetry and Multimodal Retinal Imaging: The Fundamentals

1 Microperimetry: An Introduction	3
Edoardo Midena	
2 Retinal Fixation and Microperimetry	5
Michael Crossland and Gary S. Rubin	
3 Microperimetry: Technical Remarks	13
Stela Vujosevic and Margherita Casciano	
4 OCT/SLO Microperimetry and Correlates	23
Gennady Landa, Emily Su, Patricia Garcia, and Richard B. Rosen	
5 Scotopic Microperimetry	41
Elisabetta Pilotto and Enrica Convento	
6 Multimodal Retinal Imaging: An Introduction	51
Edoardo Midena and Elisabetta Pilotto	

Part II Clinical Applications of Microperimetry and Multimodal Retinal Imaging

7 Early and Intermediate Age-Related Macular Degeneration	69
Julia-Sophie Kroisamer, Bianca S. Gerendas, and Ursula Schmidt-Erfurth	
8 Geographic Atrophy	77
Elisabetta Pilotto and Francesca Guidolin	
9 Neovascular Age-Related Macular Degeneration	89
Bianca S. Gerendas, Julia S. Kroisamer, Florian Sulzbacher, and Ursula Schmidt-Erfurth	
10 Retinal Pigment Epithelium and Choroid Graft	101
Elsbeth J.T. van Zeeburg, Matteo G. Cereda, Leigh H. Spielberg, and Jan C. van Meurs	

11 Macular Telangiectasia Type 2	111
Tjebo F.C. Heeren, Frank G. Holz, and Peter Charbel Issa	
12 Diabetes and Retinal Vascular Disorders	119
Stela Vujosevic and Edoardo Midena	
13 Myopia	129
Ichiro Maruko and Tomohiro Iida	
14 Retinal Dystrophies	137
Aakriti Garg and Stephen H. Tsang	
15 Disorders of the Vitreoretinal Interface	143
Monica Varano, Mariacristina Parravano, and Daniele De Geronimo	
16 Inflammatory Chorioretinal Disorders	157
Ahmed M. Abu El-Asrar, Marwan Abouammoh, and Hani S. Al-Mezaine	
17 Toxic Retinopathies	163
Raffaele Parrozzani and Silvia Bini	
18 Glaucoma	171
Michele Iester	
Part III The Contribution to Visual Rehabilitation	
19 Low Vision: Diagnosis and Rehabilitation	185
Samuel N. Markowitz	

Contributors

Marwan Abouammoh Department of Ophthalmology,
College of Medicine, King Saud University, Riyadh, Saudi Arabia

Ahmed M. Abu El-Asrar, MD, PhD Department of Ophthalmology,
College of Medicine, King Saud University, Riyadh, Saudi Arabia

Hani S. Al-Mezaine Department of Ophthalmology, College of Medicine,
King Saud University, Riyadh, Saudi Arabia

Silvia Bini Department of Ophthalmology, University of Padova,
Padova, Italy

Margherita Casciano Department of Ophthalmology,
University of Padova, Padova, Italy

Matteo G. Cereda Eye Clinic, Department of Clinical Science
“Luigi Sacco”, Sacco Hospital, University of Milan, Milan, Italy

Enrica Convento Department of Ophthalmology,
University of Padova, Padova, Italy

Michael Crossland, PhD Moorfields Eye Hospital NHS Foundation Trust,
London, UK

Vision and Eye Research Unit, Anglia Ruskin University, Cambridge, UK

Daniele De Geronimo GB Bietti Eye Foundation, IRCCS, Rome, Italy

Patricia Garcia Retina Center, Department of Ophthalmology,
The New York Eye and Ear Infirmary, New York, NY, USA

Aakriti Garg Department of Ophthalmology, Columbia University
College of Physicians and Surgeons, New York, NY, USA

Bianca S. Gerendas Department of Ophthalmology,
Vienna Reading Center, Medical University of Vienna, Vienna, Austria

Francesca Guidolin Department of Ophthalmology, University of Padova,
Padova, Italy

Tjebo F.C. Heeren Department of Ophthalmology, University of Bonn,
Bonn, Germany

Frank G. Holz Department of Ophthalmology, University of Bonn,
Bonn, Germany

Michele Iester, MD, PhD Laboratorio clinico anatomico-funzionale per la diagnosi e il trattamento del glaucoma e della malattie neurooftalmologiche, Clinica Oculistica, DiNOGMI, University Eye Clinic of Genoa, Genoa, Italy

Tomohiro Iida Department of Ophthalmology, Tokyo Women's Medical University School of Medicine, Tokyo, Japan

Peter Charbel Issa Department of Ophthalmology, University of Bonn, Bonn, Germany

Julia-Sophie Kroisamer Department of Ophthalmology, Vienna Reading Center, Medical University of Vienna, Vienna, Austria

Gennady Landa Retina Center, Department of Ophthalmology, The New York Eye and Ear Infirmary, New York, NY, USA

Samuel N. Markowitz, MD Low Vision Service, Department of Ophthalmology and Vision Sciences, University Health Network Hospitals, University of Toronto, Toronto, ON, Canada

Ichiro Maruko, MD Department of Ophthalmology, Tokyo Women's Medical University School of Medicine, Tokyo, Japan

Edoardo Midena, MD, PhD, FARVO, FEBO Department of Ophthalmology, University of Padova, Padova, Italy
Fondazione G.B. Bietti, IRCCS, Rome, Italy

Mariacristina Parravano GB Bietti Eye Foundation, IRCCS, Rome, Italy

Raffaele Parrozzani, MD, PhD GB Bietti Foundation, IRCCS, Rome, Italy

Elisabetta Pilotto, MD Department of Ophthalmology, University of Padova, Padova, Italy

Richard B. Rosen, MD Retina Center, Department of Ophthalmology, The New York Eye and Ear Infirmary, New York, NY, USA

Gary S. Rubin, PhD UCL Institute of Ophthalmology, London, UK
NIHR Biomedical Research Centre for Ophthalmology, London, UK

Ursula Schmidt-Erfurth, MD Department of Ophthalmology, Vienna Reading Center, Medical University of Vienna, Vienna, Austria

Leigh H. Spielberg Department of Ophthalmology, The Rotterdam Eye Hospital, Rotterdam, The Netherlands

Emily Su Retina Center, Department of Ophthalmology, The New York Eye and Ear Infirmary, New York, NY, USA

Florian Sulzbacher Department of Ophthalmology, Vienna Reading Center, Medical University of Vienna, Vienna, Austria

Stephen H. Tsang, MD, PhD Department of Ophthalmology,
Columbia University College of Physicians and Surgeons,
New York, NY, USA

Department of Pathology and Cell Biology, Columbia University
College of Physicians and Surgeons, New York, NY, USA

Department of Ophthalmology, Columbia University Harkness Eye
Institute, New York, NY, USA

Jan C. van Meurs Department of Ophthalmology, The Rotterdam
Eye Hospital, Rotterdam, The Netherlands

Elsbeth J.T. van Zeeburg Department of Ophthalmology, The Rotterdam
Eye Hospital, Rotterdam, The Netherlands

Monica Varano, MD GB Bietti Eye Foundation, IRCCS, Rome, Italy

Stela Vujosevic, MD, PhD Department of Ophthalmology,
University of Padova, Padova, Italy

Part I

**Microperimetry and Multimodal Retinal
Imaging: The Fundamentals**

Edoardo Midena

1.1 Microperimetry

The functional evaluation of the retina rests on the quantification of visual acuity, the study of the retinal threshold (mainly referred as the study of the visual field), and electrophysiologic tests. In daily clinical practice the functional efficiency of the retina is quantified by means of visual acuity testing: a classic visual function psychophysical test. Visual psychophysical tests are the cornerstone of visual function investigation, and any therapy currently applied or under investigation for retinal disorders, mainly acquired macular diseases, still has the maintenance (or improvement) of visual acuity as primary endpoint [1]. Psychophysics is a science which has developed as a way to measure the internal sensory and the perceptual responses to external stimuli. Psychophysical visual function testing may reflect the neural activity of the whole visual pathway, but it is known that these tests are valuable clinical indicators of retinal function derangements induced by local or systemic changes (i.e., diabetes mellitus, neurodegenerative disorders, or systemic drugs).

Visual acuity is still considered, in clinical practice, the gold standard of vision testing, but it

does not reflect functional vision [2]. Functional vision describes the impact of sight on quality of life, representing the patient's point of view. This approach means that a series of functional tests, mainly psychophysical, may be useful to acquire more detailed information about the different aspects of vision and better report the individual situation. The quantification of visual acuity in both high- and low-contrast conditions, contrast sensitivity in static and dynamic settings, color vision, macular recovery function, and retinal threshold in different light conditions are well-known visual function tests [3]. Apart from visual acuity, the quantification of retinal threshold is currently performed as the second step of visual function investigation. The quantification of differential retinal threshold (the shorter terms retinal threshold or retinal sensitivity are used along the text) is commonly described as visual field testing, and it may be done in different light (both background and stimuli) conditions [4]. Even if the term perimetry originally described the borders of the island of vision in preselected stimuli versus background conditions, it is commonly used as a substitute of visual field testing. Visual field testing is commonly performed using hardware and software equipped instruments and in a static way. The threshold of any tested area of the retina is collected in graphs reporting the whole explored area. Current instruments are able to obtain visual field testing (perimetry) using different settings according to the standards of psychophysical testing. Unfortunately, perimetry is inadequate to detect very small scotoma

E. Midena, MD, PhD, FARVO, FEBO
Department of Ophthalmology, University of Padova,
via Giustiniani 2 35128 Padova, Italy

Fondazione G.B. Bietti, IRCCS, Rome, Italy
e-mail: edoardo.midena@unipd.it

(an area of the retina where the retinal threshold is reduced up to no light perception) mainly when retinal fixation (for more details refer to Chap. 2) is unstable, a functional situation quite common in the most important acquired macular disorders [5]. Because perimetry depends on fixation, the quantification of retinal sensitivity during follow-up tests does not necessarily reflect the threshold of the same area previously tested. Therefore, if an exact fundus-related threshold to be used at baseline investigation and during follow-up is required, it cannot be reliably obtained using perimetry. The long-standing demand for an exact correlation between retinal morphologic changes and retinal sensitivity became a reality with the introduction of the perimetry tool of the first clinically used scanning laser ophthalmoscope (SLO, Rodenstock, Germany), an instrument which is no more commercially available [6]. This SLO fundus-related quantification of retinal sensitivity under fixation monitoring was called *microperimetry* [7]. According to the opinion of many researchers and clinicians, the term appears misleading and the more precise term *fundus-related perimetry* was proposed. Notwithstanding, *microperimetry* was used by most of the authors, mainly clinicians, and it is now the most diffuse and known term. Microperimetry is a fundus-tracking controlled visual field examination. Fundus-tracking allows now to project each stimulus (which may vary in size, brightness, and color) in an exact pre-planned retinal area both at baseline and during automatic follow-up examination [8, 9]. Fundus-tracking allows to overcome the eye movements and retinal fixation changes and to obtain precise retina-related sensitivity data. More technical details about current microperimetry instruments are reported in Chaps. 3 and 4 of this volume.

The use of microperimetry in the diagnosis and follow-up of retinal disorders is continuously growing, mainly associated with the use of other morphologic imaging tests, to offer not only more precise clinical diagnostic insights but also to quantify the visual impact (positive or negative) of commercially used and future therapies (in phase II or III clinical trials) of retinal disorders.

References

1. Midena E, Vujosevic S (2012) Visual psychophysics in diabetic retinopathy. In: Tombram-Tink J, Barnstable CJ, Gardner TW (eds) Visual dysfunction in diabetes, Ophthalmology research series. Springer Science-Business Media, LLC., New York
2. Owsley C, Sloane ME (1987) Contrast sensitivity, acuity and the perception of real world targets. *Br J Ophthalmol* 71:791–796
3. Kniestedt C, Stamper RL (2003) Visual acuity and its measurement. *Ophthalmol Clin North Am* 16: 155–170
4. Frisen L (1990) Clinical tests of vision. Raven Press, New York, pp 55–173
5. Midena E, Radin PP, Pilotto E et al (2004) Fixation pattern and macular sensitivity in eyes with subfoveal choroidal neovascularization secondary to age-related macular degeneration. *Semin Ophthalmol* 19:55–61
6. Sunness JS, Schuchard RA, Shan N et al (1995) Landmark-driven fundus perimetry using the scanning laser ophthalmoscope. *Invest Ophthalmol Vis Sci* 36:1863–1874
7. Rohrschneider K, Bultman S, Springer C (2008) Use of fundus perimetry (microperimetry) to quantify macular sensitivity. *Prog Retin Eye Res* 27:536–548
8. Midena E, Vujosevic S, Cavarzeran F, for the Microperimetry Study Group (2010) Normative age-related database for the MP1 microperimeter. *Ophthalmology* 117:1571–1576
9. Vujosevic S, Smolek MK, Lebow KA et al (2011) Detection of macular function changes in early (AREDS 2) and intermediate (AREDS 3) age-related macular degeneration. *Ophthalmologica* 225: 155–160

Michael Crossland and Gary S. Rubin

2.1 Using a Microperimeter to Evaluate Fixation

A significant advantage of microperimetry over other forms of visual field assessment is that unstable or noncentral fixation can be quantified and corrected for. Consider, first, the problem of noncentral fixation. People with vision loss from macular disease frequently use a noncentral part of the retina known as the preferred retinal locus (PRL) for fixation [1–5]. Development of a PRL is considered to be critical for successful visual rehabilitation. If the patient does not adopt a PRL on their own, there are various training methods to promote the development of one [6].

Fixating with a PRL leads to misalignment of the visual field plot created by conventional visual field testing. The visual field plot in Fig. 2.1 was taken with a conventional Humphrey Field Analyzer and shows a large area of severely reduced sensitivity on the left side. But it is not possible to determine whether the patient is using

their fovea to fixate (and the vision loss is parafoveal), or whether the field loss includes the central macular region, and the centre of the visual field plot corresponds to their PRL.

Microperimetry can not only determine the location of the PRL and correct for the resulting offset of the visual field map, but it can also compensate for shifts of fixation, which may occur during visual field testing. Together these features of microperimetry should lead to more accurate assessment of retinal sensitivity across the visual field; however, there is a lack of data comparing microperimetry with standard automated perimetry in patients with central scotomas.

Fixation characteristic can be evaluated during a visual field test, by noting the fixation location at the time the visual field stimulus is presented, or as separate procedure, by monitoring fixation location for a fixed length of time (usually 10–30 s) while the participant views a fixation stimulus in an otherwise blank field. In either case, fixation data can be evaluated to determine the location of the PRL and fixation stability.

M. Crossland, PhD
Moorfields Eye Hospital NHS Foundation Trust,
London, UK

Vision and Eye Research Unit,
Anglia Ruskin University, Cambridge, UK

G.S. Rubin, PhD (✉)
UCL Institute of Ophthalmology,
11-43 Bath Street, London EC1V 9EL, UK

NIHR Biomedical Research Centre
for Ophthalmology, London, UK
e-mail: g.rubin@ucl.ac.uk

2.2 Assessment of Fixation Location

A key benefit of microperimeters is the ability to determine the fixation location on the retina. The location of the PRL can be defined either in terms of visual field position (e.g. ‘inferior visual field’) or in retinal co-ordinates (‘superior retina’).

When discussing fixation position it is important to specify whether the location is given in visual field space or in terms of retinal location.

Pooling data from several research papers allows the fixation location to be determined for more than 1,500 eyes of people with macular disease [7–12]. This shows that 37 % use a PRL placed below their scotoma (in visual field space),

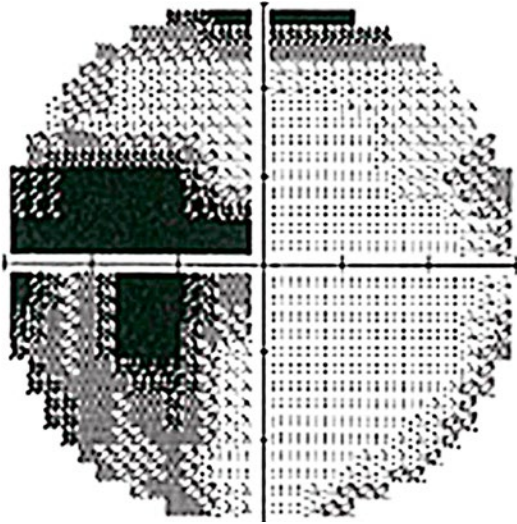


Fig. 2.1 Humphrey visual field plot for someone with central vision loss

33 % to the left of fixation, 19 % to the right of the scotoma, and 6 % above the scotoma. Less than 2 % used a central position (fixating within their scotoma), and 3 % had a mixed strategy of multiple PRLs.

There is a theoretical advantage in using a vertically shifted PRL for reading, as this reduces the effect of the scotoma when making eye movements along a line of text. If using a horizontally shifted PRL, there is an advantage to placing the PRL in the right visual field, rather than the left, as this would interfere less with the perceptual span for reading than a PRL to the left of fixation [13]. Data from normally sighted readers with simulated scotomas, who were forced to read with their peripheral vision, showed the expected right field advantage [14]. However, reading speed in people with real central scotomas is no higher for a vertically shifted PRL compared to a PRL to the left or right of their scotoma [4, 10, 12, 15]. Figure 2.2 shows the distribution of reading speed (in \log_{10} character/second) as a function of PRL location for 34 readers with advanced AMD. There is no significant difference in reading speeds for vertically shifted PRLs compared to horizontally shifted PRLs nor any difference for above vs. below or left vs. right (Mann–Whitney test, $p > 0.1$).

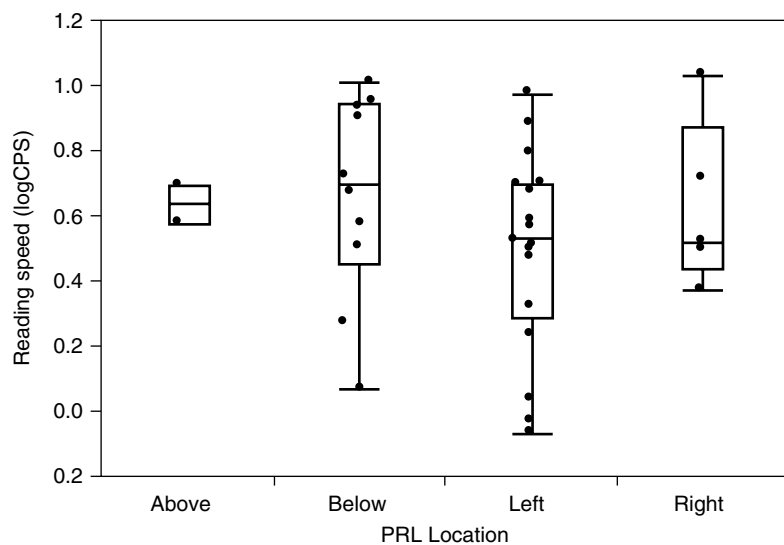
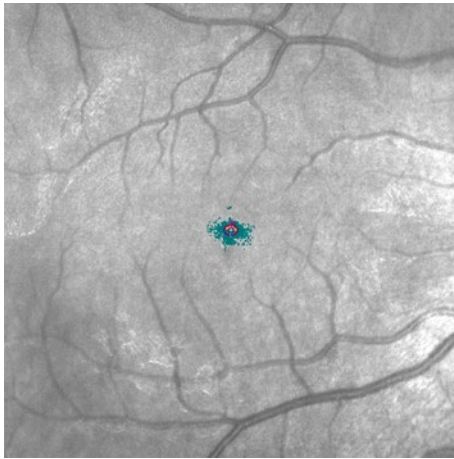


Fig. 2.2 Reading speed (in logCPS) is plotted for groups of patients with PRLs located above, below, left, and right of the scotoma (in visual field space). The box plots show the median and 25th and 75th percentiles with the vertical ‘whiskers’ extending to the 5th and 95th percentiles



Bivariate contour ellipse area:

63 % BCEA: $0.2^\circ \times 0.1^\circ$, Area = $0.1^{\circ 2}$, angle = $.0.2^\circ$

95 % BCEA: $0.6^\circ \times 0.4^\circ$, Area = $0.7^{\circ 2}$, angle = $.0.2^\circ$

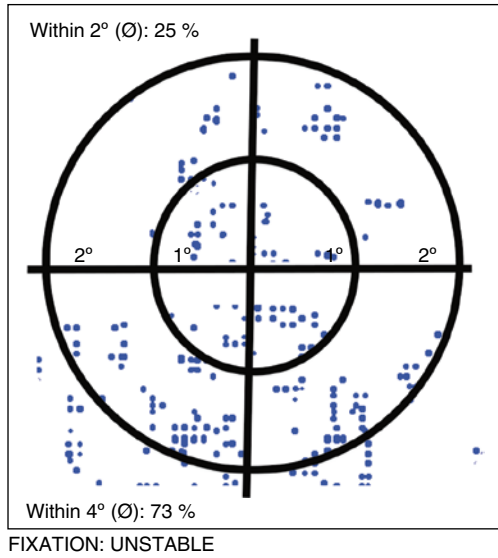


Fig. 2.3 Fixation analysis from the MAIA microperimeter (*left*) showing BCEA values for fixation for someone with no eye disease and good fixation and MP-1 (*right*) showing Fujii classification scheme

2.3 Assessment of Fixation Stability

Fixation stability can be measured during microperimetry or during a specific fixation task. In a fixation analysis, the patient is asked to keep their eye steady while observing a target (usually a cross or circle). The dispersion of fixation points is then analysed to quantify the stability of fixation:

$$BCEA = 2k\pi\sigma_H\sigma_V(1-\rho^2)^{0.5}$$

where σ_H and σ_V are the standard deviations of fixation position in the horizontal and vertical meridian, respectively, and ρ is the product-moment correlation of these two components.

The value k is dependent upon the probability area chosen

$$P = 1 - e^{-k}$$

where e is the base of the natural logarithm. Therefore, when k is 1, 63.2 % of the fixation positions lie within this area. Different authors have used different values of P , such as 0.6, 0.68, or 0.95 [7, 16–19].

A limitation of the BCEA technique is that it assumes fixation points are normally distributed

in x and y , which is often not the case. In particular, if someone has multiple PRLs, fixation points will be clustered rather than normally distributed [20, 21]. In this case, a statistical test for multimodality of fixation points can be used to determine the number of PRLs, and ‘local’ BCEAs can be calculated for each cluster [22] (Fig. 2.3).

A second method is to report the proportion of fixation points that fall within a certain area. For example, Fujii and colleagues report fixation as being stable when 75 % of fixations fall inside a 2° circle, relatively unstable when 75 % of fixations fall inside a 4° circle, and unstable when fixation is poorer than this [23]. This technique does not make allowance for the typically elliptical distribution of fixation points and also does not allow for the case of multiple PRLs. It also groups people with very different fixation into the same category: someone with good fixation could have 75 % of fixation points within a 2° circle or 100 % of fixation points inside a 0.5° circle.

We measured fixation using both of these techniques and related these values to various aspects of reading performance. We found significant relationships between BCEA values and 4 of our 5 measures of reading speed. In comparison, we found no relationship between any of our

reading outcomes and the proportion of points within 2° or 4° [24]. For this reason, we recommend using the BCEA technique to quantify fixation stability.

2.3.1 Choice of Fixation Target

What effect does the fixation target have on fixation stability? Bellmann and colleagues measured fixation stability in people with and without macular disease when observing six different fixation targets: a small (1°) cross, filled circle, and letter x; a small diamond of four points; a larger diamond of four points; and a large filled diamond. For people without eye disease, fixation stability was best for the 1° cross and poorest for the large 4-point diamond. For people with central vision loss, there was no difference in fixation stability with any of the targets selected [22]. This means that any target which is easily visible to the patient can be used for a fixation target.

2.3.2 Fixation Test Length

In general, fixation stability is measured for a period of 30 s or 1 min. What is the effect of measuring for a longer time? We measured fixation for an extended period of 4 min and compared fixation stability for the first 10 s of each minute. No significant change was found over time. This suggests that no additional information is gained from a longer test period.

2.4 Fixation Stability in Good Vision

In children, fixation stability improves from the age of 4–15 years [25]. In adulthood, fixation stability appears not to change in people without eye disease. For example, Kosnik and colleagues found no difference in stability between people with a mean age of 22 years and those with a mean age of 70 [17]. This finding was replicated

in our study of extended fixation stability: no statistically significant age effect was observed when comparing younger (19–38 years) and older (61–86 years) adults [26].

Motivation can also affect fixation stability: in a 1985 paper, Snodderly and Kurtz describe a participant who improved his fixation stability when betting a milkshake that he could improve his fixation [27]. There is some evidence that people can train themselves to have more stable fixation. Di Russo and colleagues examined fixation stability in professional shooters and in control subjects and found more stable fixation in the shooter group. Interestingly, the professional shooters had equally stable fixation with and without visual distraction (created by flashing a point target close to the fixation mark), whereas the control subjects had poorer fixation stability with distractors [28]. Of course, it is not clear whether people progress to being professional shooters because they have an innately better fixation stability or whether they have practised and trained to have more stable fixation.

2.5 Fixation Stability in Eye Disease

We have found that BCEA measurements are severely skewed when calculated in minarc^2 . Transforming BCEA to $\log \text{minarc}^2$ helps to normalise the distribution, as shown in Fig. 2.4. Fixation stability is significantly reduced in people with eye disease (BCEA gets bigger). For example, in a group of people with newly diagnosed macular disease, we found a mean BCEA of $9.04 \log \text{minarc}^2$, compared to a mean value of $3.2 \log$ units for age-matched control subjects measured on the same instrument [22].

Other types of eye disease affect fixation stability differently. For a group of people with diabetic eye disease, Dunbar found a mean BCEA value of $2.94 \log \text{minarc}^2$ eye disease, only about half a low unit less stable than her control subjects. However, some individual patients had far poorer stability, of more than $5 \log \text{minarc}^2$ [29].

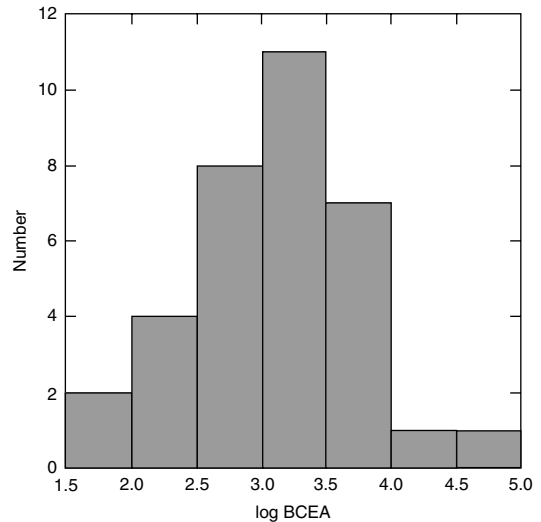
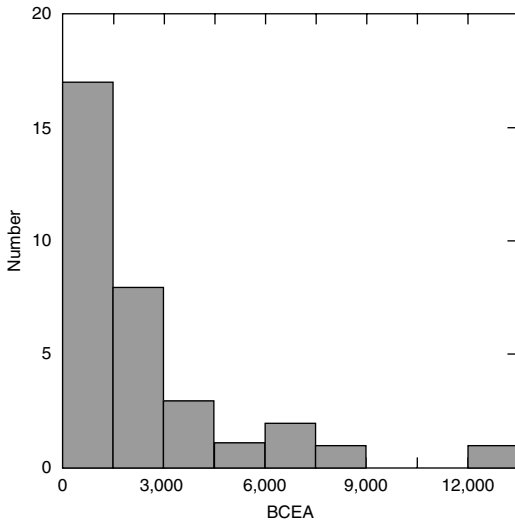


Fig. 2.4 Distribution of fixation stability measures across a group of 34 subjects with advanced AMD. When plotted in simple area co-ordinates (*left*; minarc^2), the dis-

tribution is very skewed. But when converted to $\log \text{minarc}^2$ (*right*), the distribution is more symmetric and less skewed

In a comprehensive study of fixation stability in different eye diseases, Amore and colleagues report near-normal fixation stability for people with retinitis pigmentosa, a wide range of fixation stability for people with glaucoma, and the poorest values for people with macular disease [30].

2.6 Effect of Fixation Stability on Reading

Poor fixation stability is associated with poor visual function. Unstable fixation is particularly related to poorer reading speed. In a study of 34 patients with advanced AMD, fixation stability was significantly associated with reading speed for print of optimal size ($r^2=0.25$, see Fig. 2.5). In an analysis of 120 patients with a diverse range of eye diseases, Amore found a linear relationship between reading speed and fixation stability ($r^2=0.51$, $p<0.001$) [30].

In a longitudinal study of people with macular disease, we found that reading speed is significantly associated with fixation stability for patients ($r^2=0.21$) and for control subjects ($r^2=0.44$). We also found that changes in fixation stability over a 12-month period were strongly associated with changes in reading speed ($r^2=0.54$) [22].

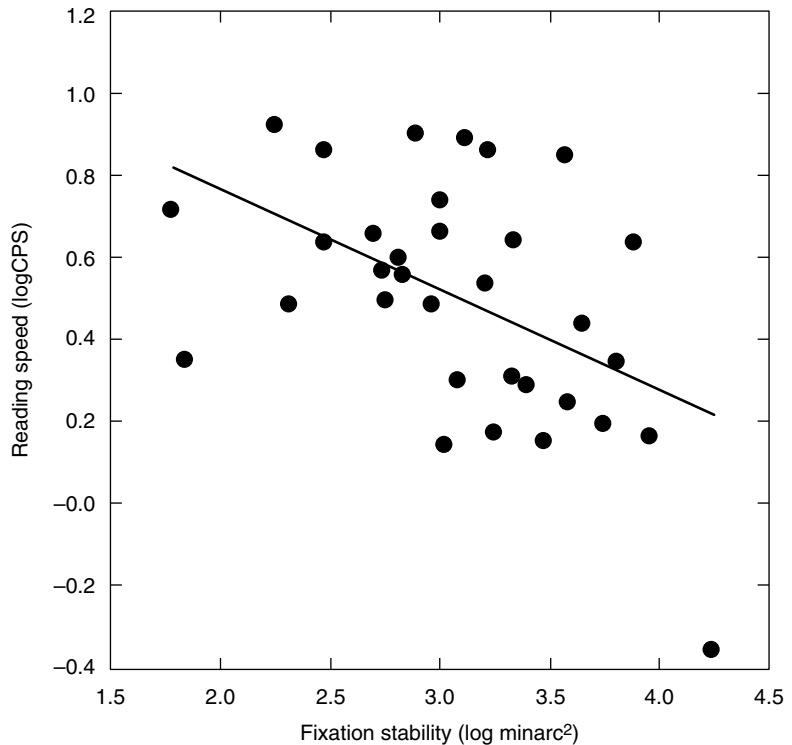
2.6.1 Overcoming Fixation Instability

Low vision centres use eccentric viewing training as a mechanism of improving visual performance in people with macular disease [11, 31–35]. Microperimetry is an important component of an eccentric viewing training programme: it can be used to determine the position of the PRL at entrance to a training programme, it can be used to train fixation location, and it can be used to determine the success of the training programme.

In a recent report, Tarita-Nistor and colleagues found that fixation stability improved by 53 % after biofeedback training on the MP-1 microperimeter [36]. This improvement occurred alongside an improvement in reading speed and in critical print size (the minimum text size which can be read at maximum fluency).

In a number of preliminary studies, Macedo has found that correcting unstable fixation (by moving text displayed on a screen in tandem with eye movements) can improve reading speed in people with macular disease. However, visual acuity is not improved when correcting unstable fixation [37, 38].

Fig. 2.5 Reading rate in log characters/second is plotted against fixation stability measured in log minarc²



Conclusion

Microperimeters record the preferred retinal locus (PRL) for fixation and fixation stability during a standard examination. Data from over 1,500 people with central scotomas due to macular disease indicate that the majority use a PRL below or to the left of their scotomas (in visual field space). Theoretical considerations suggest that reading speed should suffer for PRLs to the left, but reading performance data indicate that PRL location has little effect on reading speed. Fixation stability, on the other hand, has a significant impact on reading, with both cross-sectional and longitudinal studies demonstrating higher reading speeds for patients with more stable fixation. There is some suggestion that reducing fixation instability, either by compensating for eye movements with a gaze contingent display or by training eccentric fixation, can improve reading performance in people with macular disease, but further evidence is needed to establish when eccentric viewing training or automatic compensation for fixation instability is beneficial.

Acknowledgements GS Rubin is supported by a programme grant from fight for sight.

References

1. White JM, Bedell HE (1990) The oculomotor reference in humans with bilateral macular disease. *Invest Ophthalmol Vis Sci* 31:1149–1161
2. Fletcher DC, Schuchard RA, Livingstone CL et al (1994) Scanning laser ophthalmoscope macular perimetry and applications for low vision rehabilitation clinicians. *Ophthalmol Clin North Am* 7:257–265
3. Cheung SH, Legge GE (2005) Functional and cortical adaptations to central vision loss. *Vis Neurosci* 22:187–201
4. Crossland MD, Culham LE, Kabanarou SA, Rubin GS (2005) Preferred retinal locus development in patients with macular disease. *Ophthalmology* 112:1579–1585
5. Timberlake GT, Sharma MK, Grose SA et al (2005) Retinal location of the preferred retinal locus relative to the fovea in scanning laser ophthalmoscope images. *Optom Vis Sci* 82:177–185
6. Nilsson UL (1990) Visual rehabilitation with and without educational training in the use of optical aids and residual vision. A prospective study of patients with advanced age-related macular degeneration. *Clin Vis Sci* 6:3–10

7. Culham L, Fitzke FW, Timberlake GT (1993) Assessment of fixation stability in normal subjects and patients using a scanning laser ophthalmoscope. *Clin Vis Sci* 8:551–561
8. Guez J-E, Le Gargasson J-F, Rigaudiere F (1993) Is there a systematic location for the pseudo-fovea in patients with central scotoma? *Vision Res* 33:1271–1279
9. Sunness JS, Applegate CA, Haselwood D (1996) Fixation patterns and reading rates in eyes with central scotomas from advanced atrophic age-related macular degeneration and Stargardt disease. *Ophthalmology* 103:1458–1466
10. Fletcher DC, Schuchard RA (1997) Preferred retinal loci relationship to macular scotomas in a low-vision population. *Ophthalmology* 104:632–638
11. Nilsson UL, Frennesson C, Nilsson SE (1998) Location and stability of a newly established eccentric retinal locus suitable for reading, achieved through training of patients with a dense central scotoma. *Optom Vis Sci* 75:873–878
12. Fletcher DC, Schuchard RA, Watson G (1999) Relative locations of macular scotomas near the PRL: effect on low vision reading. *J Rehabil Res Dev* 36:356–364
13. Rayner K, Well AD, Pollatsek A (1980) Asymmetry of the effective visual field in reading. *Percept Psychophys* 27:537–544
14. Fine EM, Rubin GS (1999) Reading with simulated scotomas: attending to the right is better than attending to the left. *Vision Res* 39:1039–1048
15. Rubin GS, Feely M (2009) The role of eye movements during reading in patients with age-related macular degeneration (AMD). *Neuroophthalmology* 33:120–126
16. Steinman RM, Cunitz RJ (1968) Fixation of targets near the absolute foveal threshold. *Vision Res* 8:277–286
17. Kosnik W, Fikre J, Sekuler R (1986) Visual fixation stability in older adults. *Invest Ophthalmol Vis Sci* 27:1720–1725
18. West SK, Munoz B, Rubin GS (2005) Compensatory strategy use identifies risk of incident disability for the visually impaired. *Arch Ophthalmol* 123:1242–1247
19. Schuchard RA, Raasch TW (1992) Retinal locus for fixation: pericentral fixation targets. *Clin Vision Sci* 7:511–520
20. Lei H, Schuchard RA (1997) Using two preferred retinal loci for different lighting conditions in patients with central scotomas. *Invest Ophthalmol Vis Sci* 38:1812–1818
21. Crossland MD, Culham LE, Rubin GS (2004) Fixation stability and reading speed in patients with newly developed macular disease. *Ophthalmic Physiol Opt* 24:327–333
22. Bellmann C, Feely M, Crossland MD (2004) Fixation stability using central and pericentral fixation targets in patients with age-related macular degeneration. *Ophthalmology* 111:2265–2270
23. Fujii GY, de Juan E Jr, Sunness J (2002) Patient selection for macular translocation surgery using the scanning laser ophthalmoscope. *Ophthalmology* 109:1737–1744
24. Dolan P, Roberts J (2002) Modelling valuations for Eq-5d health states: an alternative model using differences in valuations. *Med Care* 40:442–446
25. Ygge J, Aring E, Han Y (2005) Fixation stability in normal children. *Ann N Y Acad Sci* 1039:480–483
26. Virgili G, Rubin G (2006) Orientation and mobility training for adults with low vision. *Cochrane Database Syst Rev* (3):CD003925
27. Snodderly DM, Kurtz D (1985) Eye position during fixation tasks: comparison of macaque and human. *Vision Res* 25:83–98
28. Di Russo F, Pitzalis S, Spinelli D (2003) Fixation stability and saccadic latency in elite shooters. *Vision Res* 43:1837–1845
29. Mozaffarieh M, Heinzl H, Sacu S (2005) Clinical outcomes of phacoemulsification cataract surgery in diabetes patients: visual function (VF-14), visual acuity and patient satisfaction. *Acta Ophthalmol Scand* 83:176–183
30. Amore FM, Fasciani R, Silvestri V et al (2013) Relationship between fixation stability measured with MP-1 and reading performance. *Ophthalmic Physiol Opt* 33(5):611–617
31. Goodrich GL, Quillman RD (1977) Training eccentric viewing. *J Vis Impair Blind* 71:377–381
32. Culham LE (1991) Evaluation of a low vision training programme. University of London
33. Mallinson T, Stelmack J, Vellozo C (2004) A comparison of the separation ratio and coefficient alpha in the creation of minimum item sets. *Med Care* 42(1 Suppl):I17–I24
34. Seiple W, Szyk JP, McMahon T (2005) Eye-movement training for reading in patients with age-related macular degeneration. *Invest Ophthalmol Vis Sci* 46:2886–2896
35. Vingolo EM, Salvatore S, Cavarretta S (2009) Low-vision rehabilitation by means of MP-1 biofeedback examination in patients with different macular diseases: a pilot study. *Appl Psychophysiol Biofeedback* 34:127–133
36. Tarita-Nistor L, Gonzalez EG, Markowitz SN (2009) Plasticity of fixation in patients with central vision loss. *Vis Neurosci* 26:487–494
37. Crossland MD, Macedo AF, Rubin GS (2010) Electronic books as low vision aids. *Br J Ophthalmol* 94:1109
38. Macedo AF, Crossland MD, Rubin GS (2011) Investigating unstable fixation in patients with macular disease. *Invest Ophthalmol Vis Sci* 52:1275–1280

Stela Vujosevic and Margherita Casciano

3.1 Introduction

Microperimetry is a psychophysical visual function test that offers the option to correlate clinical morphological changes of the retina with visual function and subjective visual alterations.

Kinetic and static computerized perimetry stands out to investigate the visual field in many neuro-ophthalmological disorders, but it appears insufficient for precise evaluation of chorioretinal diseases. Conventional perimetry has two principal limitations: (1) it does not display any image of the fundus and (2) its accuracy is based on the assumption that fixation during examination is central and stable. To control the influence of fixation on final results, it is mandatory to see fundus image in real time, and the main problem is that the high levels of light to illuminate the retina interfere with light stimuli. The first microperimetry device was the scanning laser ophthalmoscope (SLO, Rodenstock, Germany) that used infrared light sources to overcome this problem [1]. A helium-neon laser beam and an infrared diode laser were projected through a slightly confocal aperture onto the retina. The helium-neon laser beam produced background and light

stimuli; the retinal image was captured through an infrared diode laser. SLO allowed to analyze fixation characteristics and retinal threshold under direct fundus control [2–4]. However, the original Rodenstock software did not allow the examiner to perform fully automatic examination and adequately retest the same retinal areas, although few laboratories developed individual algorithms to perform automatic tests. The Rodenstock SLO is no longer commercially available.

In the early 2000s, a new microperimetry device was developed to overcome the SLO limitations, the microperimeter MP-1 (Nidek, Gamagori, Japan). It is not a scanning laser ophthalmoscope, but a liquid-crystal-display microperimeter that uses an infrared fundus camera to visualize the fundus. The main innovation compared with Rodenstock SLO, in addition to fully automatic examination, was the eye-tracking system, which automatically compensates eye movements and allows a correct matching between the expected stimulus position onto the retina and the actual projection position.

Other microperimetry devices have been recently developed. The Macular Integrity Assessment (MAIA, CenterVue, Padova, Italy) combines the characteristics of a SLO with the tool of an advanced microperimeter, allowing a high-quality retinal imaging and an easier automatic procedure. In this chapter the technical characteristics of both MP-1 and MAIA microperimetry devices are analyzed, describing their features and differences.

S. Vujosevic, MD, PhD (✉) • M. Casciano
Department of Ophthalmology, University of Padova,
via Giustiniani 2, 35128, Padova, Italy
e-mail: stela.vujosevic@unipd.it

3.2 Microperimeter MP-1

3.2.1 Technical Features

The MP-1 has a halogen lamp that generates an infrared (IR) light conveyed to the retina. The fundus image is acquired by a black and white IR camera, with a resolution 768×576 pixels, at 25 Hz. The field of view is 45° . The MP-1 is also supplied with an independent non-mydratric color fundus camera, with an image resolution of $1,392 \times 1,040$ pixels. The correcting system for refractive errors ranges from -12.5 D to $+16$ D.

The projection system is a 6.5" liquid crystal display, 640×480 pixels, optically conjugated with the IR camera sensor. The standard background is monochromatic white, with luminance set at 1.27 cd/m^2 ($= 4 \text{ asb}$) [5].

The most important feature of the MP-1 is the automatic tracking system of eye movements. The eye tracker monitors the eye position with the frequency of 25 Hz (every 40 ms). The system compares a baseline reference image (128×128 pixels) with each acquired frame, calculating the horizontal and vertical shifts of the eye and therefore correcting stimulus location based on the current fundus position. If the reference area moves and cannot be found, the stimulus is turned off.

MP-1 offers different choices for the fixation target. The examiner has to evaluate retinal function and anatomical characteristics in order to decide the size and shape of the fixation target.

A single, 1° , 100 asb, red cross is the standard target. The cross could vary in thickness, color, and size (from 0.5° to 20°). Four crosses or a single ring is also available as fixation target (Fig. 3.1). A small (1°), single ring is used to avoid central sensitivity bias due to the luminance of the fixation target, as with the central cross. A wider ring could be used as a paracentral fixation target, in subjects with eccentric and unstable fixation. The ring may be integrated by four straight lines crossing the ring and pointing toward the center of fixation. Wide central scotomas take advantage of four crosses as a paracentral fixation target. The patient is asked to gaze at the ideal center of the four crosses. The fixation movements and the profile become wider and more irregular with a greater fixation target.

According to Goldmann stimulus size standards, the stimulus may be varied from size I (6.5 min/arc) to V (104 min/arc). Goldmann III is the most commonly used in microperimetry, because of its high reliability, even if Goldmann I is more precise in delineating small scotoma, such as those due to macular hole. However, stimulus shape (even figures, letters or phrases) may be customized. The duration of each stimulus may be varied from 100 to 2,000 ms. The most used presentation time is 200 ms, to avoid temporal summation. Stimuli intensity range is between 0 and 20 dB, which represents maximum and minimum stimulus luminance, 400 asb and 4 asb, respectively. The MP-1 attenuation



Fig. 3.1 Different fixation targets and exams with MP-1 microperimeter. In the *left* image, a four *red crosses* fixation target has been chosen for the examination. *Blue*

points indicate subject's fixation, which is central and stable. In the *right* image the fixation target is a single 1° *red circle*, and the subject's fixation is eccentric and unstable

scale is different from the standard automatic perimetry scale, and Midena et al. previously demonstrated that a direct comparison between MP-1 microperimetry and Octopus standard automatic perimetry data is not unreliable [6].

3.2.2 Fundus Perimetry with MP-1 Microperimeter

One of the most important MP-1 tests is the fixation exam. MP-1 records the fixation during the entire microperimetry exam, in addition to a 30- or 60-s specific fixation test. Both examinations allow the examiner to evaluate the patient fixation site and stability. The preferred retinal locus (PRL) is therefore defined according to Fujii et al. as central, poor central, or eccentric if more than 50 %, more than 25 %, or less than 25 % of fixation points, respectively, are located within 1° from the anatomical fovea [7].

Fixation stability is automatically calculated, and it is termed as stable, relatively unstable, or unstable if 75 % of the fixation points are located within a 2°, 4°, or more than 4° diameter circle, positioned with respect to the gravitational center of all fixation points. Site and stability of PRL are classified separately, because an eccentric but stable PRL has a completely different functional meaning compared with a central but relatively unstable fixation [8, 9]. The classification of fixation site is displayed by the instrument after manually positioning a landmark at the center of the anatomic fovea. Statistics about distribution of fixation during each test are also available: mean speed (deg/sec), time profile (deg 0–10 s), and trajectory. The examiner may also measure the eccentricity in degrees of the PRL and the BCEA (bivariate contour ellipse area). The BCEA is the result of plotting the position of each fixation point on Cartesian axes and calculating the area of an ellipse that encompasses a given percentage of fixations. The software shows the area (square degrees) and the angle (degrees) of 68.2, 95.4, and 99.6 % ellipse areas, corresponding to 1, 2, or 3 standard deviations, according to Timberlake et al. [10].

To quantify the retinal differential light threshold, three different topographic strategies can be chosen: automatic, semiautomatic, and

manual. The most commonly used is the automatic examination. The stimulus presentation is automatically performed by randomly projecting stimuli on a preselected grid. Several standard grids are available with the software, macular and peripapillary grids, or the examiner may customize a specific grid (Fig. 3.2). The grids may be automatically centered on the PRL or manually positioned onto a chosen retinal point. With the semiautomatic test a particular retinal area is manually selected, then the software develops a grid within the area. The manual microperimetry allows to test any retinal point with stimuli of any luminance intensity. It is also possible to perform kinetic microperimetry, which is a useful exam, i.e., to precisely detect the edges of a macular scotoma. Microperimetry software enables to choose between numeric, symbolic, or interpolated presentation of the resulting light thresholds (Fig. 3.3). A “local defect map” allows plotting the differences in dB between measured thresholds and age-corrected normal values at each stimulated location, within 20° centered on the fovea (Fig. 3.4).

The most frequently used threshold strategy in clinical practice is a 4-2 staircase that allows a precise but relatively fast determination of the differential light threshold. A 4-2-1 staircase is



Fig. 3.2 Peripapillary microperimetry, performed with MP-1 microperimeter, showing glaucomatous arcuate defects. The selected fixation target is a red circle centered on the preferred retinal locus



Fig. 3.3 Interpolated color map of microperimetry performed with MP-1 microperimeter

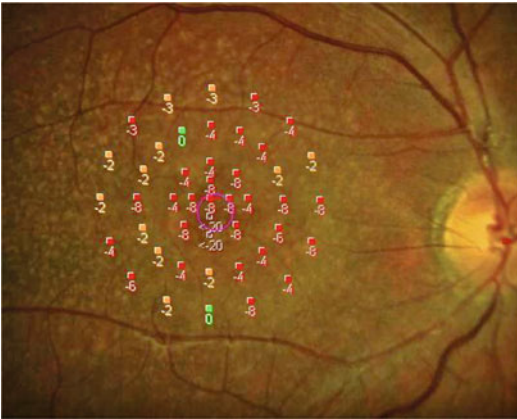


Fig. 3.4 Local defect map with MP-1 microperimeter. The red circle is the selected fixation target

often used in clinical trials, because of more precise results. A fast staircase strategy is also available, as a screening tool, i.e., to detect location and size of dense scotomas.

Even the attenuation of starting stimuli may be varied. A pretest is a useful starting option: the starting intensity for the grid points in the test will depend on the light threshold of four different retinal points previously analyzed.

For an automated real-time eye tracking, a region of interest on the infrared fundus image has to be defined prior to the microperimetry or fixation exam. The software compares the current image with the region of interest selected to track eye movements.

To evaluate patient reliability, a stimulus is periodically projected during the exam onto the blind spot selected by the operator. The instrument displays false-positive results. A high false-positive ratio indicates random clicking of the perimetry switch and a low reliability of the exam.

Using any automatic test, any subject may undergo a follow-up examination which is performed exactly over the same previously tested retinal points, independently of fixation changes, because stimuli projection depends just on anatomic landmarks. A fixation follow-up test is also available. Furthermore, to verify the progression of the disease, MP-1 shows a differential map with the differential light threshold between baseline and follow-up test.

MP-1 microperimeter allows also to perform visual rehabilitation. Through auditory stimuli it is possible to train a subject to relocate the preferred retinal locus (PRL) into a different region, called trained retinal locus (TRL), previously decided by the physician, allowing fixation rehabilitation and recovering visual abilities (i.e., reading speed) due to the improvement of fixation stability. Patients are asked to move their eyes according to an audio feedback which tells them whether they are getting closer to the TRL.

A very interesting tool of MP-1 is the option to make an overlay of microperimetry light threshold values on images obtained with other devices, such as fundus photographs, autofluorescence (FAF), and fluorescein angiography (Fig. 3.5). This tool allows an exact correlation between sensitivity thresholds and retinal abnormalities, such as atrophic areas, macular edema, or laser scars [11–14]. Pilotto et al. have recently analyzed retinal sensitivity on geographic atrophy secondary to age-related macular disease. The MP-1 sensitivity maps were overlapped on FAF images, and dense and relatively dense scotomas were evaluated during 1-year follow-up [11]. In a previous study, Vujosevic et al. demonstrated a correlation between increased autofluorescence areas and decreased sensitivity thresholds, in a patient with clinically significant diabetic macular edema [15]. After a semiautomatic overlapping of FAF image and microperimetry

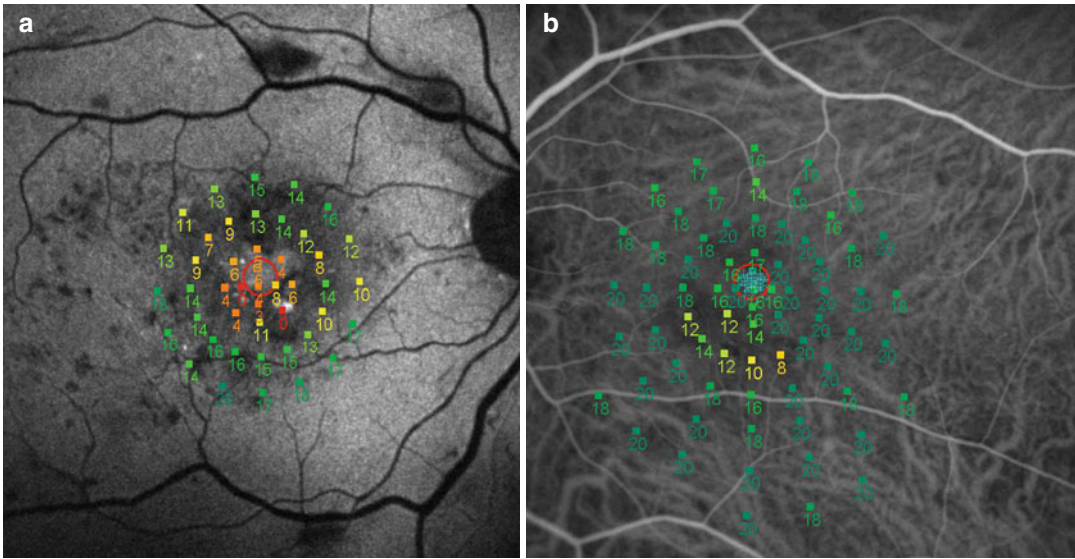


Fig. 3.5 Microperimetry exams performed with MP-1 superimposed to autofluorescence (a) and indocyanine angiography (b) images captured with Heidelberg HRA

thresholds, it is possible to manually draw areas with increased autofluorescence, obtaining an automatic calculation of mean sensitivity threshold of comprised retinal points.

A new version of MP-1 allows to perform scotopic (dark adapted) microperimetry. This topic is described in detail in a specific chapter (see Chap. 5).

3.3 Macular Integrity Assessment (MAIA)

3.3.1 Technical Features

The MAIA microperimeter is a relatively new instrument that combines a non-mydratric microperimetry with a near-infrared line SLO. It is a very compact device with a single unit, 540×560×482 mm in size. It does not require any additional computer, because it is controlled by the use of a touch screen and a two-button keypad, with an optional keyboard.

Confocal laser scanning is a technique for obtaining high-resolution and high-contrast optical images (Fig. 3.6). The key feature is the ability to acquire in-focus images from a selected

depth, avoiding to get scattered light from contiguous areas. Applying two-dimensional confocal scanning images are acquired line by line and reconstructed by a computer. A laser-like light beam is shaped as a line and focused onto the retina by an objective lens (Fig. 3.7).

The optical source is an infrared superluminescent diode with central wavelength at 845 nm and a full width at half maximum of 40 nm. MAIA has a digital camera resolution of 1,024×1,024 pixels and a field of view of 36°. The MAIA embedded display for image view is sized 10.4" with a resolution of 800×600 pixels. The optical resolution on the retina is 25 μm that allows black and white high-quality retinal imaging. The minimum pupil size is 2.5 mm, thus not requiring, in most of the cases, the use of dilating drops. The focus adjustment range is from -15 to +10 diopters.

There is no display in MAIA stimuli projection system, differently from other devices, which demands stimuli projection to an internal LCD display. The MAIA microperimeter projects stimuli by means of a stimulus projector focused onto the retina and based on a white light emitting diode (LED) and of a steering mirror for stimulus positioning. Due to a patented solution, the MAIA

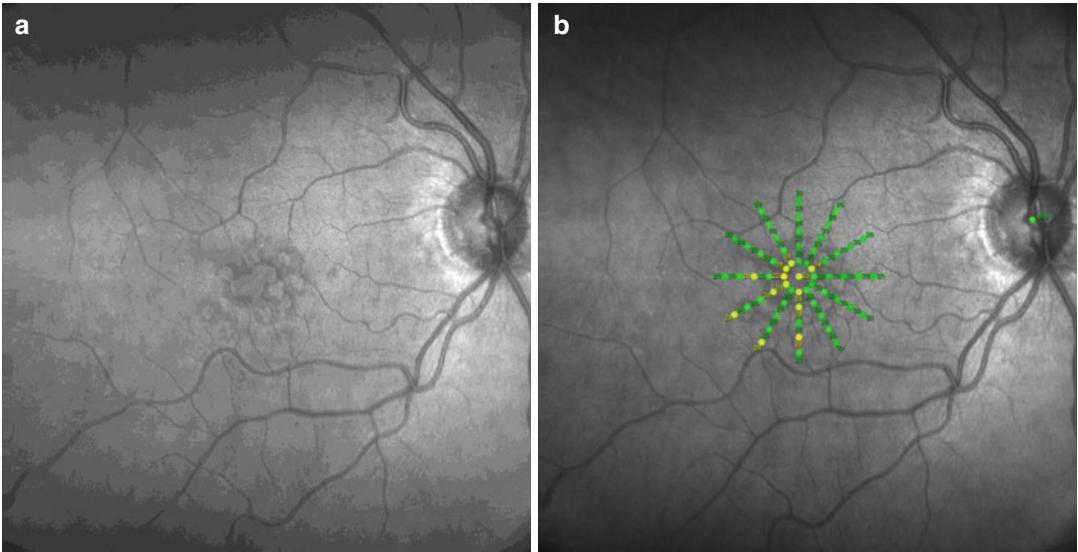


Fig. 3.6 MAIA: (a) fundus image; (b) microperimetry exam

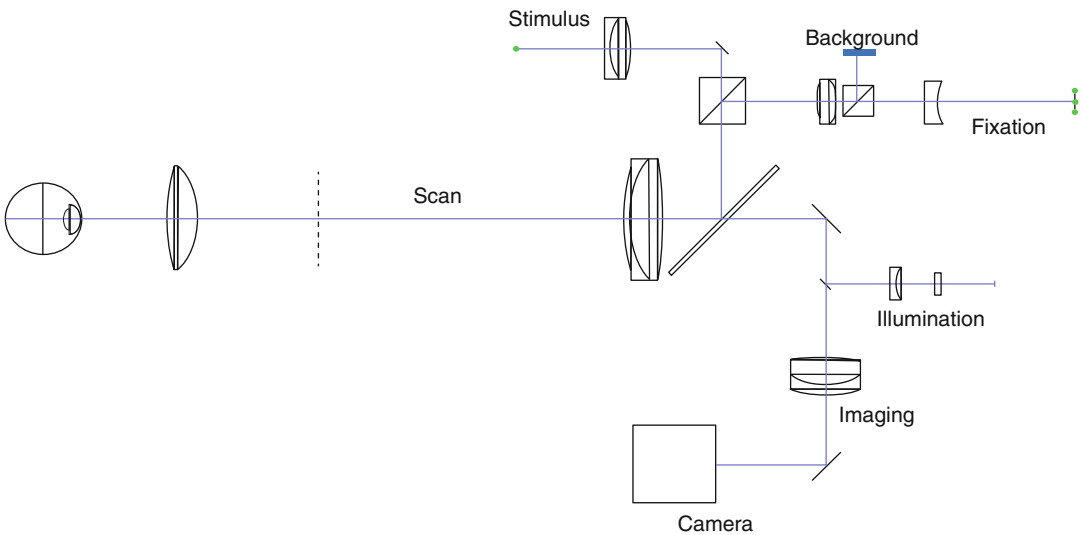


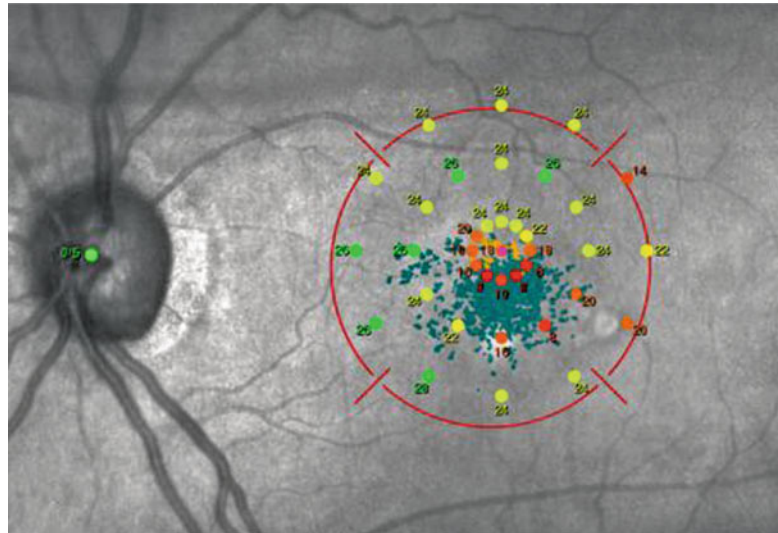
Fig. 3.7 MAIA optic scheme

stimulus projector features high precision on shape and size, and potentially no discretization or digital limits on stimulus positioning and stimulus intensity, as provided by the manufacturer. The background luminance is set at 4 asb, such as standard perimetry (Octopus 101) and MP-1. The automatic eye tracker locks onto the entire fundus image, allowing a highly precise and easy correction of stimulus location, reducing the duration of

each examination. The tracking speed is 25 times per second (25 Hz). The eye-tracking system includes a real-time feature recognition software which elaborates the retina displacement and a steering mirror which moves stimulus projector according to such displacement.

Another important characteristic of MAIA is the easy interaction between the operator and the device. MAIA is provided by an automatic eye

Fig. 3.8 Twelve-degree fixation target with MAIA microperimeter



focusing, an automatic right/left eye recognition, and a very intuitive software.

MAIA offers as fixation target a red circle with two different sizes: 1° and 12° in diameter; the latter presents 4 straight lines crossing the ring and pointing toward the center of the fixation (Fig. 3.8). The red illumination is created by a matrix of LEDs at 633 nm.

Stimuli are white, Goldmann III sized (2.26 mm). An additional property of MAIA microperimeter is a wider stimulus luminance scale that ranges from 1,000 asb (corresponding to 0 dB) to 0.25 asb (36 dB) (Table 3.1). This scale is analogous to the Octopus perimeter luminance range that varies between 0 dB (1,000 asb) and 40 dB (0.1 asb).

3.3.2 Fundus Perimetry with MAIA Microperimeter

MAIA microperimeter records fixation during the microperimetry exam. The software automatically analyzes the fixation stability according to Fujii et al. classification as stable, relatively unstable, or unstable, and it shows the percentages of fixation points located within 1° or 2° from the gravitational center of all fixation points [7]. Quantification of fixation stability is also performed by plotting the position of each fixation

Table 3.1 Different stimuli intensity scale for microperimeter MP-1 and MAIA

MAIA dB level	MAIA differential luminance (asb)	MP-1 dB level	MP-1 differential luminance (asb)
0	1000.00	–	–
1	794.33	–	–
2	630.96	–	–
3	501.19	–	–
4	398.11	0	400
5	316.23	1	317.73
6	251.19	2	252.38
7	199.53	3	200.47
8	158.49	4	159.24
9	125.89	5	126.49
10	100.00	6	100.48
11	79.43	7	79.81
12	63.10	8	63.40
13	50.12	9	50.36
14	39.81	10	40.00
15	31.62	11	31.77
16	25.12	12	25.24
17	19.95	13	20.05
18	15.85	14	15.92
19	12.59	15	12.65
20	10.00	16	10.05
21	7.94	17	7.98
22	6.31	18	6.34
23	5.01	19	5.04
24	3.98	20	4.00
25	3.16	–	–

(continued)

Table 3.1 (continued)

MAIA dB level	MAIA differential luminance (asb)	MP-1 dB level	MP-1 differential luminance (asb)
26	2.51	–	–
27	2.00	–	–
28	1.58	–	–
29	1.26	–	–
30	1.00	–	–
31	0.79	–	–
32	0.63	–	–
33	0.50	–	–
34	0.40	–	–
35	0.32	–	–
36	0.25	–	–

on Cartesian axes and calculating the area of an ellipse that encompasses a given percentage of fixations (bivariate contour ellipse area, BCEA). The software shows the area (square degrees) and the angle (degrees) of 63 % BCEA and 95 % BCEA.

To evaluate visual function, MAIA microperimeter uses two different test strategies. A fast test that performs 1 or 2 projections per stimulus, depending on the initial answer, like in a supra-threshold perimetry. It is a screening test, with a mean test time below 2 min per eye. It provides a “traffic light” for macular integrity and fixation stability (red, abnormal; yellow, suspect; green, normal). The retinal sensitivity threshold is instead measured by the expert test that uses a 4–2 threshold strategy. It provides a “traffic light” and numerical outcomes for macular sensitivity and fixation stability. The results are displayed as numeric, symbolic, or interpolated map. A pretest based on an age-related normative database determines the light threshold at 4 different retinal points, one for each quadrant.

MAIA microperimeter analysis software compares actual threshold data with age-adjusted normative values and classifies the outcome as being normal, suspect, or abnormal, calculating a percentage that represents the likelihood of the results to be functionally abnormal. Several standard grids are available within the software, but the examiner may also customize a new grid or manually preselect some retinal points to be

tested. Subject reliability is also tested, through a stimulus projected onto the patient’s blind spot selected by the operator, as with MP-1.

The eye-tracking system allows also to perform reliable follow-up tests to evaluate the progression of the disease. The follow-up test is performed regardless of the position of the PRL, and it uses the baseline thresholds as starting values of the exam. The follow-up test is therefore slightly faster than the baseline expert exam. After the follow-up test, the software compares sensitivity light thresholds and fixation points between the baseline and the following examinations. Differential point-by-point maps are also available (Fig. 3.9).

Within MAIA microperimeter a biofeedback tool is also available. The auto-tracking system calculates horizontal and vertical shifts relative to a reference frame and maps the eye movements during the examination. The system provides an audible feedback with variable frequency depending on the distance between the PRL, measured by the eye-tracking system, and the trained retinal locus (TRL). The location of the TRL is stored by the system for use in future sessions, though it can be modified at any time.

3.4 Normative Database

The remarkable value of the microperimetry is especially related to the availability of a large normative database. For each actually commercially available microperimetry device, normative studies on a large number of normal subjects have been performed, to verify average values and reliability of the instrument [6, 16–19].

Springer et al. evaluated normal values of MP-1 microperimeter, with a $27^\circ \times 18^\circ$ grid in 30 healthy subjects, between 23 and 55 years old [16]. The mean differential light threshold was 15.5 ± 0.8 dB, and mean light threshold of each retinal point was determined, to verify differences in sensitivity thresholds along the entire grid. The upper part of the visual field showed, compared to the lower part, a decreased mean light threshold. Moreover, in this study each subject underwent standard perimetric

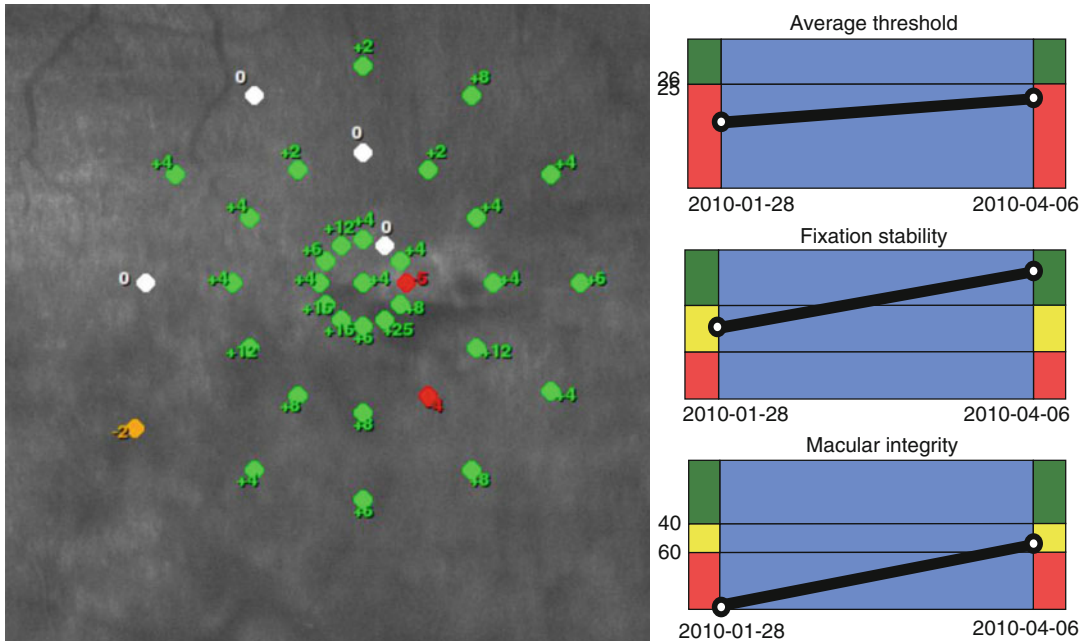


Fig. 3.9 Differential map after follow-up examination, with MAIA microperimeter

examination, with Octopus 101 (Haag-Streit AG, Switzerland), to compare microperimetric and perimetric values. A systematic difference of 11.4–18.3 dB (mean 14.6 ± 1.8 dB) of MP-1 was found when compared with Octopus 101. In a different study [6], Miedna et al. tested a 10° retinal area, centered on fovea, with both MP-1 and Octopus 101 in 18 healthy eyes. A mean differential light threshold of 19.7 ± 0.8 dB with MP-1 and of 33.1 ± 1.7 with Octopus 101 was found. A comparison, point by point, of the two instruments was furthermore impossible due to a very large and non-corresponding difference in the extension of the dB scale (4–400 asb in MP-1 versus 0.1–1,000 asb in Octopus 101). Shah and Chalam reported analogous result in an MP-1 study: a mean differential light threshold of 18.33 dB in a central 12° grid of 37 healthy subjects [17]. A large-scale (190 healthy subjects), multicentric study was conducted in eight Italian Centers to determine a normative database and repeatability values for the MP-1 microperimeter [18]. Mean sensitivities of 4 macular sectors of a 20° grid were evaluated. The superior sector showed a significantly lower mean retinal sensitivity (19.0 ± 1.1 dB) than the other

sectors (inferior sector 19.6 ± 0.7 dB, nasal sector 19.2 ± 0.9 dB, temporal sector 19.3 ± 0.9 dB), confirming the results of Springer et al. [11]. Linear regression analysis showed a statistically significant decrease in differential light threshold with increasing age ($p < 0.0001$) [18]. Repeatability measurements were achieved from ten subjects with a different grid; comparable and statistically significant repeatability was obtained from each retinal tested area even over time (1 week) [18].

A smaller number of studies are available for MAIA device. A large, multicentric study included 200 healthy volunteers evaluated with MAIA microperimeter [19]. The mean age of subjects was 69 ± 6.8 years, significantly older compares to normative MP-1 data, because they represented the age-matched control group of 200 patients affected by age-related macular degeneration. The mean differential light threshold in normals was 29.78 ± 1.71 dB, from a 61-stimuli grid, covering the central 10° of the macula. Moreover, the average threshold for each of 61 stimuli was calculated in healthy subjects and plotted for each decade from 20 to 80 years old. Therefore, the software is able to automatically compare any subject's results with an age-related

normative database, allowing at-a-glance evaluation of the outcome, displayed as “normal,” “suspect,” or “abnormal.”

Conclusion

It is well rendered how the great technical possibilities and customizable features of microperimetry devices allow multiple, stimulating choices to evaluate the functional aspect of various retinal and neurological diseases. Notwithstanding, it is important to standardize microperimetry parameters to obtain scientifically correct and comparable outcomes even with the most recent devices. More widespread use of microperimetry in the assessment of visual function may add new knowledge in the evaluation of different chorioretinal diseases and treatments.

References

1. Webb RH, Hughes GW (1981) Scanning laser ophthalmoscope. *IEEE Trans Biomed Eng* 28:488–492
2. Mainster MA, Timberlake GT, Webb RH et al (1982) Scanning laser ophthalmoscopy. Clinical applications. *Ophthalmology* 89:852–857
3. Rohrschneider K, Springer C, Bültmann S et al (2005) Microperimetry – comparison between the microperimeter 1 and scanning laser ophthalmoscope – fundus perimetry. *Am J Ophthalmol* 139:125–134
4. Menke MN, Sato E, Van De Velde FJ et al (2006) Combined use of SLO microperimetry and OCT for retinal functional and structural testing. *Graefes Arch Clin Exp Ophthalmol* 244:634–638
5. Midena E, Radin PP, Convento E (2006) Liquid crystal display microperimetry. In: Midena E (ed) *Perimetry and the fundus: an introduction to microperimetry*. Slack Inc, Thorofare, pp 15–25
6. Midena E, Radin PP, Convento E et al (2007) Macular automatic fundus perimetry threshold versus standard perimetry threshold. *Eur J Ophthalmol* 17:63–68
7. Fujii GY, de Juan E Jr, Sunness J et al (2002) Patient selection for macular translocation surgery using the scanning laser ophthalmoscope. *Ophthalmology* 109:1737–1744
8. Midena E, Radin PP, Pilotto E et al (2004) Fixation pattern and macular sensitivity in eyes with subfoveal choroidal neovascularization secondary to age-related macular degeneration. A microperimetry study. *Semin Ophthalmol* 19:55–61
9. Déruaz A, Matter M, Whatham AR et al (2004) Can fixation instability improve text perception during eccentric fixation in patients with central scotomas? *Br J Ophthalmol* 88:461–463
10. Timberlake GT, Sharma MK, Grose SA et al (2005) Retinal location of the preferred retinal locus relative to the fovea in scanning laser ophthalmoscope images. *Optom Vis Sci* 82:177–185
11. Pilotto E, Guidolin F, Convento E et al (2013) Fundus autofluorescence and microperimetry in progressing geographic atrophy secondary to age-related macular degeneration. *Br J Ophthalmol* 97:622–626
12. Vujosevic S, Midena E, Pilotto E et al (2006) Diabetic macular edema: correlation between microperimetry and optical coherence tomography findings. *Invest Ophthalmol Vis Sci* 47:3044–3051
13. Midena E, Vujosevic S, Convento E et al (2007) Microperimetry and fundus autofluorescence in patients with early age-related macular degeneration. *Br J Ophthalmol* 91:1499–1503
14. Pilotto E, Vujosevic S, Melis R et al (2011) Short wavelength fundus autofluorescence versus near-infrared fundus autofluorescence, with microperimetric correspondence, in patients with geographic atrophy due to age-related macular degeneration. *Br J Ophthalmol* 95:1140–1144
15. Vujosevic S, Casciano M, Pilotto E et al (2011) Diabetic macular edema: fundus autofluorescence and functional correlations. *Invest Ophthalmol Vis Sci* 52:442–448
16. Springer C, Bültmann S, Völcker HE et al (2005) Fundus perimetry with the Micro Perimeter 1 in normal individuals: comparison with conventional threshold perimetry. *Ophthalmology* 112:848–854
17. Shah VA, Chalam KV (2009) Values for macular perimetry using the MP-1 microperimeter in normal subjects. *Ophthalmic Res* 41:9–13
18. Midena E, Vujosevic S, Cavarzeran F, Microperimetry Study Group (2010) Normal values for fundus perimetry with the microperimeter MP1. *Ophthalmology* 117:1571–1576
19. Vujosevic S, Smolek MK, Lebow KA et al (2011) Detection of macular function changes in early (AREDS 2) and intermediate (AREDS 3) age-related macular degeneration. *Ophthalmologica* 225:155–160

Gennady Landa, Emily Su, Patricia Garcia,
and Richard B. Rosen

4.1 Functional Correlations of High-Resolution Retinal Imaging Using Combined OCT/SLO Microperimetry

Best corrected visual acuity has long been the gold standard for measuring visual function but lacks sufficient detail to fully describe visual impairment [1]. As far back as 1856, Albert Von Graefe recognized that central visual acuity was inadequate for the task and championed the use of visual fields analysis [1]. Visual experience is strongly influenced by the presence of paracentral or central scotomas which are often difficult to map with standard automated perimetry. Fundus-based perimetry or microperimetry attempts to map these visual phenomena and to relate them to corresponding fundus features [2, 3].

High-resolution spectral-domain optical coherence tomography (SD OCT) has expanded our ability to identify the anatomic correlates of retinal dysfunction and has become indispensable clinically since its commercial introduction in 2007. It provides better characterization

at the vitreoretinal surface, clearer delineation of the retinal layers, and retinochoroidal interface than its predecessor Time-Domain OCT, as well as providing 3D reconstructions. The spectral-domain OCT/SLO imaging system (OPKO, Miami, USA), like many of its competitors, provides images at twice the resolution of the original OCT/SLO (5 μm vs. 10 μm) and at speeds of up to 32 times faster (64 Hz vs. 2 Hz). Such high-speed and high-resolution imaging minimizes movement artifacts and allows many different imaging strategies to be performed quickly and with greater accuracy. Employing an 830 nm superluminescent diode as its light source, with a 40 nm bandwidth and a spectrometer which captures 28,000 A-scans/s, the OCT/SLO can acquire up to 128 longitudinal OCT scans in 2 s over a 5 mm area, allowing generation of a 3-dimensional retinal thickness map.

The OPKO Spectral-Domain OCT/SLO also incorporates an integrated system for localized visual function assessment of the fundus using an automated threshold sensitivity testing algorithm delivered in a variety of grid patterns. Microperimetry testing runs simultaneously with the SLO imaging and incorporates software which allows real-time tracking of retinal movement and records patient fixation, along with mapping of the macular sensitivity. Changes in visual function over time can be quantified utilizing a retest feature which returns to the previously tested retinal location. This enables accurate evaluation of visual change in relation to anatomic changes detected by OCT and SLO [2].

G. Landa • E. Su • P. Garcia • R.B. Rosen, MD (✉)
Retina Center, Department of Ophthalmology,
The New York Eye and Ear Infirmary,
310 East 14th Street, New York, NY 10003, USA
e-mail: ricosen@gmail.com,
richardrosen2@mac.com

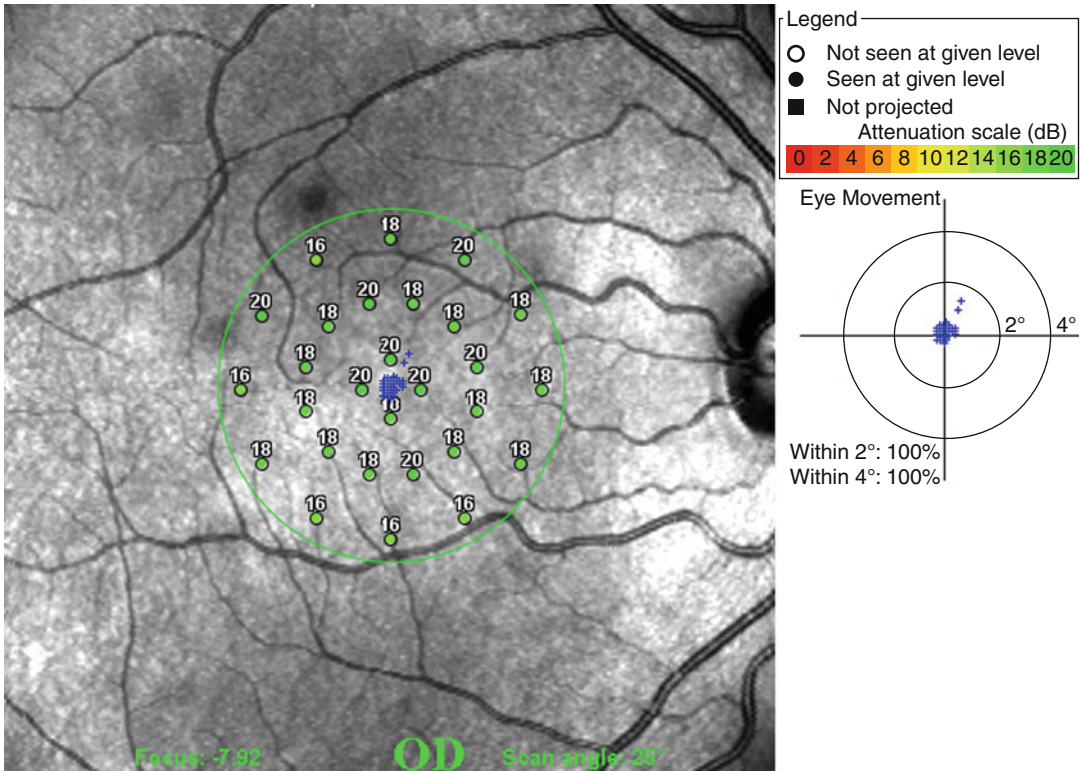


Fig. 4.1 Normal microperimetry test result. The fixation stability is shown on the right (in *blue*) and overlaid on the fundus image along with sensitivity point values

(in *green*). A color scale (from *red* to *green*), indicating the degree of attenuation, is provided for easy visual recognition

During microperimetry testing, the patient is instructed to fixate on the central target and to push the handheld button every time a stimulus is seen. Once the patient's fundus is aligned and focused, the operator designates the vessel to be used for fixation tracking and adjusts the stimulus pattern to cover the area of interest. The typical testing pattern employed is the circular grid, "polar 3," which consists of 28 dots: 4 central, 12 mid, and 12 outer rings. It features Goldman III size stimuli presented for 200 ms with a 1,500 ms interval between stimuli presentations.

The system automatically checks fundus alignment prior to each stimulus presentation, adjusting accordingly, and pauses the test automatically should the subject be unable to maintain good fixation or move out of range. In such event, the system prompts the operator to manually realign the patient, before testing is allowed to resume. At the completion of the study, each of 28 retinal test points (or loci) is scored, according to the threshold sensitivity detected at that point. The MP values range from the lowest sensitivity level, 0, to the highest, 20, as shown in Fig. 4.1.

4.2 Pathological Examples

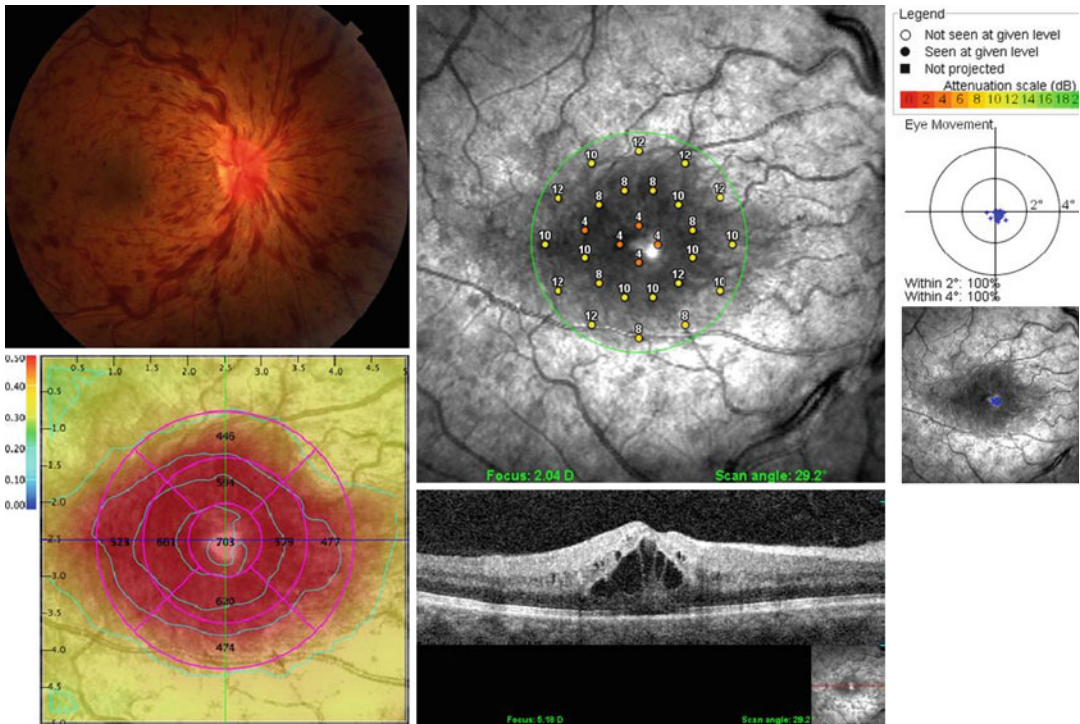


Fig. 4.2 Central retinal vein occlusion (CRVO). The patient depicted suffers from a minimally ischemic central retinal vein occlusion. While there is significant edema in the outer layers, the inner retinal layers appear minimally

disturbed. The photo shows hemorrhages but no nerve fiber layer infarcts. The microperimetry shows moderate central depression but retains some function despite the cystoid changes

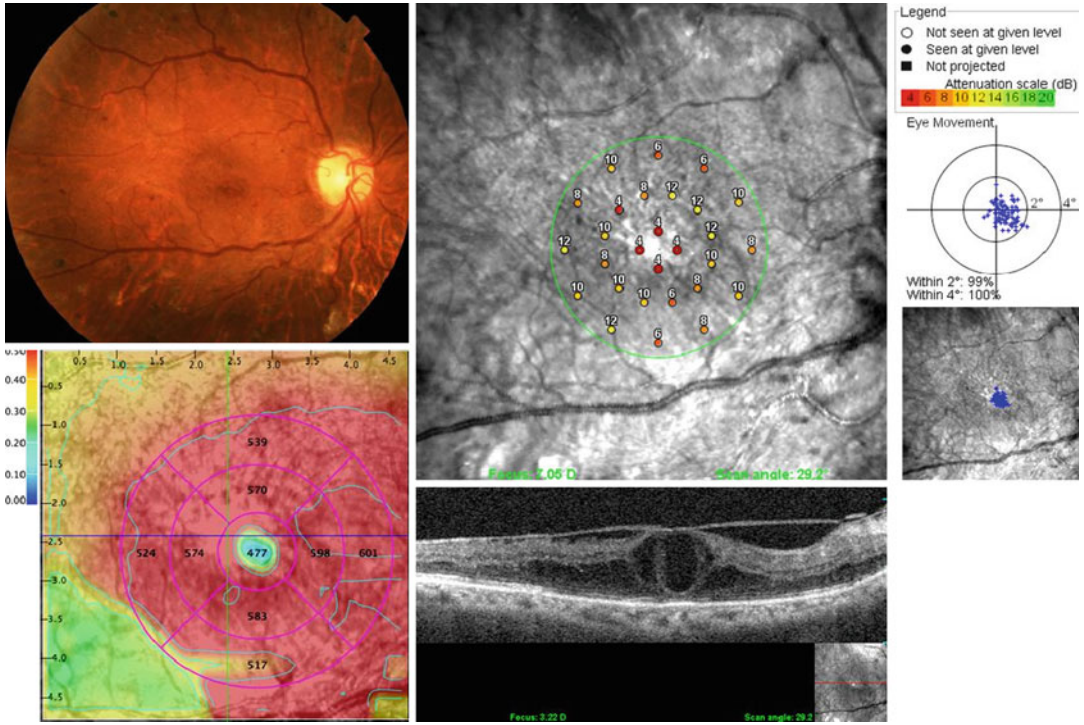


Fig. 4.3 Diabetic maculopathy. This patient has proliferative diabetic retinopathy which has been treated earlier with panretinal photocoagulation. The macula shows a membrane which is pulling the retina and creating severe cystic changes. The microperimetry shows poor central function and the inability to see the brightest stimulus

presented. Fixation appears shifted inferonasally with some degree of scatter. The poor central function is consistent with the large central cysts. The topographic map includes the dense tractional membrane as part of the retinal thickness giving it a falsely exaggerated perifoveal reading

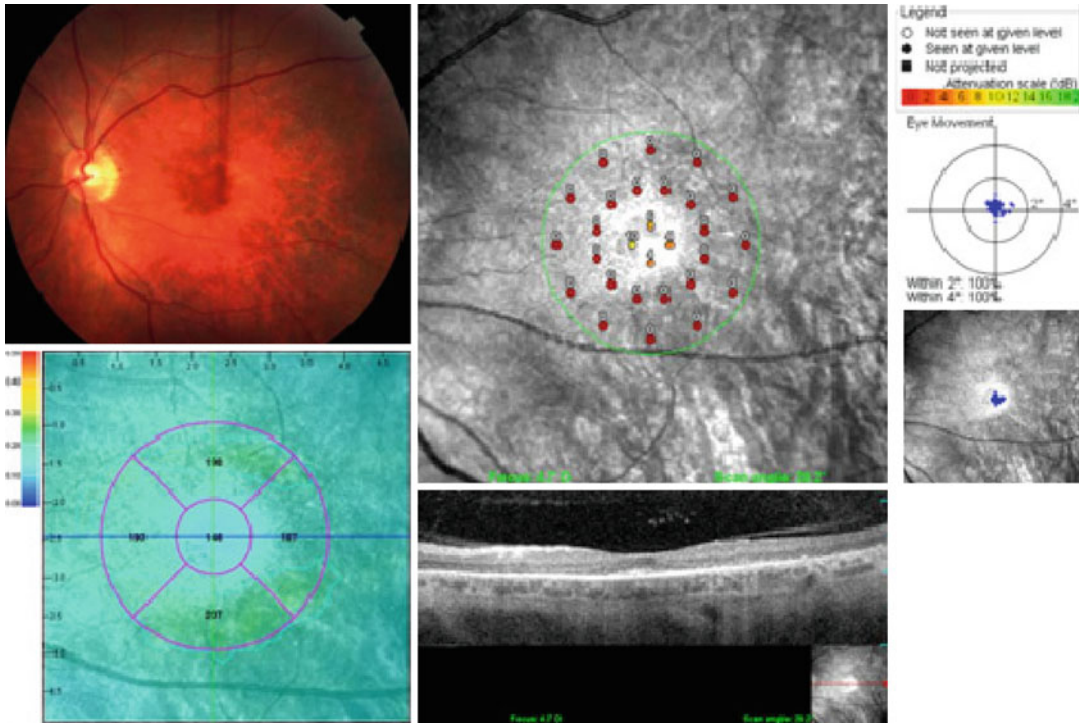


Fig. 4.4 Pigmentary degeneration with central sparing. Here is a case of retinal photoreceptor degeneration which has progressed from the periphery leaving a small area of functioning central retina. The color fundus photo in the upper left shows a prominent choroidal pattern consistent with retinal thinning. The topography below shows an

abnormally thin retina. The microperimetry demonstrates a severe macular dysfunction except in a small central area which is preserved. The visual acuity is 20/30. The OCT shows some vitreous degeneration in front of the macula and deep penetration of the illumination into the choroid, consistent with RPE atrophy



Fig. 4.5 Central serous retinopathy (CSR). This a patient with a recurrent episode of CSR. The blister-like detachment is evident in the fundus photo and the

topography. The microperimetry demonstrates the retention of good central function despite the retinal elevation

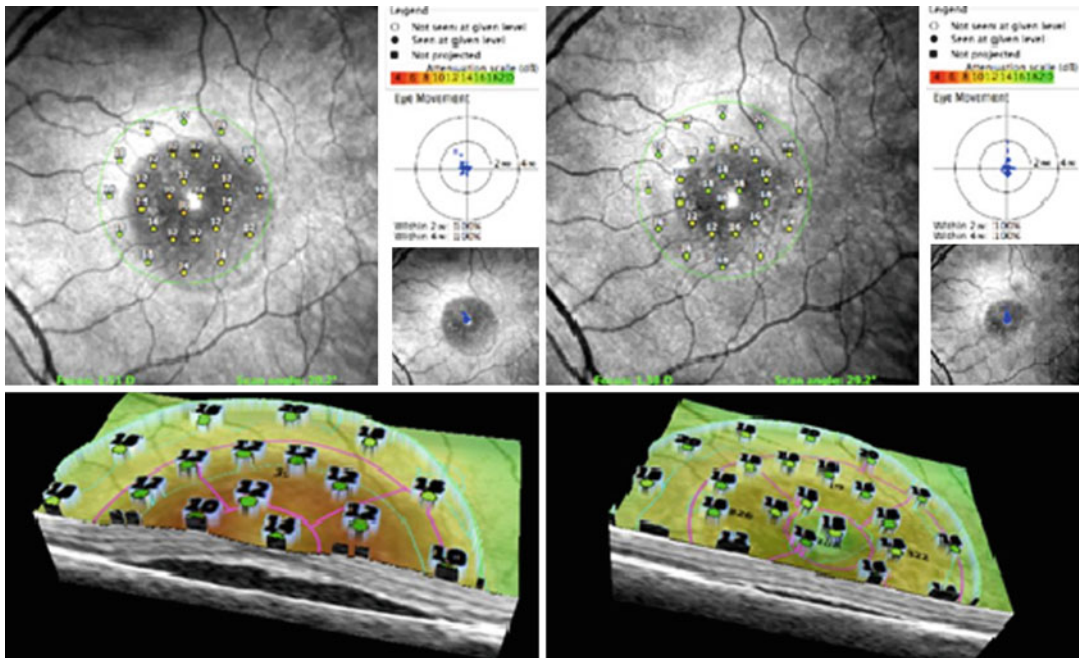


Fig. 4.6 Serial CSR exams. Microperimetry on the left was performed during an acute episode, while the study on the right was performed after most fluid has

been reabsorbed. The changes in sensitivity demonstrate the value of multimodal imaging to relate anatomy to functional performance

Macular Hole Pre and Post Repair

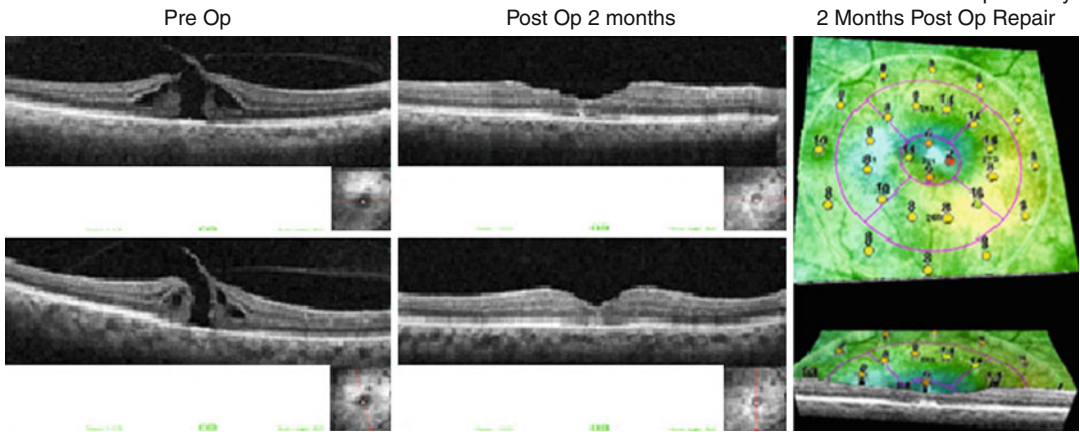


Fig. 4.7 Macular hole before and after repair. Microperimetry study on the right was performed 2 months following successful repair

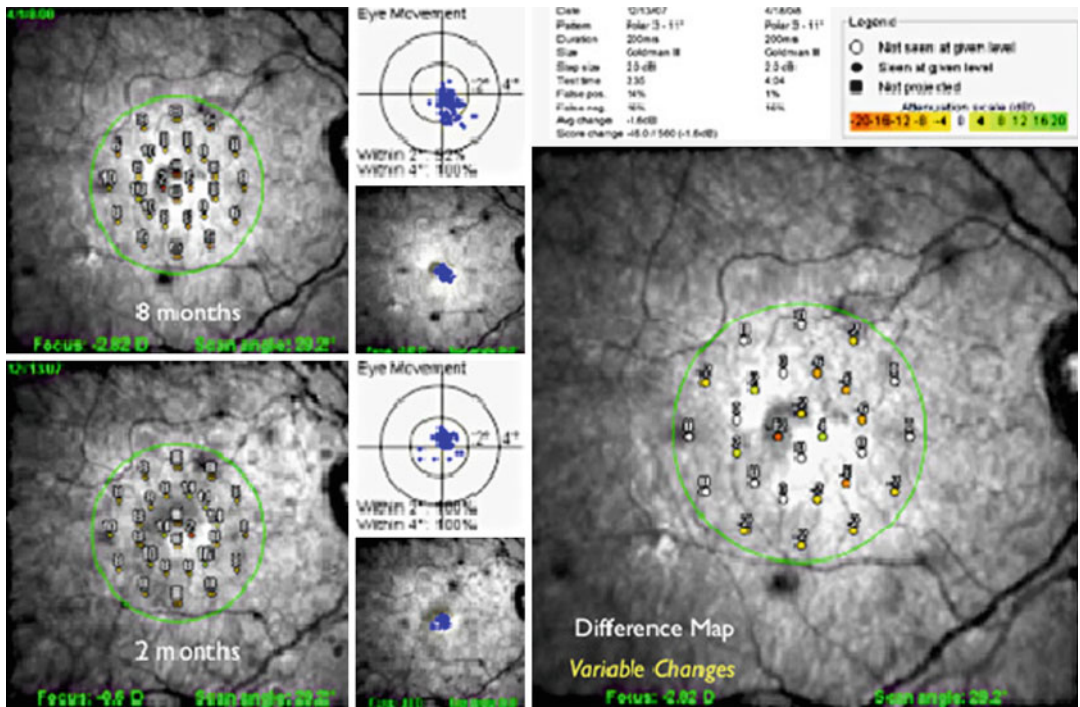


Fig. 4.8 Macular hole visual function changes at 2 and 8 months following repair. The difference map on the right demonstrates some variability in functionality which appears to have developed during the 6-month interval between the studies

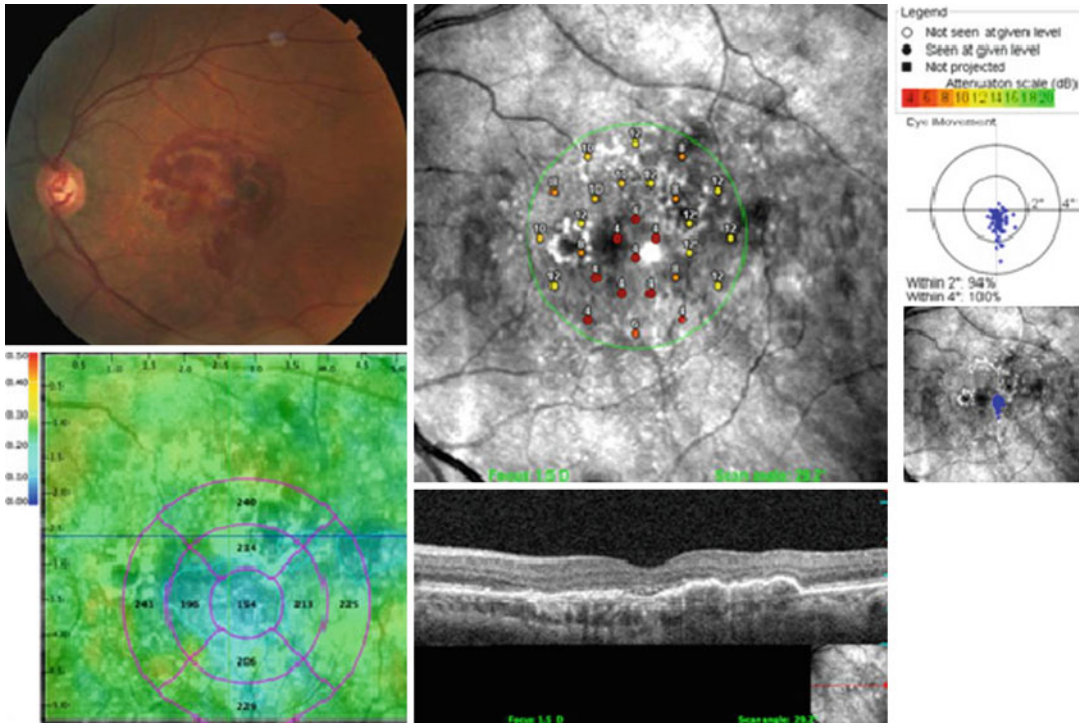


Fig. 4.9 Wet age-related macular degeneration (AMD). Microperimetry reveals the extensive functional decrease in this case of wet AMD. This is in sharp contrast to the thickness map which shows only some mild thinning

4.3 Anatomic-Functional Correlations

With the availability of enhanced anatomic detail revealed by SD OCT imaging, attention has been drawn to the status of the so-called inner outer segment junction line, now suggested to correlate to the location of the photoreceptor ellipsoid, as a predictor of functional integrity. The integration of functional and anatomic testing within the OCT/SLO insures an accurate internal registration which allowed this hypothesis to be tested in a variety of pathological states. Patients with macular degeneration and diabetes were imaged to obtain high-resolution scans.

Threshold sensitivity maps were then obtained using the microperimetry module. Each study evaluated retinal sensitivity at 28 points, and then the status of the IS-OS line was evaluated at each corresponding location. Line integrity was graded as continuous or not [3].

Analysis of 3,373 microperimetry points compared to the status of underlying IS-OS junctional layer revealed an inverse correlation between

microperimetric values (ranged 0–20) and the rate of disruptions in IS-OS layer (correlation coefficient $r = -0.77$, $p < 0.001$), suggesting that lower MP values at a specific retinal loci were more often associated with adjacent IS-OS line disruptions [3].

For each of the three groups tested – dry AMD, wet AMD, and diabetic retinopathy – correlation between percentage of IS-OS line breaks at the microperimetry test points was compared to the mean microperimetry values in each eye (Fig. 4.13a–c). AMD eyes demonstrated higher correlation than diabetic eyes. This difference may be ascribed in part to differences in the anatomic location of the pathological process. AMD primarily affects the outer retina as an inflammatory/degenerative process or choroidal vasculopathy with only secondary effects extending to the overlying inner retina. In contrast, diabetic retinopathy is a primary vasculopathy of the retinal vessels with inner retinal manifestations and only secondary outer retinal disturbances. The combination of OCT imaging and microperimetry testing nicely demonstrates this difference.

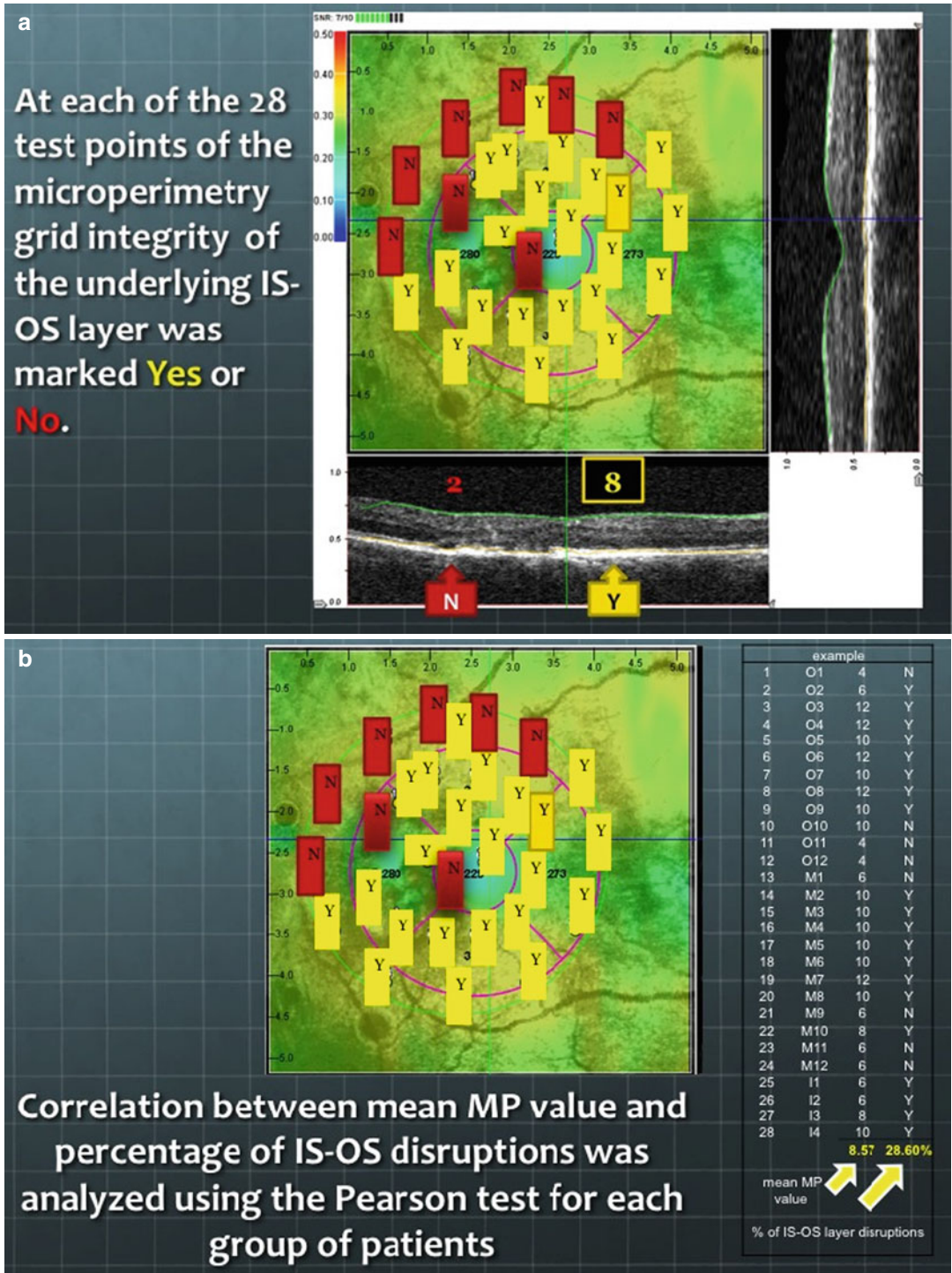


Fig. 4.10 (a) Checking IS-OS line integrity at each microperimetry test point. (b) Correlating mean microperimetry test values to percentage of IS-OS disruptions

Fig. 4.11 Percentage of IS-OS layer disruptions at microperimetry points versus microperimetry values of retinal sensitivity. Combined data of (all groups) 3,373 correlation points were analyzed. The lower the MP value, the higher the possibility of IS-OS layer disruption (correlation coefficient = -0.96)

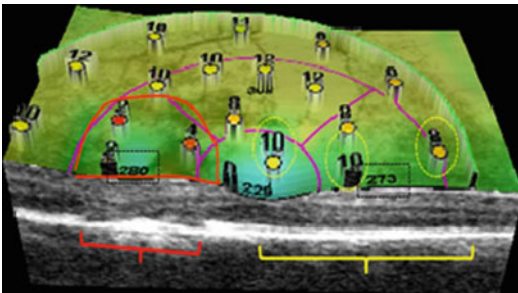
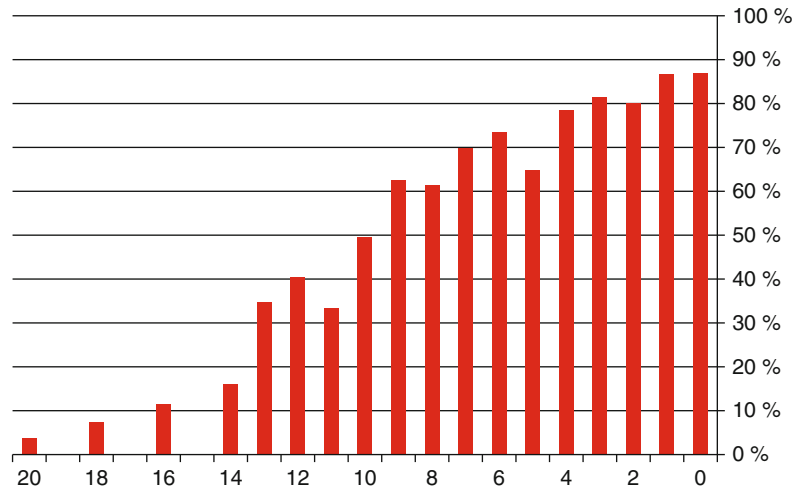


Fig. 4.12 Three-dimensional map, demonstrating reduced retinal sensitivity over the area of disrupted IS-OS layer (in red), though the retinal thickness matches a similar point on the right side of the fovea

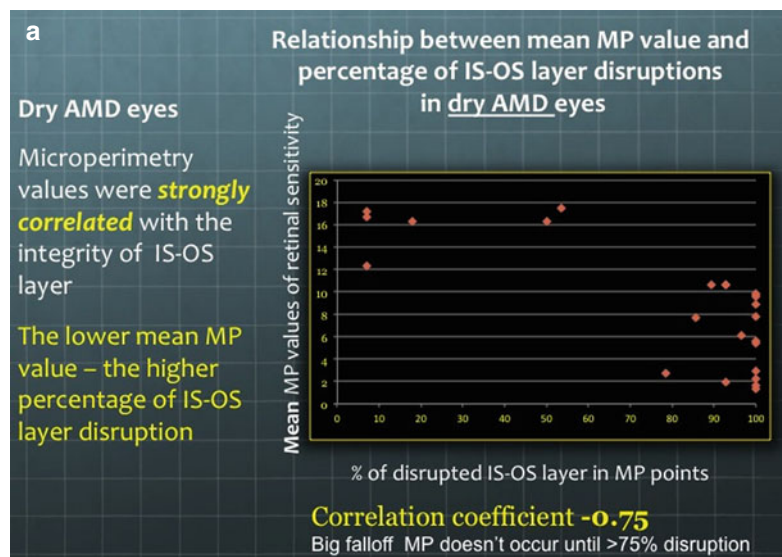
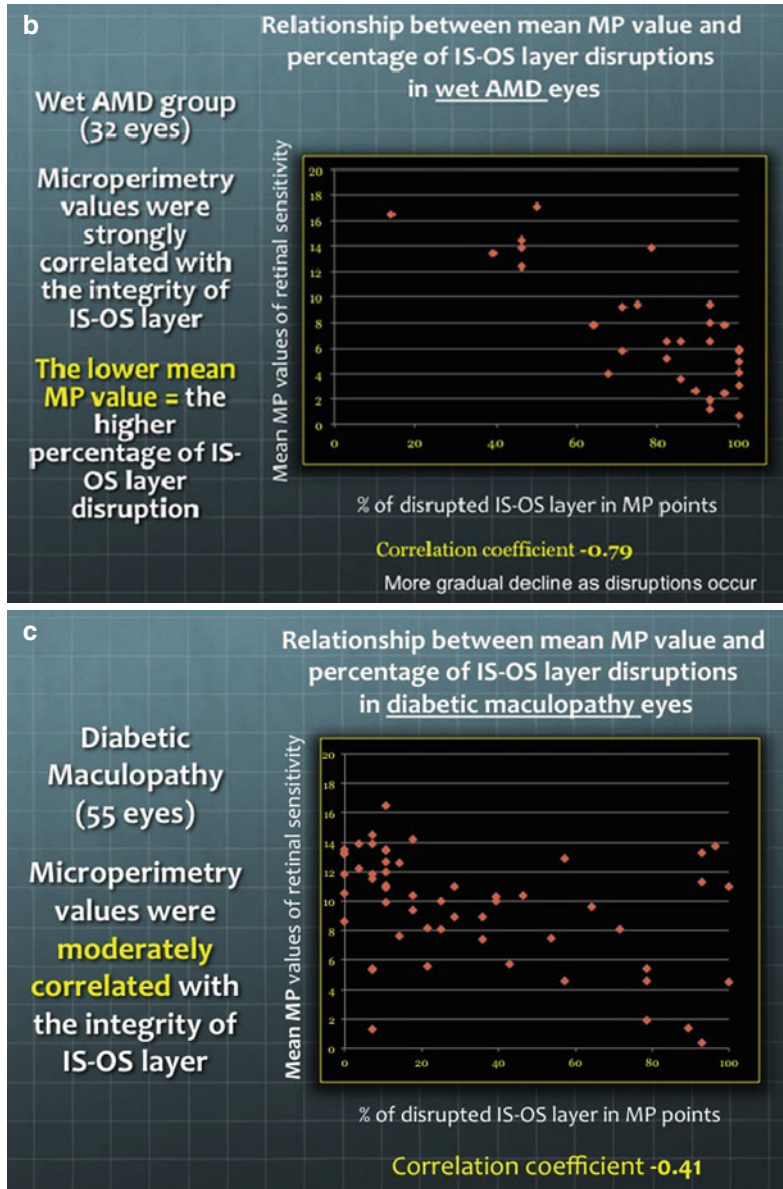


Fig. 4.13 Percentage of IS-OS line disruptions versus mean microperimetry values. (a) Dry AMD. (b) Wet AMD. (c) Diabetic maculopathy

Fig. 4.13 (continued)



4.4 Serial OCT/SLO Microperimetry of Choroidal Neovascularization Treatment

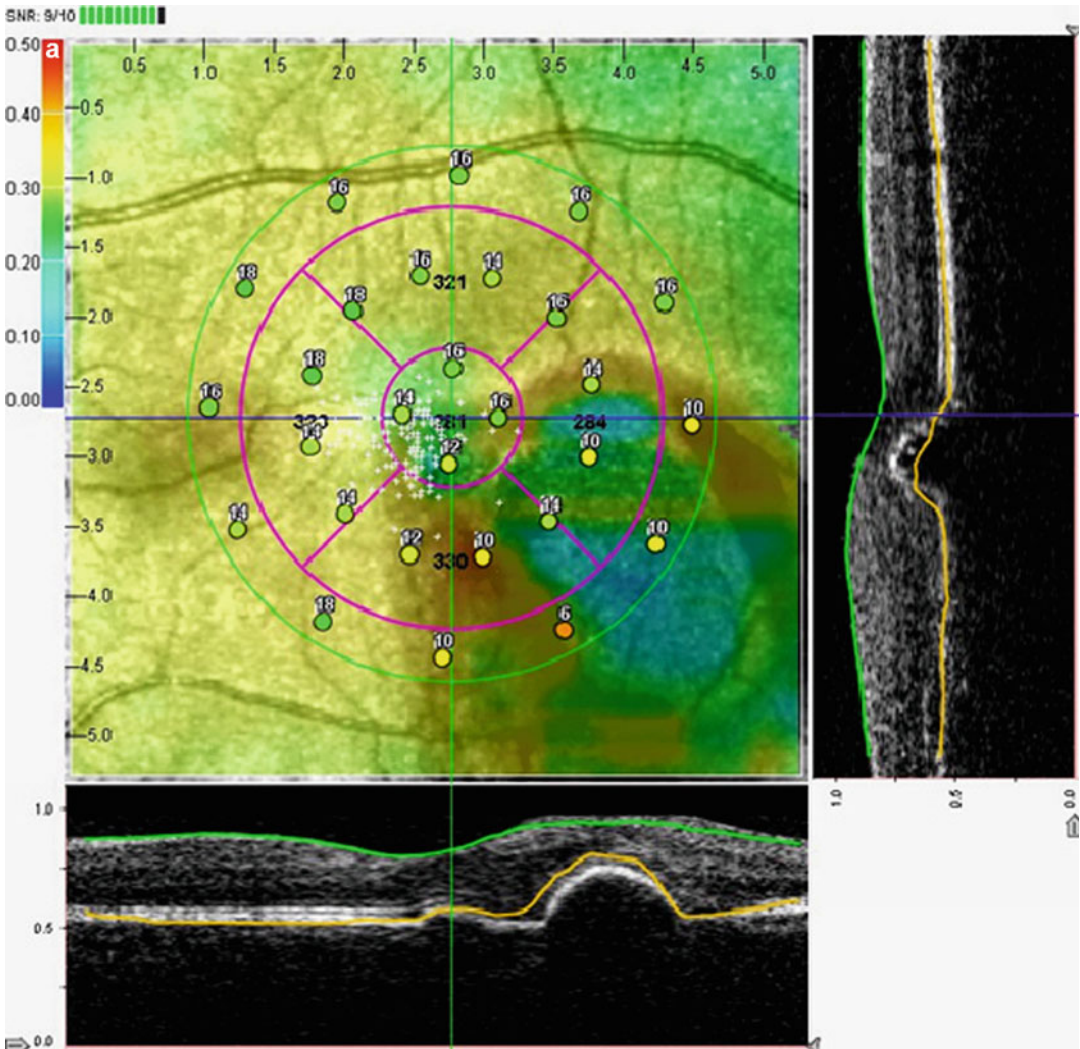


Fig. 4.14 Age-related macular degeneration. (a) Day 0: new onset choroidal neovascularization. Microperimetry reveals depressed function overlying the membrane. (b) Day 60: choroidal neovascularization, following two injections of ranibizumab. Microperimetry shows improvement in retinal function in the region overlying the membrane.

(c) Day 155: choroidal neovascularization, following five injections of ranibizumab. Microperimetry improved to near-normal levels over the regressed membrane. (d) Red-free visual function difference map. Day 155: choroidal neovascularization following five injections of ranibizumab. Microperimetry level changes from day 0

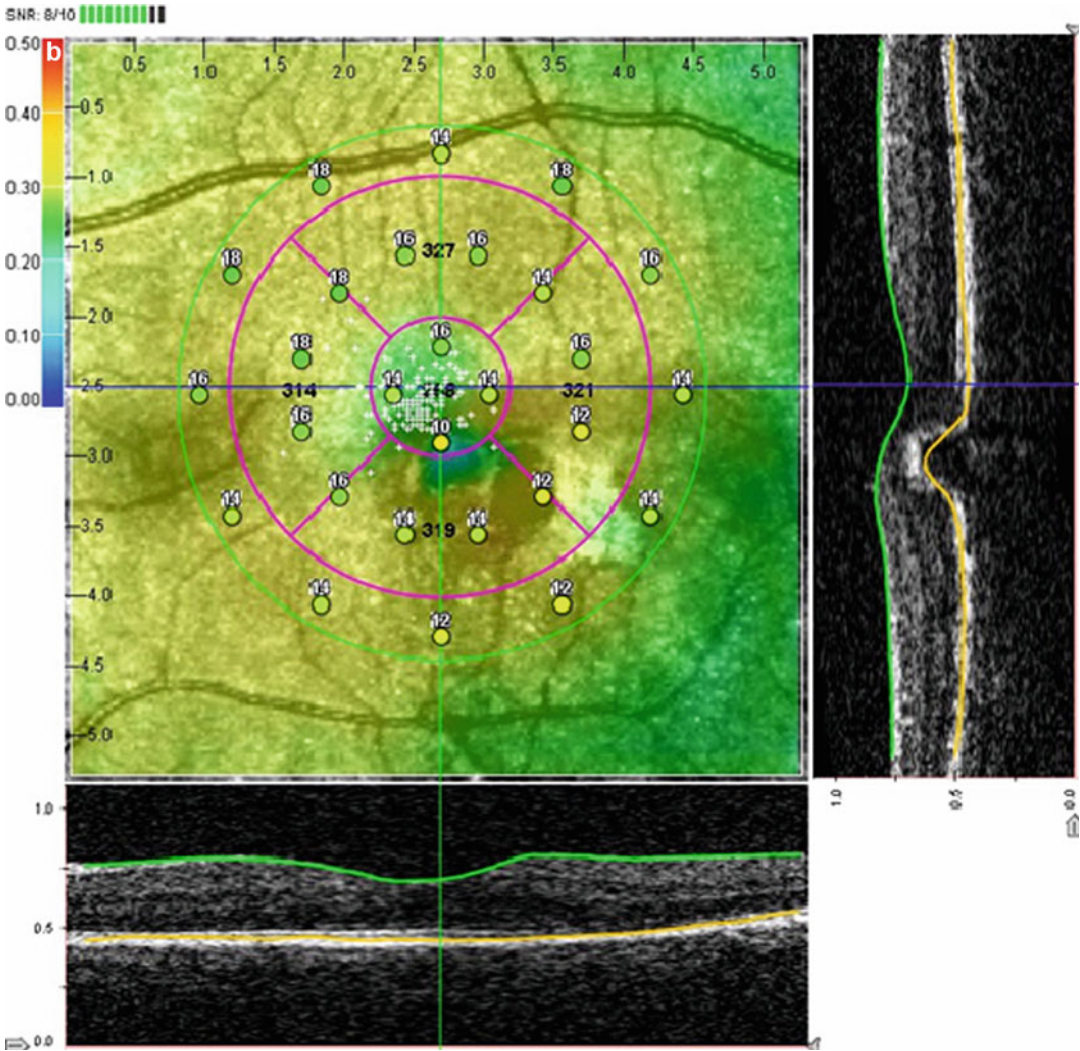


Fig. 4.14 (continued)

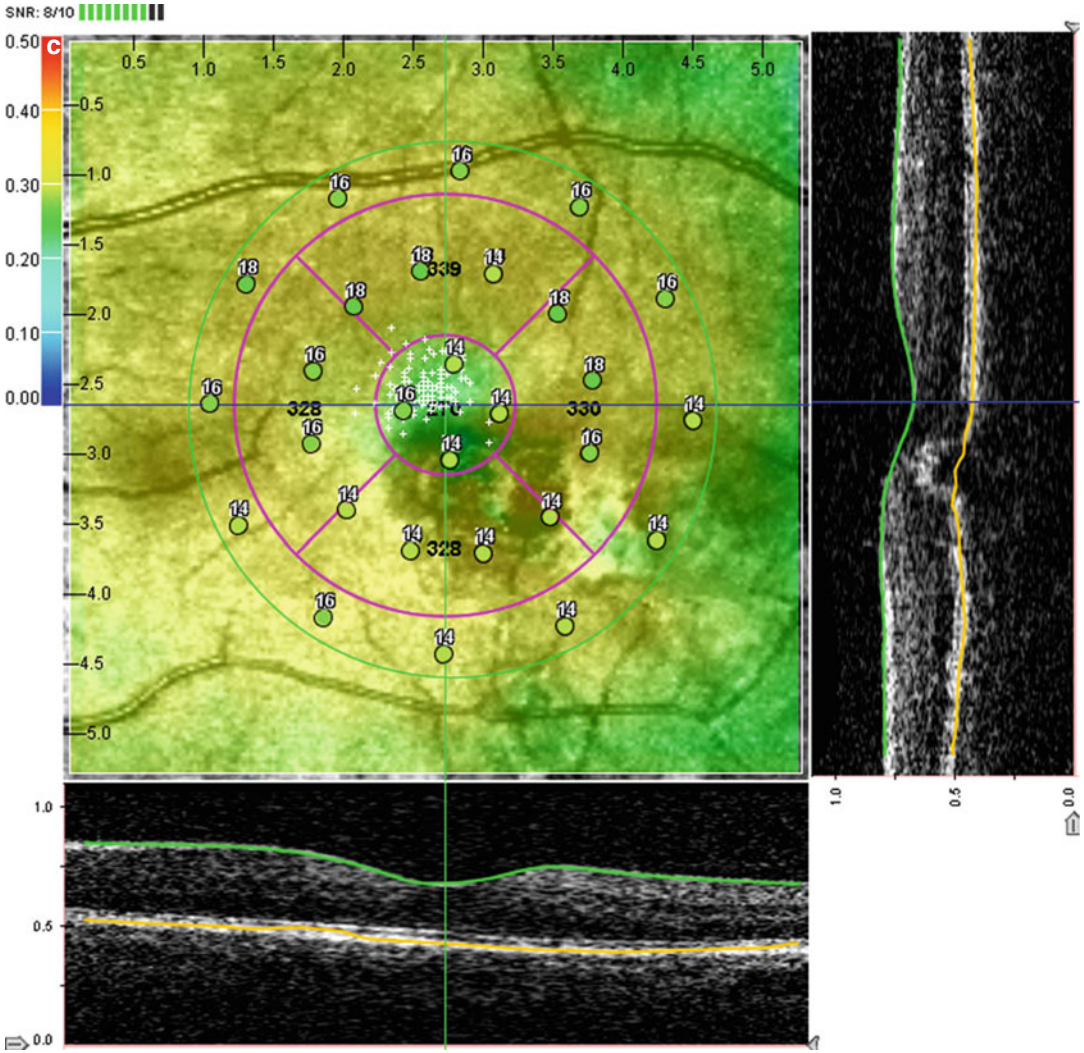


Fig. 4.14 (continued)

4.5 Microperimetry Monitoring Compared to Visual Acuity and Retinal Thickness

Microperimetry’s value as a monitoring tool in anti-VEGF treatment of choroidal neovascularization (CNV) has recently been tested and compared with changes detected in visual acuity and retinal thickness over the course of therapy. During the first months of therapy, mean retinal sensitivity showed progressive improvement with the most significant increases in mean MP scores

occurring following the first and fourth injections (Fig. 4.15). Central retinal thickness in contrast decreased after the first injection and remained almost unchanged afterwards.

Mean microperimetry and ETDRS scores showed the strongest correlation ($r=0.69$, $p<0.001$). Mean microperimetry and central macular thickness showed a strong but smaller correlation ($r=0.528$, $p=0.01$), while ETDRS score and central macular thickness showed the weakest association ($r=0.33$, $p=0.043$) (Fig. 4.16a–c).

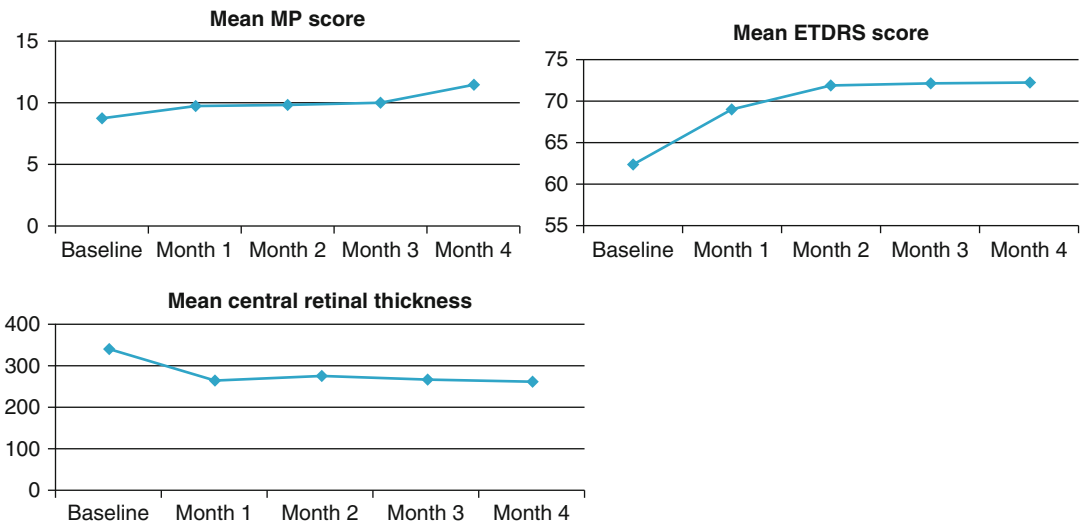
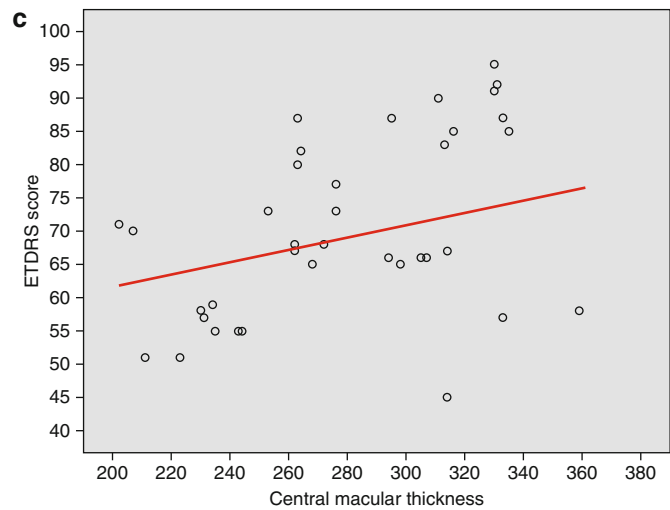
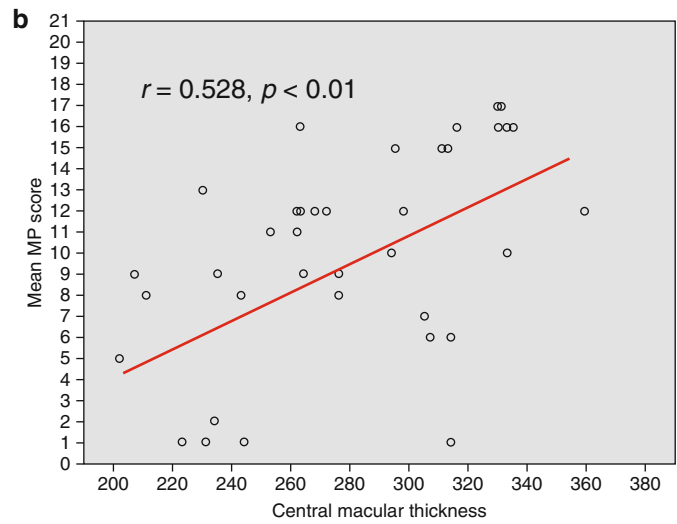
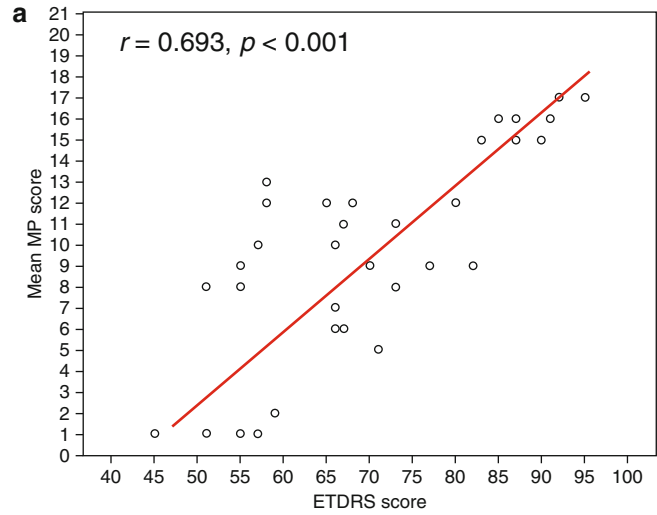


Fig. 4.15 Comparison of changes in mean microperimetry score versus mean ETDRS visual acuity versus mean central retina thickness during the first 4 months of anti-VEGF therapy with ranibizumab

Fig. 4.16 (a) Mean microperimetry scores (MP) showed *strong and significant correlation* ($r=0.69, p<0.001$) with related ETDRS scores. (b) Mean microperimetry score and central macular thickness showed a less strong though significant correlation ($r=0.528, p<0.01$). (c) ETDRS scores and CRT were the least significantly correlated ($r=0.33, p<0.043$)



References

1. Rohrschneider K, Bultmann S, Springer C (2008) Use of fundus perimetry (microperimetry) to quantify macular sensitivity. *Prog Retin Eye Res* 27:536–548
2. Landa G, Rosen RB, Garcia PM et al (2010) Combined three-dimensional spectral OCT/SLO topography and Microperimetry: steps toward achieving functional spectral OCT/SLO. *Ophthalmic Res* 43:92–98
3. Landa G, Su E, Garcia PM et al (2011) Inner segment-outer segment junctional layer integrity and corresponding retinal sensitivity in dry and wet forms of age-related macular degeneration. *Retina* 31: 364–370

Elisabetta Pilotto and Enrica Convento

5.1 Introduction

In patients affected by macular diseases, impaired vision in dim light and difficulties in recognizing the contour of objects in low-contrast conditions are common complaints even with normal visual acuity and full visual field [1–3]. Unfortunately, these topics have been rarely considered in clinical practice, and the examination of visual function at low contrast or during dark adaptation has never been considered clinically relevant. Rod photoreceptor function is reduced in many retinal diseases, both congenital and acquired, including age-related macular degeneration, diabetic retinopathy, rod-cone dystrophy, retinitis pigmentosa and retinal teleangiectasia [4–8]. In the progression of early age-related macular degeneration (AMD), rod photoreceptors degenerate earlier and more rapidly than cones both anatomically and functionally [9–11]. The greatest loss in rod function occurs in the parafoveal region of the macula, which extends from 3.5° to 10° from the fovea, where rod density is at its maximum [12]. Despite the evidence that rods fail first, clinicians and regulatory agencies monitor the progression of macular degeneration with visual tests that measure cone but not rod function.

This is typically performed in bright light, but not in dim light condition where patients struggle to perform ordinary visual tasks.

This chapter describes the contribution of newly developed scotopic microperimetry to the clinical examination of rod function, mainly in early AMD and in diabetic retinopathy.

5.2 Scotopic Sensitivity and Scotopic Visual Field Examination

Scotopic visual function was originally examined using a Goldmann-Weekers adaptometer. It allowed to measure thresholds in the fully dark-adapted state at one or more retinal loci [13]. After this standardized approach, a specifically modified perimeter such as the modified Humphrey field analyser (HFA) was proposed to perform both light- and dark-adapted visual field testing [14]. The desired target size (Goldman IV or V) and a stimulus intensity range of 5 log units were available on the modified HFA. For two-colour dark-adapted perimetry, blue-green and red stimuli were needed. Although there were coloured filters in the HFA, the 5 log unit intensity range was unavailable. Therefore, a filter was installed into the optical pathway (immediately after the projector condenser lens), housed in a filter slide. The red filter had a 650 nm peak and the blue-green, a 500 nm peak. In the filter slide, with the blue-green filter, a neutral density filter (1.2 ND) was added so that the normal

E. Pilotto, MD (✉) • E. Convento
Department of Ophthalmology, University of Padova,
via Giustiniani 2, Padova, 35128, Italy
e-mail: elisabetta.pilotto@unipd.it

upper limit for dark-adapted sensitivity to the blue-green stimulus did not exceed 63 decibels (dB), the maximum number allowable by the HFA's data collection algorithms. At maximum intensity, the energy of the 500 nm stimulus was 2.3 μW and the 650 nm stimulus was 88 μW in the beam incident on the perimeter (target size, 16 mm²). For dark-adapted testing, the two lamps that provide the background of 31.5 abs can be turned off under computer control. The HFA yellow LEDs fixation targets, which are inappropriate for dark-adapted testing, were replaced with red LEDs (640 nm peak), and a control system was installed to allow the examiner to adjust light intensity. An infrared (IR) TV system for continuous monitoring of fixation in light and dark adaptation was built. The IR sources were eight IR LEDs (940 nm peak) affixed behind holes drilled in the hemisphere around the central fixation target. A low-light-level, IR-sensitive TV camera with additional optical elements was mounted at the end of the HFA's telescope. Output of the camera was directed to a small TV monitor attached to the side of the HFA. The foveal threshold was tested using a diamond-shaped array of LEDs below the central fixation target. A dual floppy disc system was available on the HFA. Data analyses were performed on a microcomputer remote from the perimeter [13].

For a more detailed study of scotopic retinal function, fine matrix mapping (FMM) was also used [15, 16]. This technique uses a television screen to present flashes of blue stimuli under scotopic conditions. The size of the stimulus, distance between subjacent stimuli and size of the field tested are controlled by entering the desired parameters into the computer. A red-light-emitting diode attached to the television screen for fixation can be moved, depending on the retinal area of interest. Subsequent processing of the data produces a three-dimensional representation of rod thresholds: The higher the elevation from baseline, the greater the loss of function compared to normal values [15].

In this examination technique, a modified Humphrey field analyser is used. For scotopic FMM measurements, Humphrey size III target blue flashes are presented with the bowl illumination switched off under scotopic condi-

tions. Four red-light-emitting diodes in a small diamond configuration served as the fixation target. Accuracy of fixation is monitored by means of an infrared camera. The data are converted into IBM format files that are merged using custom software to produce a single matrix with a separation between test locations of 1°. The numerical matrix of the luminance sensitivity at each test locations was then used to generate a surface or contour plot showing the size and location of luminance sensitivity gradients across the grid (contour steps, 0.1 log unit). The luminance sensitivity contour plots may be superimposed onto other images, like fundus autofluorescence images obtained with a different system, with custom image-analysis software. Accurate superimposition is achieved by aligning anatomic landmarks, such as the centre of the optic disc and the fovea, with the corresponding perimetric landmarks, such as the centre of the blind spot and fixation. In addition, three-dimensional surface plots are generated. These data are also used to calculate the mean and the maximum threshold elevation from baseline.

The modified HFA became a diffused method to measure scotopic visual function. However this system does not control for fixation errors or poor fixation stability.

Microperimetry is the diagnostic technique which allows to exactly correlate, in real time, the sensitivity threshold of any individual point of the retina with its clinical (biomicroscopic) appearance. It also documents the location and stability of fixation. Microperimetry is a term introduced when scanning laser ophthalmoscope (SLO) allowed, for the first time, to easily and reliably document the above-mentioned morpho-functional correlation [17, 18]. MP-1 microperimeter was the first microperimeter that allowed light-adapted automatic microperimetry testing with modifiable parameters (examination grid, target intensity and fixation shape and intensity). This instrument, whose repeatability and clinical applications are reported in numerous papers, has been recently modified to perform rod threshold measurements. The MP-1 scotopic microperimeter (MP-1S) has new hardware and software capabilities, which are described in the following paragraphs.

5.3 Scotopic Microperimetry

The MP-1S is a modified version of the standard MP-1 and has all MP-1 capabilities. Moreover, it allows the examiner to perform localized rod sensitivity measurements of dark-adapted patients in a darkroom environment (Fig. 5.1).

Therefore, MP-1S operates in two visual function conditions: one optimized for light-adapted eyes in an examination room that has mesopic light conditions (“mesopic use”) and the other optimized for use in dark-adapted eyes in a darkroom environment (“scotopic use”). The control software is specially designed to manage both the mesopic and scotopic configurations of the instrument. For scotopic use, the MP-1S has two new optical filters that extend the dynamic range of the instrument into extremely low light levels, which are required for rod threshold measurements. MP-1S has been optimized for use in a darkroom environment, which is essential for rod sensitivity measurements in dark-adapted subjects. All stray light emissions from the instrument and the control PC are blocked and a red gel filter shield is applied on the display screen of the PC monitor.

MP-1S is equipped with a light shield made of black fabric that is designed to protect the patient from any other accidental exposure to external light sources, which may originate at the operator station. In addition, the joystick device which

is used to trigger the fundus photography procedure is disabled during scotopic examination. This prevents to expose the dark-adapted eye to uneventful bleaching.

5.3.1 Hardware Features

The MP-1S is equipped with a pair of additional filters along the internal optical pathway which modifies background, stimuli and fixation target perception. These filters consist of a 500 nm short-pass filter which prevents rod stimuli from light adapting the subject’s dark-adapted cones during the examination and a neutral density filter to reduce light emission in order to extend the dynamic range of the stimulus down to rod threshold. Both filters are combined for scotopic examination under dark-adapted conditions. Neither of them is in use during mesopic examination under light-adapted conditions. Both filters are held in a sliding holder, which can be easily inserted or removed manually by the examiner. The control software checks the position of the filter holder, preventing improper scotopic test

It is also possible to control the intensity of the internal IR source used for fundus illumination. IR level must be adjusted to the minimum level ensuring a correct patient eye fundus tracking.

Stimuli duration’s range is from 40 to 2,000 ms. The range of the *stimuli intensity* changes from the mesopic to the scotopic examination. In the mesopic modality, previously described filters are not inserted, and the stimuli intensity range is from 4 to 404 asb. In the MP-1S scotopic modality, a filter 2 OD (2 optical density) is inserted in the machine, and the maximum stimuli intensity is 0.8000 asb.

5.3.2 Software Application

All information about the parameters of any individual examination, stimulus presentation and threshold quantification are recorded into a log file. This file is stored side by side with current examination data and is available to the exported in Excel format from the MP-1S main screen.



Fig. 5.1 Microperimeter MP-1S (Nidek, Technologies, Alagnasego, Italy)

The MP-1S also provides a new co-registration software application that spatially aligns MP-1S visual stimulus coordinates with post-processing image data from cSLO retinal imaging systems, including fundus autofluorescence or infrared images. This allows detecting correlations between localized rod and cone sensitivity and local imaging features in the macula. The new software application also allows uploading into the MP-1 software a retinal image, obtained with a specific OCT device, (Heidelberg Spectralis, Germany) where the fovea is marked and highlighted. This option allows to select the stimuli pattern exactly centred on the anatomic fovea.

5.4 Scotopic Microperimetry Test

To obtain reliable data, a 4 mm pupil diameter is recommended in order to achieve ideal image and test quality. Twenty minute dark adaptation is essential for rod sensitivity measurements. All stray light emission from the instrument and the control PC are blocked and a red gel filter shield is applied on the display screen of the PC monitor. Each stimulus consists in the short presentation of a selected luminance test in the LCD background. Light stimuli range from 0 to 20 dB, on a 1 dB step scale: 0 dB represents the instrument's maximum stimulus luminance and 20 dB the minimum stimulus luminance. The stimulus colour is white. The stimulus *size* may be varied according to Goldmann size standards: from I to V (from 6.5 to 104 min/arc). For scotopic automatic perimetry, the Goldmann IV stimulus size is the most commonly used target, because of its higher reliability from a topographic point of view. The presentation time varies from 40 to 200 ms. To accurately investigate scotopic vision, it is very useful (mainly during follow-up examinations) to have the testing grid exactly centred onto the fovea. A spectral domain OCT (Heidelberg Spectralis, Germany) is used to acquire a single horizontal scan in order to acquire a high-quality single scan passing through the fovea. Then, a green vertical cursor is used to identify the centre of the fovea into the horizontal

scan. The printout of this scan is saved in bitmap. The file coming from the SD-OCT is uploaded into the MP-1S software using the "import image" function. The uploaded OCT file is included as a specific record into the MP-1 Exam list. The uploading procedure crops automatically the bitmap file from OCT considering only the area with the infrared OCT image, where the horizontal and the small vertical green lines identifying the centre of the fovea are located. The follow-up function of the MP-1S allows to perform an automatic microperimetry where the centre of the stimuli grid pattern is automatically set and corresponds to the centre of the fovea marked with the OCT procedure (Fig. 5.2).

At the end of the examination, the operator can acquire a colour fundus photograph. This image is then aligned with the IR reference frame, so that functional results (fixation area and sensitivity map) are overlapped automatically onto the colour fundus image (Fig. 5.3). This is advantageous to the clinician who may directly compare functional data with fundus details, particularly compared to previous SLO microperimeter where comparison was possible only with IR (black and white) fundus image. MP-1S software contains, as standard MP-1, an automatic tracking system of eye movements. The standard background used for MP-1S microperimetry is a white background whose background intensity is 0.0080 asb. The software offers different choices for the fixation target: Size and shape may be varied according to the patient's visual acuity and macular functional and anatomical characteristics. The most frequently used fixation target is a circle of 3° in radius. It is possible to activate the "fade-out protection mode" for circle-shaped fixation target during scotopic examination by means of the highlighted control. With this option, the circle dimension changes smoothly in order to keep active the patient fixation during scotopic examination.

According to the clinical situation, several standard psychophysical threshold strategies are available: a 4-2-1 staircase strategy, the most precise (but more time consuming) in psychophysical tests, a 4-2 staircase and a fast strategy. During microperimetry a stimulus is projected

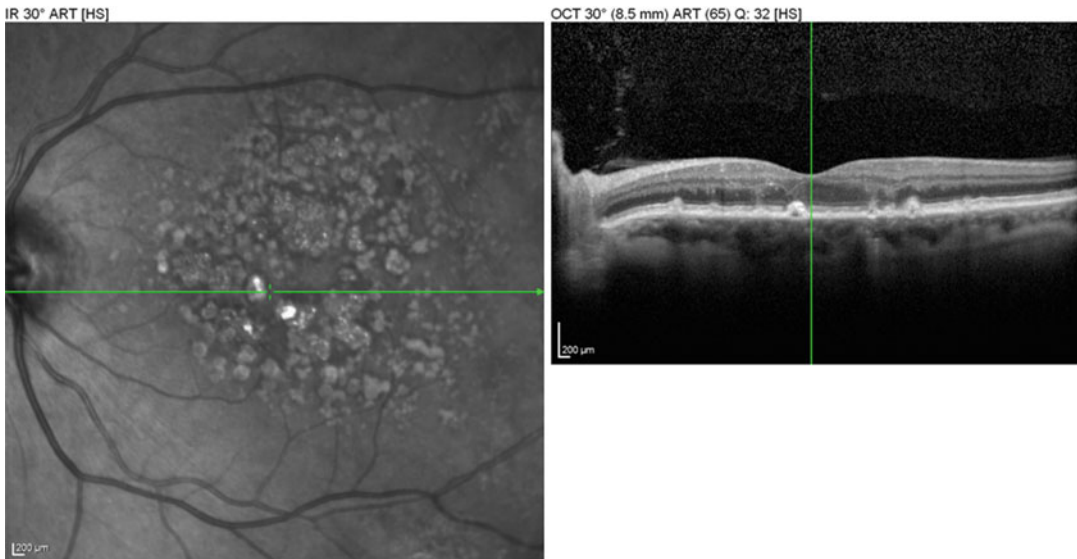


Fig. 5.2 The new software application allows to load into the MP-1 software a retinal image, obtained with a specific OCT device, the Heidelberg Spectralis® OCT, where

the horizontal and the small vertical green lines that identify the foveal point are placed. This option permits to select the stimuli pattern centre on patient's fovea



Fig. 5.3 The colour image obtained with the MP-1S is aligned with the IR reference frame of the OCT image, so that functional results are overlapped automatically onto the colour fundus image centred on the fovea. Fixation target (white circle)

onto the patient's blind spot area at selected intervals (from 20 to 60 s), to check patient reliability during examination. The ideal topographic test grid should allow to detect small scotomas avoiding unnecessary test locations. Therefore,

the choice of the test grid should be carefully considered, preferring short test sessions or individual test settings. On the other side, when performing a prospective clinical trial, the pattern should be selected to collect baseline and follow-up functional information (using an automatic follow-up test) useful to contribute to the main purposes of the study. To quantify retinal differential light threshold, the operator preliminarily chooses a given topographic strategy which may be fully automatic, semi-automatic or manual. Test results are reported in dB or pseudocolours or by interpolated pseudocolour maps. Threshold and fixation data may be reported onto the IR image or more commonly onto the fundus colour photo. The interpolated pseudocolour map may be useful as a general overview or to graphically compare microperimetry with an optical coherence tomography map. The duration of each test depends on the number of stimulated retinal points and selected strategy, starting attenuation of stimuli or pretest activated and patient's characteristics. The pure fixation test aims to evaluate location and stability of fixation. During a fixation examination, the patient is required to look at the fixation target (previously selected) projected on a background

for a given amount of time (typically 30 or 60 s): The horizontal and vertical shifts (relative to a baseline reference frame) of fundus details are recorded by the tracking system, so that fixation positions can be plotted over the reference (static) fundus image. Such analysis provides the time-dependent positions of the virtual centre of patient PRL, compared with the macular anatomic landmarks, and thus provides a quantitative and objective description of fixation characteristics. This analysis is also automatically performed during any microperimetry test, and results are shown at the end of the procedure.

5.5 Scotopic Microperimetry: Test Evaluation

Site and stability of MP-1S fixation, in relation to foveal area, are still under validation. The quantification of fixation characteristics uses the bivariate contour ellipse calculated area (BCEA) [19]. The BCEA is an area which reflects the horizontal and vertical eye positions and is calculated in minutes of arc. This is a 2-dimensional ellipse that describes the portion of retinal surface within the centre of the target imaged at least 68 % of the time. Using any automatic (even customized) static or kinetic test, the operator can perform an automatic follow-up examination during follow-up of any patient. The follow-up examination is topographically performed exactly over the previously retinal tested points, and it is independent of fixation changes, because stimuli projection depends just on stable anatomic landmarks. Moreover, a differential map displays the differential light threshold for static and kinetic tests allowing to monitor disease progression. Mean differential light threshold value and standard deviation in dB are also reported. The increasing role of microperimetry examination in most macular disorders, and the increasing use of old or new morphologic diagnostic tests of the same retinal areas (fluorescein and indocyanine green angiography, fundus autofluorescence and OCT images) oriented toward an integration of all available information. Therefore, it is possible to

import in the MP-1S microperimeter any retinal image of the same eye, performed with any different instrument, and obtain an exact and fully reliable overlapping of threshold sensitivity map and fixation parameters over the original image.

5.6 Scotopic Microperimetry in Normal Subjects

In dark-adapted conditions, a central scotopic scotoma, which corresponds to the foveal rod-free region, is detectable in people with healthy retina. By scotopic microperimetry, normal eyes show a central scotoma of the same size, and fixation is always eccentric compared to the anatomic fovea but stable [23] (Fig. 5.4). This foveal region measures about 0.35 mm and subtends approximately 1.25° [20]. Peak of rod density is reached at approximately 5° eccentricity, so a relative dark-adapted scotoma can be found within the central 10° of retina.

Recently, Crossland et al. performed scotopic microperimetry in health subjects with no retinal disease using a prototype scotopic



Fig. 5.4 In health subjects with no retinal disease, a central dense scotoma is detectable at the scotopic microperimetry. Fixation target (*white circle*)

MP-1 microperimeter [21]. They compared MP-1 scotopic findings with those collected with a modified HFA. The second-generation HFA, which is still commercially available, includes an infrared eye tracker, but a custom chipset is required to override the self-calibration programme [22]. For the purpose of their study, the authors modified the MP-1 microperimeter instrument. The screen luminance was reduced by inserting a 2.0 log unit neutral density filter in the optical path of the LCD monitor on the instrument. Stimuli were limited to blue by placing a 500 nm short-pass filter in the same position, without affecting the imaging system. Stray light was shielded from the observer by placing silk covers over vents on the MP-1 and by draping felt sheets around the chin and forehead of the device. After at least 30 min dark adaptation, perimetry was performed on the MP-1 and HFA. A central scotopic scotoma of at least 1 log unit was identified in all subjects on both tests. Scotopic MP-1 indicated that this scotoma was coincident with the foveal centre in all subjects. However, the point of minimum sensitivity was frequently distant from the centre of the HFA visual field plot, due to the lack of fixation control by this instrument.

5.7 Scotopic Microperimetry in Macular Diseases: Preliminary Data

Recently, we have evaluated retinal threshold, quantified by scotopic microperimetry, in dark-adapted eyes of diabetics without and with early nonproliferative diabetic retinopathy and in normal subjects who served as controls [23]. By scotopic microperimetry, all eyes (all groups) showed a central scotoma (of the same size), and fixation was always eccentric compared to the anatomic fovea but stable. Fixation was always central and stable in mesopic microperimetry (Fig. 5.5). Mesopic microperimetry also showed no statistically significant retinal threshold differences among

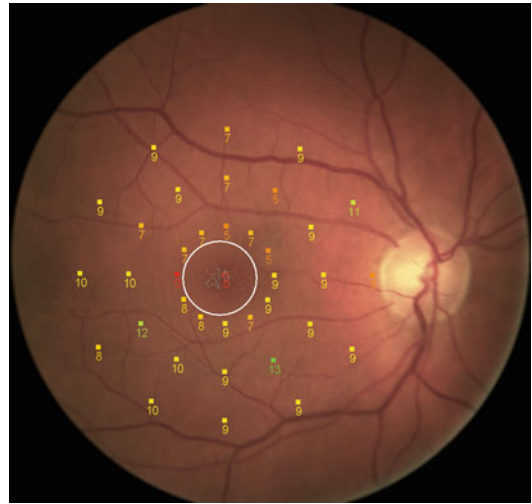


Fig. 5.5 Scotopic microperimetry in a diabetic patient without diabetic retinopathy. A central scotoma is detectable and fixation is eccentric compared to the anatomic fovea but stable. Fixation target (white circle)

groups ($p=0.21$). Diabetic subjects without clinically detectable or with early retinopathy have no signs of threshold changes when quantified by scotopic microperimetry. This study confirms that both rod and cone sensitivity thresholds are not affected in diabetes when no clinically detectable or early retinopathy is present. Otherwise, scotopic microperimetry in patients with early AMD allows to detect that the area of dense scotoma is always wider than in mesopic microperimetry (unpublished preliminary data) (Fig. 5.6). Histopathological studies on human donor retinas with AMD indicate a predilection for parafoveal loss of rod photoreceptors over cones in the early stage of the early non-exudative stage of the disease [10]. Foveal cone loss is not observed in donor retinas until later in AMD progression. Although both rods and cones in the parafovea (within 15° of the visual angle of the fovea) degenerate in AMD, rod loss precedes and is more severe than cone loss in most donor retinas evaluated [12]. In patients with early AMD, scotopic sensitivity reduces more than photopic sensitivity, and the greatest deficit is $2.5\text{--}5.0^\circ$ [24].

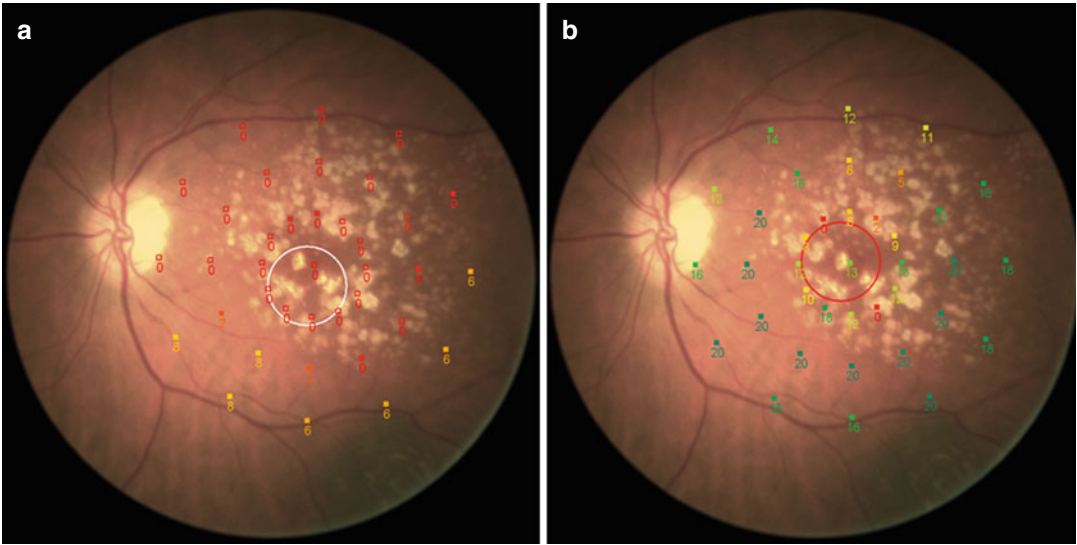


Fig. 5.6 Scotopic (a) and mesopic (b) microperimetries both obtained with the same MP-IS instrument, in a patient with non-exudative age-related macular degenera-

tion. Fixation target (*white and red circle* in scotopic (a) and mesopic (b) microperimetries respectively)

Conclusion

Scotopic microperimetry is a new approach to the psychophysical investigation of the retina. Combining reliable stimulation parameters to strict fixation control, MP-IS checks scotopic retinal threshold at predefined retinal points. The obtained scotopic sensitivity map helps to detect early functional alterations of rod photoreceptors. Scotopic microperimetry is, from a clinical point of view, in its infancy, but the perspectives are encouraging. Not only one of the major acquired retinal disorders, namely, age-related macular degeneration, but also retinal dystrophies and toxic maculopathies are under investigation by this technique.

References

1. Steinmetz RL, Haimovici R, Jubb C et al (1993) Symptomatic abnormalities of dark adaptation in patients with age-related Bruch's membrane change. *Br J Ophthalmol* 77:549–554
2. Owsley C, Jackson GR, White M et al (2001) Delay in rod-mediated dark adaptation in early age-related maculopathy. *Ophthalmology* 108:1196–1202
3. Haimovici R, Owens SL, Fitzke FW, Bird AC (2002) Dark adaptation in age-related macular degeneration: relationship to the fellow eye. *Graefes Arch Clin Exp Ophthalmol* 240:90–95
4. Lorenz B, Gyurus P, Preising M et al (2000) Early-onset severe rod-cone dystrophy in young children with RPE65 mutations. *Invest Ophthalmol Vis Sci* 41:2735–2742
5. Cella W, Greenstein VC, Zeman-Rajang J et al (2009) G1961E mutant allele in the Stargardt disease gene ABCA4 causes bull's eye maculopathy. *Exp Eye Res* 89(1):16–24
6. Arden GB, Carter RM, Hogg CR et al (1983) Rod and cone activity in patients with dominantly inherited retinitis pigmentosa: comparisons between psychophysical and electroretinographic measurements. *Br J Ophthalmol* 67:405–418
7. Schmitz-Valckenber S, Ong EE, Rubin GS et al (2009) Structural and functional changes over time in MacTel patients. *Retina* 29:1314–1320
8. Umino Y, Solessio E (2013) Loss of scotopic contrast sensitivity in the optomotor response of diabetic mice. *Invest Ophthalmol Vis Sci* 54:1536–1543
9. Owsley C, McGwin G, Jackson GR, Kallies K, Clark M (2007) Cone- and rod-mediated dark adaptation impairment in age-related maculopathy. *Am J Ophthalmol* 114:1728–1735
10. Curcio C, Medeiros NE, Millican CL (1996) Photoreceptor loss in age-related macular degeneration. *Invest Ophthalmol Vis Sci* 37:1236–1249
11. Medeiros NE, Curcio C (2001) Preservation of ganglion cell layer neurons in age-related macular degeneration. *Invest Ophthalmol Vis Sci* 42:795–803
12. Curcio CA, Owsley C, Jackson GR (2000) Spare the rods, save the cones in aging and age-related maculopathy. *Invest Ophthalmol Vis Sci* 41:2015–2018

13. Marmor MF, Aguirre G, Arden G et al (1983) Retinitis pigmentosa; a symposium on terminology and methods of examination. *Ophthalmology* 90:126–131
14. Jacobson SG, Voigt WJ, Parel JM et al (1986) Automated light- and dark-adapted perimetry for evaluating retinitis pigmentosa. *Ophthalmology* 93:1604–1611
15. Chen JC, Firzke FW, Pauleikhoff D, Bird AC (1992) Functional loss in age-related Bruch's membrane change with choroidal perfusion defect. *Invest Ophthalmol Vis Sci* 33:334–340
16. Scholl HPN, Bellmann C, Dandekar SS, Bird AC, Fitzke FW (2004) Photopic and scotopic fine matrix mapping of retinal areas of increased fundus autofluorescence in patients with age-related maculopathy. *Invest Ophthalmol Vis Sci* 45:574–583
17. Pilotto E, Midena E (2007) Scanning laser microperimetry. In: Midena E (ed) *Perimetry and the fundus: an introduction to microperimetry*. Slack Incorporated, Thorofare, pp 7–12
18. Midena E, Radin PP, Convento E (2007) Liquid crystal display microperimetry. In: Midena E (ed) *Perimetry and the fundus: an introduction to microperimetry*. Slack Incorporated, Thorofare, pp 15–25
19. Bellmann C, Feely M, Crossland MD, Kabanarou SA, Rubin GS (2004) Fixation stability using central and pericentral fixation targets in patients with age-related macular degeneration. *Ophthalmology* 111:2265–2270
20. Curcio CA, Allen KA (1990) Topography of ganglion cells in human retina. *J Comp Neurol* 300:5–25
21. Crossland MD, Luong VA, Rubin GS, Fitzke FW (2011) Retinal specific measurement of dark-adapted visual function: validation of a modified microperimeter. *BMC Ophthalmol* 11:5
22. Van de Born LI, van Schooneveld MJ, de Jong LA et al (1994) Thr4Lys rhodopsin mutation is associated with autosomal dominant retinitis pigmentosa of the cone-rod type in a small Dutch family. *Ophthalmic Genet* 15:51–60
23. Midena E, Convento E, Casciano M et al (2012) Scotopic microperimetry in diabetes. *Invest Ophthalmol Vis Sci* 53:E-Abstract 2864
24. Chen C, Wu L, Wu D et al (2004) The local cone and rod system function in early age-related macular degeneration. *Doc Ophthalmol* 10:1–8

Edoardo Midena and Elisabetta Pilotto

6.1 Introduction

In retinal and macular diseases, several efforts have been done to correlate morphological findings to functional impairment. The use of microperimetry, an exactly fundus-related psychophysical testing, allows to correlate retinal function to optical coherence tomography (OCT) findings and to the other currently imaging techniques, mainly fundus autofluorescence (FAF), fluorescein and indocyanine green angiography (FA, ICGA). This multimodal, integrated approach is nowadays widely used at baseline and during follow-up in progressing macular diseases.

This chapter introduces the reader to the concept of morpho-functional integrated multimodal diagnostic approach using some simple clinical cases, in which this diagnostic approach has been used to correlate morphologic changes and their functional impairment in patients suffering different retinal diseases. This chapter has no references, except some methodological ones, mainly for one simple reason: because they are reported and discussed in detail in each chapter

E. Midena, MD, PhD, FARVO, FEBO (✉)
Department of Ophthalmology, University of Padova,
via Giustiniani 2, 35128 Padova, Italy

Fondazione G.B. Bietti, IRCCS, Rome, Italy
e-mail: edoardo.midena@unipd.it

E. Pilotto, MD
Department of Ophthalmology, University of Padova,
via Giustiniani 2, 35128 Padova, Italy

of the second part of this volume. The selection of just a few of them was considered by us a use-less limitation.

6.2 An Illustrated Multimodal Imaging Approach

Case 1

A 20-year-old female was referred with a 1-day history of reduced visual acuity in her left eye. This episode was preceded by a 3-day history of flu-like illness. At presentation her best corrected visual acuity was 20/20 in her right eye and 20/40 in her left eye. Fundus examination revealed the presence of yellow-white placoid lesions distributed throughout the posterior pole in both eyes (Fig. 6.1). Fluorescein angiography showed areas corresponding to the placoid lesions of early hypofluorescence which later became hyperfluorescent (Fig. 6.2). Indocyanine green angiography (ICG) showed early areas of hypofluorescence. These areas only partially corresponded with those seen on fluorescein angiography; more widely smaller hypofluorescent areas were detectable on ICG angiography. These hypofluorescent areas remained as such even in the late stages of the ICG angiography (Fig. 6.3) Spectral

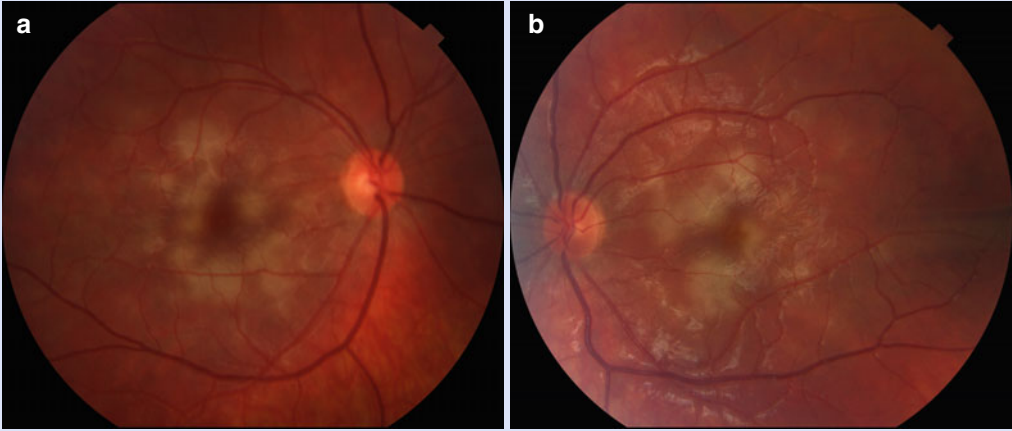


Fig. 6.1 Case 1, colour fundus photographs of the right (a) and left (b) eye of a 20-year-old female with acute posterior multifocal placoid pigment

epitheliopathy (APMPPE) show the presence of yellow-white placoid lesions distributed throughout the posterior pole in both eyes

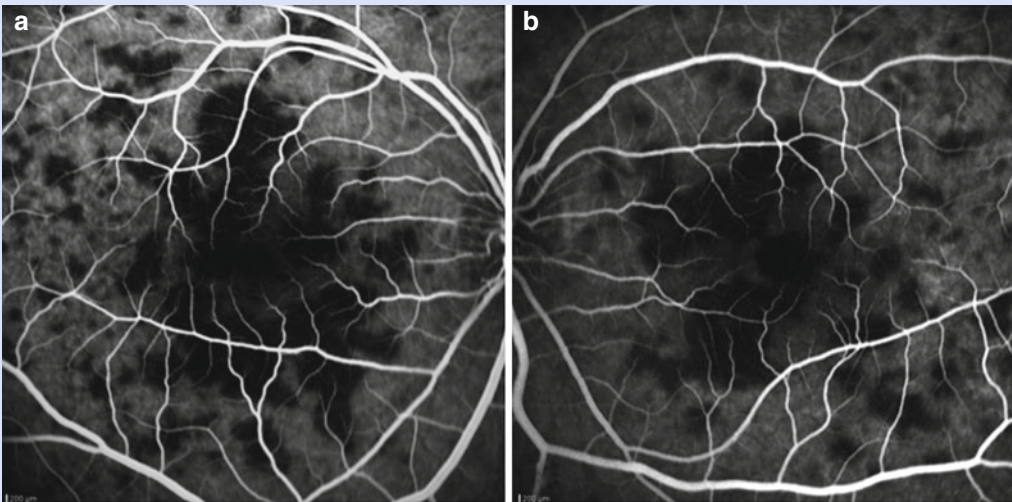


Fig. 6.2 Case 1, early (a, b) and late (c, d) phases of fluorescein angiography images show multiple lesions at the posterior pole

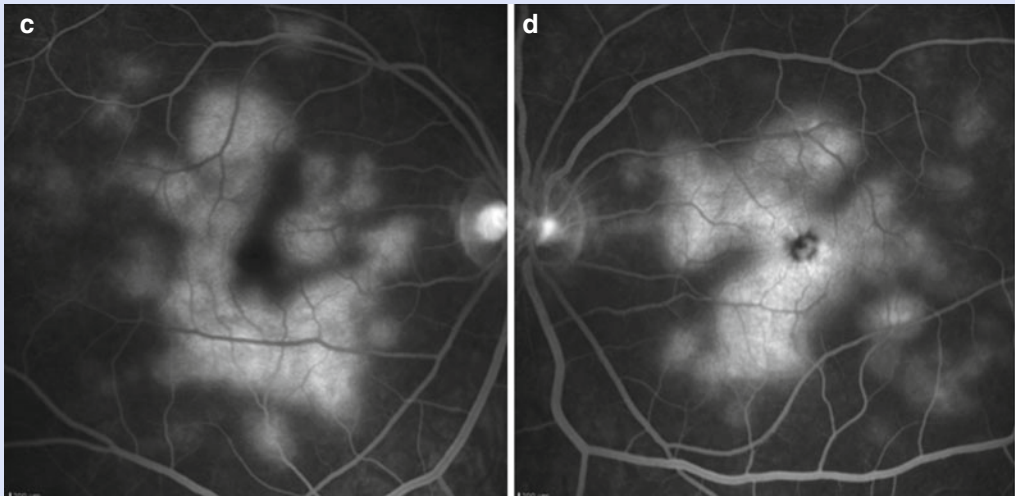


Fig. 6.2 (continued)

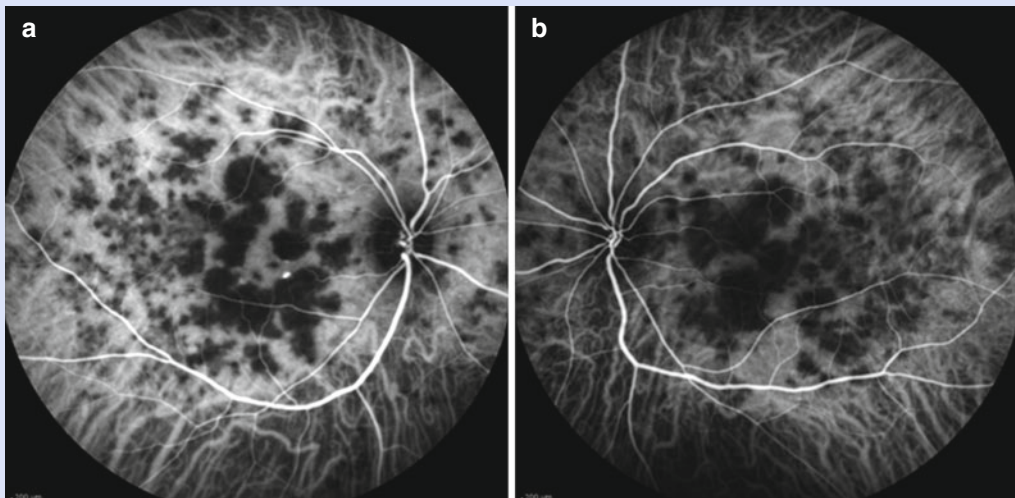


Fig. 6.3 Case 1, early (a, b) and late (c, d) phases of indocyanine green angiography images show multiple hypofluorescent areas at the posterior pole and the middle periphery

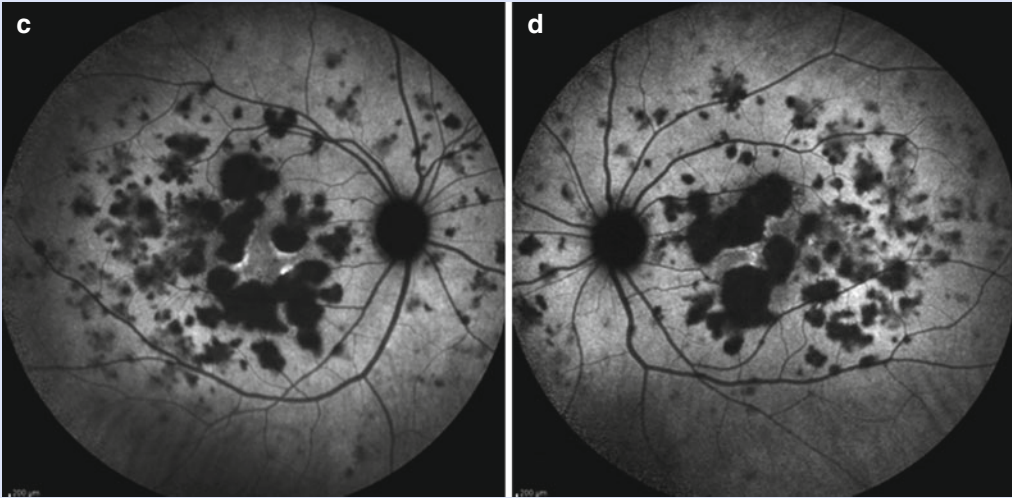


Fig. 6.3 (continued)

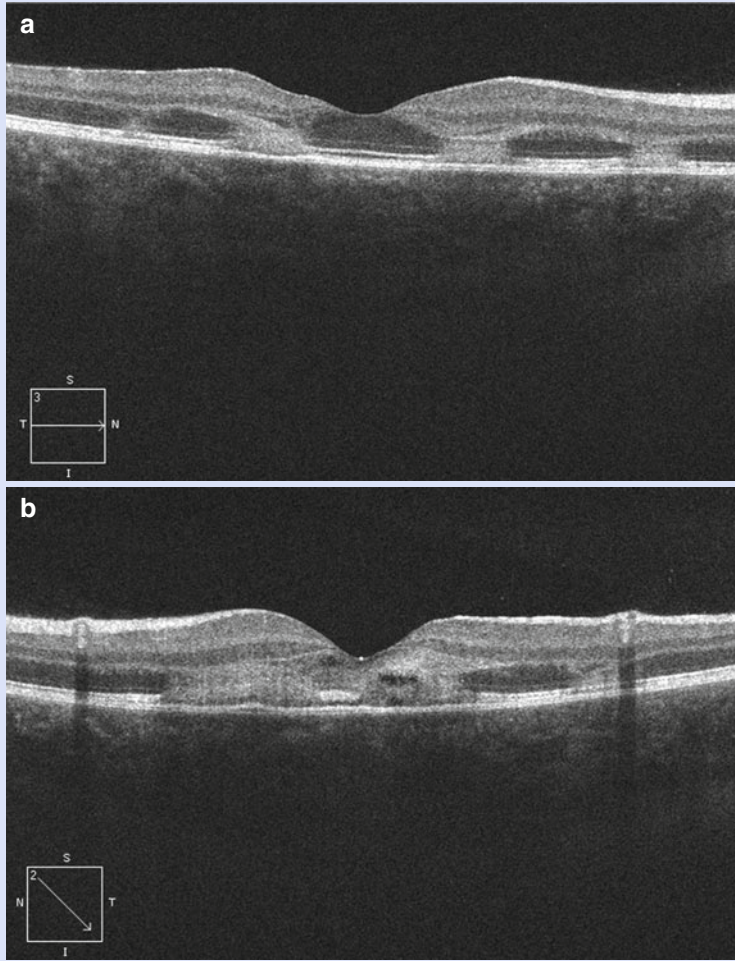
domain optical coherence tomography (SD-OCT) showed hyperreflectance at the level of the outer retinal layers corresponding to the placoid lesions in both eyes and intraretinal cysts in the outer nuclear layer consistent with intraretinal oedema on SD-OCT in the left eye (Fig. 6.4). Based on the results of performed investigations, the diagnosis of acute posterior multifocal placoid pigment epitheliopathy was established.

Acute posterior multifocal placoid pigment epitheliopathy (APMPPE) is characterized by rapid, but transient loss of visual acuity. However, in cases with poor visual acuity, corticosteroids may be beneficial. In this specific case, due to the reduction of visual acuity and foveal oedema of the left eye, general corticosteroids were administered with fast visual acuity improvement. Three weeks later, her visual acuity improved to 20/20 in the left eye, with resolution of the placoid lesions in both eyes. However, areas of retinal pigment epithelium (RPE) changes were detectable at the macula, characterized by RPE clumping in

both eyes. At this time microperimetry was performed to investigate macular sensitivity. A semiautomatic strategy was used to quantify the differential retinal light threshold. Mean retinal sensitivity was slightly reduced in both eyes. Moreover, some relative scotomas were detectable, particularly in those areas characterized by RPE changes (Fig. 6.5). Microperimetry map was overlapped to fluorescein and ICG angiography images performed at presentation in an attempt to correlate the angiographic findings and microperimetric changes detected after resolution. In the overlapped images, microperimetry detected that relative scotomas developed where ICG hypofluorescent areas were particularly confluent in the acute phase of the disease (Fig. 6.6).

This case underlines that a multimodal integrated imaging modality, which correlates morphological to functional changes, could be useful to identify APMPPE cases in which therapy might be beneficial to prevent macular sensitivity deterioration.

Fig. 6.4 Case 1, spectral domain optical coherence tomography of the right (a) and left eye (b) hyperreflectance at the level of the outer retinal layers corresponding to the placoid lesions in both eyes



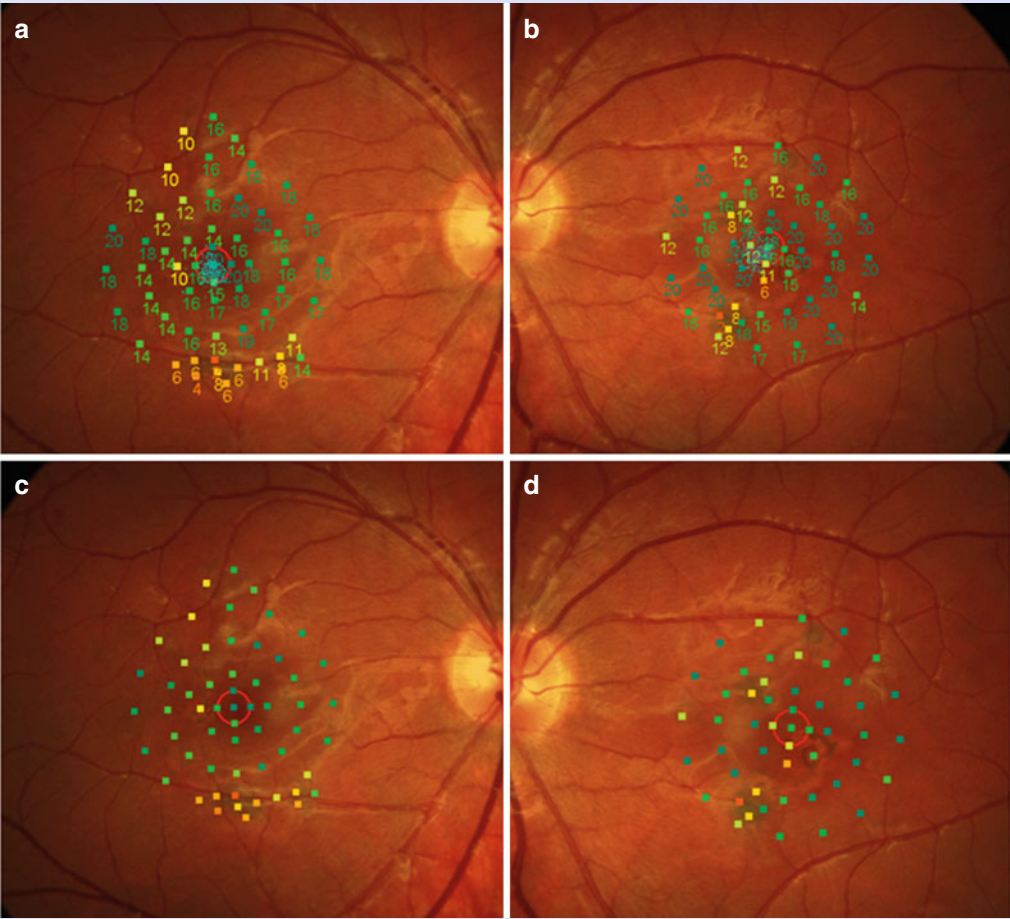


Fig. 6.5 Case 1, microperimetry sensitivity maps of both eyes: test results are reported in dB (a, b) and in pseudocolour (c, d). (Coloured boxes correspond to

different retinal sensitivity: for usual (green) to full scotoma (red); numbers correspond to retinal threshold, in dB)

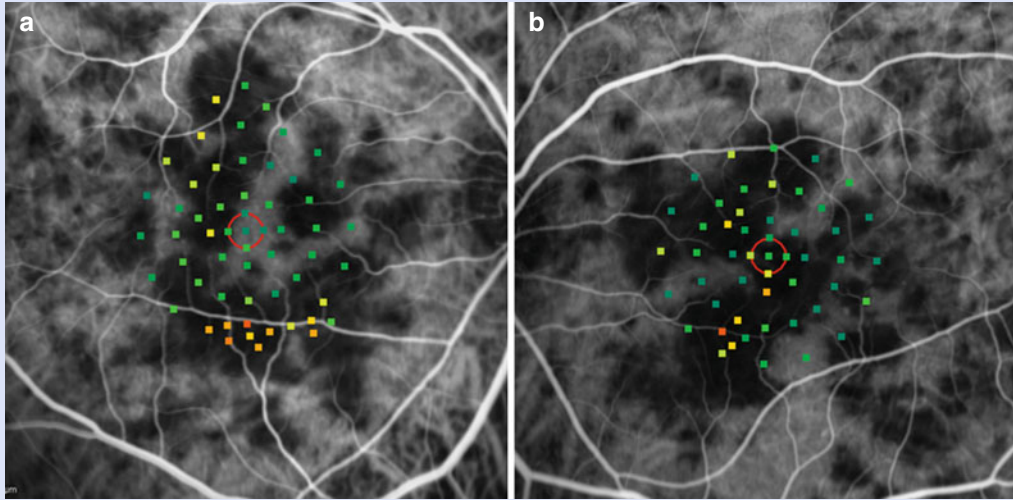


Fig. 6.6 Case 1, MPI sensitivity map was overlapped to early phase ICG angiography images performed at presentation in an attempt to correlate the angiographic findings and microperimetric changes after resolution

(a, right eye; b, left eye). In overlapped images, microperimetry detected that relative scotomas were present where ICG hypofluorescent areas were particularly confluent in the acute phase of the disease

Case 2

A 73-year-old woman had exudative age-related macular degeneration in the right eye evolved to disciform scar and progressive geographic atrophy (GA) in the fellow eye. Her best corrected visual acuity in the left eye was 20/40. On fundus photography atrophic areas appeared as sharply hypopigmented demarcated areas with enhanced visualization of deep choroidal vessels (Fig. 6.7a). Microperimetry was performed to assess retinal fixation and macular sensitivity. The sensitivity map detected that the dense scotoma area did not exactly correspond in spatial extent to the fundus colour photography atrophic area (Fig. 6.7b). Retinal fixation was central and stable and corresponded to an area with atrophic changes at fundus photography (Fig. 6.7a).

Short-wavelength FAF (SW-FAF, excitation 488 nm, emission >500 nm) and near-infrared FAF (NIR-FAF, excitation 787 nm, emission >800 nm) were performed. SW-FAF and NIR-SW-FAF images were overlapped to fixation and sensitivity data, obtained

with microperimetry. At SW-FAF overlapped image, retinal fixation corresponded to a hypo-autofluorescent (hypo-FAF) area, whose retinal threshold was characterized by a relative dense scotoma (6 dB) (Fig. 6.8a). Otherwise, at NIR-FAF overlapped image retinal fixation corresponded to a normal autofluorescent area (Fig. 6.8b). SW-FAF is an imaging method that allows topographic mapping of lipofuscin distribution in the retinal pigment epithelium (RPE) in vivo. Because of the absence of RPE lipofuscin, atrophic areas in GA show a severely reduced FAF signal at the site of atrophic areas appearing markedly hypo-FAF. The hypofluorescent areas are reported to exactly correspond to dense scotoma, as frequently documented by microperimetry. However, the central macula is particularly dark due to the absorption of the blue excitation light by lutein. Therefore, with SW-FAF, it may be sometimes difficult to distinguish between normal hypo-FAF and atrophic areas. NIR-FAF has been introduced to visualize fluorophores different from lipofuscin.

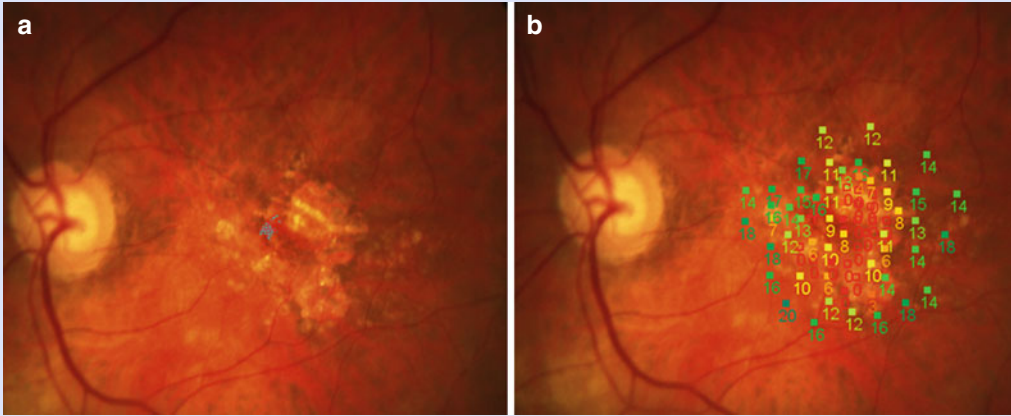


Fig. 6.7 Case 2, microperimetric retinal fixation (a) and sensitivity map (b) in a 73-year-old woman affected by geographic atrophy due to age-related

macular degeneration. Fixation is central and stable. Dense scotoma appeared as empty little *red squares*

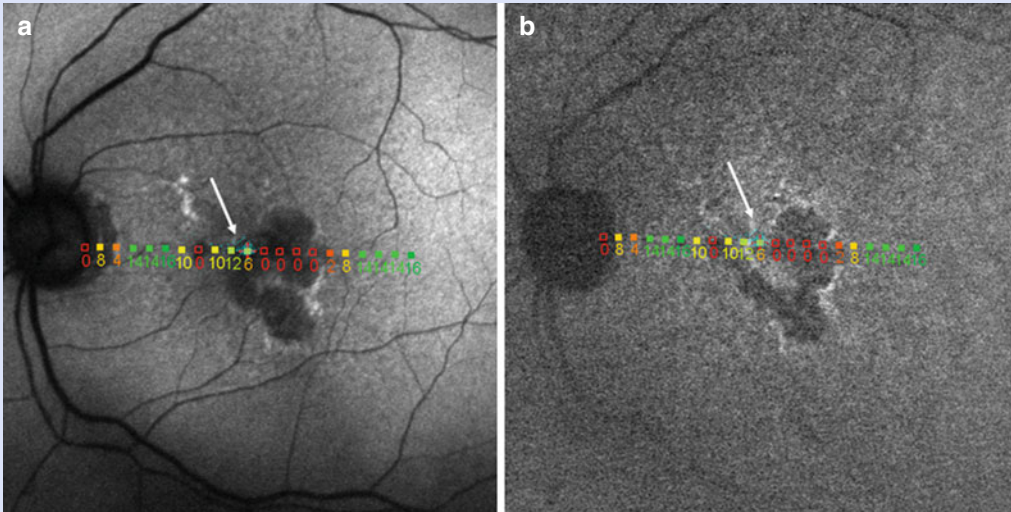


Fig. 6.8 Case 2, Short-wavelength and near-infrared fundus autofluorescence (FAF) images with overlapped sensitivity linear map. (a) Site of fixation appears to be located in hypofluorescent-FAF area (*white arrow*) on

short-wavelength-FAF. (b) This site has normal NIR-FAF (*white arrow*) and shows persisting retinal sensitivity (6 dB)

Therefore, NIR-FAF is useful to topographically map the melanin distribution in RPE in vivo. Using this imaging modality the foveal area appears normally hyper-FAF due to the physiological presence of melanin, and GA area appears markedly hypo-FAF because of the absence of RPE melanin. Therefore, both foveal areas of GA and foveal sparing may be easily visualized and quantified using NIR-FAF than SW-FAF. In this specific case, the site of retinal fixation was characterized by

a relative scotoma at microperimetry. At this retinal site the photoreceptor layer was still present as detected by means of a SD-OCT central scanned line. However, the fovea was surrounded by areas of retinal and RPE atrophy (Fig. 6.9). The use of many combined and overlapped tests allowed to better analyse the impact of individual morphologic alterations on macular function, and revealed the exact role of any individual morphologic imaging technique.

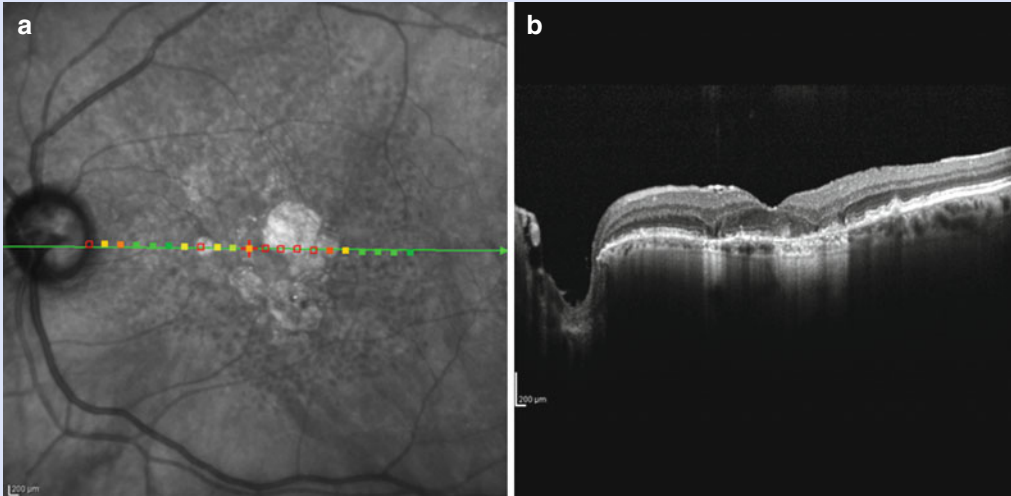


Fig. 6.9 Case 2, infrared SD-OCT image and SD-OCT linear scan. The *green line* represents the OCT scanned line where corresponding retinal sensitivity is shown by coloured squared (*green*; normal, *red* and *yellow*; relative scotoma, *empty red squares*;

dense scotoma). In the foveal area, site of fixation (*small red cross*), the photoreceptor layer is normally represented but is surrounded by atrophy of the retinal pigment epithelium and of the outer photoreceptors layers

Case 3

A 70-year-old man was referred with acute transient horizontal scotoma in the paracentral field of vision of the right eye. Six months earlier, he complained a 24-h episode of visual field constriction. The patient referred that at that time both ophthalmological and neurological examinations were negative. Visual acuity was 20/20 in both eyes. Fundus examination was normal except for diffuse narrowing of the retinal vessels in both eyes (Fig. 6.10). An automatic static perimetry was performed; a slight decrease of central retinal sensitivity was detected (Fig. 6.11). A dynamic fluorescein and indocyanine green angiography was performed. At dynamic fluorescein angiography, a localized delay of the filling of a branch of the central retinal artery could be detected in the early and laminar phases of the angiogram, no more visible in the later ones (Fig. 6.12a, b). At dynamic indocyanine angiography a normal

choroidal filling was documented (Fig. 6.12c). Otherwise, in the late ICG angiography phase an irregular mild hypofluorescent area was visible at the macula (Fig. 6.12d). A semiautomatic microperimetric strategy was performed to investigate retinal threshold (Fig. 6.13a). The sensitivity map, overlapped to the laminar phase of the fluorescein angiography, revealed an area in which retinal sensitivity was significantly reduced in the superior macular field. This area corresponded, in its spatial extent, to the retinal area perfused by the branch retinal vessel whose filling was delayed (Fig. 6.13b). The OCT scanned line performed at this level confirmed the ischaemic retinal damage, showing thinning of the inner retinal layers (Fig. 6.13c).

In this case the multimodal imaging approach allowed to correlate exactly haemodynamic retinal changes to functional visual field sequelae.

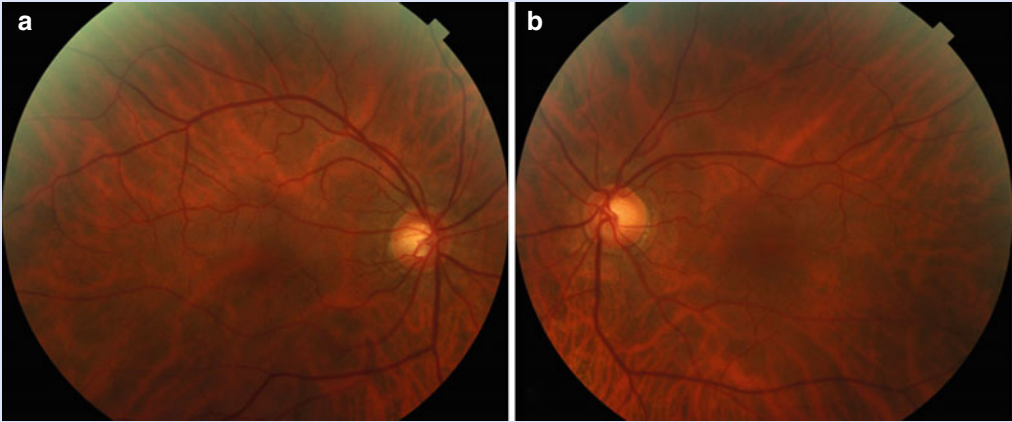


Fig. 6.10 Case 3, colour fundus photographs of the right (a) and left (b) eye of a 70-year-old man with acute transient horizontal scotoma in the paracentral field of vision of the right eye. The fundus examination appeared normal

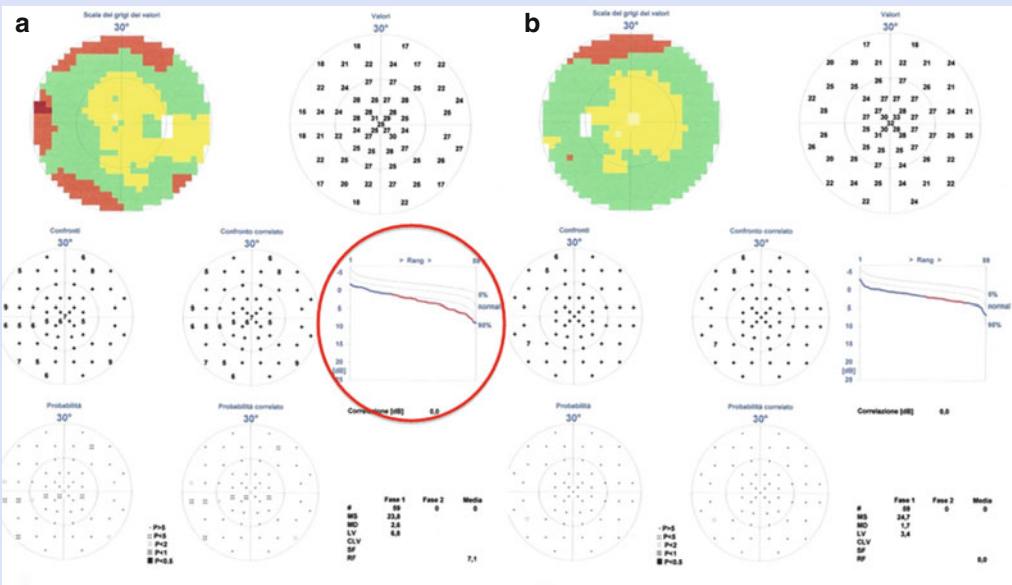


Fig. 6.11 Case 3, automatic static perimetry of both eyes. A slight decrease of central retinal sensitivity was detected in the right eye (a), left eye is unusual (b)

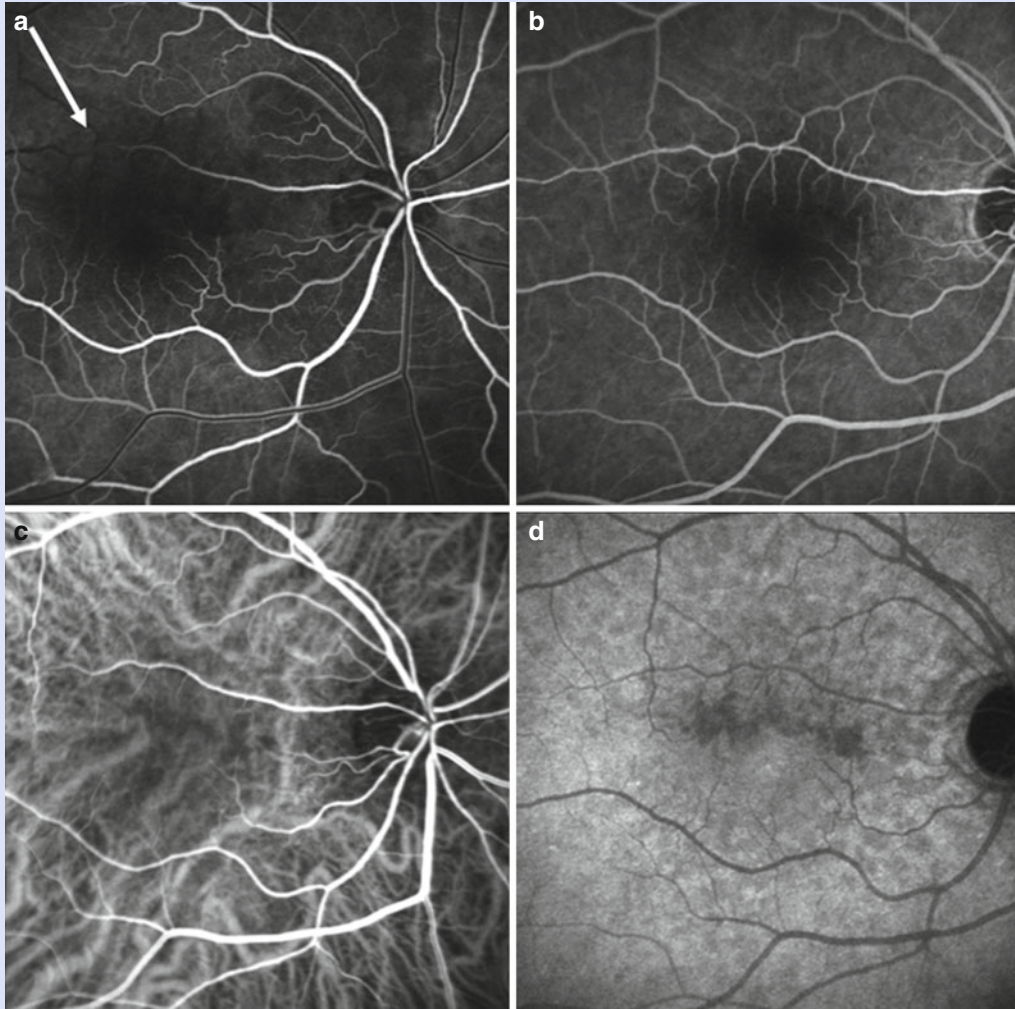


Fig. 6.12 Case 3, fluorescein (a, b) and indocyanine green angiography (c, d) of the right eye. A localized delay of the filling of a branch of the central retinal

artery can be detected in the laminar phase of the fluorescein angiogram (*white arrow*)

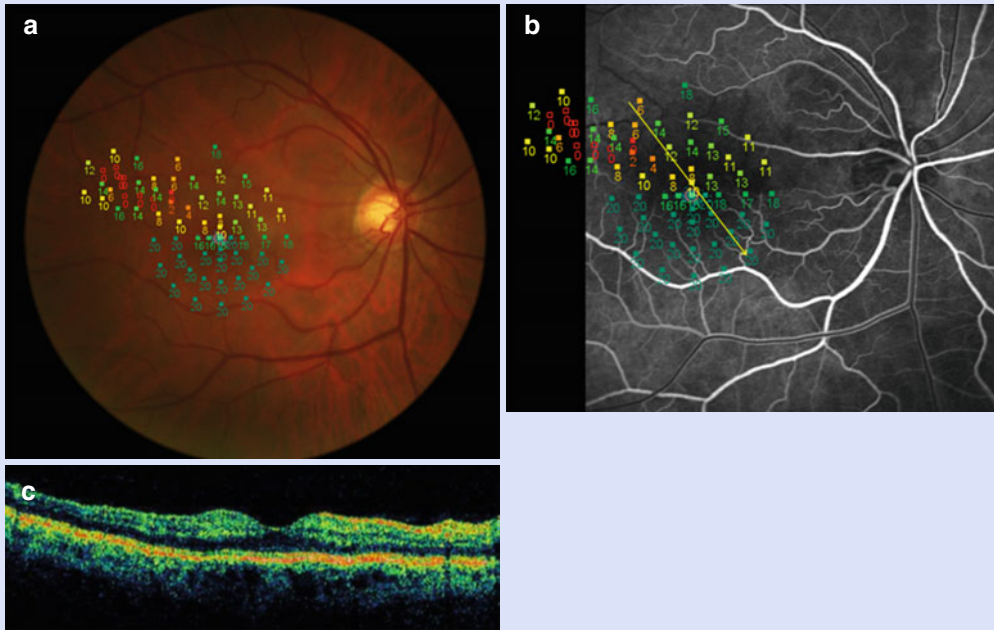


Fig. 6.13 Case 3, the microperimetric macular map (a) was overlapped to the early phase fluorescein angiography image (b). The haemodynamic retinal changes correlate in its spatial extent to the retinal sensitivity

reduction. The OCT scanned line performed at this level (yellow arrow) showed the thinning of the inner retinal layers in this area (c)

Case 4

A 28-year-old man was referred with a 15 days history of a sudden small paracentral scotoma superior to fixation in the field of his right eye. This episode was preceded by a few days history of a flu-like illness. At presentation the best corrected visual acuity was 20/20 in both eyes; however metamorphopsia was complained in the affected eye. At fundus examination, a reddish-brown wedge-shaped flat juxtafoveal lesion was detectable (Fig. 6.14a). Confocal scanning laser ophthalmoscopic (cSLO) infrared imaging showed a hyporeflective irregular area in the macular region, corresponding to the fundus lesion (Fig. 6.14b). cSLO SW-FAF and NIR-FAF imaging appeared normal (Fig. 6.15). The SD-OCT showed hyper-reflective lesions located in the outer nuclear layer and broadening of the inner segment/outer segment junction line. Retinal pigment epithelium and the

choroidal layers appeared normal (Fig. 6.16). Microperimetry detected a juxtafoveal area of relatively dense scotoma (Fig. 6.17). The macular sensitivity map was overlapped to the cSLO-infrared image, showing the spatial correspondence of the relative dense scotoma to the cSLO-infrared hyporeflective irregular area (Fig. 6.18). The diagnosis of acute macular neuroretinopathy was established.

Acute macular neuroretinopathy (AMN) is a rare disease of unknown aetiology. The advent of cSLO imaging has facilitated the identification of the retinal abnormalities. SD-OCT has become an essential diagnostic tool to clarify that the retinal lesions are localized in the outer retinal layers and not in the inner ones. The photoreceptor involvement has functional correlates, which are undetected by visual acuity quantification, but clearly quantified at both baseline and follow-up investigations with microperimetry.

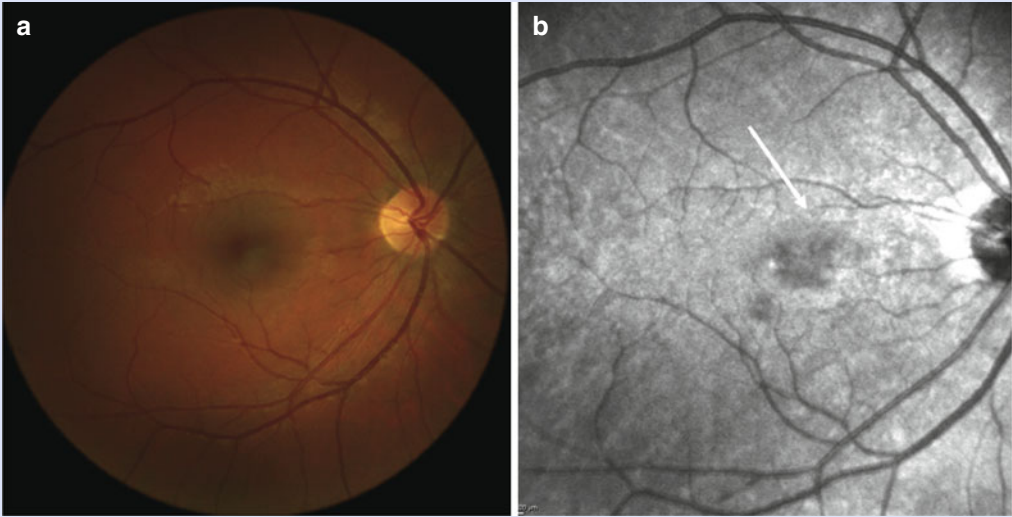


Fig. 6.14 Case 4, colour fundus photograph of the right eye (a) of a 28-year-old man with acute macular neuroretinopathy showed the presence of a reddish-

brown wedge-shaped flat juxtafoveal lesion, which appear hyporefective at the cSLO-infrared imaging (b, arrow)

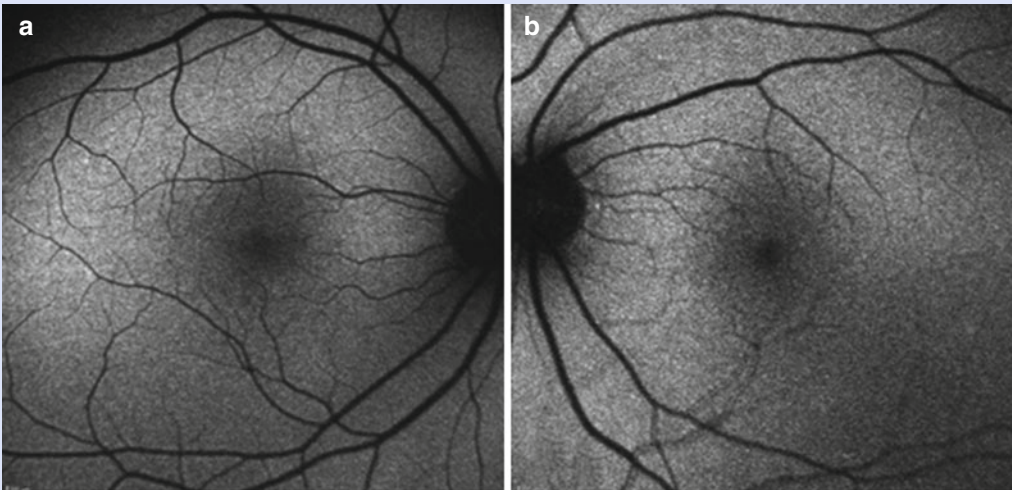


Fig. 6.15 Case 4, SW-FAF and NIR-FAF images of the right and left eyes show normal autofluorescence of the macula

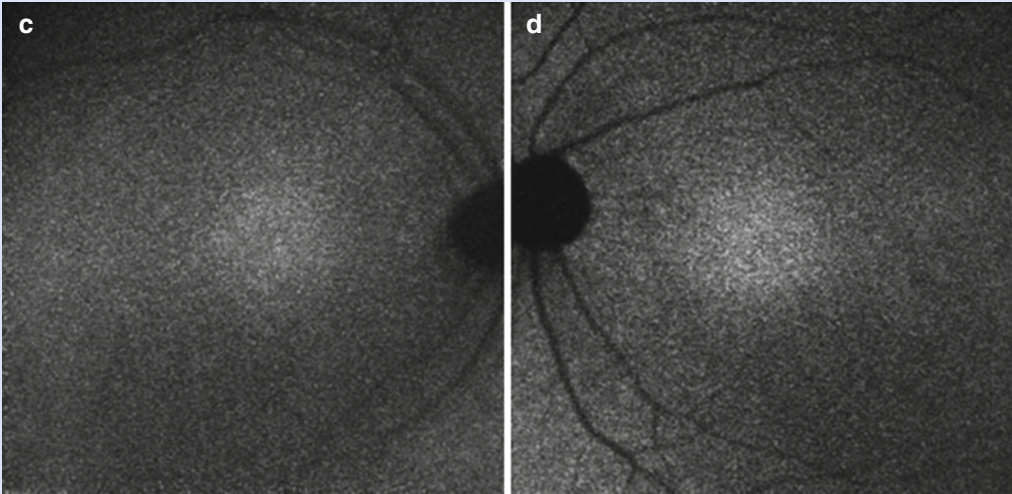


Fig. 6.15 (continued)

Fig. 6.16 Case 4, SD-OCT show hyper-reflective lesions located in the outer nuclear layer and broadening of the inner segment/outer segment junction line, whereas retinal pigment epithelium and choroidal layer, seem normal

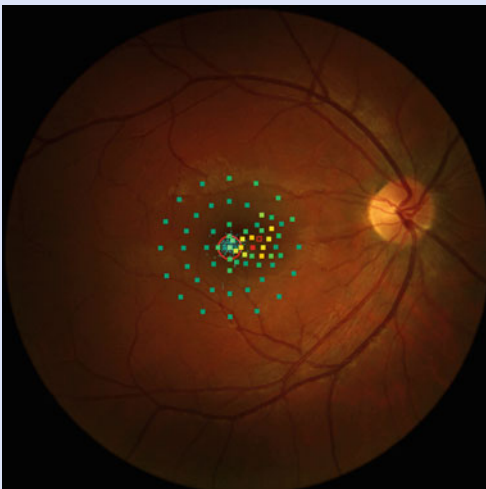
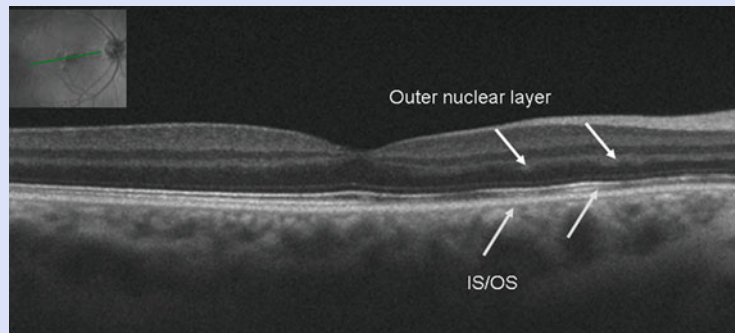


Fig. 6.17 Case 4, microperimetry sensitivity map show a juxtafoveal relative dense scotoma (yellow and red little squares)

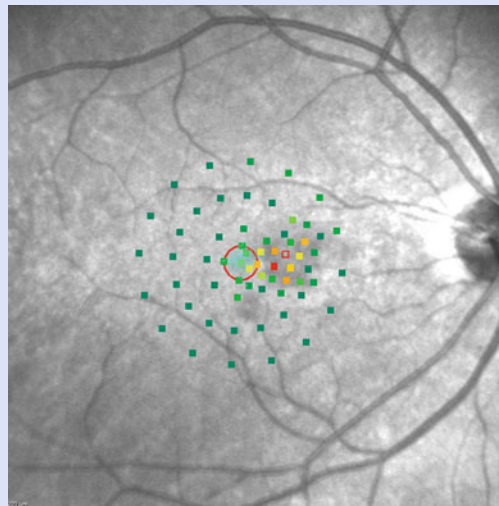


Fig. 6.18 Case 4, the sensitivity map was overlapped to the cSLO-infrared image. The relative scotoma spatially corresponded to the hyper-reflective infrared lesion (green; normal, red and yellow; relative scotoma, empty red squares; dense scotoma)

Conclusion

Many recent investigations about clinical changes due to primary or secondary retinal disorders underline the importance of combining in a precise way all information obtained by different diagnostic tests. These informations need not only to be analysed in detail, but directly overlapped to distinguish the different components of the individual disorder. The functional correlate is becoming essential to judge the effects of any therapy, even those which may seem initially very useful, but then reveals to have a dramatic negative functional impact. Therefore, the multimodal retinal imaging approach allows to systematically correlate retinal morphologic changes with their functional side in patients with different primary retinal and sometimes secondary retinal disorders. The chapters of Part II are devoted to specific disorders where the combination of morphological and functional data, the multimodal approach, is precisely defined

and highlighted, showing that the results obtained by this approach have not only dramatically modified some previous pathophysiologic interpretations, but also contributed to better understand any individual disorder and evaluate the impact of various treatments.

Bibliography

- Anderson PW (1972) More is different. *Science* 177:393–396
- Borell M (1993) Training the senses, training the mind. In: Bynum WF, Porter R (eds) *Medicine and the five senses*. Cambridge University Press, Cambridge, UK, pp 244–261
- Finger S (1994) *Origins of neuroscience*. Oxford University Press, Oxford, pp 65–95
- Galilei G (1606) *Le operazioni del compasso geometrico e militare*. Paolo Fiambotto, Padova
- Morgan M (2003) *The space between our ears*. Oxford University Press, Oxford
- Polyak SL (1941) *The retina*. University of Chicago Press, Chicago

Part II

Clinical Applications of Microperimetry and Multimodal Retinal Imaging

Julia-Sophie Kroisamer, Bianca S. Gerendas,
and Ursula Schmidt-Erfurth

7.1 Introduction

Age-related macular degeneration (AMD) is still the leading cause of blindness in people over 50 years of age in industrialized countries. According to estimates from the World Health Organization (WHO), AMD is responsible for 8.7 % of all blindness worldwide [1]. In the European population the estimated prevalence of late AMD is 1.4 % at 70 years of age, increasing exponentially with age and rising to 20 % at the age of 90 years [2]. As a result of the world's aging population, AMD will become even more important in the future, not only influencing patient's quality of life but also posing an enormous challenge for our health-care systems.

A basic clinical classification system for AMD was recently introduced by an expert group to overcome communication problems among eye specialists worldwide and facilitate evaluation

of therapeutic approaches. The classification, which is based on fundus lesions assessed within 2-disc diameters of the fovea, is as follows:

- *No apparent aging changes*: no visible drusen or AMD pigmentary abnormalities
- *Normal aging changes*: only drupelets (small drusen $\leq 63 \mu\text{m}$), no AMD pigmentary abnormalities
- *Early AMD*: medium drusen (>63 and $\leq 125 \mu\text{m}$), no AMD pigmentary abnormalities
- *Intermediate AMD*: large drusen ($>125 \mu\text{m}$) and/or any AMD pigmentary abnormalities
- *Late AMD*: neovascular AMD and/or any geographic atrophy

Eyes with at least medium drusen ($63\text{--}125 \mu\text{m}$) showed evidence of increasing risk of AMD progression in the Age-Related Eye Disease Study (AREDS) population; therefore this classification seems also to be useful for predicting AMD risk [3].

AMD is a complex disease caused by an interaction of environmental factors and genetic susceptibility. Risk factors, i.e., age, race, hyperopia, cardiovascular disease, smoking, or hypertension, were described long ago. During the last few years, the genetic architecture associated with AMD has become a major issue. For example, variants of the complement factor H (CFH), the age-related maculopathy susceptibility 2 loci (ARMS2), or apolipoprotein E polymorphisms are confirmed to play a role, even in early forms of AMD [4].

J.-S. Kroisamer • B.S. Gerendas
U. Schmidt-Erfurth, MD (✉)
Department of Ophthalmology,
Vienna Reading Center,
Medical University of Vienna,
Waehringer Guertel 18-20, 1090 Vienna, Austria
e-mail: ursula.schmidt-erfurth@meduniwien.ac.at

7.2 Therapeutic Options

Whereas there are various therapeutic concepts for neovascular AMD, headed by agents targeting vascular endothelial growth factor (VEGF) [5], only limited therapeutics are currently available for intervention in the early stages of AMD to prevent progression and significant loss of vision.

The effect of dietary supplements with high-dose vitamins and minerals (especially β -carotene, vitamin C, vitamin E, and zinc) has been evaluated in various studies. The Age-Related Eye Disease Study (AREDS), for example, demonstrated the benefit of these antioxidant supplements for slowing AMD progression, albeit providing no evidence for prevention of the disease or delaying its onset [6, 7]. Although side effects (gastrointestinal symptoms, lung cancer in smokers, heart failure, prostate cancer, etc.) have been described in the literature [6, 8, 9], recommending supplements containing the AREDS formulation for patients with early and intermediate AMD still seems reasonable.

Food frequency questionnaires indicate that supplements of omega-3 long-chain polyunsaturated fatty acids and the xanthophylls which compose macular pigment (lutein and zeaxanthin) protect against the progression of AMD [10]. Studies indicate that macular pigment density is reduced in patients with AMD and that supplementation with lutein and zeaxanthin increases macular pigment and might prevent the progression of AMD [11, 12]. The AREDS 2 study is currently evaluating the effect of omega-3 fatty acids and lutein plus zeaxanthin in reducing the risk of developing advanced AMD [13].

Randomized trials have suggested a protective effect of aspirin; however, these findings were statistically nonsignificant [14]. Studies have yielded inconsistent findings concerning the benefit of patients taking statins [15, 16].

Functional, morphological, and genetic studies over the last decade have helped us to understand the pathophysiologic features leading to AMD, a crucial step for developing new therapeutic agents for prevention and early intervention. Unfortunately, results regarding the effectiveness of complement or inflammasome-targeting

components, interference with the light cycle in photoreceptors, or neuroprotective agents like the ciliary neurotrophic factor are still today only limited [17].

7.3 Multimodal Imaging and Functional Testing

The introduction of optical coherence tomography (OCT) into ophthalmology in 1991 and its enhancements has definitely been one of the most important developments in ophthalmologic imaging, influencing the clinical routine of monitoring patients in a tremendous way and providing some of the major outcome values for most studies concerning the living human retina today. OCT is a noncontact, noninvasive imaging modality providing high resolution, cross-sectional 3D images of a tissue. Due to motion artifacts the evaluation of the retinal pigment epithelium (RPE) was often difficult using time-domain OCT (TD-OCT). However, current technologies (spectral-domain OCT (SD-OCT) or Fourier-domain OCT (FD-OCT)) provide a high acquisition speed, resulting in fewer eye motion artifacts, and additional features such as averaging of scans, real-time tracking, and 3D visualization are available to improve scan quality [18].

Drusen, one of the hallmarks of AMD, is defined as deposits of extracellular debris between the retinal pigment epithelium (RPE) and Bruch's membrane. They appear in OCT as elevations of the RPE, visible as a highly reflective band, with variable internal reflectivity caused by the different composition of the underlying material. A disruption of the inner-outer segment (IS-OS) junction of the photoreceptors, irregularity of the external limiting membrane (ELM), or thinning of the outer nuclear layer can also be observed in the drusen area [19]. Furthermore, other drusen types like "reticular pseudodrusen" (also called "subretinal drusenoid deposits") or "basal laminar drusen" (also called "cuticular drusen") can, with the help of OCT, easily be distinguished from "typical" AMD drusen. Besides efforts to describe the morphological features of drusen qualitatively, various

algorithms to analyze the drusen area automatically have been introduced and evaluated for repeatability in the last years [20–22]. Changes in the RPE caused by AMD (hypertrophy, proliferation, migration, etc.) can also be visualized with OCT, mainly as an increased or decreased reflectivity of the structure itself or the underlying tissue (shadowing effect) [19].

AMD is never evaluated by a single modality but always with a multimodal imaging procedure. Color fundus photography (CF), fundus autofluorescence (FAF), near-infrared reflectance (NIR), near-infrared autofluorescence (NIA), fluorescein angiography (FA), and indocyanine green angiography (ICGA) are often used to complete information acquired with OCT.

Color fundus photography has been used in many studies, including AREDS, to evaluate drusen in AMD. However, the detection of small drusen or RPE irregularities (including small areas of geographic atrophy) is often difficult, especially when image quality is low due to opacity of the ocular media. Although typical characteristics can be seen in fundus photography, differentiating between drusen types without 3D information is challenging: “Typical” AMD drusen are yellow-white and their center may appear lighter than their edges (Fig. 7.1). Cuticular drusen are usually smaller than typical AMD drusen and

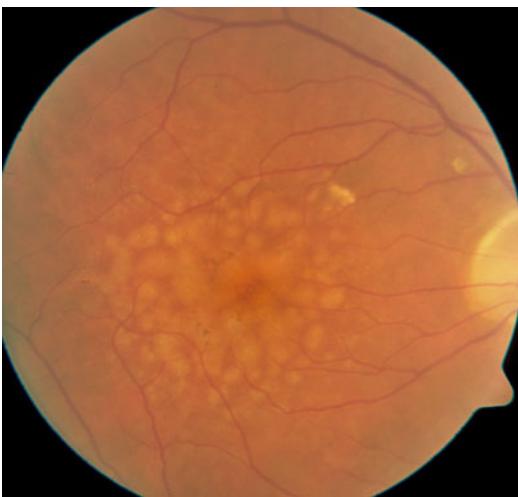


Fig. 7.1 Color fundus photography of a 73-year-old patient with large, confluent drusen, and RPE irregularities (Image provided by Ferdinand Schlanitz, MD)

round and densely packed (starry sky appearance). Subretinal drusenoid deposits appear whiter than typical AMD drusen and are sometimes almost blue [23]. Fundus autofluorescence, generated by RPE lipofuscin, used to play an important role in the evaluation of geographic atrophy and can detect even small satellites of atrophy (Fig. 7.2). However, modern OCT techniques are probably more precise to determine foveal involvement [24]. Near-infrared fundus autofluorescence, a relatively new method, derives from melanin and can visualize subretinal pathologies. Fluorescein and indocyanine green angiography are essential for detecting and differentiating neovascular AMD. Drusen can cause either an increase or decrease in the signal resulting from these imaging devices, mainly caused by irregularities of the retinal pigment epithelium [25].

Besides other functional tests (like contrast sensitivity testing, reading speed and ability, or Amsler charts), best-corrected visual acuity (BCVA) is still of major value in monitoring the macular function of patients with AMD in clinical practice and study settings. However, BCVA

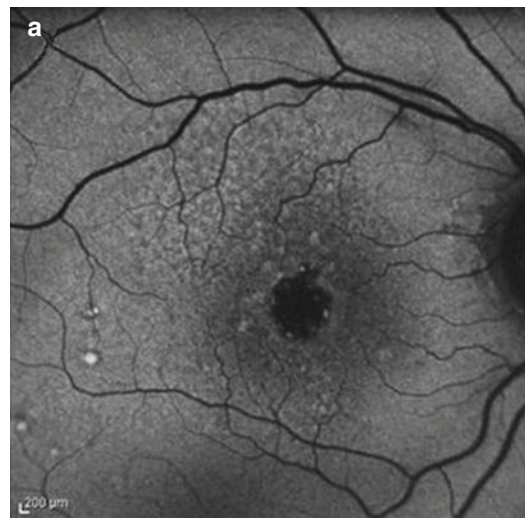


Fig. 7.2 (a) Fundus autofluorescence of a 71-year-old patient with central geographic atrophy surrounded by drusen. (b) Central SD-OCT B-scan of the same patient confirming central geographic atrophy. Drusen, RPE, and IS-OS line irregularities are visible. The green box represents the total area scanned by OCT. The green arrow indicates the position of the scan displayed at the right side (Image provided by Ramzi G. Sayegh, MD)

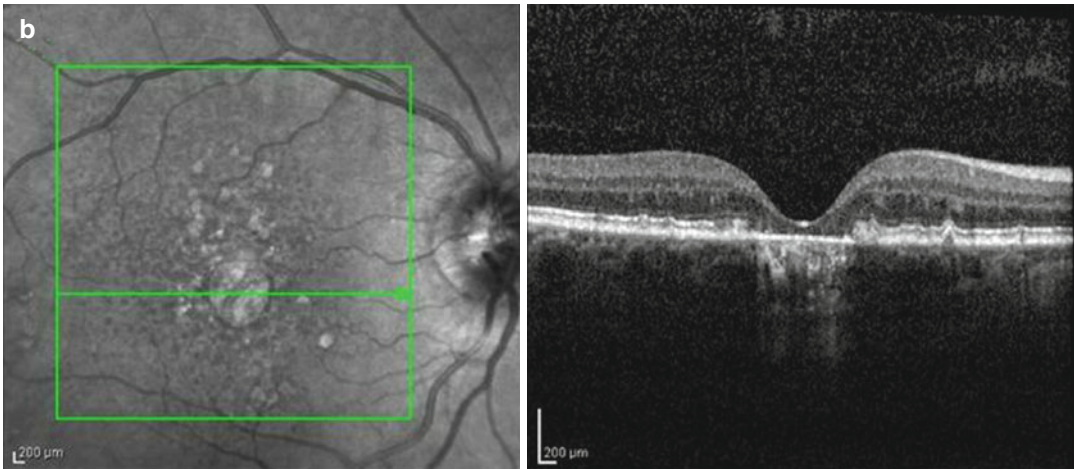


Fig. 7.2 (continued)

is only a single aspect of visual function and is not sufficient to investigate patients' comprehensive "quality of vision." An expert consensus pointed out that testing visual acuity should be completed with other functional investigations and that microperimetry may be the best tool to objectify patients' ability of managing daily visual tasks independently [26].

Microperimetry studies in patients with early or intermediate AMD revealed a statistically significant reduction in retinal sensitivity in areas overlying drusen, even in patients with good BCVA (Figs. 7.3 and 7.4). A correlation between retinal sensitivity and drusen volume, irregularities of the retinal pigment epithelium (RPE), and the junction between the inner and outer segments of the photoreceptors (IS-OS junction) detected in OCT or FAF was found [27–29].

The value of multimodal imaging including microperimetry and other functional tests for diagnosis and for following up patients with early or intermediate AMD in clinical routine and study settings is indisputable. However, one question comes to mind with multimodal imaging: Is there a value or a combination of findings that could help to identify patients who are at imminent risk of developing advanced stages of AMD? Such a value or combination would help clinicians to adapt examination intervals to provide adequate support to patients without exceeding the limits of health-care systems.

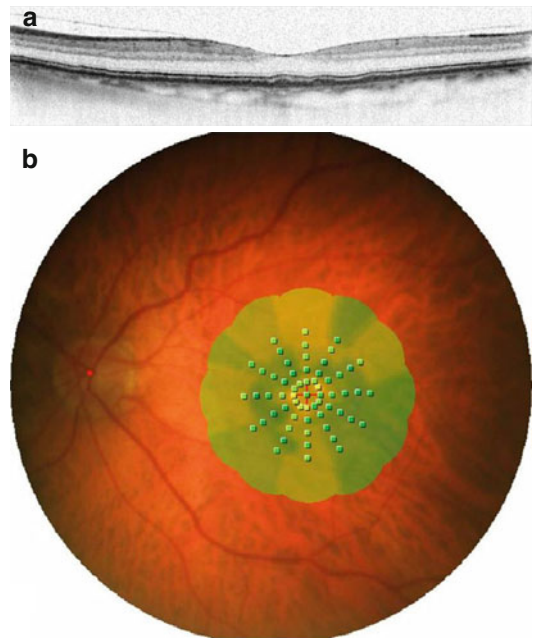


Fig. 7.3 (a) Central SD-OCT B-scan of a 78-year-old woman with drusen, IS-OS line is intact. (b) The corresponding microperimetric examination showed a slight reduction in sensitivity over drusen

In addition to evaluating well-known risk factors for the progression to advanced AMD (i.e., drusen diameter or drusen area), evaluating changes in fixation patterns occurring prior to progression to advanced AMD forms by common microperimetric devices is useful [30]. The

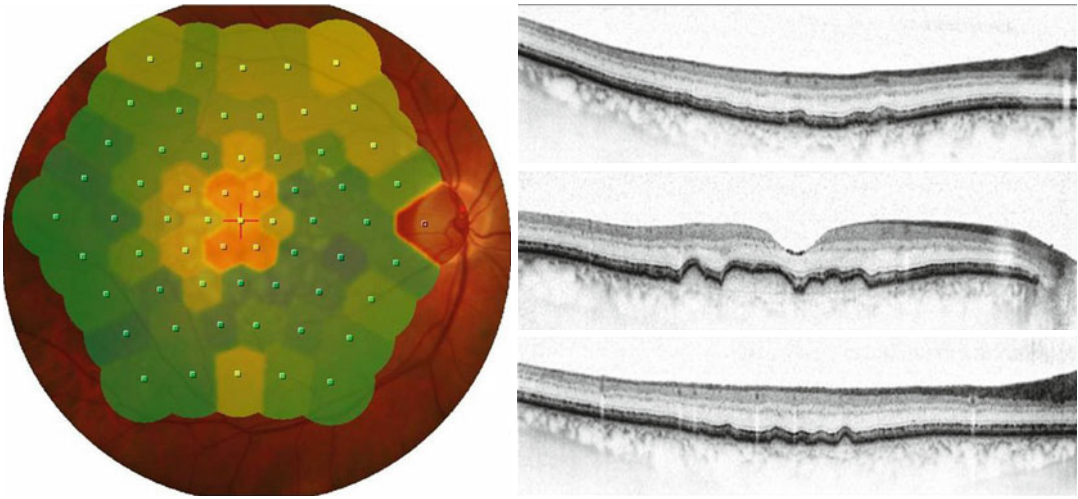


Fig. 7.4 Microperimetry (*left*) and SD-OCT results (*right*) of a 72-year-old patient with large, confluent drusen, and irregularities in the IS-OS line. A reduction in retinal sensitivity is visible, especially in the central area

inner retinal migration of hyperreflective foci detected in OCT may also serve as a biomarker for AMD progression as it is associated with higher incidences of geographic atrophy [31]. Furthermore, microperimetry and OCT add useful information when the fluorescein angiogram is negative or suspect [32].

7.4 Aspects for the Future

The above-mentioned commonly used and commercially available imaging devices are complemented by new developments promising further gains in knowledge of AMD.

Whereas conventional intensity-based OCT cannot differentiate between structures, polarization-sensitive OCT (PS-OCT) measures the polarization state of light to obtain additional information on the tissue. Several structures in the eye, including the retinal pigment epithelium (RPE), alter the polarization state of light and therefore lead to a measurable signal in PS-OCT images [33]. This helps to differentiate between tissues, which is often difficult in pathology when the normal layer structure is disrupted. The RPE overlying drusen has been shown to be hugely variable in integrity, mainly influenced by drusen size, shape, and reflectivity [34, 35].

Imaging devices equipped with adaptive optics (AO) provide high axial and lateral resolution by correcting higher-order aberrations of the eye. These instruments can visualize *in vivo* single cones, even in the foveal region (Fig. 7.5), and rods in the retinal periphery (Fig. 7.6) of healthy volunteers [36, 37]. In addition, temporal changes in the human cone photoreceptor mosaic can be observed, providing a better insight into regular physiological processes during normal photoreceptor renewal [38, 39]. However, the quality of AO images of patients with AMD is lower than that of young and healthy subjects, probably due to fixation problems, media opacity, and tear film instability in older age. Drusen appear in these images as hyperreflective areas [40]. The images have revealed irregularities in the photoreceptor mosaic, even in the early stages of AMD, due to drusen formation and have identified small drusen that are otherwise undetectable with standard clinical imaging techniques [41].

These new imaging devices should supply us with a deeper insight into the pathophysiologic features leading to AMD and help us to monitor even minor changes in our study populations better. Hopefully, they will one day lead to an improved concept for patient care and prevent severe vision loss.

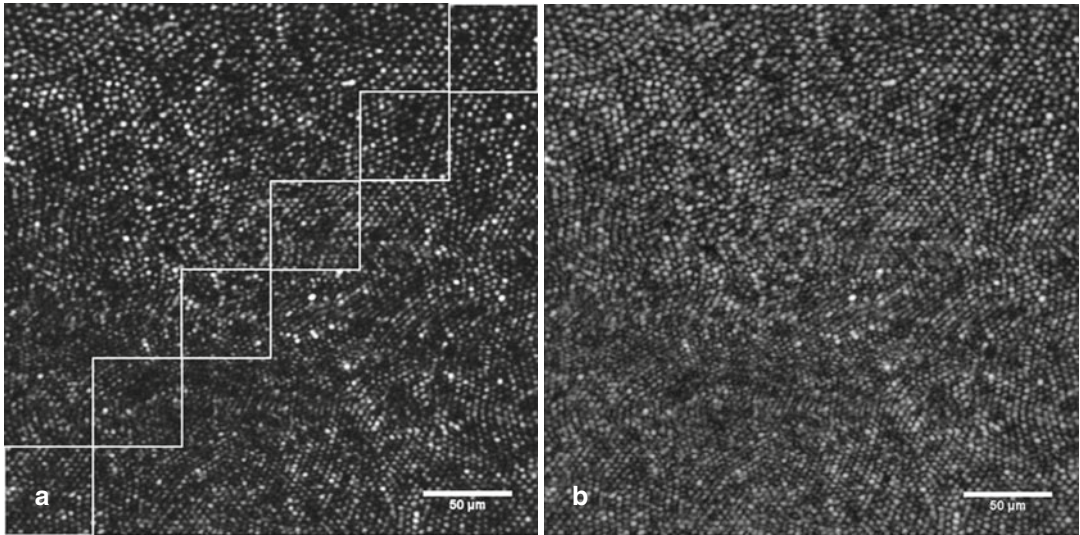


Fig. 7.5 AO-SLO image of the fovea of a 27-year-old healthy volunteer. Scanning angle $\sim 1^\circ \times 1^\circ$. (a) Results displayed on a linear scale. (b) Results displayed on a logarithmic scale (Reprinted from [10])

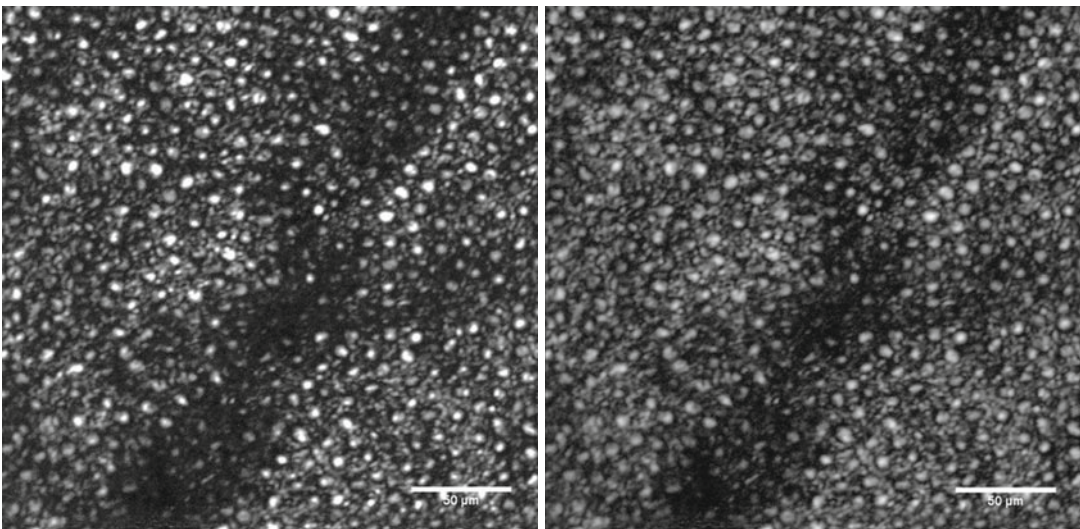


Fig. 7.6 Images of rod photoreceptors from a 30-year-old volunteer at $\sim 7^\circ$ eccentricity temporal to the fovea. *Left*, linear scale; *right*, logarithmic scale (Reprinted from [10])

References

1. Vision 2020: right to sight. Blindness and visual impairment: global facts. <http://www.iapb.org/vision-2020>. Accessed Mar 2013
2. Rudnicka AR, Jarrar Z, Wormald R et al (2012) Age and gender variations in age-related macular degeneration prevalence in populations of European ancestry: a meta-analysis. *Ophthalmology* 119:571–580
3. Ferris FL 3rd, Wilkinson CP, Bird A, Chakravarthy U, Chew E, Csaky K, Sadda SR (2013) Clinical classification of age-related macular degeneration. *Ophthalmology* 120:844–851
4. Holliday EG, Smith AV, Cornes BK et al (2013) Insights into the genetic architecture of early stage age-related macular degeneration: a genome-wide association study meta-analysis. *PLoS One* 8(1):e53830
5. Schmidt-Erfurth U, Pollreis A, Mitsch C, Bolz M (2010) Antivascular endothelial growth factors in

- age-related macular degeneration. *Dev Ophthalmol* 46:21–38
6. Age-Related Eye Disease Study Research Group (2001) A randomized, placebo-controlled, clinical trial of high-dose supplementation with vitamins C and E, beta carotene, and zinc for age-related macular degeneration and vision loss: AREDS report no. 8. *Arch Ophthalmol* 119:1417–1436
 7. Chong EW, Wong TY, Kreis AJ, Simpson JA, Guymer RH (2007) Dietary antioxidants and primary prevention of age related macular degeneration: systematic review and meta-analysis. *BMJ* 335:755
 8. Evans JR, Lawrenson JG (2012) Antioxidant vitamin and mineral supplements for slowing the progression of age-related macular degeneration. *Cochrane Database Syst Rev* (11):CD000254
 9. Klein EA, Thompson IM Jr, Tangen CM et al (2011) Vitamin E and the risk of prostate cancer: the Selenium and Vitamin E Cancer Prevention Trial (SELECT). *JAMA* 306:1549–1556
 10. Ho L, van Leeuwen R, Witteman JC et al (2011) Reducing the genetic risk of age-related macular degeneration with dietary antioxidants, zinc, and omega-3 fatty acids: the Rotterdam study. *Arch Ophthalmol* 129:758–766
 11. Kaya S, Weigert G, Pemp B, Sacu S et al (2012) Comparison of macular pigment in patients with age-related macular degeneration and healthy control subjects – a study using spectral fundus reflectance. *Acta Ophthalmol* 90:e399–e403
 12. Ma L, Yan SF, Huang YM et al (2012) Effect of lutein and zeaxanthin on macular pigment and visual function in patients with early age-related macular degeneration. *Ophthalmology* 119:2290–2297
 13. Chew EY, Clemons T, SanGiovanni JP et al (2012) The Age-Related Eye Disease Study 2 (AREDS2): study design and baseline characteristics (AREDS2 report number 1). *Ophthalmology* 119:2282–2289
 14. Christen WG, Glynn RJ, Ajani UA et al (2001) Age-related maculopathy in a randomized trial of low-dose aspirin among US physicians. *Arch Ophthalmol* 119:1143–1149
 15. Fong DS, Contreras R (2010) Recent statin use and 1-year incidence of exudative age-related macular degeneration. *Am J Ophthalmol* 149:955–958.e1
 16. McGwin G Jr, Xie A, Owsley C (2005) The use of cholesterol-lowering medications and age-related macular degeneration. *Ophthalmology* 112:488–494
 17. Miller JW (2013) Age-related macular degeneration revisited – piecing the puzzle: the LXIX Edward Jackson memorial lecture. *Am J Ophthalmol* 155:1–35.e13
 18. Geitzenauer W, Hitzenberger CK, Schmidt-Erfurth UM (2011) Retinal optical coherence tomography: past, present and future perspectives. *Br J Ophthalmol* 95:171–177
 19. Keane PA, Patel PJ, Liakopoulos S et al (2012) Evaluation of age-related macular degeneration with optical coherence tomography. *Surv Ophthalmol* 57:389–414
 20. Gregori G, Wang F, Rosenfeld PJ et al (2011) Spectral domain optical coherence tomography imaging of drusen in nonexudative age-related macular degeneration. *Ophthalmology* 118:1373–1379
 21. Schlanitz FG, Ahlers C, Sacu S et al (2010) Performance of drusen detection by spectral-domain optical coherence tomography. *Invest Ophthalmol Vis Sci* 51:6715–6721
 22. Yehoshua Z, Wang F, Rosenfeld PJ et al (2011) Natural history of drusen morphology in age-related macular degeneration using spectral domain optical coherence tomography. *Ophthalmology* 118:2434–2441
 23. Spaide RF, Curcio CA (2010) Drusen characterization with multimodal imaging. *Retina* 30:1441–1454
 24. Sayegh RG, Simader C, Scheschy U et al (2011) A systematic comparison of spectral-domain optical coherence tomography and fundus autofluorescence in patients with geographic atrophy. *Ophthalmology* 118:1844–1851
 25. Forte R, Querques G, Querques L et al (2012) Multimodal imaging of dry age-related macular degeneration. *Acta Ophthalmol* 90(4):e281–e287
 26. Piermarocchi S, Sartore M, Bandello F et al (2006) Quality of vision: a consensus building initiative for a new ophthalmologic concept. *Eur J Ophthalmol* 16:851–860
 27. Hartmann KI, Bartsch DU, Cheng L et al (2011) Scanning laser ophthalmoscope imaging stabilized microperimetry in dry age-related macular degeneration. *Retina* 31:1323–1331
 28. Iwama D, Tsujikawa A, Ojima Y et al (2010) Relationship between retinal sensitivity and morphologic changes in eyes with confluent soft drusen. *Clin Experiment Ophthalmol* 38:483–488
 29. Midena E, Vujosevic S, Convento E et al (2007) Microperimetry and fundus autofluorescence in patients with early age-related macular degeneration. *Br J Ophthalmol* 91:1499–1503
 30. Dinc UA, Yenerel M, Gorgun E et al (2008) Assessment of macular function by microperimetry in intermediate age-related macular degeneration. *Eur J Ophthalmol* 18:595–600
 31. Christenbury JG, Folgar FA, O’Connell RV et al (2013) Progression of intermediate age-related macular degeneration with proliferation and inner retinal migration of hyperreflective foci. *Ophthalmology* 120:1038–1045
 32. Simader C, Michels S, Geitzenauer W et al (2005) Functional macular mapping in patients with progression from dry to neovascular AMD. Paper presented at the SOE
 33. Pircher M, Hitzenberger CK, Schmidt-Erfurth U (2011) Polarization sensitive optical coherence tomography in the human eye. *Prog Retin Eye Res* 30:431–451
 34. Schlanitz F, Bolz M, Baumann B et al (2012) Drusentypen und ihr Einfluss auf das retinale

- Pigmentepithel – In-vivo-Evaluation mit Hilfe der Polarisationssensitiven OCT. Paper presented at the DOG
35. Schlanitz FG, Baumann B, Spalek T et al (2011) Performance of automated drusen detection by polarization-sensitive optical coherence tomography. *Invest Ophthalmol Vis Sci* 5:4571–4579
 36. Dubra A, Sulai Y, Norris JL et al (2011) Noninvasive imaging of the human rod photoreceptor mosaic using a confocal adaptive optics scanning ophthalmoscope. *Biomed Opt Express* 2:1864–1876
 37. Felberer F, Kroisamer JS, Hitzenberger CK et al (2012) Lens based adaptive optics scanning laser ophthalmoscope. *Opt Express* 20:17297–17310
 38. Jonnal RS, Besecker JR, Derby JC et al (2010) Imaging outer segment renewal in living human cone photoreceptors. *Opt Express* 18:5257–5270
 39. Pircher M, Kroisamer JS, Felberer F et al (2010) Temporal changes of human cone photoreceptors observed in vivo with SLO/OCT. *Biomed Opt Express* 2:100–112
 40. Kroisamer JS, Felberer F, Hitzenberger CK et al (2012) Evaluation of an adaptive optics SLO in patients with AMD. Paper presented at the ARVO
 41. Boretsky A, Khan F, Burnett G et al (2012) In vivo imaging of photoreceptor disruption associated with age-related macular degeneration: A pilot study. *Lasers Surg Med* 44:603–610

8.1 Introduction

Geographic atrophy (GA) represents the atrophic late-stage manifestation of age-related macular degeneration (AMD) [1]. It affects about 3.5 % of people aged 75 and over, and its prevalence raises to over 20 % in people older than 90 years old [2–4]. GA, which is commonly bilateral, is characterized by the development of areas of retinal pigment epithelium and neural retina atrophy, which slowly progress over time at a median rate of 1.5–2.1 mm² per year [5–7]. Patients with primary GA tend to be older than those with exudative AMD at the time of initial presentation. It has been speculated that GA occurs in subjects in which exudative AMD has not yet developed [8]. Currently, there is no treatment available to slow GA progression, but several therapeutic strategies for this macular disease are under investigation [9–11]. Based on data of large natural history studies exploring the progression of this macular disease, the GA progression rate has been approved by the Food and Drug Administration (FDA) as primary outcome measure in clinical trials on GA [12, 13]. Progressive enlargement of atrophy was usually assessed by color fundus images [5]. More recently, short-wavelength fundus autofluorescence (SW-FAF, excitation 488 nm, emission >500 nm) and near-infrared

fundus autofluorescence (NIR-FAF, excitation 787 nm, emission >800 nm) imaging modalities have been claimed to be useful to monitor GA progression [7, 14]. Microperimetry is used to exactly measure macular retinal sensitivity, and it is useful to follow-up relative scotomas in progressing GA [14–16].

This chapter describes recent investigations in functional macular damage and the correlations between morphologic changes and their functional impairment in patients with GA.

8.2 Geographic Atrophy and Functional Impairment

Severe visual acuity loss secondary to GA occurs in about 20 % of all patients with AMD [2, 17]. Hence, GA is a common cause of legal blindness in AMD patients. Atrophic areas initially occur in the parafoveal retina, and patients are unaware of their functional condition. Over time several atrophic areas may coalesce and new atrophic areas may occur. In more advanced stages, atrophic areas form an atrophic ring around the fovea, which can remain stable for a long time, a phenomenon known as “foveal sparing” [18]. The areas of GA are characterized by a dense scotoma whose extension corresponds to the atrophic area and a significant retinal sensitivity reduction at their margins [19, 20]. Therefore, the progression of GA is always associated with progressive loss of visual function [5]. Because the fovea is unaffected, retinal fixation maintains central and

E. Pilotto, MD (✉) • F. Guidolin
Department of Ophthalmology, University of Padova,
via Giustiniani 2, Padova 35128, Italy
e-mail: elisabetta.pilotto@unipd.it

stable until the fovea is preserved (Fig. 8.1). This means that even small residual area of retinal sensitivity is useful for fixating in patients with progressive atrophic lesions due to AMD, as in other slowly progressive atrophic disorders involving the macula [21]. Otherwise, patients with GA who have normal visual acuity often report impaired vision in dim light and difficulties in

recognizing the contour of objects in low contrast conditions. This underlines that rod photoreceptors degenerate earlier and more rapidly than cones both anatomically and functionally in retinal areas that are not yet dense scotoma due to atrophy [22–25].

Fixation patterns in eyes with GA and central scotoma were studied in detail by Sunness et al. [26]. Using SLO microperimetry, the authors looked at the location of the preferred retinal locus (PRL) in patients with GA who had lost foveal function and had visual acuity in the 20/80 to 20/200 range. PRL is located at the edge of the main area of atrophy, presumably because this location is closer to the foveal region, thus providing the best functional result. However, the position of the central scotoma relative to the PRL is a driving factor in the choice of PRL location. For patients with GA, the preferred fixation pattern is placing fixation to have the scotoma on the right side of the visual field. The second adaptation choice is to have the scotoma above fixation [27–29] (Fig. 8.2). This phenomenon, which is visual cortex controlled, is partly reading driven. It prevents that the left-to-right reader has the scotoma projected over the beginning of the text. The long-term follow-up of these patients showed that most of them retained the fixation pattern developed at baseline visit [26]. Some



Fig. 8.1 Macular microperimetry (MP1) fixation superimposed to color fundus photograph in an eye affected by geographic atrophy (GA). Foveal sparing and stability of retinal fixation

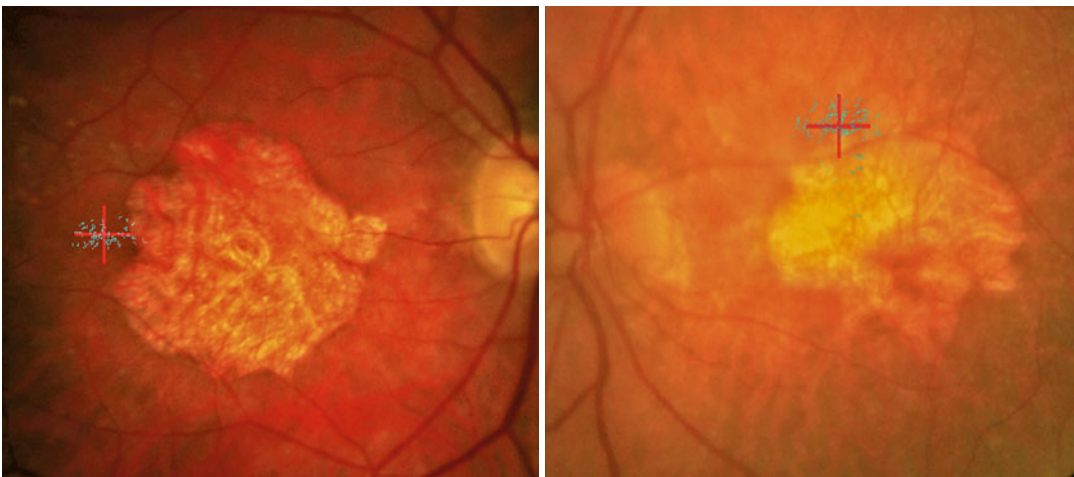


Fig. 8.2 Preferred retinal locus (PRL) in two patients affected by geographic atrophy (GA) with foveal involvement. Patient A (on the *left*) fixation site is on the left side

of GA area to have a scotoma on the right side of the visual field. In patient B (on the *right*) fixation site is above the GA area

patients with a large area of GA surrounding a preserved central foveal area may have and use two fixation sites: a central PRL and a second one at the peripheral edge of the atrophy. The central fixation site allows good visual acuity, but a very limited seeing area. On the other hand, the peripheral fixation site allows lower visual acuity but a larger useful area surrounding it [30].

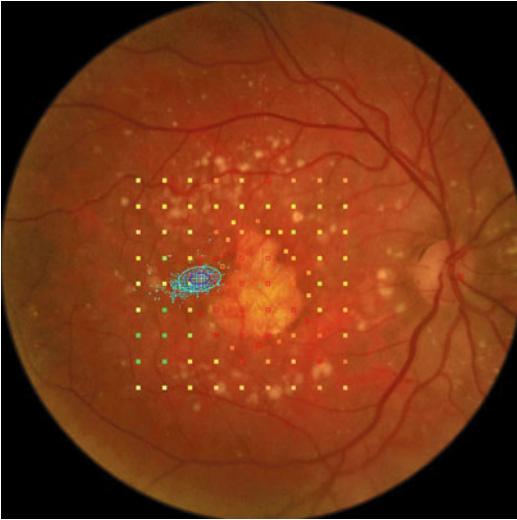


Fig. 8.3 Quantification of fixation stability by microperimetry (MP1): bivariate contour ellipse area (BCEA)

Fixation stability is another important parameter that influences visual performance. The quantification of fixation characteristics may be performed using the bivariate contour ellipse calculated area (BCEA) (Fig. 8.3). BCEA is an area which quantifies the horizontal and vertical eye positions and is expressed in degrees² (deg²). This is a 2-dimensional ellipse that describes the portion of retinal surface within the center of the target imaged at least 68 % of the time (BCEA 68), 95 % of the time (BCEA 95), and 99 % of the time (BCEA 99) [31]. The calculation of the BCEA is automatically performed by the MP1 Microperimeter (Nidek, Gamagori, Japan) and MAIA (CenterVue, Padova, Italy). BCEA correlates with reading ability in patients with macular diseases [32]. Recently, it has been demonstrated that in patients with progressive GA, mean BCEA may significantly decrease during follow-up due to a more stable fixation [14]. This finding confirms that even if GA area progresses, fixation may become more stable as previously detected in end-stage AMD [33] (Fig. 8.4).

Areas of GA are characterized by a dense scotoma which generally corresponds in spatial extent exactly to the atrophic area [19]. Microperimetry is used to exactly measure macular

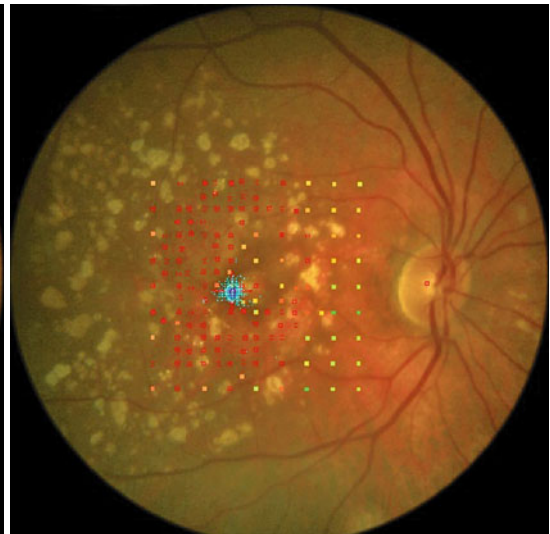
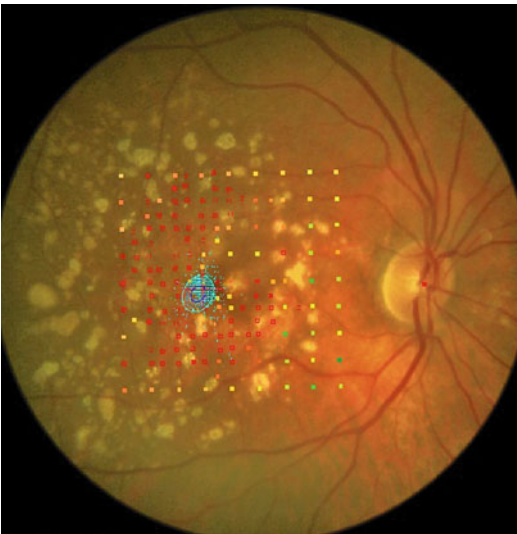


Fig. 8.4 Quantification of fixation stability by bivariate contour ellipse area (BCEA) in a patient with geographic atrophy (GA): baseline (on the *left*) and follow-up (on the

right). The decreasing of BCEA reveals that the fixation has become more stable during follow-up

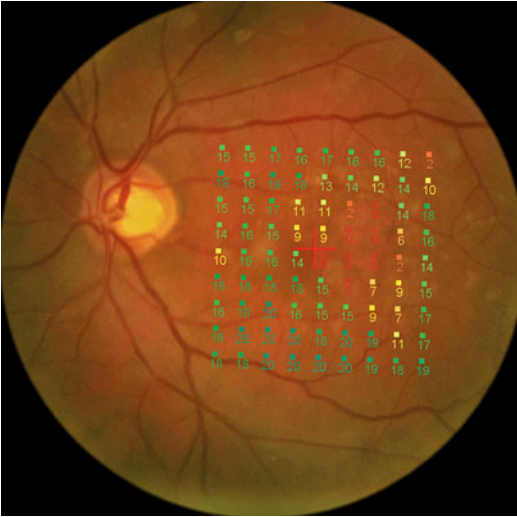


Fig. 8.5 Macular microperimetry (MP1) sensitivity map superimposed to color fundus photograph in an eye affected by geographic atrophy (GA). Areas of GA are characterized by dense scotomas (*red empty scores*)

retinal sensitivity, and it is useful to map dense and relative scotomas in GA [15] (Fig. 8.5). The progressive enlargement of GA is associated with the changes in the number of scotomatous points in the macular area [14, 15]. In patients with GA, retinal sensitivity in areas outside of the GA lesion is usually lower than that found in equivalent areas in healthy aged subjects [15, 34]. Therefore, functional decline in GA involves both the increase in size of the absolute scotoma and a diffuse decrease in macular sensitivity. Meleth et al. analyzed retinal sensitivity changes of retinal points in the junctional zone of GA (perilesional points) or in areas further away from GA (extralesional points). The authors detected that perilesional points had lower sensitivity compared with extralesional points. Also, while there was a statistically significant relationship between the decrease in mean sensitivity of perilesional points and follow-up time, the relationship between mean sensitivity of extralesional points and follow-up time was not statistically significant. Extralesional points also showed a slight non-significant increase in mean sensitivity at 6 and 12 months and declined slightly at 18 and 24 months. Mean sensitivity of perilesional points

also demonstrated a greater and more general decrease with time than extralesional points. Therefore, the more generalized loss of macular sensitivity in areas around GA lesion seems to occur as a separate process from the local expansion of the GA lesion itself [15]. These findings underline that pathophysiology of GA progression still remains largely unknown. For this reason, more efforts have been recently done to investigate further morpho-functional correlations in patients with progressive GA.

8.3 Imaging of Geographic Atrophy

Geographic atrophy has been usually assessed by color fundus photo [5] (Fig. 8.6). More recently, fundus autofluorescence (FAF) imaging has been shown to be useful to detect GA and to accurately monitor its progression [15, 35, 36] (Fig. 8.7). Short-wavelength FAF (SW-FAF, excitation 488 nm, emission >500 nm) is an imaging method that allows topographic mapping of lipofuscin distribution in the retinal pigment epithelium (RPE) in vivo [35–39]. Because of the absence of RPE lipofuscin, atrophic areas in GA show a severely reduced FAF signal at the site of atrophic areas, appearing markedly hypo-autofluorescent (hypo-FAF). The hypo-fluorescent areas correspond to dense scotoma, as documented by microperimetry (Fig. 8.8). The high contrast difference between atrophic and non-atrophic retina allows for much better delineation of atrophic area with FAF imaging compared to conventional fundus photographs. In contrast to fluorescein angiography, FAF is a noninvasive and less time-consuming method. Customized image analysis software enables automatic segmentation of atrophic areas by a region algorithm using FAF imaging to detect and to quantify atrophic areas [40]. Moreover, an abnormal autofluorescence pattern in the junctional zone of GA (the area between atrophy and normal retina) has been demonstrated using confocal scanning laser ophthalmoscope (cSLO) systems. Areas of increased SW-FAF in the junctional zone precede the enlargement of preexisting



Fig. 8.6 Color fundus photograph in an eye affected by geographic atrophy (GA): baseline (on the *left*) and follow-up (on the *right*)

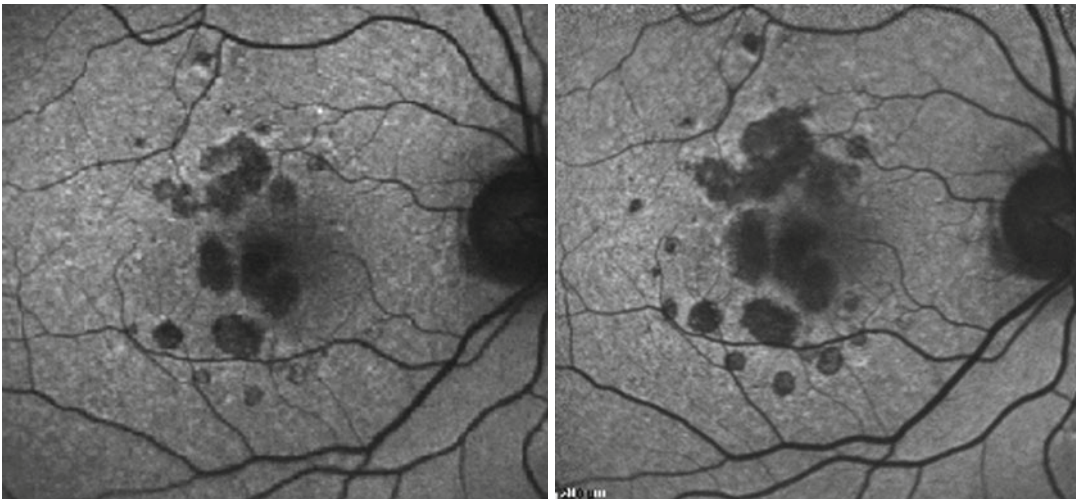


Fig. 8.7 Short-wavelength fundus autofluorescence (SW-FAF) in an eye affected by geographic atrophy (GA): baseline (on the *left*) and follow-up (on the *right*)

atrophy and the development of new atrophic patches over time [41]. Using SW-FAF imaging distinct phenotypes of these areas of increased FAF have been detected, with a high degree of intraindividual symmetry [31, 42].

The fundus autofluorescence in Age-Related Macular Degeneration Study demonstrated that the great variability and range of atrophy enlargement between patients is largely dependent on the specific pattern of SW-FAF abnormalities at baseline outside the atrophic patches. Eyes with

the banded and the diffuse SW-FAF patterns have a more rapid enlargement rate than eyes without FAF abnormalities and the focal FAF pattern [7]. A high degree of concordance for SW-FAF pattern and GA progression has been observed in eyes of patients with bilateral GA [43] (Fig. 8.9).

However, the central macula is particularly dark due to the absorption of the blue excitation light by lutein. Therefore, with SW-FAF, it may be sometimes difficult to distinguish among normal hypo-FAF, atrophic areas, and drusen [44].

Recently, near-infrared FAF (NIR-FAF, excitation 787 nm, emission >800 nm) has been introduced to visualize fluorophores different from lipofuscin [39]. Gibbs et al. have experimentally shown that NIR-FAF signal represents novel fluorophores specific to melanosomes both in the RPE and choroid [45]. Lipofuscin granules of the

RPE and many other potential fluorophores of the neural retina and RPE do not detectably contribute to the NIR-FAF signal [45]. Therefore, NIR-FAF is useful to topographically map the melanin distribution in RPE *in vivo*. Using this imaging modality the foveal area appears normally hyper-FAF due to the physiological presence of melanin, and GA area appears markedly hypo-FAF because of the absence of RPE melanin. Therefore, both foveal areas of GA and foveal sparing may be easier visualized and quantified using this imaging technique than with SW-FAF [36, 37, 46] (Fig. 8.10). Recently, NIR-FAF has been used to quantify GA extension comparing it to SW-FAF [36, 46]. It has been detected that the total area of GA is always significantly larger at NIR-FAF compared to SW-FAF at baseline and during follow-up. Otherwise, the annual rate of GA progression based on NIR-FAF is not greater than on SW-FAF [14]. Besides, some hypo-FAF areas at NIR-FAF may appear normal at SW-FAF [14, 47]. The source of maximum SW-FAF signal has histologically been detected in the RPE and photoreceptor (PR) outer segments [45]. Therefore, it has been speculated that normal SW-FAF may be due to persistent PR layer over a damaged RPE, which corresponds to hypo-NIR-FAF [36]. Similar findings have been

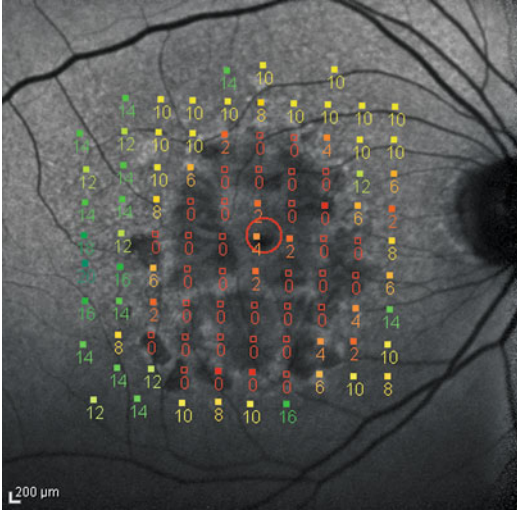


Fig. 8.8 Macular microperimetry (MP1) sensitivity map superimposed to short-wavelength fundus autofluorescence (SW-FAF) in an eye affected by geographic atrophy (GA): areas of hypo-autofluorescence correspond to dense scotomas and macular sensitivity is diffusely decreased

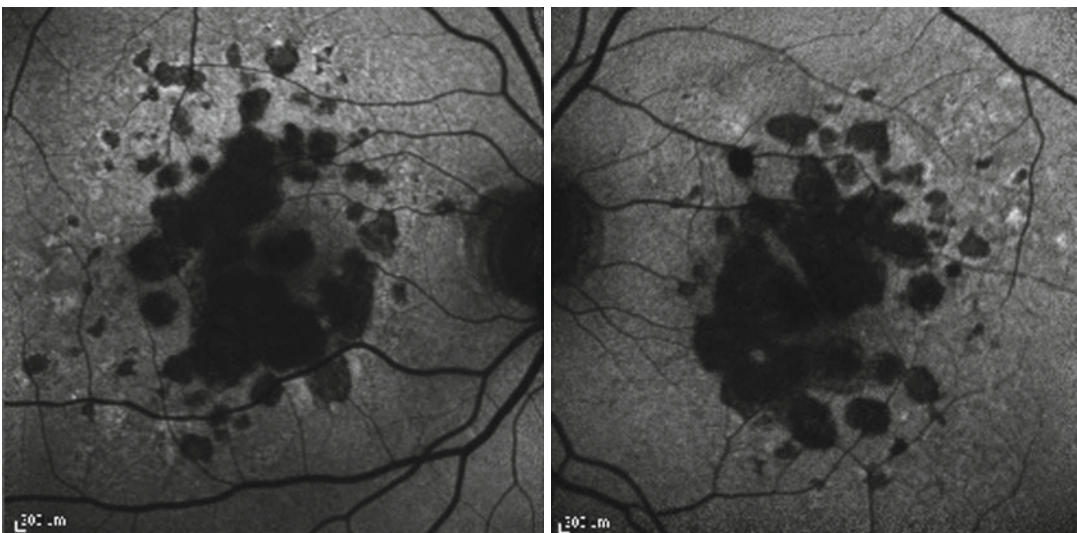


Fig. 8.9 Patient affected by geographic atrophy: both eyes have the same short-wavelength pattern

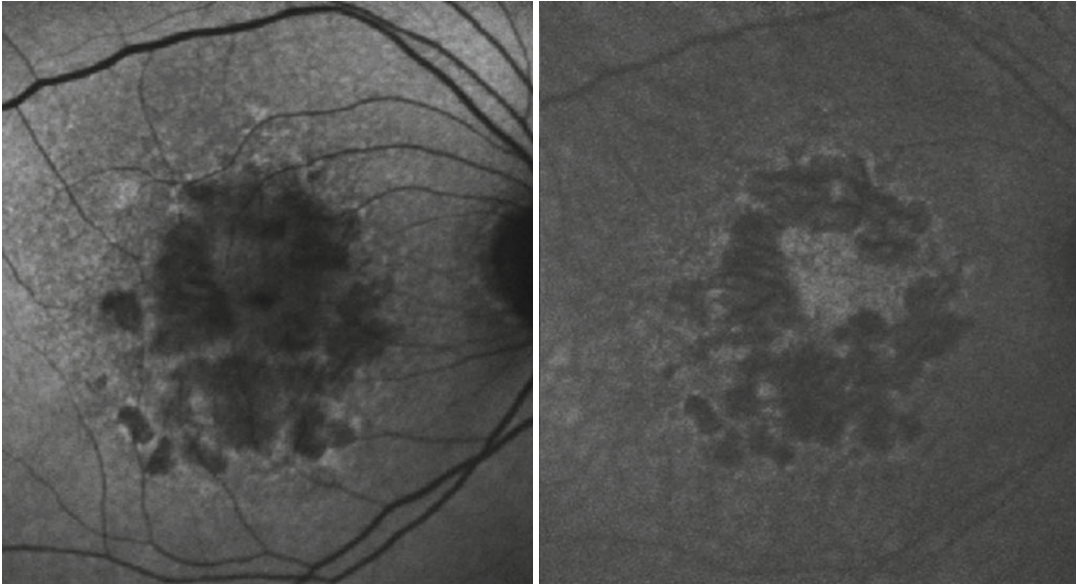


Fig. 8.10 Short-wavelength fundus autofluorescence (on the *left*) and near-infrared fundus autofluorescence (on the *right*) in an eye affected by geographic atrophy (GA):

foveal areas of geographic atrophy (GA) and foveal sparing are easier visualized at NIR-FAF

observed in patients with Stargardt disease and cone-rod dystrophy [48].

Recently, spectral domain optical coherence tomography (SD-OCT) has been introduced with further improvements in imaging speed and resolution compared with previous time domain OCT imaging. With SD-OCT, a wide spectrum of morphological changes has been detected both in the atrophic area and in the surrounding tissue [18, 49–54]. In the perilesional area, elevations of the outer retinal layers, thickening, and spikes of the outer OCT hyperreflective band as well as clumps at different neurosensory retinal levels have been described. At the junction between the two zones, a highly variable loss of the outer retinal layers has been observed. Within the GA area, hyperreflective clumps at different retinal levels, segmented plaques of the outer band, and elevations with variable reflectivity have been visualized [51].

The simultaneous recording of cSLO and SD-OCT images in one instrument with an exact topographic overlay during image acquisition now allows for accurate orientation of cross-sectional SD-OCT scans at anatomic sites of interest and also the serial examinations at the same location [52]. Using this technology, the

dynamic retinal changes can be followed over time [18, 52, 53]. Besides, with the advent of this system it has become possible to obtain simultaneous FAF and OCT images, making it easier to find small changes in FAF and to analyze them on OCT [54] (Fig. 8.11). In a cross-sectional analysis, two distinct patterns of structural changes at the margins of GA on SD-OCT corresponding to specific SW-FAF patterns have been detected [50]. Those areas showing increased FAF had a corresponding irregular margin on SD-OCT as compared with the second group with no abnormal SW-FAF at the margins and corresponding smooth margin on SD-OCT [50].

Besides using SD-OCT retinal segmentation techniques, single retinal layer measurement is now available [55–57] (Fig. 8.12). Even if GA secondary to AMD is a macular disease that primarily affects the outer retina, the inner retina is also involved, as recently reported. Pilotto et al. detected, in a prospective study, that even if retinal thickness (RT) significantly decreases in progressing GA, its thinning is only moderately correlated to outer retinal layers (ORL) thinning. A more strong inverse correlation has been detected between ORL thinning and inner retinal layer

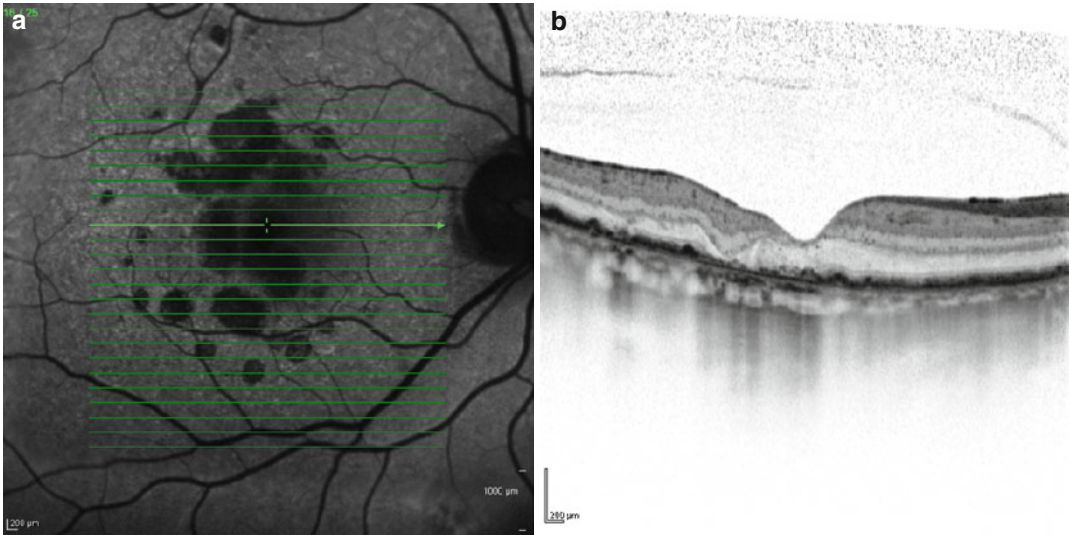


Fig. 8.11 Short-wavelength fundus autofluorescence (SW-FAF) and spectral domain optical coherence tomography (SD-OCT) obtained simultaneously in an eye affected by geographic atrophy (GA). Green lines on

SW-FAF individuate the position of the linear scans performed, and the OCT scan on the right correspond to the scan passing through the fovea (*white line*)



Fig. 8.12 Retinal layering in a normal eye using a spectral domain optical coherence tomography (SD-OCT) retinal segmentation technique (Spectralis, Heidelberg Engineering, Heidelberg, Germany)

(IRL) thickening [57]. Because the cell body of Müller cells is located in the IRL, Pilotto et al. speculate that the hypertrophy of the Müller cells could justify the IRL thickening detected in their study [57]. This hypothesis is supported by some clinical and histological findings recently reported. Foveal swelling related to thickening of the Henle's fiber layer in patients with foveal sparing secondary to GA has been also described [18, 58]. Changes in the thickness and optical reflectivity of individual retinal layers in sodium iodate-induced retinal damage in a rat model of outer retinal degeneration have been detected by means of ultrahigh resolution OCT and histologically confirmed [59]. Retinal remodelling and Müller cells changes induced by oxidative stress have been assessed in an animal light-induced retinal damage model [60]. DiLoreto et al. reported that Müller cells swelling preceded the degeneration of

photoreceptors spatially and temporally in a rat model of AMD [61]. Müller cell hypertrophy has also been described histologically by Curcio et al. [62]. Cohen et al. recently described in GA retinal pseudocysts, intraretinal lesions corresponding to optically empty spaces, mainly located in the inner nuclear layer, and commonly detected at the margin of GA areas [63]. These authors hypothesize that these intraretinal lesions may be caused by Müller cell degeneration or loss [63].

8.4 Integrating Morphology and Function in Geographic Atrophy

In GA several efforts have been done to correlate morphological findings to functional impairment. Fine matrix visual field mapping of junctional

regions showing increased SW-FAF documented a severe reduction in scotopic sensitivity, with moderate reduction in photopic sensitivity [64]. The use of microperimetry, an exactly fundus-related perimetry, allows to correlate retinal function to SD-OCT findings and to FAF pattern at baseline and during follow-up in progressing macular diseases. Schmitz-Valckenberg et al., using SLO microperimetry, found reduced retinal sensitivity in the areas of increased FAF bordering GA compared to areas with normal FAF [65]. This finding suggests that pathologic lipofuscin accumulation in the RPE surrounding areas of GA has reduced retinal sensitivity as functional correlate. Preliminary data also suggest that NIR-FAF better correlates to retinal sensitivity changes compared to SW-FAF [14, 16]. But reduced retinal sensitivity may directly depend on alterations in photoreceptor (PR) function along the border of GA as recently hypothesized by Bearely et al. [49]. Two hypotheses about the pathogenesis of GA secondary to AMD are under investigation. The first one is that RPE atrophy causes secondary choriocapillaris loss and PR degeneration [66]. The second one is that choroidal vascular insufficiency results in dysfunction of the RPE and PR degeneration. In postmortem specimens obtained from patients with GA due to AMD, a linear relationship between the loss of RPE and choriocapillaris atrophy has been observed [66]. But a complete loss of choriocapillaris was never observed, even if atrophy was clinically documented. The surviving choriocapillaris showed structural changes as vasoconstriction and loss of fenestrations [66]. These histological data were confirmed by experimental observations [67, 68]. However, there are some evidences suggesting that the PR layer may play a key role in GA onset and progression [23]. Recently, Bearely et al. analyzed PR layer loss at the margins of GA using SD-OCT. These authors found that PR loss occurred in 65 % of cases bridging across the GA, in 29 % inside GA margins, while only in 6 % entirely outside GA margins [49]. These findings emphasize the intimate temporal relationship between PR loss and RPE loss in GA. Pilotto et al. detected that GA boundaries with normal FAF, but functionally compromised

at microperimetry, were less frequent at NIR-FAF than at SW-FAF (0.4 % versus 4.5 %, $p=0.000$). On the contrary, GA boundaries with hyper-FAF, but also functionally compromised at microperimetry, were significantly more frequent at NIR-FAF than at SW-FAF (3.3 % versus 1.6 %, $p=0.022$) [36]. Moreover, the increase of NIR-FAF signal has a higher predictive value of progression of GA than normo-NIR-FAF [14]. Different SW-FAF and NIR-FAF patterns have shown different relative risk of progression from relative to dense scotoma. The risk of any relative dense scotoma to progress to dense scotoma is significantly correlated to each individual FAF pattern both at SW-FAF and NIR-FAF. Relative dense scotomas characterized by hypoSW-FAF or hyperNIR-FAF have a higher risk of evolving to dense scotoma than normo- and hyper-FAF at SW-FAF (O.R.=2.62 and O.R.=2.77, respectively), and normo NIR-FAF (O.R.=2.96) [14]. The correlation between FAF pattern and retinal layers changes by mean of SD-OCT have been recently investigated [57]. RT and ORL thickness were correlated both at SW-FAF and at NIR-FAF imaging modalities. However, in hyper NIR-FAF tested points RT was thicker than in hyper SW-FAF due to higher thickness of ORL. Moreover, the photoreceptor inner segment/outer segment (IS/OS) junction integrity was significantly correlated to FAF pattern at both FAF imaging modalities. Tested points with absence of photoreceptor IS/OS junction appeared more frequently hypo-FAF at SW-FAF and at NIR-FAF.

NIR-FAF is primarily derived from the RPE and the choroid. Increased autofluorescence at NIR-FAF probably identifies areas of increased melanogenesis, melanolipofuscin formation, or increased oxidized melanin: a response to increased phagocytotic activity due to photoreceptors degeneration [69]. It may be speculated that the impairment of photoreceptors, functionally confirmed by microperimetry, determines increased NIR-FAF due to increased phagocytosis and melanogenesis. At this time photoreceptor IS/OS junction is still present. The subsequent reduction of NIR-FAF, due to a decline of melanosomes, is associated to photoreceptor IS/OS disruption. Therefore, it seems that NIR-FAF

imaging better detects not only GA enlargement but also the impairment of both photoreceptors and RPE.

Conclusion

Recent investigations in functional macular damage describe the correlations between morphologic changes and their functional impairment in patients with geographic atrophy. GA model shows that morpho-functional evaluation is useful to detect the progression of this disease and evaluate the efficacy of any therapeutic approach. Retinal sensitivity changes during follow-up of GA are correlated to inner and outer retinal layers thickness changes and to photoreceptor IS/OS junction integrity. FAF pattern remains a relevant parameter in predicting GA evolution. However, different FAF patterns assessed by both SW-FAF and NIR-FAF have different relative risk of evolving to dense scotoma.

References

1. Klein R, Klein BE, Knudtson MD et al (2007) Fifteen-year cumulative incidence of age-related macular degeneration: the Beaver Dam Eye Study. *Ophthalmology* 114:253–262
2. Wang JJ, Rochtchina E, Lee AJ et al (2007) Ten-year incidence and progression of age-related maculopathy: the blue Mountains Eye Study. *Ophthalmology* 114:92–98
3. Augood CA, Vingerling JR, de Jong PT et al (2006) Prevalence of age-related maculopathy in older Europeans: the European Eye Study (EUREYE). *Arch Ophthalmol* 124:529–535
4. Klaver CC, Wolfs RC, Vingerling JR et al (1998) Age-specific prevalence and causes of blindness and visual impairment in an older population: the Rotterdam Study. *Arch Ophthalmol* 116:653–658
5. Sunness JS, Margalit E, Srikrumaran D et al (2007) The long-term natural history of geographic atrophy from age-related macular degeneration. *Ophthalmology* 114:271–277
6. Schatz H, McDonald H (1989) Atrophic macular degeneration: rate of spread of geographic atrophy and visual loss. *Ophthalmology* 96:1541–1551
7. Holz FG, Bindewald-Wittich A, Fleckenstein M et al (2007) Progression of geographic atrophy and impact of fundus autofluorescence patterns in age-related macular degeneration. *Am J Ophthalmol* 143:463–472
8. Cruickshanks KJ, Klein R, Klein BE (1993) Sunlight and age-related macular degeneration. The Beaver Dam Eye Study. *Arch Ophthalmol* 111:514–518
9. Kauper K, McGovern C, Sherman S et al (2012) Two-year intraocular delivery of ciliary neurotrophic factor by encapsulated cell technology implants in patients with chronic retinal degenerative diseases. *Invest Ophthalmol Vis Sci* 53:7484–7491
10. Tseng WA, Thein T, Kinnunen K et al (2013) NLRP3 inflammasome activation in retinal pigment epithelial cells by lysosomal destabilization: implications for age-related macular degeneration. *Invest Ophthalmol Vis Sci* 54:110–120
11. Wong WT, Dresner S, Forooghian F et al (2013) Treatment of geographic atrophy with subconjunctival sirolimus: results of a phase I/II clinical trial. *Invest Ophthalmol Vis Sci* 54:2941–2950
12. Fleckenstein M, Schmitz-Valckenberg S, Sunness JS et al (2013) Geographic atrophy. In: Holz FG, Pauleikhoff D, Spaide R et al (eds) *Age-related macular degeneration*. Springer, Berlin/Heidelberg, pp 121–138
13. Csaky KG, Richman EA, Ferris FL 3rd (2008) Report from the NEI/FDA Ophthalmic Clinical Trial Design and Endpoints Symposium. *Invest Ophthalmol Vis Sci* 49:479–489
14. Pilotto E, Guidolin F, Convento E et al (2013) Fundus autofluorescence and microperimetry in progressing geographic atrophy secondary to age-related macular degeneration. *Br J Ophthalmol* 97:622–626
15. Meleth AD, Mettu P, Agrón E et al (2011) Changes in retinal sensitivity in geographic atrophy progression as measured by microperimetry. *Invest Ophthalmol Vis Sci* 52:1119–1126
16. Querques L, Querques G, Forte R et al (2012) Microperimetric correlations of autofluorescence and optical coherence tomography imaging in dry age-related macular degeneration. *Am J Ophthalmol* 153:1110–1115
17. Sunness JS, Gonzales-Baron J, Applegate CA et al (1999) Enlargement of atrophy and visual acuity loss I geographic atrophy form of age-related macular degeneration. *Ophthalmology* 106:1768–1779
18. Schmitz-Valckenberg S, Fleckenstein M, Helb HM et al (2009) In vivo imaging of foveal sparing in geographic atrophy secondary to age-related macular degeneration. *Invest Ophthalmol Vis Sci* 50:3915–3921
19. Sunness JS, Bressler NM, Maguire MG (1995) Scanning laser ophthalmoscopic analysis of the pattern of visual loss in age-related geographic atrophy of the macula. *Am J Ophthalmol* 119:143–151
20. Hartmann KI, Bartsch DU, Cheng L et al (2011) Scanning laser ophthalmoscope imaging stabilized microperimetry in dry age-related macular degeneration. *Retina* 31:1323–1331
21. Pilotto E, Vujosevic S, Grigic AV et al (2010) Retinal function in patients with serpinginous choroiditis: a microperimetric study. *Graefes Arch Clin Exp Ophthalmol* 248:1331–1333

22. Owsley C, McGwin G, Jackson GR, Kallies K et al (2007) Cone- and rod-mediated dark adaptation impairment in age-related maculopathy. *Am J Ophthalmol* 114:1728–1735
23. Curcio C, Medeiros NE, Millican CL (1996) Photoreceptor loss in age-related macular degeneration. *Invest Ophthalmol Vis Sci* 37:1236–1249
24. Curcio CA, Owsley C, Jackson GR (2000) Spare the rods, save the cones in aging and age-related maculopathy. *Invest Ophthalmol Vis Sci* 41:2015–2018
25. Sunness JS, Rubin GS, Applegate CA et al (1997) Visual function abnormalities and prognosis in eyes with age-related geographic atrophy of the macula and good acuity. *Ophthalmology* 104:1677–1691
26. Sunness JS, Applegate CA (2005) Long-term follow-up of fixation patterns in eyes with central scotomas from geographic atrophy that is associated with age-related macular degeneration. *Am J Ophthalmol* 140:1085–1093
27. Tarita-Nistor L, González EG, Markowitz SN et al (2008) Fixation characteristics of patients with macular degeneration recorded with the mp-1 microperimeter. *Retina* 28:125–133
28. Cacho I, Dickinson CM, Reeves BC et al (2007) Visual acuity and fixation characteristics in age-related macular degeneration. *Optom Vis Sci* 84:487–495
29. Sunness JS (2008) Face fields and microperimetry for estimating the location of fixation in eyes with macular disease. *J Vis Impair Blind* 102:679–689
30. Sunness JS (2007) Atrophic age-related macular degeneration. In: Midena E (ed) *Perimetry and the fundus: an introduction to microperimetry*. Slack Incorporated, Thorofare, pp 67–73
31. Bellmann C, Feely M, Crossland MD et al (2004) Fixation stability using central and pericentral fixation targets in patients with age-related macular degeneration. *Ophthalmology* 111:2265–2270
32. Crossland MD, Dunbar HM, Rubin GS (2009) Fixation stability measurement using the MP1 microperimeter. *Retina* 29:651–656
33. Ishiko S, van de Velde F, Yoshida A (2010) Paradoxical improvement of visual acuity in macular disease. *Curr Eye Res* 35:651–656
34. Shah VA, Chalam KV (2009) Values for macular perimetry using the MP-1 microperimeter in normal subjects. *Ophthalmic Res* 41:9–13
35. Schmitz-Valckenberg S, Fleckenstein M, Scholl HPN et al (2009) Fundus autofluorescence and progression of age-related macular degeneration. *Surv Ophthalmol* 54:96–117
36. Pilotto E, Vujosevic S, Melis R et al (2011) Short wavelength fundus autofluorescence versus near-infrared fundus autofluorescence, with microperimetric correspondence, in patients with geographic atrophy due to age-related macular degeneration. *Br J Ophthalmol* 95:1140–1144
37. Delori FC, Dorey CK, Staurengi G et al (1995) In vivo fluorescence of the ocular fundus exhibits retinal pigment epithelium lipofuscin characteristics. *Invest Ophthalmol Vis Sci* 36:718–729
38. Lois N, Owens SL, Coco R et al (2002) Fundus autofluorescence in patients with age-related macular degeneration and high risk of visual loss. *Am J Ophthalmol* 133:341–349
39. Keilhauer CN, Delori FC (2006) Near-infrared autofluorescence imaging of the fundus: visualization of ocular melanin. *Invest Ophthalmol Vis Sci* 47:3556–3564
40. Schmitz-Valckenberg S, Brinkmann CK, Alten F et al (2011) Semiautomated image processing method for identification and quantification of geographic atrophy in age-related macular degeneration. *Invest Ophthalmol Vis Sci* 52:7640–7646
41. Holz FG, Bellman C, Staudt S et al (2001) Fundus autofluorescence and development of geographic atrophy in age-related macular degeneration. *Invest Ophthalmol Vis Sci* 42:1051–1056
42. Holz FG, Bellmann C, Margaritidis M et al (1999) Patterns of increased in vivo fundus autofluorescence in the junctional zone of geographic atrophy of the retinal pigment epithelium associated with age-related macular degeneration. *Graefes Arch Clin Exp Ophthalmol* 237:145–152
43. Fleckenstein M, Schmitz-Valckenberg S, Adrion C et al (2011) Progression of age-related geographic atrophy: role of the fellow eye. *Invest Ophthalmol Vis Sci* 52:6552–6657
44. Sunness JS, Ziegler MD, Applegate CA (2006) Issues in quantifying atrophic macular disease using retinal autofluorescence. *Retina* 26:666–672
45. Gibbs D, Cideciyan AV, Jacobson SG et al (2009) Retinal pigment epithelium defects in humans and mice with mutation in MYO7A: imaging melanosome-specific autofluorescence. *Invest Ophthalmol Vis Sci* 50:4386–4393
46. Kellner U, Kellner S, Weinitz S (2010) Fundus autofluorescence (488 nm) and near-infrared autofluorescence (787 nm) visualize different retinal pigment epithelium alterations in patients with age-related macular degeneration. *Retina* 30:6–15
47. Forte R, Querques G, Querques L et al (2012) Multimodal imaging of dry age-related macular degeneration. *Acta Ophthalmol* 90:281–287
48. Kellner S, Kellner U, Weber BH et al (2009) Lipofuscin- and melanin-related fundus autofluorescence in patients with ABCA4-associated retinal dystrophies. *Am J Ophthalmol* 147:895–902
49. Beareilly S, Chau FY, Koreishi A et al (2009) Spectral domain optical coherence tomography imaging of geographic atrophy margins. *Ophthalmology* 116:1762–1769
50. Brar M, Kozak I, Cheng L et al (2009) Correlation between spectral-domain optical coherence tomography and fundus autofluorescence at the margins of geographic atrophy. *Am J Ophthalmol* 148:439–444
51. Fleckenstein M, Charbel Issa P, Helb HM et al (2008) High-resolution spectral domain-OCT imaging in geographic atrophy associated with age-related macular degeneration. *Invest Ophthalmol Vis Sci* 49:4137–4144

52. Fleckenstein M, Schmitz-Valckenberg S, Adrion C et al (2010) Tracking progression with spectral-domain optical coherence tomography in geographic atrophy caused by age-related macular degeneration. *Invest Ophthalmol Vis Sci* 51:3846–3852
53. Helb HM, Charbel Issa P, Fleckenstein M et al (2010) Clinical evaluation of simultaneous confocal scanning laser ophthalmoscopy imaging combined with high-resolution, spectral-domain optical coherence tomography. *Acta Ophthalmol* 88:842–849
54. Wolf-Schnurrbusch UE, Enzmann V, Brinkmann CK et al (2008) Morphologic changes in patients with geographic atrophy assessed with a novel spectral OCT-SLO combination. *Invest Ophthalmol Vis Sci* 49:3095–3099
55. Seigo MA, Sotirchos ES, Newsome S et al (2012) In vivo assessment of retinal neuronal layers in multiple sclerosis with manual and automated optical coherence tomography segmentation techniques. *J Neurol* 259:2119–2130
56. Albrecht P, Ringelstein M, Müller AK et al (2012) Degeneration of retinal layers in multiple sclerosis subtypes quantified by optical coherence tomography. *Mult Scler* 18:1422–1429
57. Pilotto E, Benetti E, Convento E et al (2013) Microperimetry, fundus autofluorescence, and retinal layer changes in progressing geographic atrophy secondary to age-related macular degeneration. *Can J Ophthalmol* 2013;48:386–393
58. Monés J, Biarnés M, Trindade F et al (2013) Optical coherence tomography assessment of apparent foveal swelling with foveal sparing secondary to geographic atrophy. *Ophthalmology* 120:829–836
59. Hariri S, Moayed AA, Choh V et al (2012) In vivo assessment of thickness and reflectivity in a rat outer retinal degeneration model with ultrahigh resolution optical coherence tomography. *Invest Ophthalmol Vis Sci* 53:1982–1989
60. Marc RE, Jones BW, Watt CB et al (2008) Extreme retinal remodeling triggered by light damage: implications for age related macular degeneration. *Mol Vis* 14:782–806
61. DiLoreto DA Jr, Martzen MR, del Cerro C et al (1995) Müller cell changes precede photoreceptor cell degeneration in the age-related retinal degeneration of the Fischer 344 rat. *Brain Res* 698:1–14
62. Curcio CA, Messinger JD, Sloan KR et al (2011) Human chorioretinal layer thicknesses measured in macula-wide, high-resolution histologic sections. *Invest Ophthalmol Vis Sci* 52:3943–3954
63. Cohen SY, Dubois L, Nghiem-Buffer S et al (2010) Retinal pseudocysts in age-related geographic atrophy. *Am J Ophthalmol* 150:211–217
64. Sholl HP, Bellman CDS, Bird AC et al (2004) Photopic and scotopic fine matrix mapping of retinal areas of increased fundus autofluorescence in patients with age-related macular degeneration. *Invest Ophthalmol Vis Sci* 45:574–583
65. Schmitz-Valckenberg S, Bültmann S, Dreyhaupt J et al (2004) Fundus autofluorescence and fundus perimetry in the junctional zone of geographic atrophy in patients with age-related macular degeneration. *Invest Ophthalmol Vis Sci* 45:4470–4476
66. McLeod DS, Grebe R, Bhutto I et al (2009) Relationship between RPE and choriocapillaris in age-related macular degeneration. *Invest Ophthalmol Vis Sci* 50:4982–4991
67. Leonard DS, Zhang XG, Panozzo G et al (1997) Clinicopathologic correlation of localized retinal pigment epithelium debridement. *Invest Ophthalmol Vis Sci* 38:1094–1109
68. Korte GE, Reppucci V, Henkind P (1984) RPE destruction causes choriocapillary atrophy. *Invest Ophthalmol Vis Sci* 25:1135–1145
69. Kayatz P, Thumann G, Luther TT et al (2001) Oxidation causes melanin fluorescence. *Invest Ophthalmol Vis Sci* 42:241–246

Bianca S. Gerendas, Julia S. Kroisamer,
Florian Sulzbacher, and Ursula Schmidt-Erfurth

9.1 Introduction

The progression of neovascular age-related macular degeneration (nAMD), the most frequent macular disease, to a sight-threatening manifestation can nowadays be prevented by modern therapeutic agents. However, early diagnosis and adequate treatment are of crucial importance in the management and prognosis of this disease. Diagnosis can be best made using multimodal ophthalmic imaging in addition to a standard clinical examination. To date no fixed treatment regimen has been identified as good enough for every patient. Individualized treatment regimens will have to be established in the future but until then, monthly disease monitoring based on visual acuity testing and multimodal ophthalmic imaging outcomes will continue to be necessary [1]. Visual acuity testing such as best-corrected visual acuity (BCVA) or microperimetry (MP) can be

used to monitor vision loss. A variety of imaging devices including spectral domain (SD) optical coherence tomography (OCT), fluorescein angiography (FA), color fundus photography (CF), fundus autofluorescence (FAF) imaging, indocyanine green angiography (ICGA), near-infrared autofluorescence (NIA), and red free fundus (RF) imaging are available to monitor pathologic changes in the retina and disease activity. These devices can be used for macular imaging or wide-field imaging depending on the stage of disease, the subtype of choroidal neovascularization (CNV) and the morphologic changes. This chapter gives an overview of the different imaging modalities and its appropriate applications for diagnosing and monitoring nAMD.

9.2 SD-OCT in nAMD

Management of nAMD gained considerably from the introduction of OCT in ophthalmology in the 1990s. SD-OCT, a fast, noninvasive, and high-resolution imaging technique, is currently the most important imaging modality for the diagnosis and monitoring of nAMD. Morphologic alterations seen on SD-OCT together with a clinical examination often allow a first diagnosis of nAMD. SD-OCT and FA complement each other. FA is the gold standard in clinical practice today for distinguishing between CNV subtypes and assessing disease activity [2]. However, it is hoped that less invasive angiographic imaging techniques will be needed as SD-OCT advances.

B.S. Gerendas • J.S. Kroisamer
U. Schmidt-Erfurth, MD (✉) • F. Sulzbacher
Department of Ophthalmology,
Vienna Reading Center, Medical University of Vienna,
Waehringer Guertel 18-20, 1090 Vienna, Austria
e-mail: ursula.schmidt-erfurth@meduniwien.ac.at

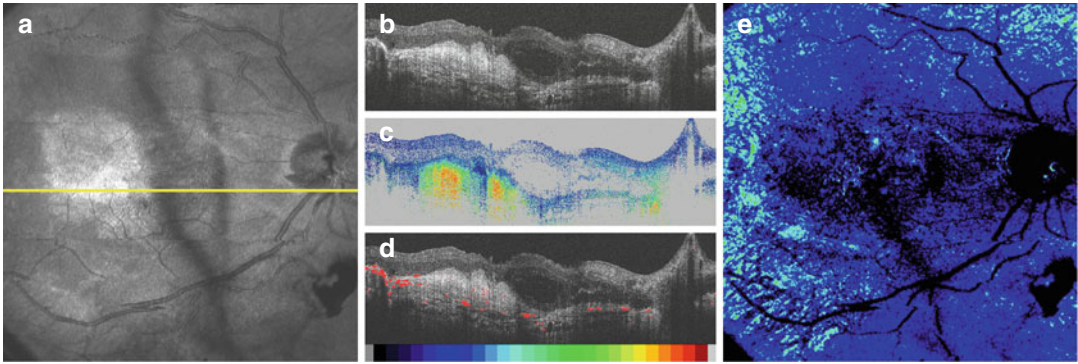


Fig. 9.1 Polarization-sensitive OCT, degenerative cysts. Images of CNV from a patient with fibrotic scarring. (a) Pseudo-SLO $40^\circ \times 40^\circ$. (b) Representative intensity B-scan (location marked in a) showing degenerative cysts. (c) Retardation (color scale: $0\text{--}90^\circ$). (d) Segmented

depolarizing material overlaid to (b) showing RPE defects in fibrotic area. (e) Thickness of depolarizing material (color scale: $0\text{--}160\ \mu\text{m}$) (Images provided by Pircher, M. and Hitzenberger C., Center for Medical Physics and Biomedical Engineering, Medical University of Vienna)

Classification systems based on SD-OCT that do not need FA have already been suggested [3]. Newer SD-OCT technologies currently mostly used for research might replace FA in the long term. Doppler OCT is already able to image retinal vessels but cannot image leakage [4]. Therefore, FA is still of great importance to the ophthalmic community. Polarization-sensitive OCT allows tissues to be distinguished by measuring the stage and change in polarization of different tissues [5]. Thus, retinal pigment epithelium cells, which are often altered in end-stage nAMD within a scar or fibrosis, can be highlighted on OCT scans to distinguish between diseased and healthy tissues (Fig. 9.1). Adaptive optics increase transverse resolution and allow each photoreceptor variation to be analyzed, for example, for toxic effects of the intra- and subretinal fluid of the CNVs [6]. Swept-source imaging speeds image acquisition up to approximately 100,000–350,000 A-scans/sec compared with the 25,000–55,000 A-scans/sec of the SD-OCT devices most commonly used in the clinic today [7, 8]. This helps to overcome bad patient fixation in nAMD. Long-wavelength SD-OCT devices allow a higher penetrance into tissue than short-wavelength OCT and can therefore image the full extent of the choroidal layer or the entire tissue of a CNV, scar, or fibrosis by reducing shadowing effects [9] (Figs. 9.2, 9.3, and 9.4).

Depending on the disease stage, central vision loss which impairs patients' fixation is often a

problem for obtaining good quality images. Current SD-OCT systems overcome the problem either by using an eye tracker or high speeds for fast acquisition in combination with large fixation targets. Large and tightly spaced raster scans allow an extensive overview of the most important anatomical pathologic findings even after fixation loss.

Type I and type II lesions are the most important nAMD subtypes that can be differentiated by SD-OCT and are classified by their localization of CNV. Other subtypes are type III lesions (so-called retinal angiomatous proliferations (RAP lesions) and polypoidal choroidal vasculopathy (PCV) lesions. The most common type I lesions are choroidal neovascularizations localized underneath the retinal pigment epithelium (RPE) (mostly corresponding to occult lesions on FA) above Bruch's membrane. Type I neovascularizations and pure pigment epithelium detachments (PEDs) are hard to distinguish from each other [3]. A fibrovascular pigment epithelial detachment can usually be seen in type I lesions during their silent period. When disease activity increases, exudative processes can be seen on SD-OCT. The most important morphologic findings are subretinal fluid (SRF) and a cystoid macular edema, which appears at a late disease stage. Type II lesions are located subretinal above the RPE (mostly corresponding to classic lesions on FA). They usually originate from beneath the RPE and break through the RPE at some point. The inner-outer photoreceptor segment (IS-OS)

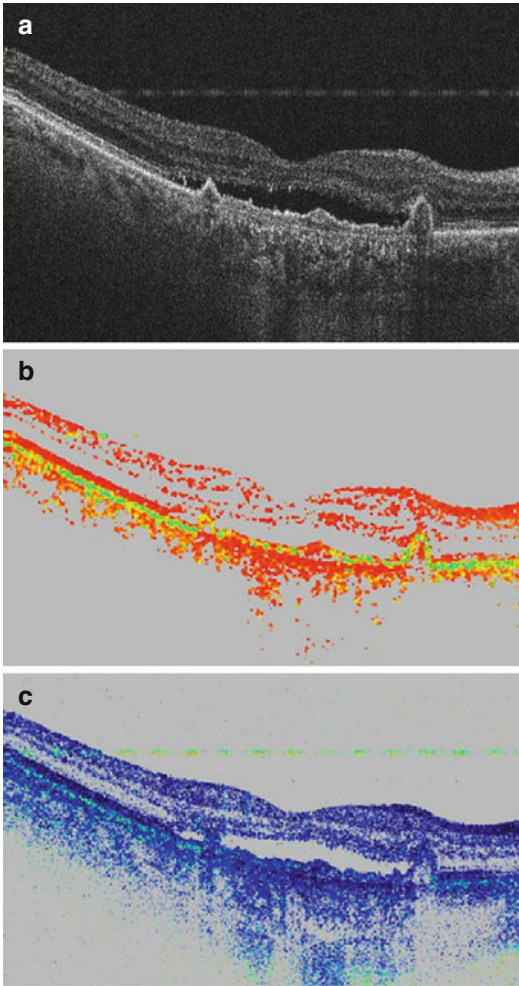


Fig. 9.2 Polarization-sensitive SD-OCT. Images of an active CNV lesion in nAMD from a 1,050-nm polarization sensitive SD-OCT, single frame, no averaging. (a) Representative foveal intensity B-scan showing subretinal fluid. (b) DOPU image with RPE defects. (c) Retardation image (Images provided by Torzicky, T. and Hitzenberger C., Center for Medical Physics and Biomedical Engineering, Medical University of Vienna)

line is therefore often disrupted. Intraretinal cysts (IRC) are usually the first sign of type II lesions. As the disease progresses SRF can be seen and later a subretinal fibrosis. The neurosensory layers are thinned and irreversibly damaged. PCV lesions are a subtype of type I lesions and are therefore also located in the space beneath the RPE. Many PEDs of different sizes can be observed with connective tissue in between them (“bola sign”). A cystoid edema in combination

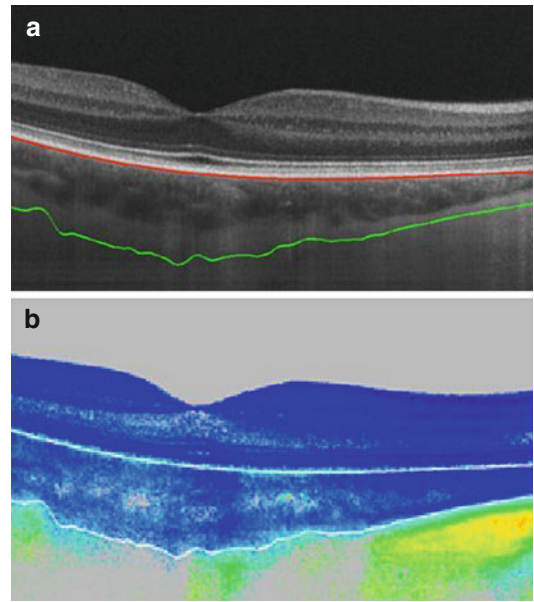


Fig. 9.3 Choroidal imaging. Images of a healthy choroidal layer from a 1,050-nm polarization-sensitive SD-OCT, 50 frames averaged. (a) Representative foveal intensity B-scan showing segmentation of the choroidal layer. (b) Retardation image with segmentation of the choroidal layer (Images provided by Torzicky, T. and Hitzenberger C., Center for Medical Physics and Biomedical Engineering, Medical University of Vienna)

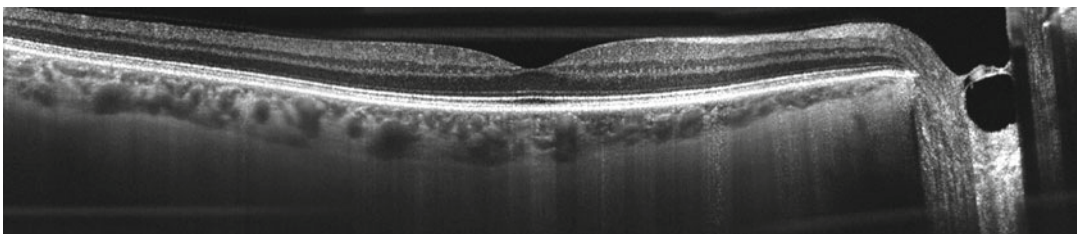


Fig. 9.4 Wide-field SD-OCT. Image of a representative healthy fovea taken with 1,050-nm SD-OCT, 50 frames averaged, 50° scan width (Image provided by Torzicky, T.

and Hitzenberger C., Center for Medical Physics and Biomedical Engineering, Medical University of Vienna)

with a pigment epithelial detachment can often be observed on SD-OCT. It is unclear if RAP lesions originate from retinal or choroidal vessels, but in most cases a retinal-choroidal anastomosis can be seen. A neurosensory cell loss and thinning of outer retinal layers can be seen in the late stages on SD-OCT [3].

Until now evaluation of retinal thickness on OCT has been the gold standard on which to base retreatment decisions during anti-VEGF therapy for nAMD. All OCT devices provide retinal thickness topography maps, which are usually based on the early treatment diabetic retinopathy study (ETDRS) grid. This grid gives an overview of the current state of edema in each of the subfields, most importantly in the foveal central millimeter subfield. All devices have the possibility to correct the foveal position and the automatically segmented thickness values to avoid errors by technical artifacts that are very common in nAMD because of bad patient fixation and various morphologic patterns [10]. In general, thickening and thinning retina are activity signs – thickening indicates exudation and thinning progressive retinal cell loss in atrophy and fibrosis. With the introduction of SD-OCT and its continuous improvement, morphology-based retreatment criteria will become the gold standard in the future. Therefore, besides the quantitative evaluation of retinal thickness, the most important qualitative morphologic findings on SD-OCT in nAMD, which include pathologic RPE configurations like drusen and PEDs, SRF, IRC, fibrosis, and scars, also have to be evaluated.

Drusen and PEDs are mostly the first signs of AMD. They appear long before the wet stages of AMD and are seen long before SRF and cysts. Drusen can be seen more frequently when early AMD stages advance to nAMD and are well described in Chap. 7. PEDs can be distinguished by their size and content, and can roughly be divided into serous PEDs and fibrovascular PEDs. Zayit and colleagues define serous PED secondary to AMD as “a localized, relatively pronounced dome-shaped elevation of the external high reflective band that appears scatter-free, optically empty with sharp margins sometimes

associated with reflections from the deeper choroid” and a fibrovascular PED as “a well-defined elevation of the RPE with a deeper area of back-scattering corresponding to fibrous proliferation” on OCT [11]. The prognosis of a serous PED in nAMD is better than that of a fibrovascular PED. When anti-VEGF therapy is applied, a PED usually contracts and therefore high protruding PEDs have a higher risk of undergoing an RPE rip that leads to a bad prognosis for visual acuity recovery. RPE rips and other abnormal RPE configurations including RPE thickening can also be seen on SD-OCT. In the natural course of a serous PED, the optically empty space becomes more organized and forms into a fibrovascular PED. The prognosis for a full visual acuity recovery is poor, but the risk of an RPE rip decreases in this state.

SRF usually appears in the case of active type I CNV lesions. It accumulates in the space between photoreceptors and RPE, where these lesions are typically located. SRF can also be a sign of the progress of a serous PED without CNV forming a type I CNV lesion [12]. The fluid can be recorded by SD-OCT as a hyporeflective area which is homogenous when it begins and can get denser and gain reflectivity as it persists. SRF is assumed to become increasingly toxic as it gains reflectivity, impairing recovery of visual acuity [13]. SRF is usually either dome-shaped or flat, but when associated with a PED appears as a triangular shape on OCT B-scans surrounding the PED to form a ring around it [12]. Finally, SRF can cover smaller or larger areas and appears in different locations but measurements of its entire volume correlate best with macular function [14].

IRC are seen in advanced nAMD and usually indicate progressed active disease [15]. Typically, treatment is required as fast as possible. IRC, similar to SRF, are hyporeflective areas which are round or oval in shape when they begin and are optically empty as only clear fluid is visible. If blood or other cells accumulate in these cystic areas, they can gain reflectivity. IRC typically appear in the outer nuclear layer, the inner nuclear layer, or the ganglion cell layer. Because of the disease pathway in nAMD, the cysts are highly

likely to appear in the outer layers before they are seen in the inner layers (outer nuclear layer>inner nuclear layer>ganglion cell layer).

Another type, cystic degeneration, should not be confused with IRC in active disease. Degenerative cysts typically appear strictly above disciform scars and fibrotic lesions, when the CNV is no longer active, and are seen with thickened RPE in end-stage nAMD. Cystic degeneration typically appears with a sharp border to the healthy tissue beside it. Visual acuity recovery at this disease stage is highly improbable.

Other features in addition to the morphologic structures that are well-established as disease modulators and were identified during the era of time domain OCT are also assumed to be important in the course of nAMD. These can only be seen with the possibilities of high-resolution SD-OCT. Recent studies have shown that the vitreomacular interface configuration has a substantial impact on the therapeutic effect of intravitreal drugs [16, 17]. Disruption of the so-called external limiting membrane (ELM), IS-OS line, and the photoreceptor end tips is also an important morphologic criterion when evaluating the possible recovery of visual function in nAMD [18, 19]. Microfoci are strongly hyperreflective speckles that are assumed to be micro-exudates because they have a polarizing character on polarization-sensitive SD-OCT similar to hard exudates that can be seen macroscopically and appear in early and advanced nAMD [20, 21].

Because unlike FA, SD-OCT is noninvasive, it can be applied frequently and is not only the modality of choice for diagnosis but also for disease monitoring, follow-up examinations, and (re-)treatment decisions. The smallest traces of intraretinal fluid and the smallest changes in the configuration of the retinal structures and the CNV can be monitored.

9.3 FA in nAMD

FA is still the gold standard imaging modality for the diagnosis of nAMD. A hyperfluorescent leakage from the retinal vessels into the surrounding

retinal and subretinal tissue is noted in all nAMD types. CNVs can be classified into different subtypes and its localization in the macula can be subfoveal, juxtafoveal, or extrafoveal [22]. Not only the recently proposed SD-OCT classification system but also the established FA classification system distinguishes between lesion types, which are classic and occult lesions [3]. Classic lesions are those that have penetrated the RPE and therefore appear in the subretinal space (mostly corresponding to type II lesions on SD-OCT). Occult lesions are seen in the sub-RPE compartment “hiding” below the RPE (mostly corresponding to type I lesions on SD-OCT). Classic lesions progress faster than occult lesions and impair BCVA more but as known from the past (the laser era of nAMD treatment), they also respond better to laser therapy. This seems less important in the current anti-VEGF era for nAMD treatment [22]. The terms predominantly classic and minimally classic are a more distinct way of subdividing mixed CNV lesions in FA. Predominantly classic lesions are where more than half of the area of the lesion is classified as “classic” and minimally classic lesions are where less than half of the area of the lesion is classified as “classic” [23].

A typical finding in FA in nAMD is a bright uniform hyperfluorescence intensifying throughout the FA phases and leaking in the late FA phase (classic lesion), a stippled hyperfluorescence from a fibrovascular PED in mid-phase FA that also leads to late-phase FA leakage but is more distinct in character than a classic lesion (first type of occult lesion), or late-phase leakage of undetermined source (second type of occult lesion) that does not correspond to any pathologic structure in the early or mid-phase (Fig. 9.5). If other pathophysiologic features are seen in a patient (hemorrhage, pigment, scar, serous PED), the leakage may be blocked or intensified when it can mask the CNV. This is an additional factor that has to be taken into account when measuring the size of the CNV lesion. The contrast between the CNV lesion in FA and the rest of the retina can be described as poorly defined/demarcated or well defined/demarcated, but these definitions do not state anything about the lesion type [23].

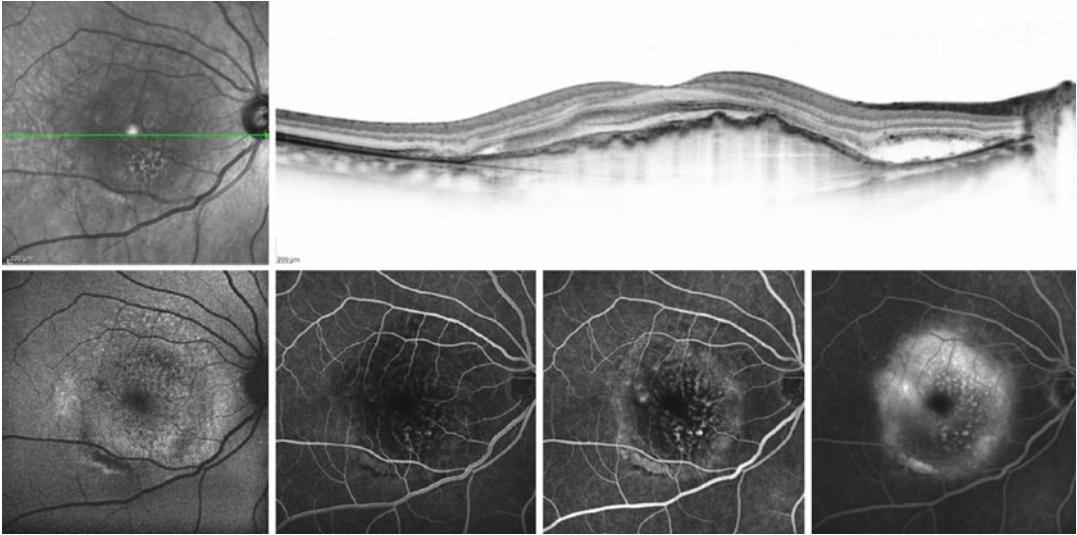


Fig. 9.5 Multimodal imaging in nAMD. Foveal SD-OCT B-scan from a patient with occult-type CNV (not entirely visible on foveal scan) with infrared fundus image (*top*), corresponding FAF image (*bottom left*), and early-, mid-, and late-phase FA images (*bottom two middle* images and *right* image); the size of the diseased area cannot be

estimated on the infrared image; the area can be estimated roughly on the FAF image and can be confirmed by FA imaging the fibrovascular PED with late-phase leakage (occult CNV) (Images provided by Vienna Study Center, Department of Ophthalmology and Optometry, Medical University of Vienna)

FA is also important when looking at the prognosis of nAMD treatment. Individualized anti-VEGF treatment with the medication, dose, and dosing interval matching the needs of each patient is growing in importance over the uniform dose and dosing scheme of standard medication. Recent studies suggest that, for example, a larger CNV area and a (predominantly/minimally) classic lesion predict that the gain in visual acuity score will not be so high as for smaller and occult/RAP lesions after 1 year of anti-VEGF therapy [24].

9.4 ICGA and Choroidal Imaging in nAMD

ICGA is especially important in nAMD when the patient is suspected to have PCV lesions. These lesions were originally described as a choroidal disorder but are now believed to be a subtype of neovascularizations seen in the sub-RPE compartment. PCV lesions are seen as choroidal polyps on ICGA [25]. In the occult/type I nAMD subtype, hyperfluorescent plaques can be seen on ICGA; other types of CNV lesions often show as nonspecific hot spots in ICGA [26].

Recently, other techniques of choroidal imaging have been established. The choroid has been of great interest and many ongoing studies give reason to expect more interesting findings about the choroidal layer in nAMD that will attach value to this layer. Clinicians and scientists can use SD-OCT not only for an en face picture of the choroidal structures as seen in ICGA but also for a three-dimensional picture of this important layer. Polarization-sensitive OCT detects the choroidal-scleral interface by using the birefringence of the sclera to measure the choroidal thickness between the depolarizing RPE and the sclera [27] (Fig. 9.3). Long-wavelength SD-OCT operating at 1050 nm allows a higher penetration and therefore high accuracy in thickness measurements than short-wavelength SD-OCT [8, 28] (Figs. 9.2, 9.3, and 9.4). Another possibility is to use the enhanced depth imaging (EDI) mode in standard clinical SD-OCT devices. EDI involves setting the choroid adjacent to the zero delay line, which allows enhanced visualization of the choroid down to the sclera by preventing the disadvantages of the sensitivity roll-off characteristics of SD-OCT systems [28]. This mode still operates

at a short-wavelength though without higher depth penetration like long-wavelength SD-OCT.

9.5 Wide-Field Imaging in nAMD

Wide-field imaging has gained interest in the past few years since the introduction of wide-field imaging lenses for angiography and fundus photography. The most important use of wide-field imaging in nAMD is for discovering very rare peripheral choroidal neovascularizations and potentially finding peripheral ischemic areas. Peripheral drusen and autofluorescence patterns can also be imaged (see below “FAF in nAMD”) [29].

SD-OCT imaging also advances to wider areas. The regular field of imaging in today’s most common clinical OCTs is 20° (~6 mm scan width, covering approximately the size of the macula). Newer devices scan areas up to 50° covering the entire posterior pole including the macula, optic nerve head, and parts of the retinal periphery. The scans allow better assessment of the curvature of the posterior pole and interpretation of the vitreoretinal interface as a whole because they give an impressive overview of vitreous adhesion, traction, and release from the retina [30] (Fig. 9.4).

9.6 CF, FAF, RF, and NIA in nAMD

CF, FAF, RF, and NIA use different technical methods but all capture a two-dimensional en face image of the retina. CF is regular photography, RF uses a red free light source for image capturing, and FAF and NIA autofluorescence patterns at different wavelengths. Although they use different techniques, they can be described in this chapter because their images have similar two-dimensional en face appearances for the clinician.

Color fundus images can capture most alterations that can be seen in funduscopy. The most important findings in nAMD are hemorrhage, exudates, edema, drusen, pigment changes, disciform scars, and atrophy. They correlate with funduscopy findings and are therefore not explained separately in this chapter.

In general, blockage by SRF, CNV, or hemorrhage reduces autofluorescence in FAF or NIA imaging. Exudative activity can usually be observed better on FAF images because it induces hyper-autofluorescence [31] (Fig. 9.5).

FAF shows up differently in nAMD. PEDs that are hypofluorescent on FA are hyper-autofluorescent in FAF images. Old PEDs also tend to show increased autofluorescence, which even persists after regression of the PED. CNVs show irregular autofluorescence being hypo- and hyper-autofluorescent in some areas. The edges usually show as increased autofluorescence and disciform scars as decreased autofluorescence [32]. In most cases of CNV, a hypoautofluorescent central area is surrounded by a hyper-autofluorescent ring forming a halo-like shape [33]. Recent studies found that when the area of imaging is extended from the usual central 20–30° to wide-field peripheral imaging, granular (discrete areas of bright, increased hyper-autofluorescence), nummular (small to medium areas of discrete, uniformly decreased autofluorescence), and mottled (areas of generally decreased autofluorescence) peripheral autofluorescence patterns can be seen in nAMD [29].

NIA imaging can be useful, for example, in nAMD for early diagnosis of an RPE rip. Recent studies found that NIA imaging can predict an RPE rip in 87 % of the cases on average 2 months before its appearance [34]. Most nAMD CNV lesions show as a bright area with a dark halo around the lesion, often identically to the leakage area on FA. Classic CNV lesions are usually well bordered and show as a bright ring around the lesion. This ring is less bright in predominantly or minimally classic lesions in the occult part. Occult lesions do not show a sharp border on NIA images. RAP lesions show a speckled focal increase on NIA images. After anti-VEGF treatment, NIA can increase as leakage decreases [35]. The bright appearance of lipids which can be seen on RF images (see below) in vascularized PEDs of type I CNV can also be seen on NIA images [36].

RF imaging is important when imaging retinal lipids, which, for example, are seen in vascularized PEDs as layered hyperreflective bands in the sub-RPE space on SD-OCT, mostly in type I CNV. This is called the “onion sign.” The lipids

are seen as yellow-gray exudates on CF images and through a funduscope, but have a bright appearance on RF (and NIA) images [36].

9.7 MP in nAMD

As discussed above, the clinical course of nAMD is multifactorial and is marked by a series of morphological changes in the retina, below the retina, at the level of the RPE, and even in the choroidal layers. These changes include CNV, SRF, IRC, and PEDs but their progression leading to a substantial visual function loss is unpredictable. Present therapy targets the inhibition of VEGF as one of the leading pathogenic factors in the development and progression of nAMD [37, 38]. Therapy decision is currently made based on

fluid detection in clinical examination and OCT or visual acuity variations in BCVA. MP is one way of testing visual acuity. Based on the concept of structure-function correlation, MP can provide useful additional information to that obtained with other imaging modalities [39].

MP can particularly give insight into disease pathways and help to identify structures that in addition to the aforementioned might be important for visual acuity and predicting visual function worsening and the possibility of its recovery after therapy (Fig. 9.6). With most MP devices, however, a retinal sensitivity map that can be superimposed manually on SD-OCT data cannot be extracted. This would allow a point-to-point analysis of morphological findings and the impact of microstructural alterations on visual function at corresponding spots.

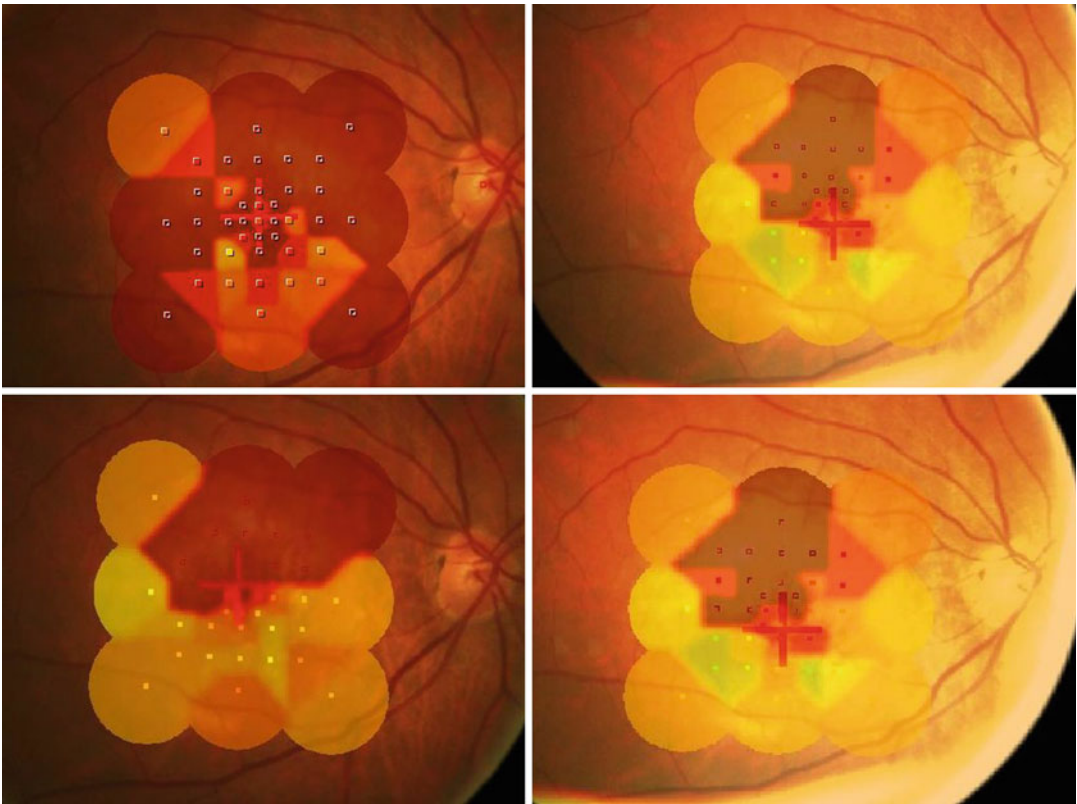


Fig. 9.6 Changes in microperimetry. Patient showing an occult CNV lesion. At baseline (*top left*) there is a total functional loss beneath the neovascular complex lesion site. After 3 months (*bottom left*) of anti-VEGF therapy, the macular edema was resorbed completely and a

functional benefit can be detected. Function increases in month 6 (*top right*) and month 9 (*bottom right*) of therapy (Images provided by Vienna Study Center, Department of Ophthalmology and Optometry, Medical University of Vienna)

Evaluation of treatment-naïve CNV lesions due to nAMD revealed that a neovascular complex is associated with a complete loss of macular function, independent of the presence of cysts or diffuse intraretinal fluid. Detailed analyses at these sites showed disrupted RPE and absent photoreceptor integrity. Sites of macular edema presenting as SRF, IRC, or diffuse macular edema alone were characterized by a moderate

loss of retinal function with no marked differences in the degree of severity between the compartment locations, whereas the combined manifestation of SRF and diffuse macular edema was associated with severe loss of macular function. An isolated PED was associated with variable macular sensitivity. A serous PED had a greater deficiency of macular function than a fibrovascular PED [40] (Fig. 9.7).

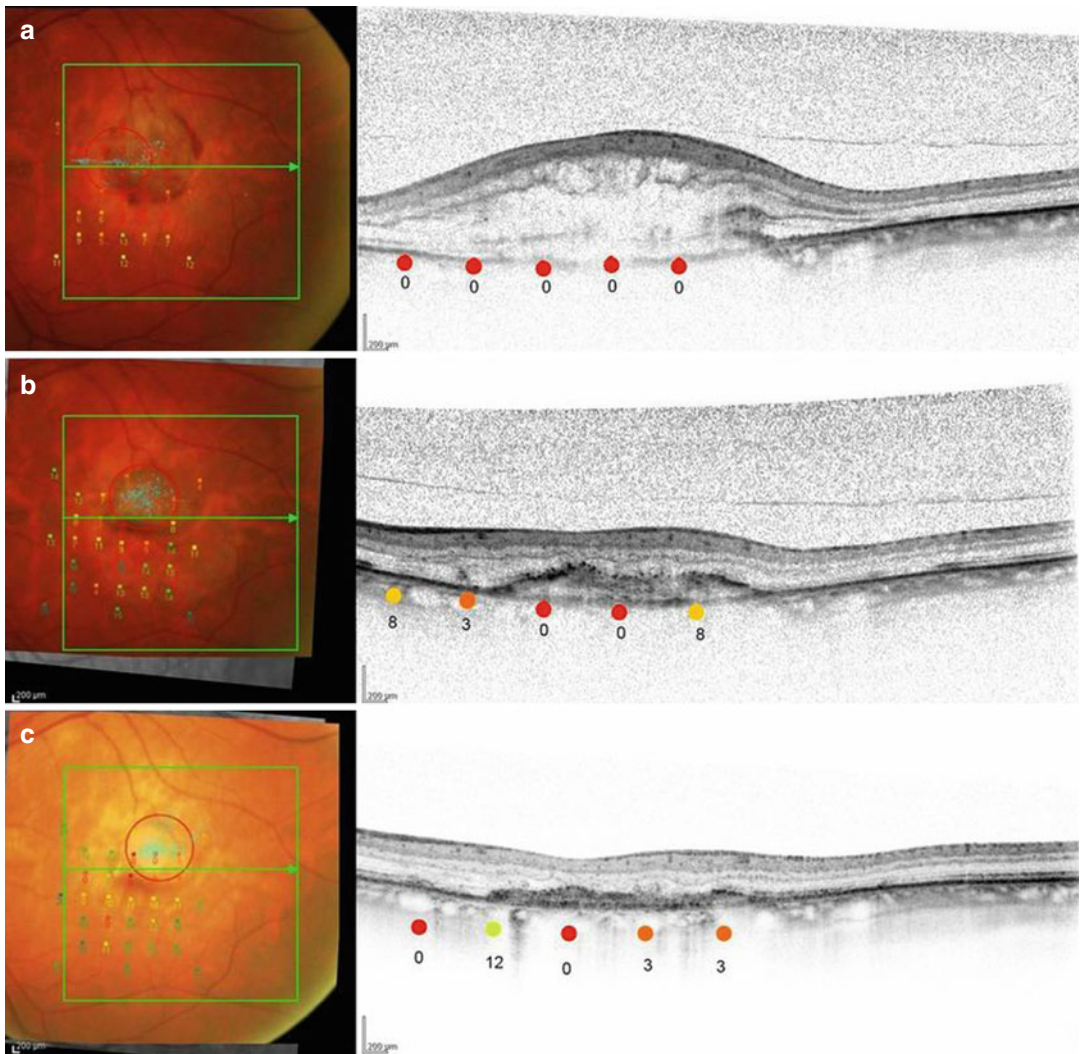


Fig. 9.7 Microperimetry in nAMD. SD-OCT B-scans of CNV with corresponding retinal sensitivity values in decibel (dB) measured by microperimetry (spot size 132 μ m). Scan from a 69-year-old male patient with classic CNV showing a neovascular complex with additional intraretinal cystoid space. At baseline (a) there is a total functional

loss beneath the neovascular complex lesion site. After 3 months (b) and after 12 months (c), macular edema have been completely resorbed leaving a fibrotic scar. The functional benefit of anti-VEGF therapy was limited, but measurable (Image from Sulzbacher et al. [41])

Modern SD-OCT and MP devices allow a very sensitive follow-up using a tracking mode with a reference examination. This makes it possible to re-examine the exact same position on the retina after a certain time to monitor changes at a certain point of interest. If the device does not allow this superimposition, overlay with an SD-OCT is possible with external software. In this way, the response of each initial morphologic alteration to treatment and its specific visual acuity can be investigated.

An initial CNV without cysts may resolve after monthly anti-VEGF treatment to a normal retinal configuration with a marked functional benefit, whereas a CNV with additional cysts is associated with fibrosis development and a reduced functional response in MP. Retinal fluid, regardless of its location, is associated with a substantial functional benefit from treatment, whereas a PED predicts various outcomes with a better benefit in the case of a serous PED and a lower benefit in the case of fibrovascular PED. This corresponds to the disease state. CNVs including IRC and a fibrovascular PED are advanced stages of nAMD, which in MP indicate a low probability that treatment will result in improved visual function outcomes [41].

An appropriate method to identify photoreceptor functional and morphological damage, such as a tracked, tightly spaced, high-resolution raster scanning SD-OCT with integrated MP, and the possibility of an exact definition of which points in SD-OCT to monitor during the MP examination must be found, either by improving an existing or establishing a new method. This is of fundamental importance for the future when decisions about treatment and retreatment will be made based on predictions of the morphologic treatment response and functional prognosis of each individual patient.

References

1. Frampton J (2013) Ranibizumab: a review of its use in the treatment of neovascular age-related macular degeneration. *Drugs Aging* 30:331–358
2. Geitzenauer W, Hitzemberger CK, Schmidt-Erfurth UM (2011) Retinal optical coherence tomography: past, present and future perspectives. *Br J Ophthalmol* 95:171–177
3. Freund KB, Zweifel SA, Engelbert M (2010) Do we need a new classification for choroidal neovascularization in age-related macular degeneration? *Retina* 30:1333–1349
4. Blatter C, Klein T, Grajciar B et al (2012) Ultrahigh-speed non-invasive widefield angiography. *J Biomed Opt* 17:070505–070501
5. Pircher M, Hitzemberger CK, Schmidt-Erfurth U (2011) Polarization sensitive optical coherence tomography in the human eye. *Prog Retin Eye Res* 30(6):431–451
6. Felberer F, Kroisamer J-S, Hitzemberger CK et al (2012) Lens based adaptive optics scanning laser ophthalmoscope. *Opt Express* 20:17297–17310
7. Liu JJ, Grulkowski I, Kraus MF et al (2013) In vivo imaging of the rodent eye with swept source/Fourier domain OCT. *Biomed Opt Express* 4:351–363
8. Torzicky T, Marschall S, Pircher M et al (2013) Retinal polarization-sensitive optical coherence tomography at 1060 nm with 350 kHz A-scan rate using an Fourier domain mode locked laser. *J Biomed Opt* 18:026008–026008
9. Torzicky T, Pircher M, Zotter S et al (2012) High-speed retinal imaging with polarization-sensitive OCT at 1040 nm. *Optom Vis Sci* 89:585–592, 510.1097/OPX.1090b1013e31825039be
10. Han IC, Jaffe GJ (2010) Evaluation of artifacts associated with macular spectral-domain optical coherence tomography. *Ophthalmology* 117:1177–1189. e1174
11. Zayit-Soudry S, Moroz I, Loewenstein A (2007) Retinal pigment epithelial detachment. *Surv Ophthalmol* 52:227–243
12. Bolz M, Simader C, Ritter M et al (2010) Morphological and functional analysis of the loading regimen with intravitreal ranibizumab in neovascular age-related macular degeneration. *Br J Ophthalmol* 94:185–189
13. Ahlers C, Golbaz I, Einwallner E et al (2009) Identification of optical density ratios in subretinal fluid as a clinically relevant biomarker in exudative macular disease. *Invest Ophthalmol Vis Sci* 50: 3417–3424
14. Golbaz I, Ahlers C, Stock G et al (2011) Quantification of the therapeutic response of intraretinal, subretinal, and subpigment epithelial compartments in exudative AMD during anti-VEGF therapy. *Invest Ophthalmol Vis Sci* 52:1599–1605
15. Giani A, Luiselli C, Esmaili DD et al (2011) Spectral-domain optical coherence tomography as an indicator of fluorescein angiography leakage from choroidal neovascularization. *Invest Ophthalmol Vis Sci* 52(8):5579–5586
16. Mayr-Sponer U, Waldstein S, Kundi M et al (2013) Influence of the vitreomacular interface on outcomes of ranibizumab therapy in neovascular age-related macular degeneration. *Ophthalmology*. pii: S0161-6420(13)00489-2. doi:10.1016/j.ophtha.2013.05.032

17. Waldstein S, Mayr-Sponer U, Ritter M et al (2013) Impact of the vitreous configuration on the efficacy of quarterly, pro-re-nata and monthly treatment in multi-center trials evaluating ranibizumab for neovascular age-related macular degeneration, ARVO Abstract 3818. In: ARVO annual meeting 2013, Seattle
18. Shin HJ, Chung H, Kim HC (2011) Association between foveal microstructure and visual outcome in age-related macular degeneration. *Retina* 31:1627–1636, 1610.1097/IAE.1620b1013e31820d31823d31801
19. Spaide RF, Curcio CA (2011) Anatomical correlates to the bands seen in the outer retina by optical coherence tomography: literature review and model. *Retina* 31:1609–1619, 1610.1097/IAE.1600b1013e3182247535
20. Bolz M, Schmidt-Erfurth U, Deak G et al (2009) Optical coherence tomographic hyperreflective foci: a morphologic sign of lipid extravasation in diabetic macular edema. *Ophthalmology* 116:914–920
21. Lammer J, Bolz M, Baumann B et al Detection and analysis of hard exudates by polarization sensitive optical coherence tomography in patients with diabetic maculopathy (unpublished data)
22. Lim LS, Mitchell P, Seddon JM et al (2012) Age-related macular degeneration. *Lancet* 379:1728–1738
23. American Academy of Ophthalmology (2012) Age-related macular degeneration and other causes of choroidal neovascularization. In: Basic and clinical science course, section 12: Retina and vitreous, part II, chapter 4, subchapter: Neovascular AMD. American Academy of Ophthalmology, San Francisco, pp 63–70
24. Ying G-S, Huang J, Maguire MG et al (2013) Baseline predictors for one-year visual outcomes with ranibizumab or bevacizumab for neovascular age-related macular degeneration. *Ophthalmology* 120:122–129
25. Koh AHC, Chen L-J, Chen S-J et al (2013) Polypoidal choroidal vasculopathy: evidence-based guidelines for clinical diagnosis and treatment. *Retina* 33:686–716, 610.1097/IAE.1090b1013e3182852446
26. Cachulo L, Silva R, Fonseca P et al (2011) Early markers of choroidal neovascularization in the fellow eye of patients with unilateral exudative age-related macular degeneration. *Ophthalmologica* 225:144–149
27. Torzicky T, Pircher M, Zotter S et al (2012) Automated measurement of choroidal thickness in the human eye by polarization sensitive optical coherence tomography. *Opt Express* 20:7564–7574
28. Adhi M, Duker JS (2013) Optical coherence tomography-current and future applications. *Curr Opin Ophthalmol* 24:213–221
29. Tan CS, Heussen F, Sadda SR (2013) Peripheral autofluorescence and clinical findings in neovascular and non-neovascular age-related macular degeneration. *Ophthalmology* 120(6):1271–1277
30. Pircher M, Zotter S, Roberts P et al (2012) Imaging of retinal lesions in age related macular degeneration using wide field polarization sensitive optical coherence tomography. In: Biomedical Optics, Biomed Poster Session II (BTu3A), Optical Society of America, Miami, 28 Apr – 2 May 2012, p BTu3A.71. doi:[10.1364/BIOSED.2012.BTu3A.71](https://doi.org/10.1364/BIOSED.2012.BTu3A.71)
31. Kellner U, Kellner S, Weinitz S (2010) Fundus autofluorescence (488 nm) and near-infrared autofluorescence (787 nm) visualize different retinal pigment epithelium alterations in patients with age-related macular degeneration. *Retina* 30:6–15. doi:[10.1097/IAE.1090b1013e3181b8348b](https://doi.org/10.1097/IAE.1090b1013e3181b8348b)
32. Von Rückmann A, Fitzke FW, Bird AC (1997) Fundus autofluorescence in age-related macular disease imaged with a laser scanning ophthalmoscope. *Invest Ophthalmol Vis Sci* 38:478–486
33. Semoun O, Guigui B, Tick S et al (2009) Infrared features of classic choroidal neovascularisation in exudative age-related macular degeneration. *Br J Ophthalmol* 93:182–185
34. Bastian N, Fonseca S, Clemens CR et al (2013) Prädiktive Nahinfrarot-SLO-Merkmale für Risse des retinalen Pigmentepithels bei altersabhängiger Makuladegeneration. *Klin Monatsbl Augenheilkd* 230:270–274
35. Theelen T, Berendschot TJM, Hoyng C et al (2009) Near-infrared reflectance imaging of neovascular age-related macular degeneration. *Graefes Arch Clin Exp Ophthalmol* 247:1625–1633
36. Mulkamala SK, Costa RA, Fung A, Sarraf D, Gallego-Pinazo R, Freund KB (2012) Optical coherence tomographic imaging of sub-retinal pigment epithelium lipid. *Arch Ophthalmol* 130:1547–1553
37. Schmidt-Erfurth UM, Richard G, Augustin A et al (2007) Guidance for the treatment of neovascular age-related macular degeneration. *Acta Ophthalmol Scand* 85:486–494
38. Heier JS, Brown DM, Chong V et al (2012) Intravitreal aflibercept (VEGF trap-eye) in wet age-related macular degeneration. *Ophthalmology* 119:2537–2548
39. Charbel Issa P, Troeger E, Finger R et al (2010) Structure-function correlation of the human central retina. *PLoS One* 5:e12864
40. Sulzbacher F, Kiss C, Kaider A et al (2012) Correlation of SD-OCT features and retinal sensitivity in neovascular age-related macular degeneration. *Invest Ophthalmol Vis Sci* 53:6448–6455
41. Sulzbacher F, Kiss C, Kaider A et al (2013) Correlation of OCT characteristics and retinal sensitivity in neovascular age-related macular degeneration in the course of monthly ranibizumab treatment. *Invest Ophthalmol Vis Sci* 54:1310–1315

Elsbeth J.T. van Zeeburg, Matteo G. Cereda,
Leigh H. Spielberg, and Jan C. van Meurs

10.1 Introduction

This chapter explores the use of microperimetry in patients with exudative age-related macular degeneration (AMD) who have undergone a retinal pigment epithelium (RPE) and choroid graft translocation. Microperimetric data are analyzed and correlated with other more conventional imaging and examination techniques.

The spectral domain optical coherence tomography (SD-OCT) and phase-resolved Doppler OCT have been used to detect early revascularization of an RPE-choroid graft by a noninvasive method [1, 2]. Changes in the vascular structure of the graft can be visualized using the SD-OCT, and intravascular flow can be measured in the vessels of the graft using the Doppler OCT [1, 2]. This demonstration of graft

revascularization is valuable information, as a non-perfused graft will dysfunction and visual acuity will deteriorate [3].

However, successful functional outcome of RPE-choroid graft surgery depends not only on graft perfusion. Other factors include the extent of preoperative RPE damage and the condition of the overlying retina, with patient selection and the peroperative course weighing as major factors [4]. In patients with a perfused graft, visual acuity (VA) varies widely [5]. Visual acuity alone, however, is only one measure of graft function and does not necessarily correlate with the patient's visual function. Besides microperimetry, other measures, such as metamorphopsia, reading visual acuity, contrast sensitivity, and quality of life might correlate with graft function.

The microperimeter is able to accurately determine retinal sensitivity, measured in dB, over the graft with high specificity, which may help to interpret functional and anatomical changes [5–14].

Using three well-documented patients as examples, the potential advantages of microperimetry are discussed below. Limitations and difficulties in patients with low visual acuity will also be discussed, with suggestions of potential improvements of the technique.

E.J.T. van Zeeburg (✉) • L.H. Spielberg
J.C. van Meurs
Department of Ophthalmology,
The Rotterdam Eye Hospital,
Rotterdam, The Netherlands
e-mail: e.vanzeeburg@oogziekenhuis.nl

M.G. Cereda
Eye Clinic, Department of Clinical Science
“Luigi Sacco”, Sacco Hospital, University of Milan,
Milan, Italy

10.2 Patients and Methods

Transplantation of free grafts of RPE and choroid after removal of the submacular neovascular complex has previously been shown to be effective in some patients with advanced exudative AMD [2, 5, 12, 13, 15–17]. Patients eligible for this surgery were patients who presented with a large submacular hemorrhage but who were ineligible for treatment with recombinant tissue plasminogen activator, patients with an RPE tear or macular fibrosis, and patients who have not responded to less invasive treatment such as anti-vascular endothelial growth factor [8, 18–20].

During surgery a full-thickness graft of autologous midperipheral RPE, Bruch's membrane, choriocapillaris, and choroid was harvested and placed under the macula via a retinotomy in the raphe, using either an aspiration-reflux spatula or fine or bent forceps (Dutch Ophthalmic Research Center [DORC], Zuidland, The Netherlands) [2, 5, 21]. At the end of surgery, silicone oil was used as a tamponade, which was removed approximately 3 months later. Lensectomy or phacoemulsification and insertion of an intraocular lens was performed in phakic patients during first or second surgery [2, 5, 13].

Pre- and/or postoperative examination of RPE-choroid graft patients was performed using the MP-1 microperimeter (Nidek Technologies, Padova, Italy), and the results were integrated with spectral domain optical coherence tomography (SD-OCT) (Spectralis HRA; Heidelberg engineering, Heidelberg, Germany), autofluorescence (AF) (Spectralis HRA; Heidelberg engineering, Heidelberg, Germany, or TOPCON, Tokyo, Japan), and fluorescein angiogram (FA) images (TOPCON, Tokyo, Japan).

10.3 Results

10.3.1 Exact Location of Function and Dysfunction

Retinal sensitivity can be determined with the microperimeter with high specificity [5–14].

These data can be used to help interpret functional and anatomical changes.

Patient 1 presented with a submacular hemorrhage and an RPE-tear due to age-related macular degeneration (Fig. 10.1a–c). VA was 1.32 logMAR. The patient was unable to perform the Radner reading acuity test, and the Sine Amsler score was 1 [22, 23].

The preoperative microperimetry exam (Fig. 10.1b) showed no detectable retinal sensitivity over the foveal area (Fig. 10.1c). Fixation was unstable and was not located over the fovea. Mean sensitivity of the preoperative tested area with the microperimeter was 0.4 dB.

After surgery, the location of the preoperative microperimetry turned out not to be centered on the later graft location. Therefore, the same test was repeated 6 months after surgery, but now centered on the graft (Fig. 10.1e), and 1 year after surgery a follow-up exam of the 6 months' exam was performed (Fig. 10.1h). In both the 6 months' and 1 year's exam, mean sensitivity had increased to 3.2 dB, and measurable sensitivity was seen on almost the entire graft; however, in the fovea, an area of relative or absolute scotoma was observed (Fig. 10.1e, h).

This area of decreased sensitivity corresponded to an RPE defect, visible as a hypoautofluorescent area, rectangular in shape, on the graft on AF (Fig. 10.1d, g), and visible on SD-OCT as absence, thinning, or mottling of the highly reflective band of the RPE layer (Fig. 10.1f, i). The SD-OCT also revealed foveal retinal atrophy; the outer nuclear layer, external limiting membrane, and inner/outer segment photoreceptor layer were absent, which also contributed to the low sensitivity (Fig. 10.1f, i).

One year after surgery, VA had increased to 0.9 logMAR, reading acuity improved to 1.0 logRAD, and the Sine Amsler score improved to 0. According to the 6 months' and the, more pronounced, 1-year's microperimetry, SD-OCT, and AF, the macular area was damaged and displayed little retinal sensitivity. However, the patient had a stable fixation during both the 6 months' and 1 year's microperimetry exams, and stable fixation on both separate fixation examinations. The fixation target (single cross 3° or circle 2°) had only

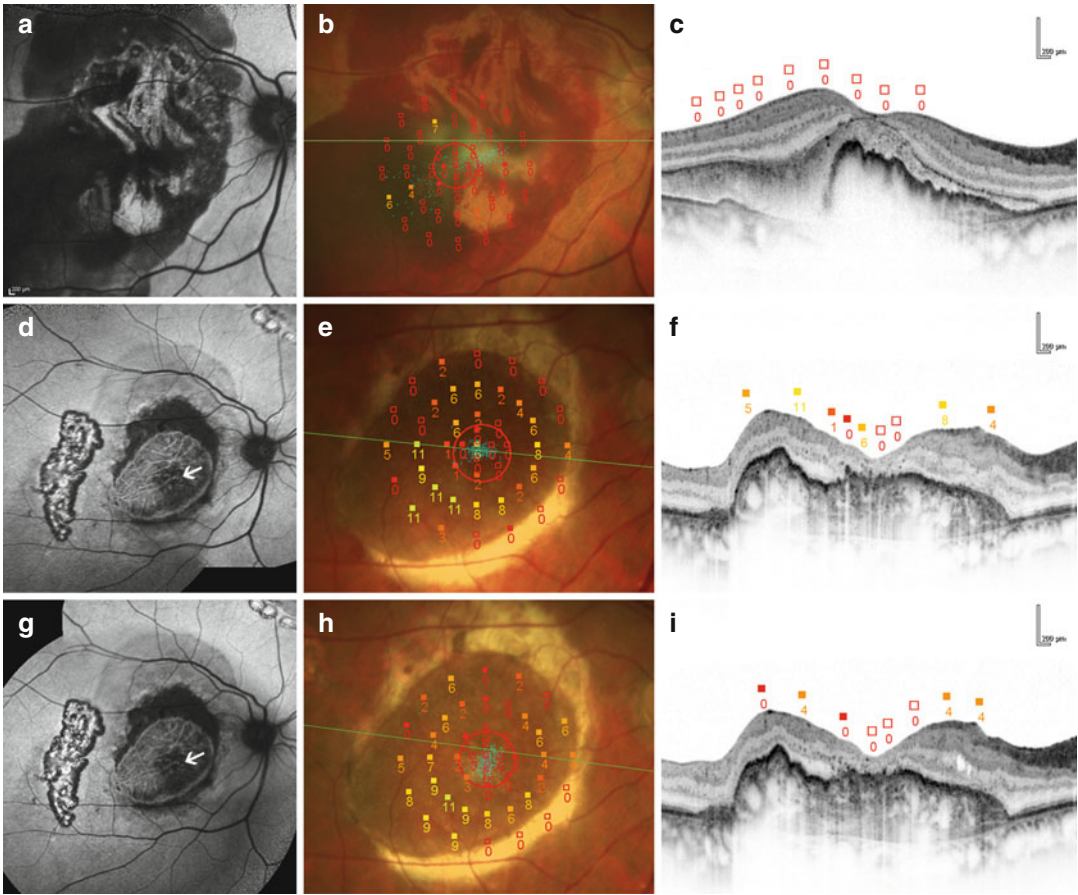


Fig. 10.1 Exact location of function and dysfunction before and after a retinal pigment epithelium-choroid graft translocation. Autofluorescence (**a, d, g**), microperimetry (**b, e, h**), and SD-OCT (**c, e, f**). Preoperative (**a, b, c**), 6 months (**d, e, f**), and 1 year (**g, h, i**) after RPE-choroid graft translocation surgery of patient 1 who presented with a macular hemorrhage and an RPE-tear. (**b, e, h**) A macular, 12° , 10 dB pattern, with 45 test loci, with a 2° circle as fixation target, centered on the hemorrhage (**b**) or graft (**e, h**) was tested automatically with a 4-2 staircase threshold strategy, with white Goldmann II stimulus displayed for 200 ms. The brightness of the test stimuli ranged from 0 to 20 dB (400 to 4 asb). Mean sensitivity preoperatively was 0.4 dB with a minimum of 0 dB and a maximum of 7 dB. Mean sensitivity of both 6 months' and 1 year's follow-up exam was 3.2 dB, with a minimum of 0 and a maximum of 11 dB. The visual acuity was 1.32

logMAR preoperatively, 0.8 logMAR 6 months after surgery, and 0.9 logMAR 1 year postoperatively. (**b, c, e, f, h, i**) The retinal sensitivity values in the SD-OCT images and the green line in the microperimetry image were placed after superimposing the microperimetry results on the matching AF and IR images. This patient illustrates RPE damage most likely following (excessively) firm gripping of the graft with the bent forceps during surgery, which can be identified as the dark area, rectangular in shape, (*white arrows*) located on the center of the graft and oriented towards the inferonasal edge on the AF images (**d, g**), and disturbances in the highly reflective RPE layer on SD-OCT (**f, i**). In the same macular area, retinal atrophy is visible on SD-OCT (**f, i**). The area with RPE damage and retinal atrophy corresponds to the area with lower sensitivity, as measured with the microperimeter (**e, f, h, i**)

a luminance of 100 asb (6 dB). Thus, despite retinal and RPE damage, fixation could still be measured over the macular area using only a dim stimulus; furthermore, the patient had reading acuity. Therefore, we hypothesize that there might be more (areas with some) retinal sensitiv-

ity in the macula than the microperimeter could detect. Our hypothesis is that, even though the macular area was (partly) damaged, a brighter stimulus, or a stimulus of a longer duration than 200 ms, might have been visible. This hypothesis will be further addressed later in this chapter.

10.3.2 Long-Term Follow-Up and Fixation Location and Stability over the Graft

Locating (foveal) fixation is another measure of retinal function over the graft. This can be performed with a slit lamp, or more accurately, with the microperimeter.

Patient 2 presented with an occult neovascular membrane and a fibrotic scar and a visual acuity of 0.7 logMAR. Two months after surgery, VA was still 0.7 logMAR, and the mean sensitivity of the microperimetry exam was 1.6 dB (Fig. 10.2a). As the MP1 was momentarily available in our hospital, a regular follow-up exam could not be performed. Therefore, the same pattern as was used on the first exam was manually customized on the microperimeter for the second test of this patient at 80 months (Fig. 10.2b). Mean sensitivity of this second test was 5.6 dB, with most sensitivity displayed on the superonasal edge of the graft, which most likely represents the location of the preoperative fovea. A comparable distribution of sensitivity was found at the third exam (Fig. 10.2d) at 107 months (this was a follow-up exam of the 80 months' exam), while mean sensitivity had slightly decreased to 4.6 dB.

Just as the mean microperimetric sensitivity increased at the second exam, so did the visual acuity increase, to 0.42 logMAR. The Sine Amsler score at the second exam was 3 and reading acuity was 0.92 logRAD.

Although the mean sensitivity decreased slightly at the third exam, VA increased to 0.34 logMAR; reading acuity improved to 0.71 logRAD; and the Sine Amsler score improved to 0.

Despite these relatively good sensitivity results over a long follow-up period, fixation was difficult to interpret in these microperimetry sensitivity exams, as the patient was specifically asked to look in between the four crosses, and thus no clear fixation point could be determined. Fixation was ranked as relatively unstable and as unstable at the second and third visit, respectively. Additionally, fixation was also tested in a separate fixation exam, and at both 80 months' follow-up and the 107 months' follow-up, fixation was stable on the edge of the graft (Fig. 10.2c, e). Therefore, a separate fixation test, especially when the four crosses are used as a fixation target in the sensitivity exam, is mandatory. We could now clearly correlate the fixation and the area with sensitivity on the superonasal edge (macular area) of the graft, which most likely explains the relatively good VA and the reading ability of the patient.

10.3.3 Combining Information About Function/Dysfunction, Anatomical Changes, and Fixation Over Time Can Help to Reinterpret Earlier Imaging

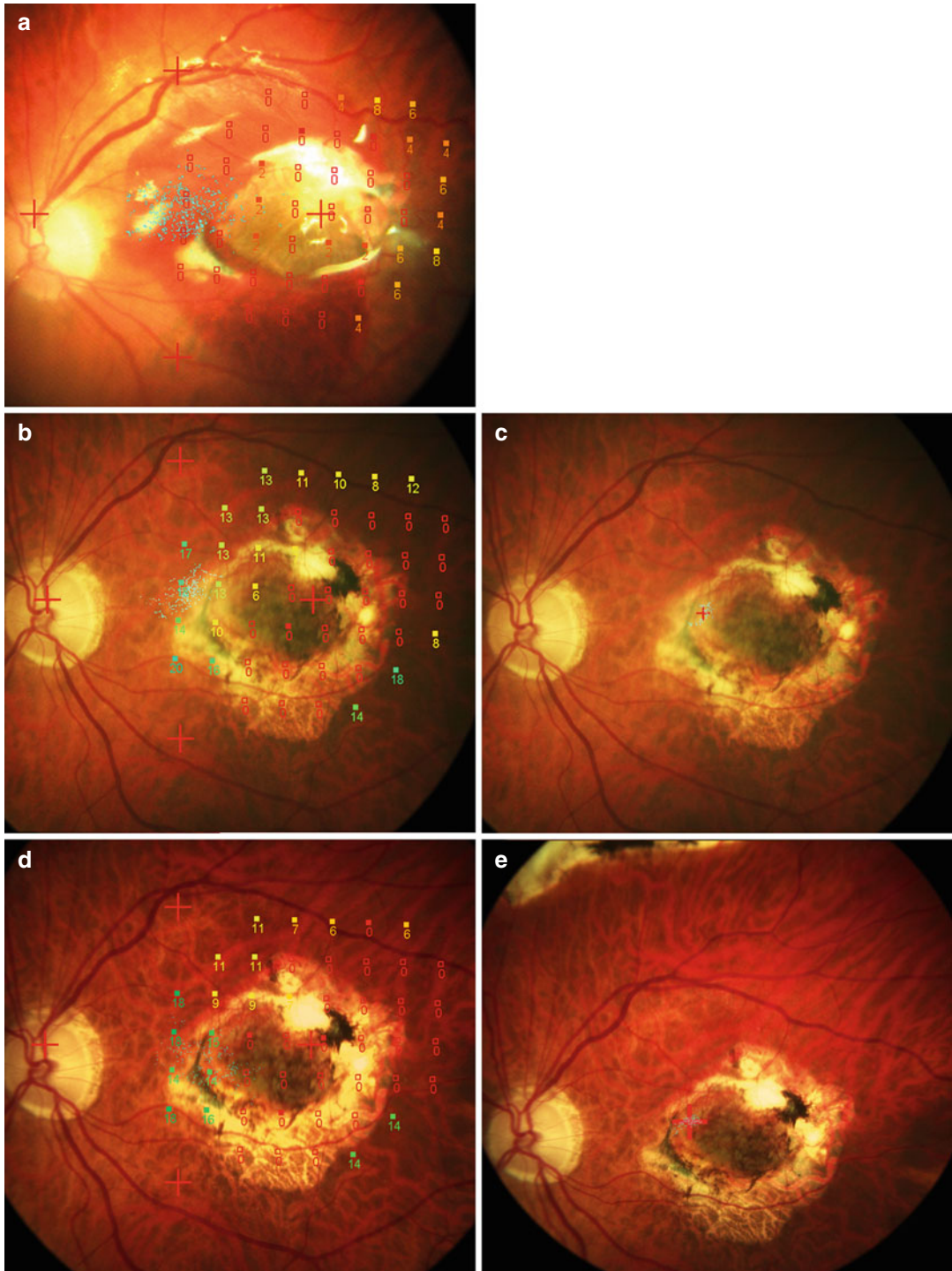
With the lessons learned from patients 1 and 2 about function in relation to anatomical changes, fixation, and long-term follow-up, we have combined microperimetry results with SD-OCT, AF, and FA images over time in patient 3. Because the information gathered from all images together can provide insights into the course of anatomical changes and function, existing RPE damage

Fig. 10.2 Long-term follow-up: sensitivity, fixation location, and fixation stability over the graft. Microperimetry sensitivity (a, b, d) and fixation (c, e) exams at 2 months (a: slight reflections due to silicone oil tamponade), 80 months (b, c), and 107 months (d, e) after RPE-choroid graft translocation surgery of patient 2, who presented with an occult neovascular membrane and a fibrotic scar. A customized pattern (47 test loci, 4-2 staircase threshold strategy, white 200 ms Goldmann III stimulus, fixation target of 4 crosses of 2° at 20° distance) tested a mean sensitivity of 1.6 dB (range 0–8 dB) at 2 months (a), 5.6 dB (range 0–20 dB) at

80 months (b), and 4.6 dB (range 0–18 dB) at 107 months (d) after surgery. Visual acuity at the same time points was 0.7, 0.42, and 0.34 logMAR. Fixation was difficult to interpret in the sensitivity exams (b, d), as 4 crosses were used as fixation target. Separate fixation exams at 80 months (single cross, 1°) (c) and 107 months (single cross, 3°) (e) show stable fixation on the superonasal edge of the graft, corresponding to the area of the graft with the highest measurable sensitivity and, most likely, the foveal area (b From *Ophthalmologica* 2012; 228(suppl 1):40. S. Karger AG Basel)

could at a later time point be correlated with decreased sensitivity and loss of function, which was followed by a shift in fixation location.

This third patient presented with a hemorrhagic pigment epithelium detachment, a fibrotic scar, and a preoperative VA of 1.6 logMAR



(Figs. 10.3a,b). RPE damage can be distinguished at the same area at the 18-month AF (Fig. 10.3c) and on the 58-month FA (Fig. 10.3d). On FA a window defect due to the atrophy of the RPE is visible as a whiter area on the graft, which corresponds with an area with less retinal sensitivity measured with the microperimeter (Fig. 10.3d). The 86-month microperimetry exam transposed onto the AF exam (Fig. 10.3f) confirms that the area with less sensitivity and decreased autofluorescence can be correlated with each other, although now more areas of the graft have lost retinal sensitivity. Also, the SD-OCT B-scan through the macula was now able to pinpoint very accurately the area with hypoautofluorescence and decreased sensitivity. In these areas, the hyperreflective RPE layer is disturbed or absent. At the mid-nasal side of the graft, intact retinal layers and a continuous RPE layer correlate to presence of retinal sensitivity on microperimetry (6 and 11 dB), while at the nasal edge of the graft an area without RPE corresponds to a retinal sensitivity of 0 dB. In the fovea and at the temporal side of the graft no outer retinal layers are visible on SD-OCT, corresponding to a retinal sensitivity of 0 dB.

At 58 months, VA had increased to 0.6 logMar, the mean sensitivity of the microperimetry exam was 4.4 dB, and a relatively unstable fixa-

tion was measured both during the sensitivity exam as on a separate fixation exam. However, during the fixation examination, fixation was located over the foveal area with the RPE damage, instead of over the superotemporal location revealed during the sensitivity exam (4D).

At 86 months' follow-up, the patient was able to read (1.155 logRAD), with a slightly decreased VA of 0.76 logMAR and a Sine Amsler of 0. Mean sensitivity at 86 months (a follow-up exam of the first microperimetry exam was performed) had decreased to 2.5 dB, with a relatively unstable, superotemporal, fixation. But now the separate fixation exam showed stable fixation also over the superotemporal side of the graft. Clearly it can be seen that (at least) part of the fovea is located in the RPE damaged area (Fig. 10.3e, f), so fixation was no longer in the fovea.

Therefore, fixation had shifted from an unstable, foveal (inferotemporal) fixation at 58 months, to a stable fixation at a macular superotemporal location; a new preferred retinal locus (PRL), where RPE was not damaged and retinal sensitivity over the graft could be measured [24]. The slight VA decrease between the two exams might also correlate with the shifted preferred location of fixation of the patient to a new preferred visual locus as the foveal area seems no longer to be used for fixation.

Fig. 10.3 Combining information about function/dysfunction, anatomical changes, and fixation over time as a help for reinterpretation of earlier imaging. Preoperative fluorescein angiogram of patient 3 showing a hemorrhagic pigment epithelium detachment (a). Still image taken from video recording of RPE-choroid graft translocation surgery (b), on which a large hemorrhage with fibrotic component can be distinguished. Preoperative VA was 1.6 logMAR. At 18 months after surgery, VA was 0.1 logMAR, and on AF (c) a clearly demarcated area of RPE damage on the inferotemporal edge of the graft is visible. At 58 months' follow-up, VA was 0.6 logMAR; on the microperimetry sensitivity exam (macula 12°, 10 dB pattern, 200 ms Goldmann II stimulus, 45 test loci centered on the graft, with a 2° circle as fixation target) transposed onto a FA image (d), an area with lower sensitivity can be distinguished, corresponding to the RPE damaged area imaged on (c), which also seems to correspond with a window defect area visible on FA. Mean sensitivity was

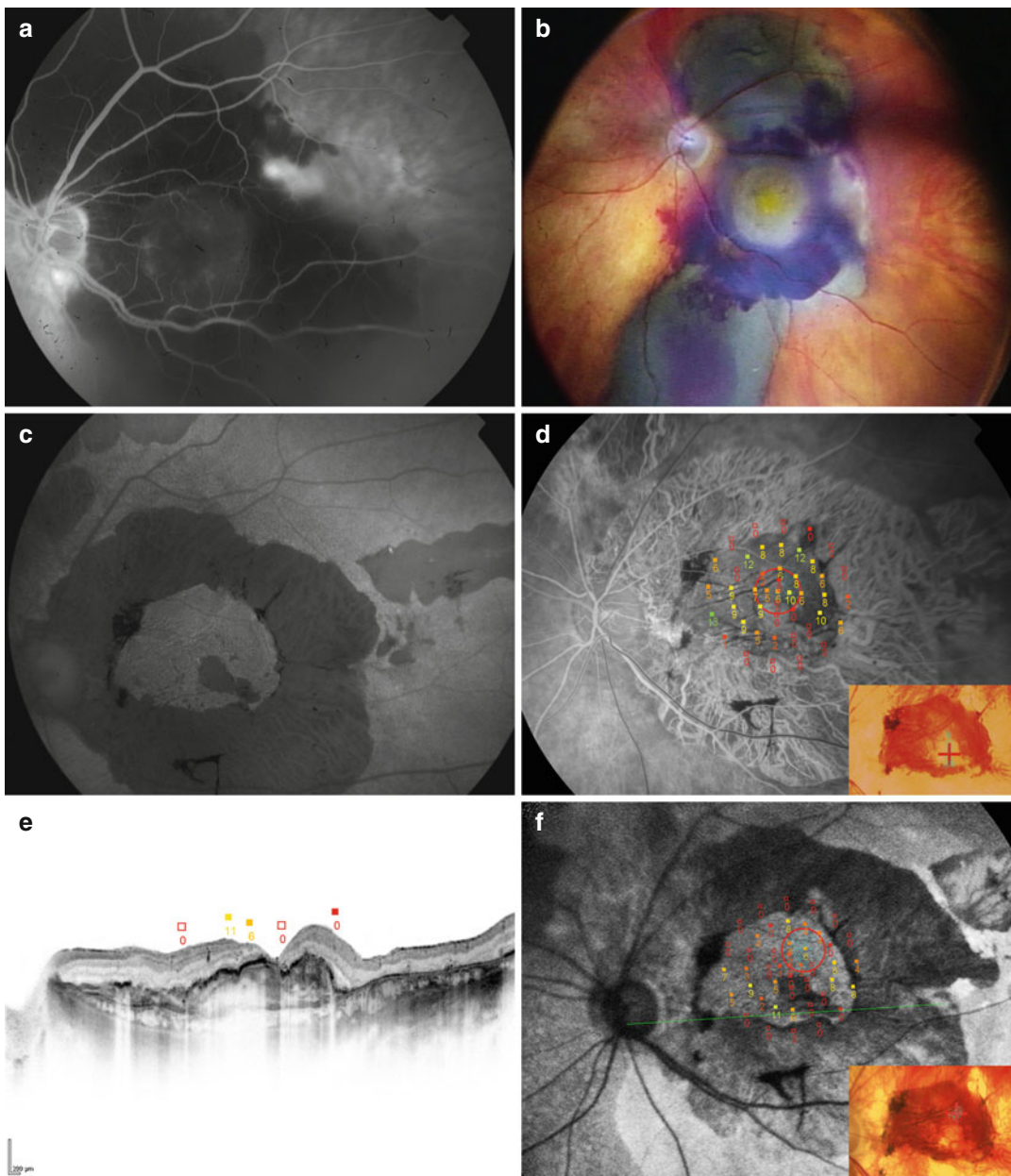
4.4 dB (range 0–13 dB). Fixation exam (single cross, 3°) of 58 months (*inset* in d) shows a relatively unstable inferotemporal fixation. (e) A B-scan of the macular area of the graft with an SD-OCT at 86 months' follow-up with a VA of 0.76 logMAR. According to the integrated microperimetry results, (part of) the macular area does not have retinal sensitivity. This area corresponds to the areas where the highly reflective RPE band is distorted or absent. The areas with intact RPE and intact retinal layers do show sensitivity. On the microperimetry exam transposed onto an AF image (f), the RPE damaged area with less sensitivity is well demarcated. The *green line* is the location where the B-scan (e) was taken. Fixation exam of 86 months (*inset* in f) shows a stable superotemporal fixation. The fovea is located at the inferior edge of the graft, and the new fixation location measured with the microperimeter at the superotemporal edge of the graft is therefore a new preferred retinal locus

10.4 Discussion

10.4.1 Visual Acuity and Its Correlation with Sensitivity Results over the Graft

Visual acuity and microperimetry results may correlate, but not consistently so [11, 17]. Patient 1's VA improved significantly from 1.32 logMAR

preoperatively to 0.8 logMAR after 6 months. The mean sensitivity also increased from 0.4 to 3.2 dB. The slight decrease in VA from 0.8 to 0.9 logMAR from 6 months to 1 year after surgery was not mirrored by a decrease in sensitivity, which remained stable at 3.2 dB. For patient 2 also an increase in VA from 0.7 logMAR 2 months after surgery to 0.42 logMAR 80 months after surgery corresponded to an increase in dB from



1.6 to 5.6 dB. However, the examination at 107 months revealed a slightly better VA, 0.34 logMAR, but the sensitivity had slightly decreased to 4.6 dB. Patient 3 had a VA of 0.6 logMAR at 58 months and of 0.76 logMAR at 86 months of follow-up. This decrease in VA was also visible in a decrease in sensitivity from 4.4 to 2.5 dB.

Therefore, a marked difference in VA corresponds to a marked change in dB, but small changes in VA are harder to correlate with the changes in sensitivity. Larger studies will be needed to be able to clearly correlate VA and sensitivity changes in grafts.

10.4.2 Correlation Between Damage of the Retinal Pigment Epithelium and Retinal Layers and Sensitivity Measurements over the Graft

In two of the cases described, a correlation was demonstrated between structural change, represented by RPE damage and retinal layer disturbance on AF, FA, and SD-OCT, and functional change, represented by a decrease in retinal sensitivity on microperimetry. Correlation between areas with RPE defect and retinal sensitivity loss over an RPE-choroid graft have been described [9, 10]. Also, correlation has previously been found between intact retinal structures over a graft and areas with retinal sensitivity [7–9]. In our first patient, the foveal area at 6 months' and 1 year's follow-up shows less retinal sensitivity than other areas of the graft (Fig. 10.1e, h). The SD-OCT reveals a damaged retina at the 6-month scan and a very thin and sometimes absent RPE (Fig. 10.1f). At the 1-year scan, the foveal retinal layers are also damaged, and the RPE is very thin or absent in some locations. Here, minimal microperimetric sensitivity could be detected (Fig. 10.1i). Although most retinal layers over the graft in patient 3 at the 86-month SD-OCT scan (Fig. 10.3e) seem to be quite intact, areas with less or absent RPE are visible. These areas correspond to the areas with less retinal sensitivity. At the areas with an intact retina and an intact layer of RPE, retinal sensitivity was indeed measured with the microperimeter. Therefore, it is

clear that damage of retinal layers and damage of RPE decreases sensitivity and therefore VA.

The intraoperative course has already been found to play a major role in graft function [4]. For patient 1, the RPE damage, likely a result of excessively firm gripping of the graft during surgery, visible on AF and SD-OCT, correlated with the decreased retinal sensitivity. Further, patient 3 clearly shows that RPE damage alone can already have a devastating effect on retinal sensitivity. Retinal damage may have occurred earlier due to the pathology before surgery but may also occur during surgery, when, for instance, fibrotic components, strongly attached to the retina, need to be peeled off. These examples underscore our need to search for more delicate instruments and techniques for this surgery.

10.4.3 Improvements and Future Possibilities

Although very detailed information of retinal sensitivity over the graft can be obtained with the MP-1, we think more information about RPE-choroid graft patients could be gained if stimuli brighter than 0 dB could be displayed. A clear example is patient 1: at 1 year, this patient was able to read nearby, had a relatively good VA of 0.9 logMar, was able to see the fixation target of 6 dB, and had a stable fixation. Although her RPE and retinal layers were damaged in the fovea, and foveal microperimetric sensitivity was severely decreased, fixation was located over the fovea. We think it would be very useful to test the function over that area with brighter stimuli. We hypothesize that the patient experienced difficulty concentrating on the fixation ring and was unable to simultaneously distinguish the projected stimuli in the same area. It is possible that a brighter stimulus would have allowed this patient detect the stimuli, and thus demonstrate residual sensitivity. Also, for patients with very low VA, who now cannot be tested with the MP-1, brighter stimuli might give the option to test if there is any retinal sensitivity over the graft.

Another idea would be to project a stimulus of a longer duration; up to 2,000 ms is possible with

the MP-1. We have tested this option in another patient with an RPE-choroid graft with relatively good VA, and this allowed the patient to see less bright stimuli. Unfortunately, in this setting, local defect maps, and therefore mean sensitivity and mean defect values, are unavailable. Thus, comparison with other reports, which almost exclusively use the 200 ms as default, is difficult. Further, with long stimulus duration, the interval between projected stimuli becomes shorter, which, in our experience, was not beneficial for the accuracy of the test. Therefore, brighter stimuli with the same duration of 200 ms, longer-duration stimuli with standard interstimulus intervals, and a set of normative data so local defect maps can be obtained, would all be very useful.

Conclusion

This study suggests that microperimetry can provide useful information regarding retinal sensitivity over an RPE-choroid graft, by correlating function with anatomical changes on FA, AF, and SD-OCT. Furthermore, microperimetry can provide accurate information on fixation location and its stability over the graft over time.

It is not yet clear whether microperimetric sensitivity information provides additional advantage for diagnosis and follow-up of an RPE-choroid graft. Future studies should address whether microperimetry results correlate with visual acuity, reading acuity, metamorphopsia, and/or quality of life.

Acknowledgements We would like to thank Kristel Maaijwee for collection of the early data.

Funding/Support

1. Royal Visio, Rotterdam, The Netherlands
2. The Rotterdam Eye Hospital Flieringa Research Foundation
3. Combined Ophthalmic Research Rotterdam
4. Stichting Coolsingel
5. MD fonds

Financial Disclosure

Last author J. C. van Meurs is the partial owner of a patent: vibration device for tissue release, with Dutch Ophthalmic Research Center (DORC), Zuidland, the Netherlands, one prototype. The other authors have no financial disclosure.

References

1. Braaf B, Vermeer KA, Sicam VA et al (2011) Phase-stabilized optical frequency domain imaging at 1-microm for the measurement of blood flow in the human choroid. *Opt Express* 19:20886–20903
2. Van Zeeburg EJ, Cereda MG, van der Schoot J et al (2011) Early perfusion of a free RPE-choroid graft in patients with exudative macular degeneration can be imaged with spectral domain-OCT. *Invest Ophthalmol Vis Sci* 52:5881–5886
3. Maaijwee K, van den Biesen PR, Missotten T et al (2008) Angiographic evidence for revascularization of an rpe-choroid graft in patients with age-related macular degeneration. *Retina* 28:498–503
4. Maaijwee K, Missotten T, Mulder P et al (2008) Influence of intraoperative course on visual outcome after an RPE-choroid translocation. *Invest Ophthalmol Vis Sci* 49:758–761
5. Van Zeeburg EJ, Maaijwee KJ, Missotten TOAR et al (2012) A free retinal pigment epithelium-choroid graft in patients with exudative age-related macular degeneration: results up to 7 years. *Am J Ophthalmol* 153:120–127
6. Petersen J, Ritzau-Tondrow U, Hoerauf H et al (2008) Autologous translocation of large retinal pigment epithelium choroid patches in age-related macular degeneration. *Klin Monbl Augenheilkd* 225:286–291
7. Caramoy A, Liakopoulos S, Menrath E et al (2010) Autologous translocation of choroid and retinal pigment epithelium in geographic atrophy: long-term functional and anatomical outcome. *Br J Ophthalmol* 94:1040–1044
8. Caramoy A, Fauser S, Kirchhof B (2011) Retinal stimuli can be restored after autologous transplant of retinal pigment epithelium and choroid in pigment epithelium tears. *Acta Ophthalmol* 89:e490–e495
9. Chen FK, Uppal GS, Rubin GS et al (2008) Evidence of retinal function using microperimetry following autologous retinal pigment epithelium-choroid graft in macular dystrophy. *Invest Ophthalmol Vis Sci* 49:3143–3150
10. Chen FK, Patel PJ, Uppal GS et al (2009) A comparison of macular translocation with patch graft in neovascular age-related macular degeneration. *Invest Ophthalmol Vis Sci* 50:1848–1855
11. Chen FK, Uppal GS, MacLaren RE et al (2009) Long-term visual and microperimetry outcomes following autologous retinal pigment epithelium choroid graft for neovascular age-related macular degeneration. *Clin Experiment Ophthalmol* 37:275–285
12. Heussen FM, Fawzy NF, Joeres S et al (2008) Autologous translocation of the choroid and RPE in age-related macular degeneration: 1-year follow-up in 30 patients and recommendations for patient selection. *Eye (Lond)* 22:799–807
13. Maaijwee K, Heimann H, Missotten T et al (2007) Retinal pigment epithelium and choroid translocation in patients with exudative age-related macular degeneration: long-term results. *Graefes Arch Clin Exp Ophthalmol* 245:1681–1689

14. Maaijwee K, van Meurs JC (2007) Retinal pigment epithelium and choroid translocation in patients with exudative age-related macular degeneration. In: Soubrane G (ed) *Les DLMA*s. Masson, Paris, pp 562–567
15. Jousseaume AM, Heussen FM, Joeres S (2006) Autologous translocation of the choroid and retinal pigment epithelium in age-related macular degeneration. *Am J Ophthalmol* 142:17–30
16. MacLaren RE, Bird AC, Sathia PJ (2005) Long-term results of submacular surgery combined with macular translocation of the retinal pigment epithelium in neovascular age-related macular degeneration. *Ophthalmology* 112:2081–2087
17. Treumer F, Bunse A, Klatt C (2007) Autologous retinal pigment epithelium-choroid sheet transplantation in age related macular degeneration: morphological and functional results. *Br J Ophthalmol* 91:349–353
18. Van Zeeburg EJ, van Meurs JC (2013) Literature review of recombinant tissue plasminogen activator used for recent-onset submacular hemorrhage displacement in age-related macular degeneration. *Ophthalmologica* 229:1–14
19. Hwang JC, Del Priore LV, Freund KB (2011) Development of subretinal fibrosis after anti-VEGF treatment in neovascular age-related macular degeneration. *Ophthalmic Surg Lasers Imaging* 42:6–11
20. Rosenfeld PJ, Shapiro H, Tuomi L (2011) Characteristics of patients losing vision after 2 years of monthly dosing in the phase III ranibizumab clinical trials. *Ophthalmology* 118:523–530
21. Maaijwee K, Koolen T, Rosenbrand D (2008) Threshold amplitude and frequency for ocular tissue release from a vibrating instrument: an experimental study. *Invest Ophthalmol Vis Sci* 49:1629–1632
22. Maaijwee K, Mulder P, Radner W (2008) Reliability testing of the Dutch version of the Radner Reading Charts. *Optom Vis Sci* 85:353–358
23. Bouwens MD, van Meurs JC (2003) Sine Amsler Charts: a new method for the follow-up of metamorphopsia in patients undergoing macular pucker surgery. *Graefes Arch Clin Exp Ophthalmol* 241:89–93
24. Crossland MD, Engel SA, Legge GE (2011) The preferred retinal locus in macular disease: toward a consensus definition. *Retina* 31:2109–2114

Tjebo F.C. Heeren, Frank G. Holz,
and Peter Charbel Issa

11.1 Introduction

Beginning in 2005, the Macular Telangiectasia Project (“MacTel Project”; <http://www.mactelresearch.org>) has initiated major research activities on MacTel type 2. In an effort involving a number of worldwide clinical centers and basic science laboratories, this privately funded project aims to develop a better understanding of the clinical features and natural history of the disease, to elucidate a genetic association, to identify animal models which may improve the understanding of intrinsic pathogenetic mechanisms, and, ultimately, to identify and test potential treatments.

This increased research interest in MacTel type 2 has helped to gain new insights in the disease in several ways. Characteristic phenotypic findings have been identified using various imaging techniques that now allow an improved clinical differentiation of this entity from other retinal diseases [1]. Moreover, the description of affected but asymptomatic family members of patients together with the higher than expected prevalence in population-based studies should clearly increase the awareness of the disease [2, 3].

T.F.C. Heeren • F.G. Holz • P. Charbel Issa (✉)
Department of Ophthalmology, University of Bonn,
Ernst-Abbe-Str. 2, D-53127, Bonn, Germany
e-mail: peter.issa@ukb.uni-bonn.de

11.2 Clinical Findings

MacTel type 2 is confined to the central oval macular area, while the peripheral retina appears to be unaffected. Five stages of the disease have been proposed by Gass and Blodi based on funduscopy and fluorescein angiography (FA) [4]. Stage 1 is ophthalmoscopically un conspicuous but shows hyperfluorescence in late-phase FA. Stage 2 is defined by a reduced parafoveal retinal transparency seen as a peculiar greying. Stage 3 is characterized by the presence of so-called right-angled vessels that end with a blunted tip and seem to bend into deeper retinal layers. Stage 4 is defined by ophthalmoscopically visible retinal pigment hyperplasia, probably due to proliferation of pigment epithelial cells. Stage 5 is defined by the presence of a secondary neovascular complex. The origin of these lesions appears to be different from choroidal neovascularization and rather seems to originate from the retinal vasculature. It should be noted that a neovascular complex may develop at any time point in the disease process. Thus, it rather represents a complication of the disease and not the natural end point [1]. Eventually, function is determined by an outer retinal atrophy which is the common finding in late disease stages [1]. Table 11.1 summarizes the disease stages and more general clinical findings that do not define subsequent stages in the currently most frequently followed classification system.

Table 11.1 Stages of macular telangiectasia (MacTel) type 2 according to Gass and Blodi [4]

General clinical findings	Stage	Specific clinical findings
Bilateral telangiectasia, minimal exudation, outer retinal thinning or atrophy, superficial retinal crystalline deposits	1	Diffuse hyperfluorescence in late-phase fluorescein angiography
	2	Reduced retinal transparency parafoveally
	3	Dilated right-angled vessels
	4	Intraretinal pigment clumping
	5	Secondary intraretinal neovascular complex

Application of various imaging modalities in MacTel type 2 has led to a better understanding of the disease phenotype. High-resolution optical coherence tomography (OCT) may show disruption of the photoreceptor inner segment-outer segment border, hyporeflective cavities at the level of the inner or outer retina, and atrophy mainly of the outer retina in later stages [1, 5].

MacTel type 2 shows a unique depletion of the macular pigment in the central retina [6, 7], resulting in increased reflectivity on confocal blue reflectance imaging and an increased fundus autofluorescence signal due to reduced absorption of the excitation light [1, 8].

11.3 Functional Impairment

In early stages, functional impairment may be mild with no or only slight reduction in best corrected visual acuity (BCVA). Epidemiologic studies revealed a mean BCVA of 20/40 in over 500 eyes [9]. Approximately half of the eyes had a BCVA of 20/32 or better and 16 % of 20/20 or better. A BCVA worse than 20/200 is rarely observed in MacTel type 2. However, reduced visual abilities such as reading difficulties proportional to the level of BCVA are frequently reported and may affect the patient's quality of life significantly [10]. Patients may also report perception of metamorphopsia and/or a positive

scotoma [11]. Microperimetry was therefore performed in several studies to further elucidate the nature of functional deficits in patients with MacTel type 2 [12–17].

A first microperimetry study was conducted in 53 eyes of 30 patients assuming that functional deficits are topographically related to the fundus-ographically and angiographically visible abnormalities which have their epicenter temporal/temporal inferior to the foveal center. Eyes were assigned to group A (disease stages 1–3) or group B (disease stages 4 and 5) [13]. Temporal to the fovea, each eye of group B had an absolute scotoma [13]. Topographically, the areas with scotoma correlated well with the angiographically hyperfluorescent areas or retinal pigmentations and showed a sharp demarcation from areas with normal light sensitivity (Fig. 11.1). However, within areas with angiographic alterations, at least some test locations exhibited preserved sensitivity in group B eyes; in 51 % of group A eyes, none of those test locations showed abnormal light sensitivity. Fixation stability seemed to be relatively unaffected [13].

Paracentral scotomata in patients with MacTel type 2 usually are small and well defined. Only in very progressed disease stages, they may enlarge to cover a central area of up to about 8–10° horizontally and less vertically. The epicenter of function loss in MacTel type 2 was shown to be located about 2° temporal/temporal inferior to the foveal center [13].

Efficient reading requires not only a sufficient visual acuity to resolve the letters but also a certain extent of central visual field of usually at least 4° to sufficiently process words and perform adequate eye movements [18]. Therefore, reading ability was investigated in patients with MacTel type 2 and correlated to vision loss as assessed by microperimetry testing [10]. Patients exhibited a significantly reduced reading acuity and reduced reading speed compared to controls. The reduced reading ability was shown to be associated with presence of a paracentral scotoma [10]. Both visual acuity and such scotomata were significant predictors for both reading speed and reading acuity. Therefore, microperimetry may be a surrogate marker for the highly variable assessment of reading ability.

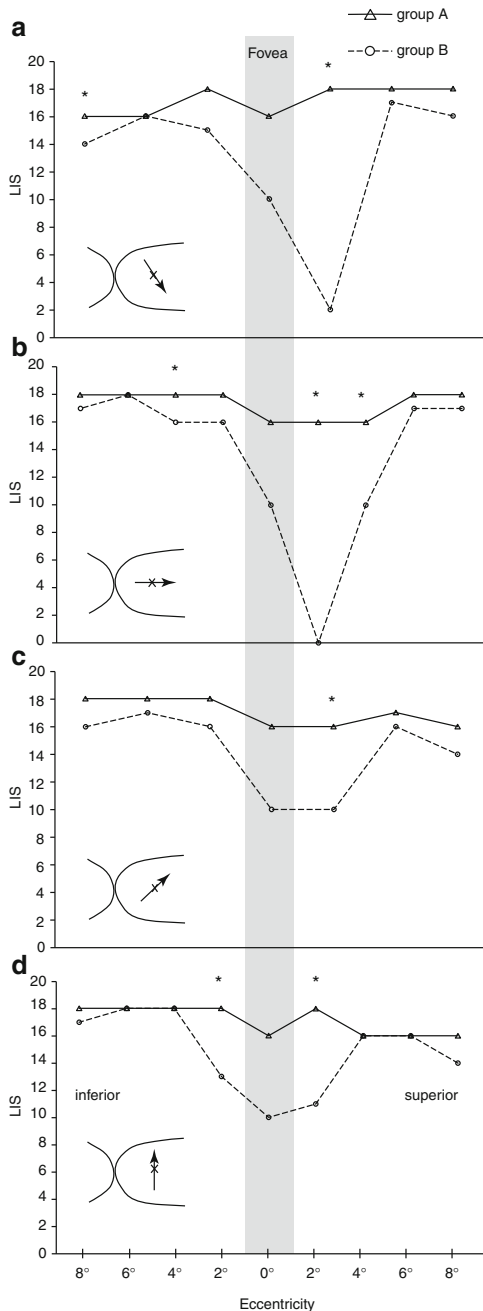


Fig. 11.1 Summary of the microperimetric examination results. Each *triangle* and *circle* represents the median light sensitivity of the corresponding individual testing points along the axis, as specified in the schematic fundus within each diagram (a–d). The *continuous line with triangles* represents group A, and the *dashed line with circles* represents group B. *Asterisks* indicate testing points with a statistically significant difference between group A and group B eyes, respectively. LIS Light increment sensitivity (in decibel), where 0 represents the brightest luminance of the test stimulus. (Figure printed from Charbel Issa et al. [13], copyright 2013, ARVO)

11.4 Structure-Function Correlation

In various diseases such as diabetic macular edema or central serous chorioretinopathy, there appears to be an association of retinal function with retinal thickness measures. However, in MacTel type 2, conclusions on retinal function based on total retinal thickness measurements may be less valid due to low-grade retinal edema over a partial atrophic retina [12]. Therefore, it is more appropriate to qualitatively analyze the retinal morphology for identifying structural associations with functional deficits in MacTel type 2.

An example for such an approach is provided in Fig. 11.2: functional preservation on microperimetry testing can be found if degeneration spares the photoreceptors, but causes quite extensive disruption of the inner retina. However, degenerative alterations of the photoreceptor layer result in an absolute and well-demarcated paracentral scotoma. Another possible correlation with findings on retinal imaging was proposed by Zeimer and co-workers. They found a correlation between loss of macular pigment and reduced retinal function as determined by microperimetry testing [17].

It was noted previously that an absolute scotoma is always present in MacTel type 2 stages 4 and 5 (see above). However, we have observed a substantial number of patients presenting with an absolute scotoma in stage 3 disease (unpublished observations). Probably photoreceptor atrophy as the underlying structural correlate appears earlier in the course of the disease than the ophthalmoscopically visible signs of stage 4 and 5. This emphasizes the importance of high-resolution OCT and microperimetry testing in this disease entity to fully understand individual disease manifestations and their functional relevance.

11.5 Microperimetry to Assess Diseases Progression and Therapeutic Effects

Longitudinal studies on loss of function as observed on microperimetry testing have not yet been performed systematically in patients with

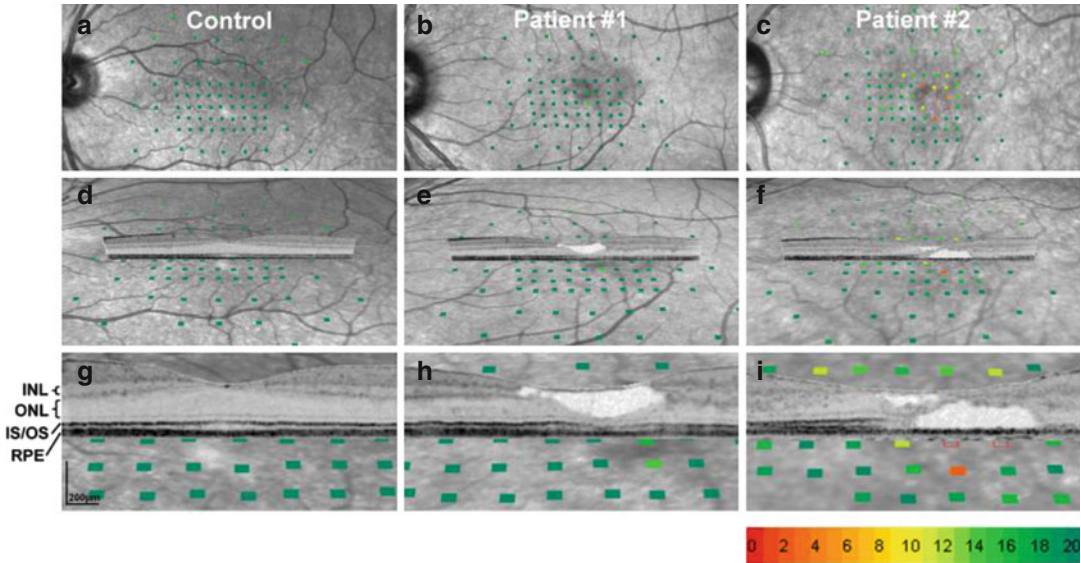


Fig. 11.2 Correlation of topographic and tomographic retinal imaging with functional mapping. Retinal sensitivity data derived from microperimetry are presented according to the scale below (i). *Open rectangles* demonstrate absolute defects. The *first column (a–c)* illustrates findings in a normal subject, the *middle and right column* in two patients with macular telangiectasia type 2. The *first row* shows functional maps superimposed on near-infrared confocal scanning laser ophthalmoscopy (cSLO) images of the central retina. The *second and third rows (d–i)* show the functional maps superimposed on the back-tilted cSLO images and a high-resolution spectral-domain optical coherence tomography (SD-OCT) scan.

The *lower panels (g–i)* show enlarged cutouts of the *middle row (d–f)*. For the normal subject, selected anatomical layers of the retina are indicated for orientation on the left-hand side of panel **g** (*INL* inner nuclear layer, *ONL* outer nuclear layer, *IS/OS* junction of the inner and outer photoreceptor segment, *RPE* retinal pigment epithelium). The tissue defect within the inner retina (**e, h**) is associated with a normal or slightly decreased retinal light sensitivity (*green squares*), whereas damage to the outer retina (the photoreceptor layers) was accompanied by a strong loss of retinal sensitivity (*red filled and red open squares; f, i*) (Figure from Charbel Issa et al. [20])

MacTel type 2. However, individual case reports and series support the usefulness of this method to monitor functional decline in this disease [1, 19, 20] (Figs. 11.3 and 11.4). Notably, microperimetry appears to be superior compared to visual acuity testing for detecting functional changes in MacTel type 2: while BCVA may remain stable over the observational periods, development or enlargement of the characteristic paracentral

scotomata may occur [1, 20]. This relative preservation of visual acuity may be explained by the delayed atrophy of photoreceptors in the foveal center (the integrity of which is needed for good performance on single optotype BCVA testing) compared to those in the paracentral temporal area. Notably, microperimetry may also be useful to monitor treatment effects in stage 5, i.e., once a neovascular complex has developed (Fig. 11.5).

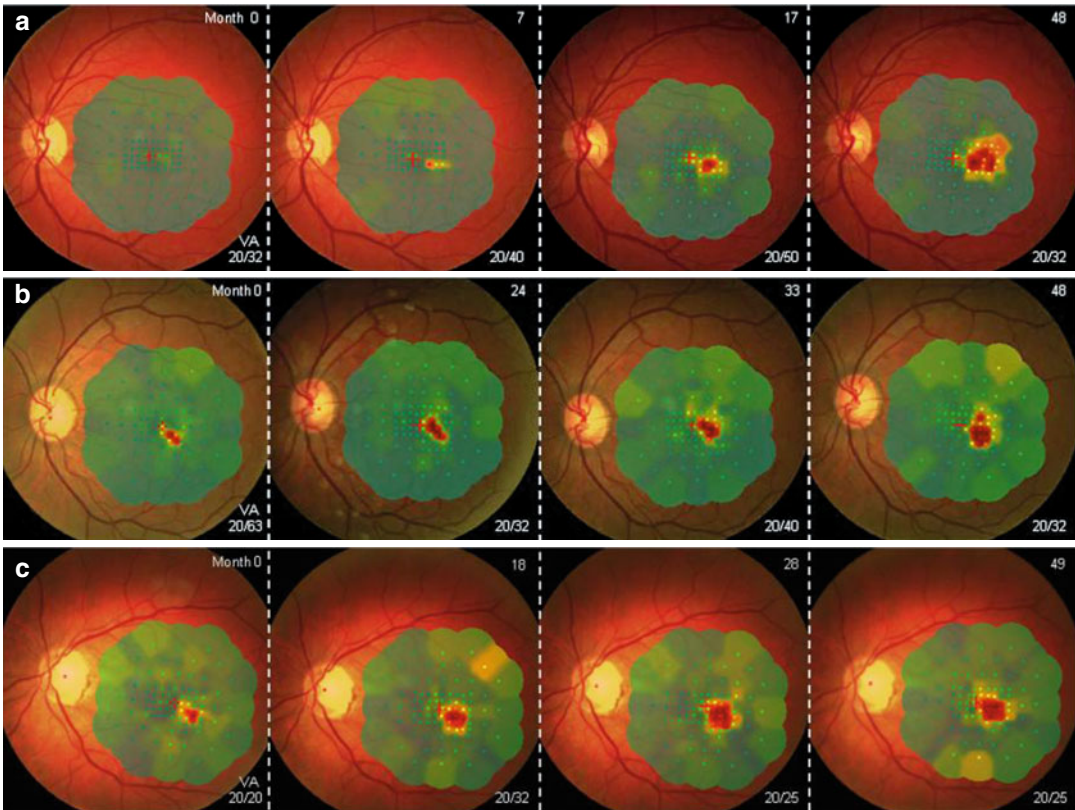


Fig. 11.3 Microperimetry in three different patients (rows **a–c**) with MacTel type 2 over a 4-year follow-up. Absolute scotoma temporal to the fovea (*deep red color*)

progresses considerably, whereas visual acuity (VA) remains largely stable (Reprinted from Charbel Issa et al. [1], Copyright (2013), with permission from Elsevier)

Another method of functional testing, fine matrix mapping, allows measurements of the scotopic function within the central visual field. Studies revealed an earlier decrease and more severe affection of scotopic rod compared to photopic cone function [15]. A subsequent longitudinal observation of nine eyes over 1 year suggested

a superior sensitivity of scotopic fine matrix mapping to monitor progression of the functional deficit compared with microperimetry [21]. Assessment of scotopic macular function using fine matrix mapping is, however, time consuming and not widely available. Therefore, it may not be suitable for larger patient cohorts in clinical trials.

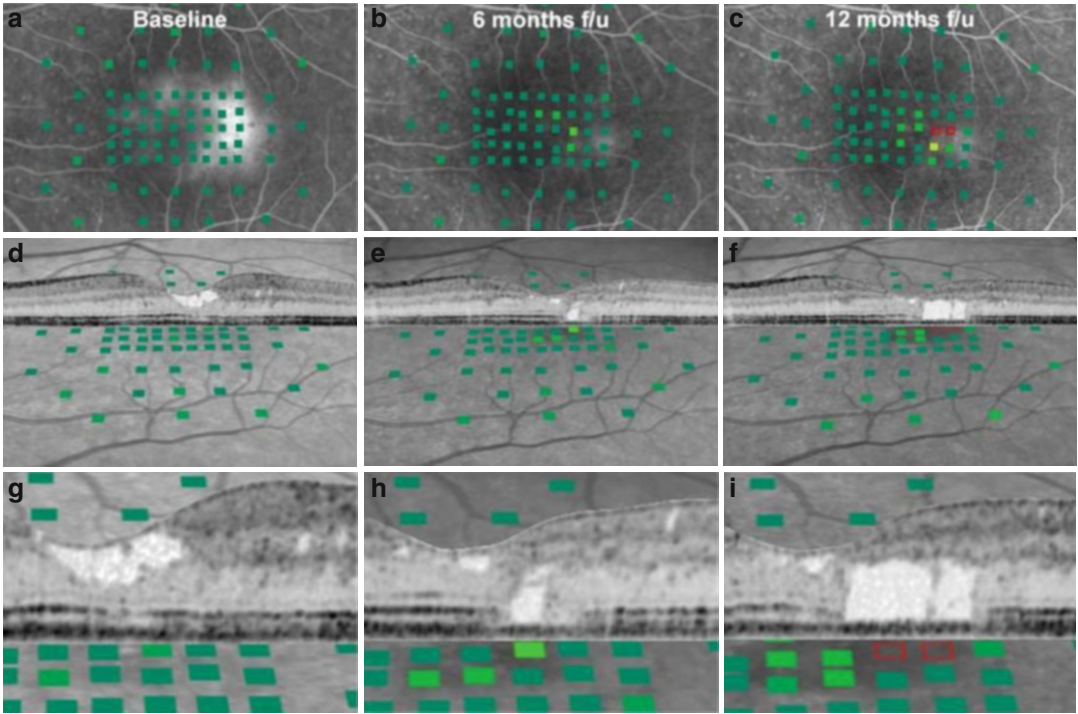


Fig. 11.4 Longitudinal structure-function correlation in macular telangiectasia type 2 in an interventional trial. The *first row* shows functional maps superimposed on late-phase fluorescein angiography images. Treatment with monthly ranibizumab considerably reduced such leakage (**a–c**). However, the patient developed loss of retinal sensitivity and showed an absolute scotoma (*open red rectangles*) after 12 months (**c**). The *second and third rows* (enlarged cutouts of the *middle row*) show corresponding OCT images superimposed on back-tilted infrared fundus images and the same functional map as shown in the *upper row*. At baseline, the patient shows consider-

able abnormality of inner retinal anatomy (**d, g**). Retinal sensitivity was normal. After 6 months of treatment, outer retina abnormalities developed affecting the photoreceptor layer (**e, h**). This alteration measuring about 100 μm appeared to be too small to be detected by fundus-controlled microperimetry. However, after 12 months of treatment, enlarged damage of the outer retina was associated with a strong loss of retinal sensitivity (**f, i**). Visual acuity at baseline was 20/40 and remained unchanged over the study period despite such pronounced loss of paracentral visual function (Figure from Charbel Issa [20])

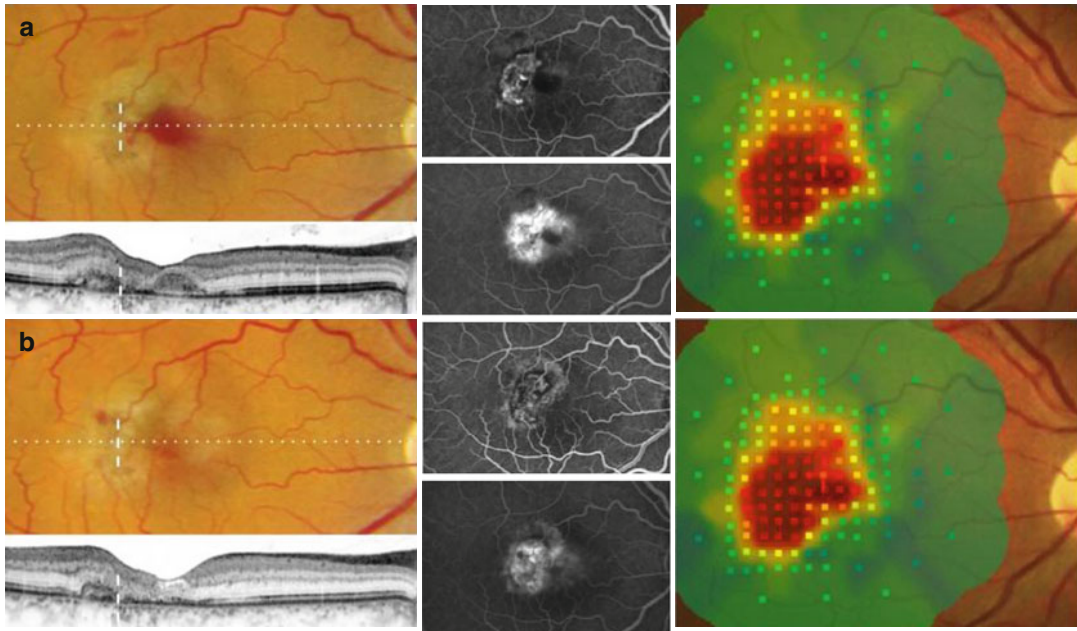


Fig. 11.5 Effects of intravitreal bevacizumab therapy in neovascular macular telangiectasia type 2 (stage 5). (a) Findings at baseline visit: foveal hemorrhage, neovascular membrane with leakage in fluorescein angiography (*top*, early phase; *bottom*, late phase). On microperimetry testing, there is a large absolute scotoma which encompasses the foveal center. Four months after one single treatment

with intravitreal bevacizumab (b), the hemorrhage had been resorbed and leakage was reduced. The scotoma has decreased considerably. The foveal center shows only a relative defect and visual acuity has improved from 20/80 to 20/50 (Reprinted from Charbel Issa et al. [1], Copyright (2013), with permission from Elsevier)

References

- Charbel Issa P, Gillies MC, Chew EY et al (2013) Macular telangiectasia type 2. *Prog Retin Eye Res* 34:49–77
- Gillies MC, Zhu M, Chew EY et al (2009) Familial asymptomatic macular telangiectasia type 2. *Ophthalmology* 116:2422–2429
- Klein R, Blodi BA, Meuer SM et al (2010) The prevalence of macular telangiectasia type 2 in the Beaver Dam Eye Study. *Am J Ophthalmol* 150:55–62
- Gass JD, Blodi BA (1993) Idiopathic juxtafoveolar retinal telangiectasis. Update of classification and follow-up study. *Ophthalmology* 100:1536–1546
- Gaudric A, De Ducos LG, Cohen SY et al (2006) Optical coherence tomography in group 2A idiopathic juxtafoveolar retinal telangiectasis. *Arch Ophthalmol* 124:1410–1419
- Charbel Issa P, Van Der Veen RLP, Stijfs A et al (2009) Quantification of reduced macular pigment optical density in the central retina in macular telangiectasia type 2. *Exp Eye Res* 89:25–31
- Helb HM, Charbel Issa P, Van Der Veen RLP et al (2008) Macular pigment density and distribution in patients with type II macular telangiectasia. *Retina* 28:808–816
- Charbel Issa P, Berendschot TT, Staurengi G et al (2008) Confocal blue reflectance imaging in type 2 idiopathic macular telangiectasia. *Invest Ophthalmol Vis Sci* 49:1172–1177
- Clemons TE, Gillies MC, Chew EY et al (2010) Baseline characteristics of participants in the natural history study of macular telangiectasia (MacTel) MacTel Project Report No. 2. *Ophthalmic Epidemiol* 17:66–73
- Finger RP, Charbel Issa P, Fimmers R et al (2009) Reading performance is reduced due to parafoveal scotomas in patients with macular telangiectasia type 2. *Invest Ophthalmol Vis Sci* 50:1366–1370
- Charbel Issa P, Holz FG, Scholl HPN (2009) Metamorphopsia in patients with macular telangiectasia type 2. *Doc Ophthalmol* 119:133–140
- Charbel Issa P, Helb HM, Holz FG et al (2008) Correlation of macular function with retinal thickness in nonproliferative type 2 idiopathic macular telangiectasia. *Am J Ophthalmol* 245:169–175
- Charbel Issa P, Helb HM, Rohrschneider K et al (2007) Microperimetric assessment of patients with type II macular telangiectasia. *Invest Ophthalmol Vis Sci* 48:3788–3795
- Maruko I, Iida T, Sekiryu T et al (2008) Early morphological changes and functional abnormalities in group 2A idiopathic juxtafoveolar retinal telangiectasis

- using spectral domain optical coherence tomography and microperimetry. *Br J Ophthalmol* 92:1488–1491
15. Schmitz-Valckenberg S, Fan K, Nugent A et al (2008) Correlation of functional impairment and morphological alterations in patients with group 2A idiopathic juxtafoveal retinal telangiectasia. *Arch Ophthalmol* 126:330–335
 16. Wong WT, Forooghian F, Majumdar Z et al (2009) Fundus autofluorescence in type 2 idiopathic macular telangiectasia: correlation with optical coherence tomography and microperimetry. *Am J Ophthalmol* 148:573–583
 17. Zeimer MB, Padge B, Heimes B et al (2010) Idiopathic macular telangiectasia type 2: distribution of macular pigment and functional investigations. *Retina* 30:586–595
 18. Trauzettel-Klosinski S (2002) Reading disorders due to visual field defects: a neuro-ophthalmological view. *Neuroophthalmology* 27:79–90
 19. Charbel Issa P, Finger RP, Holz FG et al (2008) Eighteen-month follow-up of intravitreal bevacizumab in type 2 idiopathic macular telangiectasia. *Br J Ophthalmol* 92:941–945
 20. Charbel Issa P, Tröger E, Finger R et al (2010) Structure-function correlation of the human central retina. *PLoS One* 5(9):e12864
 21. Schmitz-Valckenberg S, Ong EE, Rubin GS et al (2009) Structural and functional changes over time in MacTel patients. *Retina* 29:1314–1320

Stela Vujosevic and Edoardo Midena

12.1 Introduction

Diabetic retinopathy and retinal vascular disorders (the most common retinal vein occlusions) are one of the major causes of permanent visual acuity loss in the working population. Macular edema is the major cause of vision loss in both diabetic patients and those with retinal vein occlusion. Although different treatment options are currently available for the treatment of macular edema due to diabetes mellitus and retinal vein occlusions, still we face pitfalls due to unpredictable results. This is probably due to the presence of different phenotypes of macular edema. The use of combined, noninvasive, multimodal imaging techniques (such as optical coherence tomography, fundus autofluorescence, scanning laser ophthalmoscope in the retromode and microperimetry) might help in the better classification of macular edema, follow-up, and in the evaluation of safety and efficacy of new treatments.

S. Vujosevic, MD, PhD (✉)
Department of Ophthalmology,
University of Padova, via Giustiniani 2, 35128
Padova, Italy
e-mail: stela.vujosevic@unipd.it

E. Midena, MD, PhD, FARVO, FEBO
Department of Ophthalmology, University of Padova,
via Giustiniani 2, 35128 Padova, Italy
Fondazione G.B. Bietti, IRCCS, Rome, Italy

12.2 Diabetic Macular Edema

Diabetic macular edema (DME) is the leading cause of legal blindness in diabetic patients [1]. Approximately 14 % of all diabetics are affected by DME, and the 10-year incidence of DME in patients with newly diagnosed type 2 diabetes is approximately 20 % [2, 3]. DME can occur at any stage of diabetic retinopathy (DR), although it is more likely to occur as the disease progresses [4]. The pathophysiological mechanisms leading to DME are still poorly understood due to its complex and multifactorial origin. It is generally believed that vascular microangiopathy, with endothelial cell damage, pericyte loss, and consecutive breakdown of the inner blood-retinal barrier, is involved in the pathogenesis of DME [2, 3]. Moreover, other factors such as hypoxia, altered blood flow, retinal ischemia, and inflammation are also associated with the progression of DME [5]. However, recently an increasing body of evidence suggests that neurodegeneration precedes the earliest clinical manifestation of diabetic retinal vasculopathy [6, 7]. In fact, early clinical changes in visual function have been found by means of color contrast sensitivity, dark adaptation (nyctometry), electroretinography, and more recently by microperimetry, confirming the precocious occurrence of visual abnormalities in diabetic patients [8–11].

DME is currently evaluated with biomicroscopy, color fundus photography, optical coherence tomography (OCT), fluorescein angiography (FA) and scanning laser ophthalmoscopy in the

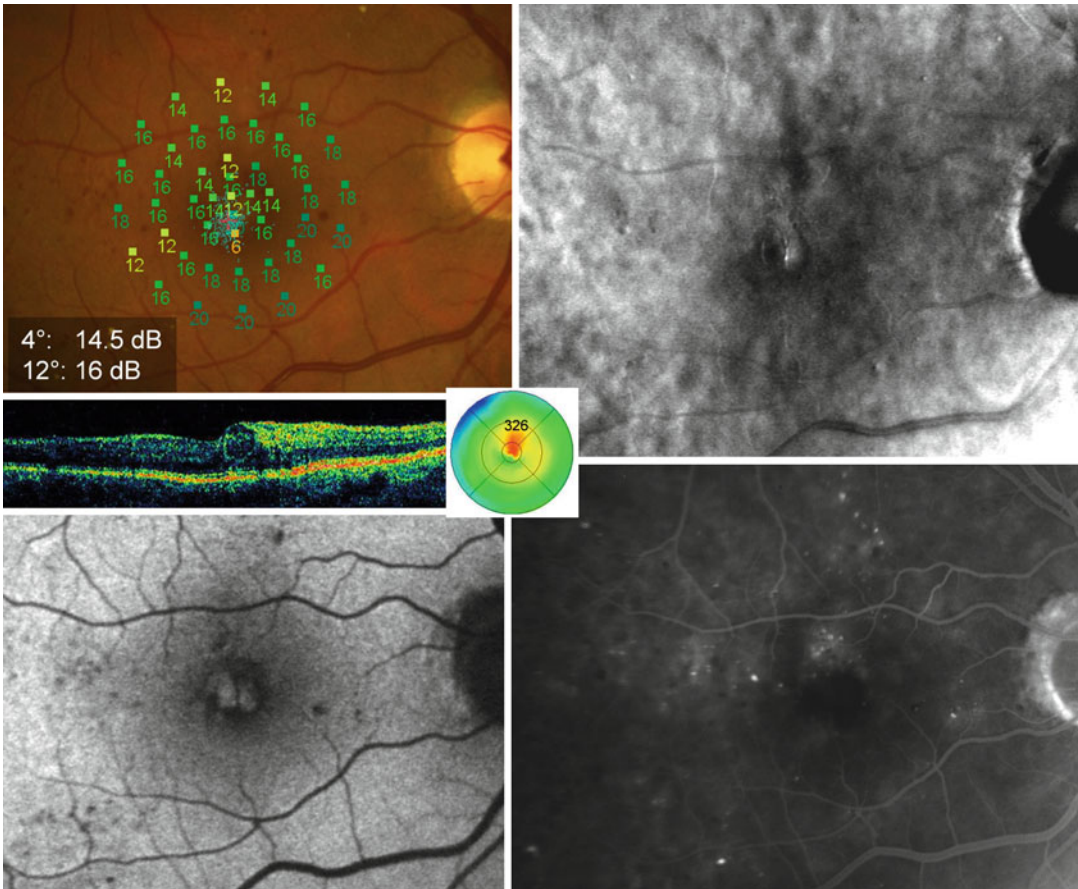


Fig. 12.1 Multimodal imaging in cystoid diabetic macular edema (DME). Microperimetry optical coherence tomography (OCT) line scan (at 90°) and OCT map (*top left*). Retromode scanning laser ophthalmoscopy (RM-SLO; *top right*), fundus autofluorescence (*bottom left*), and fluorescein angiography (*bottom right*) of the right eye of cystoid DME. Microperimetry shows

decreased central retinal sensitivity both in central 4° and 12°. RM-SLO shows intraretinal cysts (small and large ones). Location and extension of SND and macular edema are also easily evaluated. Fundus autofluorescence shows multiple spots of increased foveal autofluorescence. Fluorescein angiography shows macular leakage

retromode as morphologic tests, and mainly visual acuity (VA) as functional test [12–14] (Fig. 12.1). Whereas the use of FA has been progressively decreased, due to its invasiveness and potentially severe side effects, OCT has been proposed as the new gold standard diagnostic technique to quantify and monitor DME [15, 16]. Recently, the Diabetic Retinopathy Clinical Research Network reported only modest correlation between VA- and OCT-measured center point thickness in diabetic patients. They also found modest correlation of changes in retinal thickening and VA after focal laser treatment for

DME, suggesting that OCT measurement alone may not be a good surrogate for VA as a primary outcome in the studies of DME [16]. Therefore, other functional tests need to be evaluated and compared to OCT in order to better understand DME evolution and treatment outcome. Besides visual acuity other functional tests have been used to evaluate functional alterations in diabetic patients. These include both psychophysical tests (such as color vision, contrast sensitivity, dark adaptation (nyctometry), perimetry, and more recently microperimetry) and electrophysiological tests (multifocal electroretinography,

visual-evoked potentials). Among these tests, only microperimetry allows for exact, point-by-point correlation between retinal morphology and function.

12.3 The Role of Microperimetry in Diabetic Retinopathy

The integration of retinal details with function has been achieved by microperimetry. Microperimetry allows for the exact topographic correlation between fundus abnormalities and corresponding functional alterations by integration, with different methods, of differential light threshold (more commonly known as retinal sensitivity) and fundus imaging. It also allows to quantify fixation characteristics, by exactly defining location and stability of foveal or extrafoveal (PRL) fixation, as well as to determinate the size, site, and shape of scotoma, and to show macular sensitivity maps. Automatic follow-up examination which allows to evaluate exactly the same retinal points tested at baseline, regardless any change in fixation characteristics, is a valuable tool of this technique, mainly in the evaluation of treatment outcome and side effects. Microperimetry offers several advantages versus standard perimetry in the quantification of macular sensitivity, such as direct real-time fundus control, direct correlation between sensitivity and fundus changes, detection of central microscotomata, and continuous monitoring of fixation.

Lately, microperimetry has gained an increasing importance in evaluation of functional impairment in diabetic patients [17–24]. In DME, microperimetry has been used for the quantification of macular sensitivity, the correlation of macular sensitivity to macular thickness, visual acuity and fundus autofluorescence data, the knowledge of fixation patterns in different stages and types of edema, and the evaluation of treatment outcomes (laser treatment and intravitreal therapies). Different studies report the correlation between retinal sensitivity, determined with microperimetry, and VA in patients with clinically significant diabetic macular edema (CSME) [17, 20–22]. In DME, a significant

inverse correlation between macular thickness and macular sensitivity exists [18–22]. Different authors reported that reduced retinal sensitivity is related to increasing retinal thickness [19–21]. In a study published by Vujosevic et al., a significant inverse relationship was found, in patients with CSME, between retinal sensitivity and normalized retinal thickness values obtained with OCT, with a decay of 0.83 dB ($p < 0.0001$) for every 10 % of deviation of retinal thickness from the normal values [20]. This means that normalized macular thickness is better correlated to macular function than any absolute value [20]. Microperimetry seems to represent a better functional testing than VA to quantify visual function in diabetic patients, because it incorporates a functional measure that may potentially supplement the predictive value of OCT and visual acuity [20, 21, 25]. Deak et al. performed a systematic correlation between the morphology of single retinal layers, determined by spectral domain OCT, and function and determined by microperimetry in DME [22]. These authors found that large retinal cysts located in the outer nuclear layer and subfoveal neuroretinal detachment are the two morphologic changes with the greatest negative impact on retinal function [22]. Soliman et al. found a significant association between decrease in retinal sensitivity and cystoid macular edema (both foveal petaloid pattern and extrafoveal honeycomb pattern), outer and inner nuclear layer cysts, hard exudates, and foveal thickening in DME [23]. Nittala et al. reported a progressive decrease in macular sensitivity with increasing stage of DR and even an early loss of retinal sensitivity (both in the fovea and up to central 20°) in patients with diabetes but no retinopathy versus normal subjects [24]. This data supports a loss of retinal function before the development of structural abnormalities in the retina probably due to neuronal changes occurring before the onset of vascular dysfunction [24]. Unoki et al. reported a decrease in retinal sensitivity in areas of capillary nonperfusion resulting from severe nonproliferative or proliferative DR corresponding to specific alterations detected on OCT [26]. Microperimetry may be also useful to clarify the pathophysiology of DR,

more precisely DME. It has been recently demonstrated by Vujosevic et al., who analyzed DME using noninvasive imaging modalities such as fundus autofluorescence and microperimetry as functional correlates [27]. These authors demonstrated that in DME, fundus autofluorescence increases in 75 % of affected eyes and that these hyperfluorescent areas are characterized by reduced retinal sensitivity [27]. Therefore, DME with increased FAF pattern is, at least functionally, more severe than DME with a normal FAF pattern. Moreover, the authors hypothesized that increased fundus autofluorescence may depend on activated retinal glial cells, introducing the role of retinal glial cells in the pathophysiology of visual loss in diabetes [27, 28]. The precocious involvement of retinal glial cells has been confirmed with recent clinical studies that evaluated in vivo single intraretinal layer structure in diabetic patients without DR or with early stages of DR using spectral domain OCT [29].

Moreover, microperimetry allows for determination of fixation location (central, relatively eccentric and eccentric) and stability (stable, relatively unstable and unstable). Fixation characteristics (location and stability) are relevant parameters to fully understand the individual quality of vision, especially reading ability, and its knowledge may be especially important in planning laser treatment [21, 25, 30]. Reading ability better correlates with subjective quality of vision rather than for visual acuity [31]. Published data about fixation characteristics in DME eyes is quite contrasting mostly due to the differences in examined populations, especially differences in DME duration [19, 25, 32]. Kube et al. found decreased fixation stability in patients with DME using SLO-microperimetry [19]. Carpineto et al. found that all eyes with eccentric or unstable fixation had cystoid DME [32]. Hatef et al. found in their DME cohort that the majority of eyes had stable and central fixation [33]. Vujosevic et al. reported, in a well-defined group of CSME eyes, that location and stability of fixation were normal, except when hard exudates were located in the fovea [25]. Topographical extension of DME (focal or diffuse) or OCT type of edema (cystoid, sponge-like, subfoveal neuroretinal detachment) did not influence stability or

location of fixation [25]. Moreover, fixation pattern was not significantly influenced by the presence of subfoveal serous neuroretinal detachment, showing a different fixation behavior compared to age-related macular degeneration [34]. Therefore, the only parameter influencing fixation in DME is the presence of subfoveal hard exudates. In these cases, the knowledge of fixation characteristics is fundamental in order to avoid complications due to the photocoagulation of newly developed fixation area [25]. The fixation results in DME patients indicate that the survival and functional reserve of photoreceptor cells undergoing mechanical and toxic stress induced by edema is a long-standing phenomenon, depending mostly on duration of DME and probably not related to intraretinal cysts formation. The photoreceptor loss is preceded by retinal neurodegeneration in DR [20]. Therefore, microperimetry may be of value in predicting the functional outcome of DME after interventions that seem equally effective in restoring normal foveal thickness. This hypothesis has been confirmed by a randomized and prospective study conducted by Vujosevic et al. These authors have demonstrated that subthreshold micropulse diode laser is as effective as modified ETDRS photocoagulation in reducing central retinal thickness in patients with center-involving DME. But, with subthreshold treatment, retinal macular sensitivity stabilizes or improves, whereas with standard photocoagulation, it significantly deteriorates, manifesting as progressive microscotomata [35] (Fig. 12.2). FAF showed no changes after MPDL treatment, whereas definite laser spots were easily seen on FAF images after modified ETDRS treatment [35]. Moreover, other laser wavelengths (such as yellow at 577 nm) used with micropulse mode showed to equally preserve retinal function as diode laser [36]. Therefore, less invasive treatment options, providing the same efficacy as standard treatments, should become more widespread, as recently reported [35, 36].

Microperimetry has also been used to evaluate macular function after intravitreal treatments [37–40]. Karacorlu et al. reported a short-term significant increase in central 20° macular sensitivity and improvement in fixation location after intravitreal injection of triamcinolone in DME

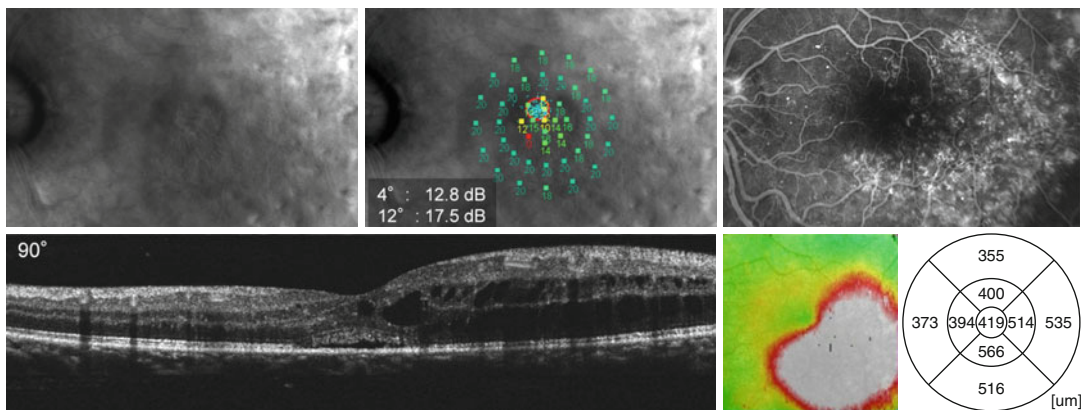


Fig. 12.2 Multimodal imaging in cystoid diabetic macular edema (DME) treated with modified ETDRS macular laser. Retromode scanning laser ophthalmoscopy (RM-SLO; *top left*), microperimetry exam overlapped on RM-SLO image (*top middle*), fluorescein angiography (*top right*), spectral domain optical coherence tomography (SD-OCT) line scan (at 90°), and OCT map (*bottom left and right*). RM-SLO shows the extension of DME as

well as depressions (corresponding to laser scars) and intraretinal cysts. Microperimetry shows decreased central retinal sensitivity both in central 4° and 12°. Fluorescein angiography shows a significant macular leakage. Location and extension of subfoveal neuroretinal detachment are also easily evaluated on RM-SLO and SD-OCT

[37]. Grenga et al. reported a longer functional benefit (increase in retinal sensitivity within central 10°) of intravitreal triamcinolone in eyes with long-standing DME [38]. Rinaldi et al. documented a significant correlation between increase in macular sensitivity and decrease in foveal thickness after 3 consecutive intravitreal injections of pegaptanib in DME, up to 48 weeks follow-up [39]. Querques et al. showed short-term improvement in central 8° retinal sensitivity after a single intravitreal injection of ranibizumab in DME [40] (Fig. 12.3).

12.4 Retinal Vein Occlusion

Retinal vein occlusion (RVO) is a common retinal vascular disorder with the potential for significant vision-related morbidity [41, 42]. Retinal vein occlusion is classified as either branch retinal vein occlusion (BRVO), central retinal vein occlusion (CRVO), or hemiretinal vein occlusion (HRVO) based on the specific occlusion site. Macular edema (ME) is the most vision-threatening complication of RVO. Grid laser photocoagulation is an evidence-based treatment for ME associated with BRVO, yet with limited

improvement in visual acuity [43]. Until recently, no proven treatment existed for ME in eyes with CRVO. The recent development of intravitreal therapy has demonstrated benefit with vascular endothelial growth factor (VEGF) agents and corticosteroids for the treatment of RVO-associated macular edema. The intravitreal use of anti-VEGF drugs (ranibizumab and bevacizumab) and sustained release dexamethasone implant and preservative-free triamcinolone has significantly expanded the treatment options and replaced standard of care for treatment of RVO-associated macular edema. Although these intravitreal agents are effective, the knowledge of their specific indications and long-term roles is still evolving [44].

12.5 The Role of Microperimetry in Retinal Vein Occlusion

In BRVO eyes with macular edema, visual prognosis is influenced by various factors, such as the duration of ME, age, initial visual acuity (VA), history of coronary artery disease, and presence of retinal ischemia [45–47]. The assessment of VA and the measurement of foveal thickness by

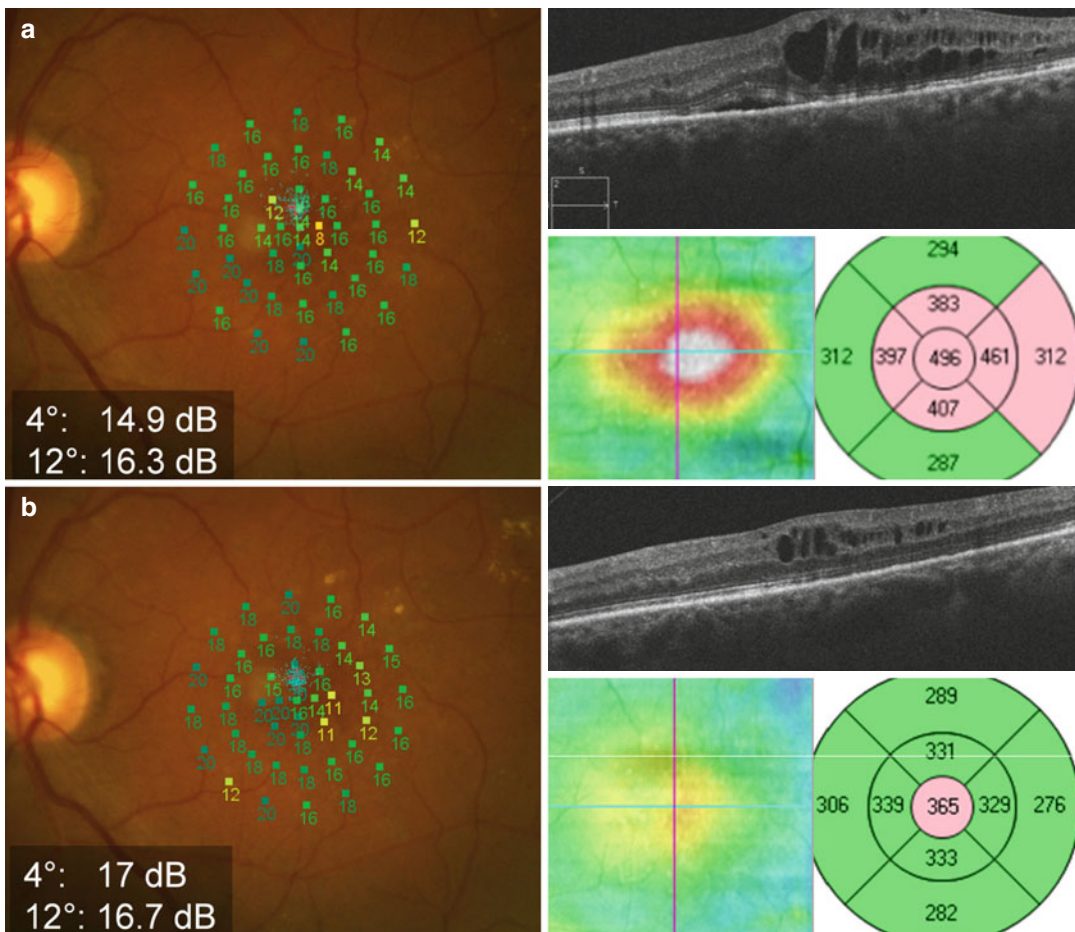


Fig. 12.3 Microperimetry and OCT before and after intravitreal ranibizumab in diabetic macular edema. (a) Baseline examination: Microperimetry, spectral domain OCT images (line scan and retinal thickness map) of a diabetic patient with cystoid macular edema and shallow neuroretinal detachment treated with modified ETDRS macular laser treatment. Microperimetry shows decreased

central retinal sensitivity both in central 4° and 12°. (b) Follow-up examination after 3 intravitreal injections of ranibizumab: An increase in both 4° and 12° central retinal sensitivity is documented by microperimetry examination. OCT shows a significant decrease in central retinal thickness and a complete resolution in subfoveal neuroretinal detachment

OCT are widely considered to be useful to determine the treatment strategy in patients with RVO [47]. However, RVO, both BRVO and CRVO, causes retinal pathological changes (such as retinal hemorrhages, hard exudates, cotton wools spots, retinal edema, retinal ischemia) that not only affect foveal region but also extend into the macular and peripheral regions. Therefore, measurement of just VA as a visual function parameter is limited to just foveal function evaluation. Moreover, patients with good VA sometimes have difficulty in seeing certain objects, and the

opposite may also occur [48]. Microperimetry showed that retinal sensitivity is more closely associated to retinal thickness and volume than visual acuity in patients with ME due to BRVO [48–50]. Cystoid macular edema, a common complication in BRVO patients is associated with reduced retinal sensitivity [51]. On the contrary, the presence of subfoveal neuroretinal detachment was not associated with more reduced retinal sensitivity (central 4°, 10°, and 20°) compared to cystoid macular edema, even if VA was significantly decreased [51]. This may be due to the fact

Fig. 12.4 Microperimetry in hemiretinal vein occlusion. Microperimetry examination of a patient with hemi-central retinal vein occlusion showing a significant decrease in retinal sensitivity over the areas of hard exudates and in the fovea



that subfoveal neuroretinal detachment is usually associated with breaks in the external limiting membrane (ELM) at the fovea [50]. Loss of the ELM barrier often results in damage to the outer segments of foveal photoreceptors and impairment in visual acuity [52]. Thus, evaluation of both VA and sensitivity may be important in BRVO patients to detect the real effects of macular edema and to fully evaluate visual function (Fig. 12.4). Moreover, Ogino et al. showed a good correlation between changes in multifocal ERG and retinal sensitivity (and not VA) in patients with ME due to BRVO [53].

A single intravitreal bevacizumab injection showed to be effective in increasing retinal sensitivity in the central 10° determined by microperimetry MP1 and decreasing retinal thickness in patients with ME, due to both BRVO and CRVO, as reported by Yamaike et al. [48]. The increase in retinal sensitivity was detected immediately after treatment and lasted up to 6 months. Kriechbaum et al. showed that after multiple intravitreal bevacizumab injections in a flexible dosing regimen (3 consecutive IVB injections at

4 weeks and thereafter as per needed), the mean area of absolute scotoma was reduced from $21.4\% \pm 21\%$ of the central visual field to $6.4\% \pm 11\%$ at 6 months of follow-up and remained stable up to 1 year in both BRVO and CRVO patients with macular edema [54]. Moreover, mean retinal sensitivity in the central 12° increased from 6 ± 4 dB at baseline to 10 ± 3 dB after 6 months and remained at this level (10 ± 4 dB) during the entire follow-up (1 year). Winterhalter et al. showed a significant localized increase in retinal sensitivity after intravitreal bevacizumab treatment in patients with ME due to BRVO and no change in best corrected visual acuity and reading ability to the 6-month follow-up [55]. In the CRVO group, although there was an amelioration in retinal sensitivity after IVB treatment, it did not reach a statistical significance [55]. The authors suggested that microperimetry was more convenient to detect even the subtle functional changes in BRVO than BCVA and reading ability, proposing it as a possible valuable tool in the follow-up of these patients [55].

Yamaike et al. were the first to report 4 cases with an improvement in macular sensitivity after intravitreal triamcinolone acetonide treatment in patients with BRVO [49]. Noma et al. found that improvement of retinal sensitivity in BRVO patients treated with intravitreal triamcinolone acetonide was correlated with the percent changes of retinal thickness and volume in two macular subfields (superior inner, the site of occlusion, and temporal outer) [56]. This suggests that the extent of morphological improvement in these two macular subfields may influence macular sensitivity after intravitreal triamcinolone acetonide. Therefore, the measurement of OCT parameters in these specific subfields is recommended in addition to the assessment of the fovea as part of routine clinical examination in order to provide further insight into the pathophysiology of this disease [56].

In nonischemic CRVO patients with ME, intravitreal triamcinolone treatment determined a significant increase in retinal sensitivity within central 20° at 1 and 3 months and decrease in retinal thickness, whereas the increase of retinal sensitivity was not significant at 6-month follow-up [57]. Both fixation location and stability significantly improved after intravitreal triamcinolone during all the follow-up visits [57]. The authors suggest that microperimetric parameters may also be good predictors of ME recurrence.

12.6 Retinal Artery Occlusion and Other Vascular Disorders

There is limited available data about the use of microperimetry in retinal artery occlusion or other vascular disorders. Chalam et al. reported a progressive increase in retinal sensitivity (from dense to relative scotomas) over the area of initial white edema (which became atrophic) in branch artery occlusion with preserved visual acuity [58]. Meyer et al. reported anatomical and functional impairment in a case with Purtscher's retinopathy [59]. These authors described the presence of absolute scotomas in the central and peripapillary area of cotton wool

spots corresponding to hyporeflexive area in the inner retinal layers which completely resolved after the treatment with steroids [59].

Conclusion

Diabetic retinopathy and retinal vascular disorders have an epidemiologically relevant impact on visual function, up to permanent visual acuity loss, even in early stages of these diseases. Although a huge progress has been made in the evaluation and treatment of DME and macular edema due to retinal vein occlusions, we are still unable to exactly identify and differentiate the responders from nonresponders to any individual treatment at baseline. Therefore, a more analytical structural and functional evaluation of these patients is needed in order to obtain more precise phenotyping. Microperimetry, a precise integrate functional imaging evaluation, might help in better management of these patients.

References

1. Global prevalence of diabetes mellitus and its complications (2005) In: Prevention of blindness from diabetes mellitus. WHO Report, Geneva. Accessed on 14 Jan 2006
2. Anderson JM, Van Itallie CM (1995) Tight junctions and the molecular basis for regulation of paracellular permeability. *Am J Physiol* 269:G467–G476
3. Antonetti DA, Barber AJ, Khin S et al (1998) Vascular permeability in experimental diabetes is associated with reduced endothelial occludin content: vascular endothelial growth factor decreases occludin in retinal endothelial cells. *Diabetes* 47:1953–1959
4. Lopes de Faria JM, Jalkh AE, Trempe CL et al (1999) Diabetic macular edema: risk factors and concomitants. *Acta Ophthalmol Scand* 77:170–175
5. Bhagat N, Grigorian RA, Tutela A et al (2009) Diabetic macular edema: pathogenesis and treatment. *Surv Ophthalmol* 54:1–32
6. Bresnick GH (1986) Diabetic retinopathy viewed as a neurosensory disorder. *Arch Ophthalmol* 104:989–990
7. Barber AJ (2003) A new view of diabetic retinopathy: a neurodegenerative disease of the eye. *Prog Neuropsychopharmacol Biol Psychiatry* 27:283–290
8. Midena E, Segato T, Giuliano M et al (1990) Macular recovery function (nyctometry) in diabetics without and with early retinopathy. *Br J Ophthalmol* 74:106–108
9. Midena E (2006) Fundus perimetry-microperimetry: an introduction. In: Midena E (ed) *Perimetry and the*

- fundus: an introduction to microperimetry. Slack Incorporated, Thorofare, pp 1–7
10. Ewing FM, Deary IJ, Strachan MW et al (1998) Seeing beyond retinopathy in diabetes: electrophysiological and psychophysical abnormalities and alterations in vision. *Endocr Rev* 19:462–476
 11. Vujosevic S, Midena E (2006) Diabetic retinopathy. In: Midena E (ed) *Perimetry and the fundus: an introduction to microperimetry*. Slack Incorporated, Thorofare, pp 177–179
 12. Browning DJ, Altaweel MM, Bressler NM et al (2008) Diabetic macular edema: what is focal and what is diffuse? *Am J Ophthalmol* 146:649–655
 13. Midena E, Vujosevic S (2012) Diagnosing and monitoring diabetic macular edema: structural and functional tests. *Int Ophthalmol* [Epub ahead of print]
 14. Vujosevic S, Trento B, Bottega E et al (2012) Scanning laser ophthalmoscopy in the retromode in diabetic macular oedema. *Acta Ophthalmol* 90:374–380
 15. Strøm C, Sander B, Larsen N et al (2002) Diabetic macular edema assessed with optical coherence tomography and stereo fundus photography. *Invest Ophthalmol Vis Sci* 43:241–245
 16. Diabetic Retinopathy Clinical Research Network (2007) Relationship between optical coherence tomography-measured central retinal thickness and visual acuity in diabetic macular edema. *Ophthalmology* 114:525–536
 17. Rohrschneider K, Bültmann S, Glück R et al (2000) Scanning laser ophthalmoscope fundus perimetry before and after laser photocoagulation for clinically significant diabetic macular edema. *Am J Ophthalmol* 129:27–32
 18. Mori F, Ishiko S, Kitaya N et al (2002) Use of scanning laser ophthalmoscope microperimetry in clinically significant macular edema in type 2 diabetes mellitus. *Jpn J Ophthalmol* 46:650–655
 19. Kube T, Schmidt S, Toonen F et al (2005) Fixation stability and macular light sensitivity in patients with diabetic maculopathy: a microperimetric study with a scanning laser ophthalmoscope. *Ophthalmologica* 219:16–20
 20. Vujosevic S, Midena E, Pilotto E et al (2006) Diabetic macular edema: correlation between microperimetry and optical coherence tomography findings. *Invest Ophthalmol Vis Sci* 47:3044–3051
 21. Okada K, Yamamoto S, Mizunoya S et al (2006) Correlation of retinal sensitivity measured with fundus-related microperimetry to visual acuity and retinal thickness in eyes with diabetic macular edema. *Eye* 20:805–809
 22. Deak GG, Bolz M, Ritter M et al (2010) A systematic correlation between morphology and functional alterations in diabetic macular edema. *Invest Ophthalmol Vis Sci* 51:6710–6714
 23. Soliman W, Hasler P, Sander B (2012) Local retinal sensitivity in relation to specific retinopathy lesions in diabetic macular oedema. *Acta Ophthalmol* 90:248–253
 24. Nittala MG, Gella L, Raman R (2012) Measuring retinal sensitivity with the microperimeter in patients with diabetes. *Retina* 32:1302–1309
 25. Vujosevic S, Pilotto E, Bottega E et al (2008) Retinal fixation impairment in diabetic macular edema. *Retina* 10:1443–1450
 26. Unoki N, Nishijima K, Sakamoto A et al (2007) Retinal sensitivity loss and structural disturbance in areas of capillary nonperfusion of eyes with diabetic retinopathy. *Am J Ophthalmol* 144:755–760
 27. Vujosevic S, Casciano M, Pilotto E et al (2011) Diabetic macular edema: fundus autofluorescence and functional correlations. *Invest Ophthalmol Vis Sci* 52:442–448
 28. Xu H, Chen M, Manivannan A et al (2008) Age-dependent accumulation of lipofuscin in perivascular and subretinal microglia in experimental mice. *Aging Cell* 7:58–68
 29. Vujosevic S, Midena E (2013) Retinal layers changes in human pre-clinical and early clinical diabetic retinopathy supports early retinal neuronal and Müller cells alterations. *J Diabetes Res*.2013:905058. doi:10.1155/2013/905058. Epub 2013 Jun 12
 30. Møller F, Bek T (2003) The relation between visual acuity, fixation stability, and the size and location of foveal hard exudates after photocoagulation for diabetic maculopathy: a 1-year follow-up study. *Graefes Arch Clin Exp Ophthalmol* 241:458–462
 31. Mori F, Ishiko S, Kitaya N et al (2001) Scotoma and fixation patterns using scanning laser ophthalmoscope microperimetry in patients with macular dystrophy. *Am J Ophthalmol* 132:897–902
 32. Carpineto P, Ciancaglini M, Di Antonio L et al (2007) Fundus microperimetry patterns of fixation in type 2 diabetic patients with diffuse macular edema. *Retina* 27:21–29
 33. Hatf E, Colantuoni E, Wang J et al (2011) The relationship between macular sensitivity and retinal thickness in eyes with diabetic macular edema. *Am J Ophthalmol* 152:400–405
 34. Midena E, Radin PP, Pilotto E et al (2004) Fixation pattern and macular sensitivity in eyes with subfoveal choroidal neovascularization secondary to age-related macular degeneration. A microperimetry study. *Semin Ophthalmol* 19:55–61
 35. Vujosevic S, Bottega E, Casciano M et al (2010) Microperimetry and fundus autofluorescence in diabetic macular edema: subthreshold micropulse diode laser versus modified early treatment diabetic retinopathy study laser photocoagulation. *Retina* 30:908–916
 36. Vujosevic S, Martini F, Convento E et al (2013) Morphologic and functional effects of diode(810nm) and yellow(577nm) subthreshold micropulse laser in center-involving diabetic macular edema. In: ARVO annual meeting 2013, Seattle
 37. Karacorlu M, Ozdemir H, Senturk F et al (2010) Macular function after intravitreal triamcinolone acetonide injection for diabetic macular oedema. *Acta Ophthalmol* 88:558–563

38. Grenga P, Lupo S, Domanico D (2008) Efficacy of intravitreal triamcinolone acetonide in long standing diabetic macular edema: a microperimetry and optical coherence tomography study. *Retina* 28:1270–1275
39. Rinaldi M, Chiosi F, dell’Omo R et al (2012) Intravitreal pegaptanib sodium (Macugen®) for treatment of diabetic macular oedema: a morphologic and functional study. *Br J Clin Pharmacol* 74:940–946
40. Querques G, Bux AV, Martinelli D et al (2009) Short-term fluctuation of diabetic macular edema after intravitreal ranibizumab injection. *Retina* 29:1274–1281
41. The Branch Vein Occlusion Study Group (1984) Argon laser photocoagulation for macular edema in branch vein occlusion. The Branch Vein Occlusion Study Group. *Am J Ophthalmol* 98:271–282
42. Central Vein Occlusion Study Group (1993) Baseline and early natural history report. *Arch Ophthalmol* 111:1087–1095
43. Central Vein Occlusion Study Group (1995) Evaluation of grid pattern photocoagulation for macular edema in central retinal vein occlusion. *Ophthalmology* 102:1425–1433
44. Hahn P, Fekrat S (2012) Best practices for treatment of retinal vein occlusion. *Curr Opin Ophthalmol* 23:175–181
45. Chung EJ, Hong YT, Lee SC et al (2008) Prognostic factors for visual outcome after intravitreal bevacizumab for macular edema due to branch retinal vein occlusion. *Graefes Arch Clin Exp Ophthalmol* 246:1241–1247
46. Rehak J, Dusek L, Chrapek O et al (2011) Initial visual acuity is an important prognostic factor in patients with branch retinal vein occlusion. *Ophthalmic Res* 45:204–209
47. Scott IU, VanVeldhuisen PC, Oden NL et al (2011) Standard Care versus Corticosteroid for Retinal Vein Occlusion Study Investigator Group. Baseline predictors of visual acuity and retinal thickness outcomes in patients with retinal vein occlusion: Standard Care Versus Corticosteroid for Retinal Vein Occlusion Study report 10. *Ophthalmology* 118:345–352
48. Yamaike N, Tsujikawa A, Sakamoto A et al (2009) Retinal sensitivity after intravitreal injection of bevacizumab for the treatment of macular edema secondary to retinal vein occlusion. *Retina* 29:757–767
49. Yamaike N, Kita M, Tsujikawa A et al (2007) Perimetric sensitivity with the micro perimeter 1 and retinal thickness in patients with branch retinal vein occlusion. *Am J Ophthalmol* 143:342–344
50. Noma H, Mimura T, Shimada K (2013) Retinal function and morphology in central retinal vein occlusion with macular edema. *Curr Eye Res.* 38:143–149
51. Noma H, Funatsu H, Mimura T et al (2011) Visual function and serous retinal detachment in patients with branch retinal vein occlusion and macular edema: a case series. *BMC Ophthalmol* 11:29
52. Tsujikawa A, Sakamoto A, Ota M et al (2010) Serous retinal detachment associated with retinal vein occlusion. *Am J Ophthalmol* 149:291–301
53. Oginio K, Tsujikawa A, Murakami T et al (2011) Evaluation of macular function using focal macular electroretinography in eyes with macular edema associated with branch retinal vein occlusion. *Invest Ophthalmol Vis Sci* 52:8047–8055
54. Kriechbaum K, Prager F, Geitzenauer W et al (2009) Association of retinal sensitivity and morphology during antiangiogenic treatment of retinal vein occlusion over one year. *Ophthalmology* 116:2415–2421
55. Winterhalter S, Lux A, Maier AK et al (2012) Microperimetry as a routine diagnostic test in the follow-up of retinal vein occlusion? *Graefes Arch Clin Exp Ophthalmol* 250:175–183
56. Noma H, Funatsu H, Mimura T et al (2012) Functional-morphological changes after intravitreal injection of triamcinolone acetonide for macular edema with branch retinal vein occlusion. *J Ocul Pharmacol Ther* 28:231–236
57. Senturk F, Ozdemir H, Karacorlu M et al (2010) Microperimetric changes after intravitreal triamcinolone acetonide injection for macular edema due to central retinal vein occlusion. *Retina* 30:1254–1261
58. Chalam KV, Agarwal S, Gupta SK et al (2007) Recovery of retinal sensitivity after transient branch retinal artery occlusion. *Ophthalmic Surg Lasers Imaging* 38:328–329
59. Meyer CH, Callizo J, Schmidt JC et al (2006) Functional and anatomical findings in acute Purtscher’s retinopathy. *Ophthalmologica* 220:343–346

13.1 Introduction

Myopia is functionally classified into two groups: non-pathologic myopia and pathologic myopia. Non-pathologic myopia is usually a minimal to moderate degree of myopia (usually less than 6 diopters), and includes simple myopia or “school myopia.” Non-pathologic myopia has no disorder other than reflective error and is easy to correct with glasses. Although there is no international standard definition, pathologic myopia is generally defined as either a reflective error of more than 8 diopters or an axial length of more than 26.5 mm. Pathologic myopia often causes a variety of fundus changes called myopic maculopathy, choroidal neovascularization (CNV), myopic retinoschisis, foveal retinal detachment, or macular hole [1].

The static visual field test is thought to be unsuitable to evaluate the abnormality in patients with pathologic myopia because these patients often have myopic maculopathy or a large peripapillary conus. Recently, new technology has produced the Microperimeter-1 (MP-1, NIDEK, Italy), as a detailed functional examination device. This chapter describes the abnormal visual field in pathologic myopia using MP-1.

I. Maruko, MD (✉) • T. Iida
Department of Ophthalmology,
Tokyo Women’s Medical University
School of Medicine, 8-1 Kawada-cho,
Shinjuku-ku, Tokyo, Japan
e-mail: imaruko@oph.twmu.ac.jp

13.2 Ophthalmoscopic Findings

As known, the fundus in pathologic myopia shows various changes. Tigrroid fundus is the most common myopic sign even in simple myopia. It is thought to result from the thinning of retinal pigment epithelium (RPE) associated with elongation of the axial length. Myopic conus, which is induced by dissociation between the optic disc and its surrounding tissue, is also common. Focal and/or diffuse atrophic lesions are observed in all types of high myopia and these lesions indicate RPE degeneration, which is caused by a decreased blood supply from the choriocapillaris. These lesions can appear as brown or white areas resulting from the pigmentation or depigmentation of RPE. Lacquer crack lesions are the mechanical breaking of the Bruch’s membrane. It is difficult to determine their length and width on ophthalmoscopic observation. At fundus autofluorescence, they appear as noninvasive hypofluorescent lines. Generally, posterior staphyloma develops after age 40 in severe myopia. The reason for the formation of posterior staphyloma has not yet been identified. The extent of staphyloma can be visualized using magnetic resonance imaging (MRI) according to recent reports [2, 3]. CNV appears on ophthalmoscopic examination as a gray lesion at the fovea and it is sometimes accompanied by subretinal hemorrhage. On fluorescent angiography, CNV is observed as the classic type with hyperfluorescence at the beginning of the early

phase and late leakage. Old CNV lesions remain as pigmented findings at the fovea, which are also called “Fuchs’ spots”.

13.3 Optical Coherence Tomography Findings

Optical coherence tomography (OCT) is the most valuable device for the imaging of the macular area. In pathologic myopia, OCT can visualize detailed morphologic changes that cannot be observed in a routine ophthalmic examination [4, 5]. It is very suitable to observe a foveal retinal detachment using OCT because of minimal changes. Myopic foveal retinal detachment is frequently accompanied by foveal retinoschisis. Foveal retinoschisis is one of the visual loss causes in pathologic myopia and it has recently been considered a major contributor of foveal retinal detachment and macular holes [6–8]. Foveal morphologic impairment in pathologic myopia is classified into three groups: the retinoschisis type, the foveal detachment type and the macular hole type. This classification is essential for the prediction of visual prognosis [9, 10]. It is easy to distinguish these types on the Spectral OCT domain. Recent micro-incision vitreous surgery, even for retinoschisis, is safe and effective as long as the formation of macular holes are avoided.

CNV is the main cause of central visual loss in pathologic myopia [11]. A typical case of myopic CNV is categorized as type 2 CNV, which extends into the subretinal space. Myopic CNV is generally observed as hyperreflective tissue above the RPE line.

Another type of foveal retinal detachment formation in pathologic myopia has recently been reported. Dome-shaped macula (DSM) is a new entity associated with highly myopic eyes [12]. It might be a particular type of posterior staphyloma, and defined as a convex elevation of the macula on OCT. Subretinal fluid is sometimes observed in DSM, and it may cause the choroidal outflow disorder associated with local morphological changes of choroid and sclera at the fovea [13]. Although the tilted disc

syndrome is usually associated with good visual prognosis, foveal complications, such as foveal retinal detachment, are sometimes observed. Tilted disc syndrome is often accompanied by moderate to severe myopic refractive error. Foveal retinal detachment in tilted disc syndrome, together with DSM, is thought to be a local morphologic change associated with the inferior staphyloma [14].

13.4 Microperimetry for Pathologic Myopia

OCT can capture subtle morphologic changes, but cannot evaluate functional changes. Although visual acuity is still a traditional valuable indicator for visual function, it reflects only the status of fovea and perifovea. On the other hand, the perimeter reflects a much wider macular area function than visual acuity. MP-1 microperimeter is the recently developed device that can provide the automatic lesion-related perimetry for monitoring the fundus.

The characteristics of MP-1 are the auto eye-tracking system for involuntary eye movements, the follow-up mode, the possibility of creating composed images using color fundus photos and perimetry results and the possibility of customizing patterns of stimulus points. The auto tracking system is an advantage during the examination, especially in pathologic myopia. Composite images of a fundus photo and sensitivity results are useful for evaluating the various lesions of myopic maculopathy. However, the operator should pay attention to the overlay of fundus photos and perimetry results because of the blurry images in highly myopic eyes. CNV size in pathologic myopia might be smaller than in age-related macular degeneration. It is useful to evaluate the small changes correctly using the customized stimulus points in an MP-1. A follow-up mode is helpful for measuring small changes in small lesions. There are several reports about microperimetry in eyes with pathologic myopia [15–23]; several cases are discussed in more detail below.

13.5 Case Presentation

13.5.1 Dome-Shaped Macula (DSM) (Fig. 13.1)

DSM is a new pathologic myopia-related entity, which is sometimes associated with subretinal fluid. Gaucher et al. originally reported that it can be found in the 20 % of all highly myopic eyes [12]. We evaluate DSM using spectral domain OCT and the subretinal fluid due to the relative scleral thickening at the subfovea. There are no reports of using MP-1 for DSM.

Figure 13.1 refers to a case of a 71-years-old woman with bilateral blur vision. Decimal visual acuities with intraocular lenses in both eyes are 0.9 in the right eye and 0.7 in the left eye. Her axial lengths are 34.44 mm in the right eye and 34.06 mm in the left. Both eyes show a large peripapillary conus and widespread RPE atrophy. A swept

source OCT captures the convex elevation of the macula in both eyes. Using MP-1, almost normal sensitivity is measured in the right eye and relatively low sensitivity in the left eye. These findings correlate with the higher macular elevation of the left eye compared to the right eye.

13.5.2 Tilted Disc Syndrome (TDS) (Fig. 13.2)

TDS is known as the characteristic inferonasal tilting of the optic disc, associated with congenital inferonasal crescent and inferior staphyloma. Staphyloma in TDS is often observed in the inferior ocular area, and the superior edge of the staphyloma sometimes involves the macula; this is the reason why these anatomic changes at the superior edge of the staphyloma may lead to foveal weakness and subsequent complications.

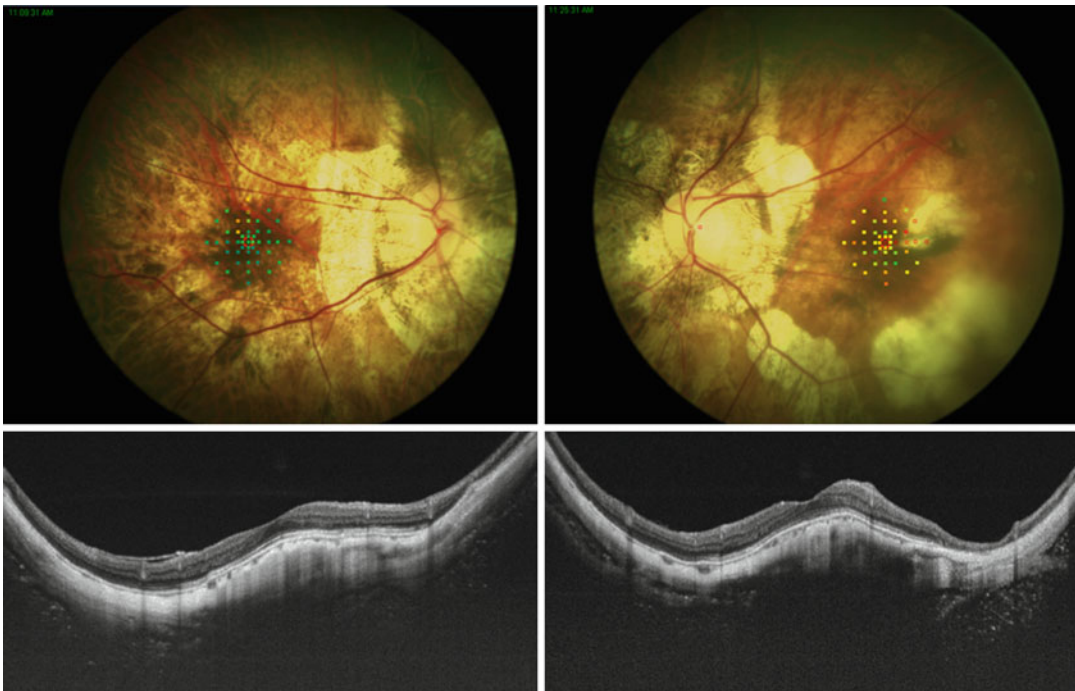


Fig. 13.1 Dome-shaped macula. A 71-year-old female. Best-collected visual acuity is 0.9 in the right eye and 0.7 in the left eye. Axial length is 34.44 mm in the right eye and 34.06 mm in the left eye (*top column*). Microperimetry-1 results with composite fundus photo in both eyes. Right eye

is almost normal, however left eye shows the partial scotoma corresponding to the chorioretinal atrophy (*bottom column*). Vertical scan images of swept source optical coherence tomography in both eyes reveal the convex elevation of the macula. There is no subretinal fluid at all

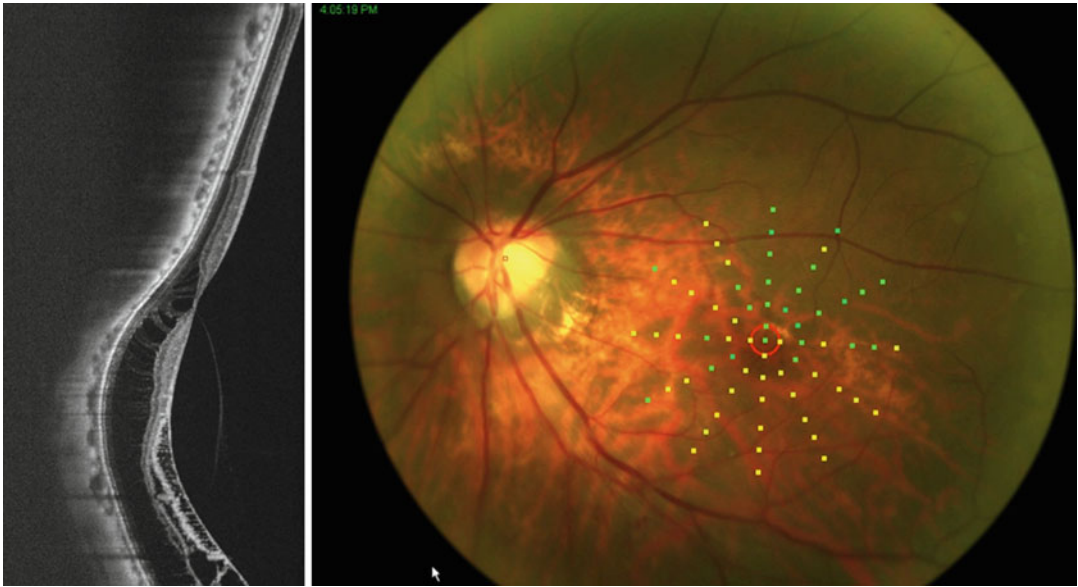


Fig. 13.2 Tilted disc syndrome. A 63-year-old female. Decimal visual acuity is 0.4 in the left eye. The spherical equivalent is -12 diopters and axial length is 27.09 mm in the left eye (*right*). Color fundus shows the inferior-nasal

tilted disc with conus. Microperimetry-1 results show relative lower sensitivity at the inferior half than superior half of the macula (*left*). Vertical scan of swept source optical coherence tomography shows retinoschisis at the inferior macula

Figure 13.2 refers to a 63-year-old woman with 0.4 decimal visual acuity in the left eye. The spherical equivalent is -12 diopters and the axial length is 27.09 mm in the left eye. Inferior staphyloma is observed with retinoschisis on swept-source OCT. Relatively less sensitivity on MP-1 is measured in correspondence of the inferior staphyloma with retinoschisis.

Figure 13.3 refers to a case of a 70-year-old woman with a history of CNV removal surgery. Axial length is 29.57, and decimal visual acuity is 0.5 in the right eye. Large RPE atrophy is observed at the macular area where a low sensitivity is also measured. One year later, MHRD appears at the macula, and MP-1 shows a further sensitivity decrease.

13.5.3 Macular Hole Retinal Detachment (MHRD) (Fig. 13.3)

MHRD is one of the most serious complications in pathologic myopia; myopic CNV is the other complication associated with severe visual loss.

13.5.4 Myopic Choroidal Neovascularization (Myopic CNV) (Fig. 13.4)

Myopic CNV induces central visual loss and scotoma. Recently, bevacizumab, an anti-vascular endothelial growth factor, has been

Fig. 13.4 Myopic choroidal neovascularization. A 72-year-old female with myopic choroidal neovascularization in the right eye. Axial length on the right eye is 28.58 mm (*top left*). Fluorescein angiography at baseline shows the classic choroidal neovascularization lesion with leakage on the early phase (*top right*). Optical coherence tomography shows the hyperreflective tissue above retinal pigment epi-

thelium representative characteristics of type 2 choroidal neovascularization lesion (*bottom left*). Microperimetry-1 results at the baseline shows the reduced sensitivity at the area of the choroidal neovascularization lesion (*bottom right*). One month after intravitreal bevacizumab, visual acuity did not change at all, but the slight improvement was measured on Microperimetry-1

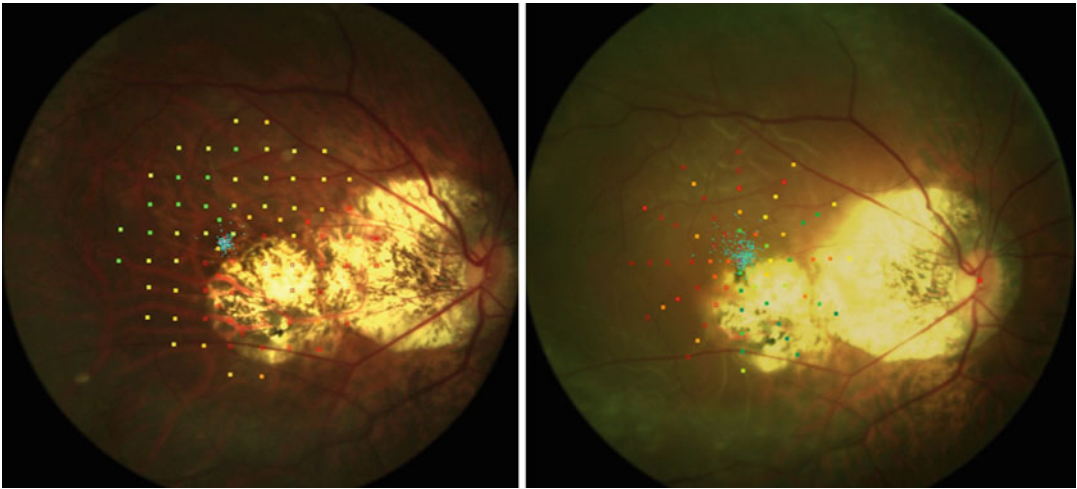
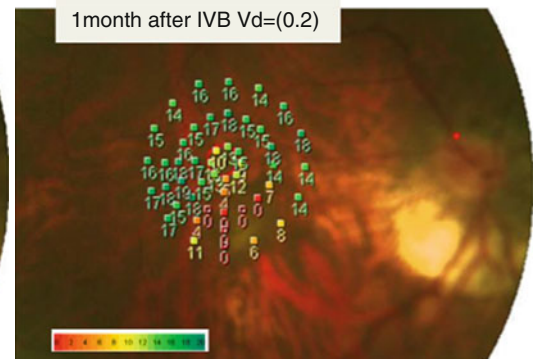
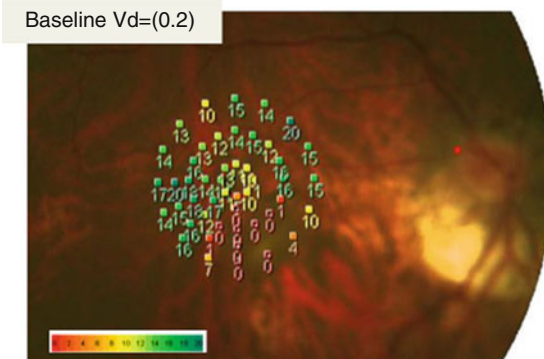
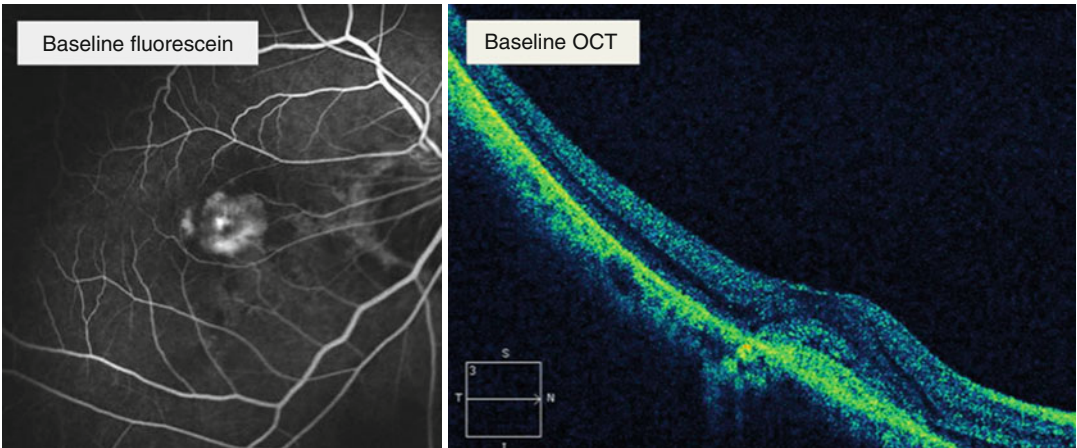


Fig. 13.3 Macular hole retinal detachment. A 70-year-old female with history of CNV removal surgery. Axial length is 29.57, and decimal visual acuity is 0.5 in the right eye (*left*). Large RPE atrophy is observed in the mac-

ular area and here a low sensitivity is measured (*right*). One year later, MHRD appears at the macula, and MP-1 shows a further sensitivity decrease



considered the most effective treatment for myopic CNV. Exudative lesions disappear for only a short time with intravitreal bevacizumab; however, a long-term follow-up still needs to be done.

Figure 13.4 refers to a case of a 72-year-old woman with myopic CNV in the right eye. Axial length of the right eye is 28.58 mm. Fluorescein angiography at the baseline shows a classic CNV lesion with early-phase leakage. OCT shows hyperreflective tissue above RPE representative characteristics of type 2 CNV. MP-1 shows the reduced sensitivity at the area corresponding to CNV. One month after intravitreal bevacizumab, visual acuity did not change at all; however, a slight improvement was measured on the MP-1.

Conclusions

Pathologic myopia often shows complications such as CNV, retinoschisis, foveal detachment, macular holes, and RPE atrophic changes. However, visual acuity is not enough a valuable index to evaluate the effectiveness of treatment or improvement in pathologic complicated myopia. Although we have several advanced devices, such as OCT, to evaluate morphological changes, we had not the possibility to measure functional changes. Now, in some cases MP-1 may provide helpful information about visual function more than visual acuity. The fixation training programs (reading test and feedback test) are also involved in MP-1 for patients with central scotoma. MP-1 is very helpful because it allows to use both research and clinical fields for pathologic myopia.

References

1. Wong WT, Brucker AJ (2005) Ocular findings in myopia. In: Midene E (ed) *Myopia and related disease*. Ophthalmic Communications Society Inc., New York, pp 54–65
2. Moriyama M, Ohno-Matsui K, Modegi T et al (2012) Quantitative analyses of high-resolution 3D MR images of highly myopic eyes to determine their shapes. *Invest Ophthalmol Vis Sci* 53:4510–4518
3. Moriyama M, Ohno-Matsui K, Hayashi K et al (2011) Topographic analyses of shape of eyes with pathologic myopia by high-resolution three-dimensional magnetic resonance imaging. *Ophthalmology* 118:1626–1637
4. Scassa C, Ripandelli G, Sciamanna M et al (2005) The role of optical coherence tomography in the differential diagnosis of macular disease in high myopia. In: Midene E (ed) *Myopia and related disease*. Ophthalmic Communications Society Inc., New York, pp 90–93
5. Brancato R, Pierro L (2005) Optical coherence tomography findings in myopia. In: Midene E (ed) *Myopia and related disease*. Ophthalmic Communications Society Inc, New York, pp 87–89
6. Hee MR, Bauman CR, Puliafito C et al (1996) Optical coherence tomography of age-related macular degeneration and choroidal neovascularization. *Ophthalmology* 103:1260–1270
7. Phillips CI, Dobbie JG (1963) Posterior staphyloma and retinal detachment. *Am J Ophthalmol* 55:332–355
8. Ripandelli G, Parisi V, Friberg TR et al (2004) Retinal detachment associated with macular hole in high myopia: using the vitreous anatomy to optimize the surgical approach. *Ophthalmology* 111:726–731
9. Sayanagi K, Morimoto Y, Ikuno Y et al (2010) Spectral-domain optical coherence tomographic findings in myopic foveoschisis. *Retina* 30:623–628
10. Ikuno Y, Sayanagi K, Soga K et al (2008) Foveal anatomical status and surgical results in vitrectomy for myopic foveoschisis. *Jpn J Ophthalmol* 52:269–276
11. Hotchkiss ML, Fine SL (1981) Pathologic myopia and choroidal neovascularization. *Am J Ophthalmol* 91:1771–1783
12. Gaucher D, Erginay A, Lecleire-Collet A et al (2008) Dome-shaped macula in eyes with myopic posterior staphyloma. *Am J Ophthalmol* 145:909–914
13. Imamura Y, Iida T, Maruko I et al (2011) Enhanced depth imaging optical coherence tomography of the sclera in dome-shaped macula. *Am J Ophthalmol* 151:297–302
14. Maruko I, Iida T, Sugano Y et al (2011) Morphologic choroidal and scleral changes at the macula in tilted disc syndrome with staphyloma using optical coherence tomography. *Invest Ophthalmol Vis Sci* 52:8763–8768
15. Pilotto E (2006) Myopic maculopathy. In: Midene E (ed) *Perimetry and the fundus: an introduction to microperimetry*. Slack Inc., New Jersey, pp 109–115
16. Qin Y, Zhu M, Qu X et al (2010) Regional macular light sensitivity changes in myopic Chinese adults: an MP1 study. *Invest Ophthalmol Vis Sci* 51:4451–4457
17. Ripandelli G, Rossi T, Scarinci F et al (2012) Macular vitreoretinal interface abnormalities in highly myopic eyes with posterior staphyloma: 5-year follow-up. *Retina* 32:1531–1538
18. Gella L, Raman R, Sharma T et al (2011) Evaluation of in vivo human retinal morphology and function in myopes. *Curr Eye Res* 36:943–946
19. Scupola A, Tiberti AC, Sasso P et al (2010) Macular functional changes evaluated with MP-1 microperimetry after intravitreal bevacizumab for subfoveal myopic choroidal neovascularization: one-year results. *Retina* 30:739–747

-
20. Varano M, Tedeschi M, Oddone F et al (2010) Microperimetric retinal changes in myopic choroidal neovascularization treated with intravitreal ranibizumab. *Retina* 30:413–417
 21. Yodoi Y, Tsujikawa A, Nakanishi H et al (2009) Central retinal sensitivity after intravitreal injection of bevacizumab for myopic choroidal neovascularization. *Am J Ophthalmol* 147:824, 824.e1
 22. Varano M, Parisi V, Tedeschi M et al (2005) Macular function after PDT in myopic maculopathy: psychophysical and electrophysiological evaluation. *Invest Ophthalmol Vis Sci* 46:1453–1462
 23. Ikuno Y, Sayanagi K, Ohji M et al (2004) Vitrectomy and internal limiting membrane peeling for myopic foveoschisis. *Am J Ophthalmol* 137:719–724

Aakriti Garg and Stephen H. Tsang

14.1 Introduction

The scope of using microperimetry to assess visual function in retinal dystrophies is wide. The advent of the Nidek MP-1 (Nidek Technologies; Padova, Italy) has allowed for correlation of structure and function, which is especially important in retinal dystrophies, as many of these conditions strike at a young age and cause progressively worsening vision [1].

This chapter will provide a background on several retinal dystrophies – retinitis pigmentosa, Stargardt disease, Best’s vitelliform dystrophy, and pattern dystrophy – and their salient features on microperimetry. We will then illustrate the possible uses of the MP-1 in monitoring disease progression with age and improvement with therapies.

A. Garg
Department of Ophthalmology,
Columbia University College of Physicians
and Surgeons, New York, NY, USA

S.H. Tsang, MD, PhD (✉)
Department of Ophthalmology,
Columbia University College of Physicians
and Surgeons, New York, NY, USA

Department of Pathology and Cell Biology,
Columbia University College of Physicians
and Surgeons, New York, NY, USA

Department of Ophthalmology,
Columbia University Harkness Eye Institute,
635 West 165th Street, Room 218,
New York, NY 10032, USA
e-mail: sht2@columbia.edu

14.2 Retinitis Pigmentosa

Retinitis pigmentosa (RP) affects one in 5000 people worldwide and is the most common type of hereditary retinal degeneration, causing the loss of rods and cones typically starting in the mid-periphery, with advancement toward the macula and fovea [2, 3]. RP is genetically heterogeneous, with over 40 genes discovered for the condition so far, and classical inheritance patterns are exhibited: X-linked (XLRP), autosomal dominant (adRP), autosomal recessive (arRP), and mitochondrial inheritance [2, 4].

14.2.1 XLRP

Carriers of XLRP have been found to have a tapetal fundus reflex, which is characterized as a brightly scintillating particulate reflection with relative sparing of the fovea on ophthalmoscopic examination [5]. In a study of 3 XLRP carriers, combined spectral domain optical coherence tomography (SD-OCT) and microperimetry using the OPKO OCT/scanning laser ophthalmoscope (SLO) microperimetry (OPKO Health, Miami, FL).

Normal retinal structure was found and showed abnormal retinal sensitivity associated with tapetal fundus changes [6]. Another study using the Nidek MP-1 tested subjects using the 10-2 pattern. It was found that total deviation (TD) defects were present in areas with and without the tapetal reflex on fundus autofluorescence (FAF) imaging [7]. The lack of correlation was

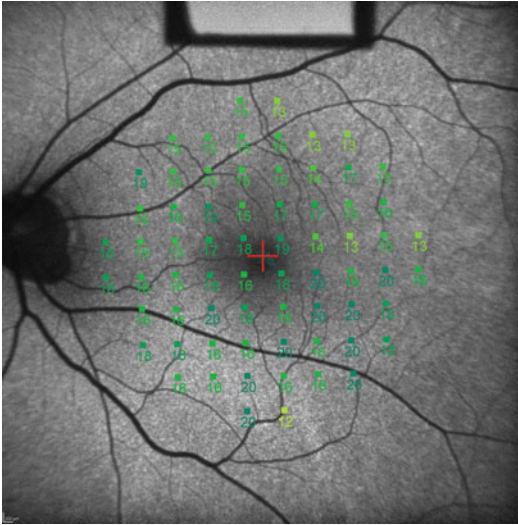


Fig. 14.1 An AF fundus image of an X-linked retinitis pigmentosa carrier reveals hyperautofluorescence in a radial pattern throughout the macula. Superimposed MP-1 map demonstrates normal visual field sensitivities throughout the macula, with a few small patches in the peripheral macula of subtle visual field sensitivity loss

explained by the difference in instrumentation, with the MP-1 having a lower luminance level as compared to the OPKO microperimeter [7]. Consistent with several other studies, patchy visual sensitivity loss was found to be greatest in the inferior retina using the Nidek MP-1 [7].

It was concluded that while microperimetry was a useful tool in monitoring XLRP carriers, it was imperfect because thresholds were mediated by a mixed rod-cone system response or by mainly a cone system response [8] (Fig. 14.1).

14.2.2 adRP

The foremost genes responsible for autosomal dominant RP (adRP) include rhodopsin (RHO), peripherin 2 (PRPH2/RDS), pre-mRNA processing factor 31 (PRPF31), and retinitis pigmentosa 1 (RP1) (Fig. 14.2) [4].

14.2.3 arRP

The leading genes responsible for autosomal recessive RP (arRP) include retinal pigment epithelium

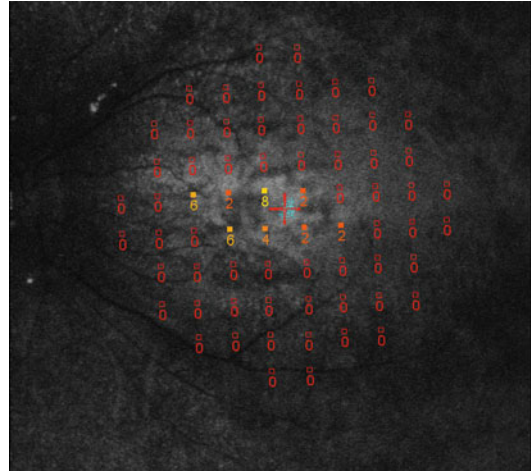


Fig. 14.2 An AF fundus image of a patient with autosomal dominant retinitis pigmentosa reveals a small area of hyperautofluorescent area peripherally, with surrounding hypoautofluorescence. Superimposed MP-1 map demonstrates moderate to severe visual field sensitivity loss corresponding with the hyperautofluorescent region and total visual field sensitivity loss throughout the macula

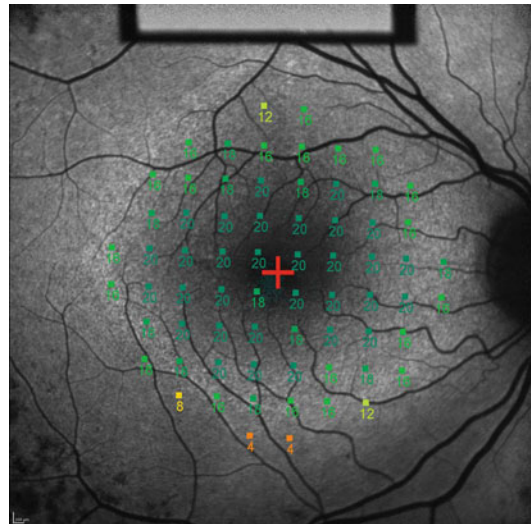


Fig. 14.3 An AF fundus image of a patient with autosomal recessive retinitis pigmentosa reveals large hyperautofluorescent ring surrounding the perifoveal region in the macula and hypoautofluorescence outside the macula. Superimposed MP-1 map demonstrates that visual field sensitivities are preserved in a pattern corresponding to the region within the ring of hyperautofluorescence with moderate visual field sensitivity loss in the surrounding hypoautofluorescent region

65 (RPE65), heterotetrameric phosphodiesterase (PDE6A, PDE6B, and PDE6G0), and the retinitis pigmentosa 25 (RP25) (Fig. 14.3) [4].

14.3 Stargardt Disease

Stargardt disease (STGD) is a genetically heterogeneous disease that is typically inherited in an autosomal recessive pattern and has an onset in childhood [9]. STGD is caused by mutations in the gene encoding the photoreceptor cell-specific ATP-binding cassette transporter (ABCA4), which is believed to cause lipofuscin accumulation in the RPE, resulting in RPE and secondary photoreceptor degeneration [10, 11]. The ability of FAF to visualize A2E and other bisretinoid components of lipofuscin in RPE and ability of SD-OCT to visualize retinal architecture in vivo make these noninvasive techniques useful to evaluate the extent of STGD [12].

A study using the Nidek MP-1 with the 10-2 program compared 97 locations with hyperautofluorescent flecks and 97 neighboring non-flecked areas and found a statistically significant difference in visual sensitivity ($p < .001$). Hyperreflective dome-shaped lesions with dislocation or disruption of the photoreceptor layer in the outer retina located at the level of the RPE were found on SD-OCT. It was hypothesized that functional alterations were likely irreversible in flecked areas where the inner segment ellipsoid (ISe) band was disrupted or completely absent. However, other studies have found that areas of hyperautofluorescence that corresponded to yellowish-white flecks and were confined to the macular area were not always associated with decreased visual sensitivity [13]. This finding suggests that changes in photoreceptor integrity noted on SD-OCT may correlate with visual sensitivity losses better than RPE changes seen on FAF.

Dark-adapted sensitivity measurements on STGD1 patients could be potentially useful in finding areas of potential improvement of retinal function. A study using the MP-1S, which is performed under dark-adapted conditions, found a significant decrease ($p < .001$) in mean sensitivity (MS) values in patients with STGD1. These sensitivity losses correlated with areas that showed changes on SLO imaging and on SD-OCT, reflecting topographical accuracy between the two imaging modalities. Changes on SD-OCT included disorganization loss of RPE, abnormal

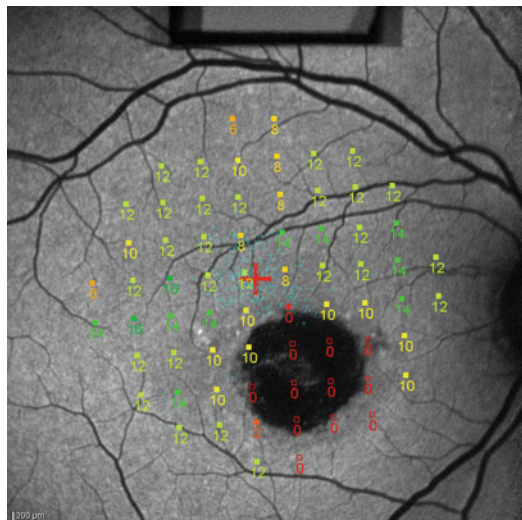


Fig. 14.4 An AF image of a Stargardt patient reveals that the condition is manifesting as a densely hypoautofluorescent bull's eye lesion in the foveal and perifoveal region, with normal autofluorescence elsewhere in the macula. Superimposed MP-1 map demonstrates visual field sensitivity loss corresponding to the hypoautofluorescent bull's eye lesion and a patchy loss in visual field sensitivities outside of this region

photoreceptor ISe band, and external limiting membrane reflectance band [14] (Fig. 14.4).

14.4 Best's Vitelliform Dystrophy

Best's vitelliform dystrophy (BVD), also known as vitelliform macular degeneration type 2, is an autosomal dominant form of macular degeneration with clinically heterogeneous defects in which changes in ophthalmoscopy and visual function do not correspond [15]. BVD is caused by a mutation in the BEST1 gene, which encodes an integral membrane protein bestrophin, which is responsible for creating the chloride channel in the RPE's basolateral membrane [16, 17]. A study using the MP-1 found highly sensitive topographic monitoring of the progression of retinal function with MP in eyes with BVD. In the early stages, central or pericentral fixation was preserved; eventually, loss of central function caused evident shift of fixation to preferred retinal location (PRL) in eyes with visual acuity of 0.2 or less. Additionally, results of static perimetry (as measured by Octopus M1) and the Nidek MP-1

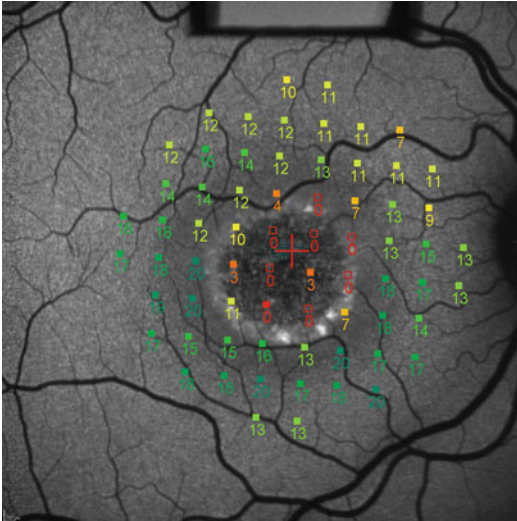


Fig. 14.5 AF fundus images of a patient with Best's vitelliform dystrophy reveal a densely hypoautofluorescent bull's eye lesion in the foveal and perifoveal region, which is surrounded by a hyperautofluorescent ring. Mild hypoautofluorescence is seen elsewhere in the macula. Superimposed MP-1 map demonstrates severe visual field sensitivity losses foveally and perifoveally that correspond with the hypoautofluorescence seen on AF. In the region outside of the hypoautofluorescent ring, the superior macula demonstrates mild to moderate visual field sensitivity losses, while the inferior macula has normal visual field sensitivities

were compared in BVD eyes and showed high correlation of static perimetry and MP results. However, the MP method was superior to automatic perimetry due to the former's ability of fundus-controlled fixation screening [15] (Fig. 14.5).

14.5 Pattern Dystrophy

Pattern dystrophy is a phenotypically variable condition described by the accumulation of lipofuscin at the level of the RPE [18]. Inheritance patterns are typically autosomal dominant, and the peripherin/RDS gene is often responsible; genetic heterogeneity has been shown [19]. Significant bilateral visual impairment and/or legal blindness is prevalent in patients with pattern dystrophy after the age of 70 [20]. Patients with BVD and pattern dystrophy have been

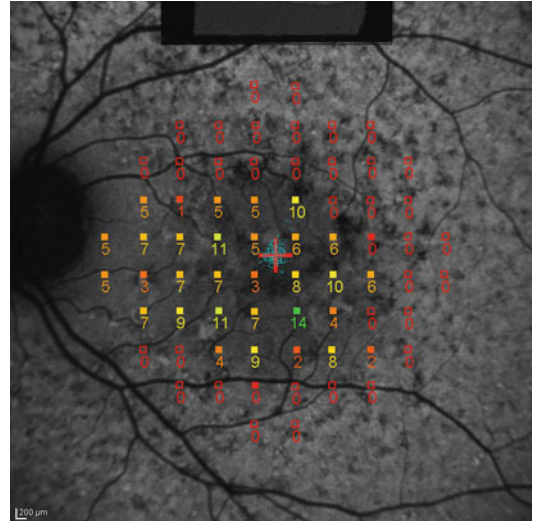


Fig. 14.6 AF fundus images of a patient with pattern dystrophy mimicking Stargardt disease reveal a mildly hypoautofluorescent patch perifoveally and hypoautofluorescent irregular flecks throughout the macula. Superimposed MP-1 map demonstrates moderate visual field sensitivity loss perifoveally and nasally and severe visual field sensitivity loss elsewhere in the macula

shown to have decreased visual field sensitivities, which were associated with dense rings of hyperautofluorescence surrounding hypoautofluorescent regions on FAF [13] (Fig. 14.6).

14.6 Shortcomings

Unstable fixation is an obstacle that cannot be entirely overcome even with the eye-tracking feature of the MP-1, making values variable. Additionally, SLO imaging and MP-1 sensitivity maps may not be in the same position relative to the fovea and may not perfectly align when comparing two juxtaposed retinal locations.

Conclusion

Atrophic macular disease is a prominent feature of many inherited retinal dystrophies such as RP and STGD. Progression and/or improvement in these conditions are particularly difficult to evaluate, as visual acuity can remain stable in spite of the growth of perifoveal atrophy and the area of atrophy is a difficult to

measure accurately as rates of enlargement vary [21, 22] and there is a lack of definition on FAF imaging. Slowing the progression of functional or visual loss is the aim of therapy in atrophic macular disease, and microperimetry offers a useful tool for evaluations of subtle functional vision loss with stable visual acuity and fixation [23].

A study from Moorfields Eye Hospital found that in those patients with progressive atrophic macular disease and stable acuity, the MPI could detect significant change in regional retinal sensitivity within 12 months [23]. Microperimetry also allows for the prediction of the location of relative or dense scotoma, a feature that clinical and imaging modalities are not always able to detect in dystrophies [15, 24].

Microperimetry is a useful method for detecting functional decline and may be an integral accompaniment to anatomical evaluation of patients with inherited retinal dystrophies. This is especially relevant since gene therapy trials are on the horizon for patients suffering from these conditions. Monitoring disease progression and improvement with modalities that can integrate evaluation of structural integrity and functional status will be essential in determining the efficacy of future therapies and directing treatment.

References

- Rohrschneider K, Bultmann S, Springer C (2008) Use of fundus perimetry (microperimetry) to quantify macular sensitivity. *Prog Retin Eye Res* 27:536–548
- Rivolta C, Sharon D, DeAngelis MM, Dryja TP (2002) Retinitis pigmentosa and allied diseases: numerous diseases, genes, and inheritance patterns. *Hum Mol Genet* 11:1219–1227
- Hartong DT, Berson EL, Dryja TP (2006) Retinitis pigmentosa. *Lancet* 368:1795–1809
- Ferrari S, Di Iorio E, Barbaro V, Ponzin D, Sorrentino FS, Parmeggiani F (2011) Retinitis pigmentosa: genes and disease mechanisms. *Curr Genomics* 12: 238–249
- Cideciyan AV, Swider M, Aleman TS et al (2005) ABCA4-associated retinal degenerations spare structure and function of the human parapapillary retina. *Invest Ophthalmol Vis Sci* 46:4739–4746
- Genead MA, Fishman GA, Lindeman M (2010) Structural and functional characteristics in carriers of X-linked retinitis pigmentosa with a tapetal-like reflex. *Retina* 30:1726–1733
- Acton JH, Greenberg JP, Greenstein VC et al (2013) Evaluation of multimodal imaging in carriers of X-linked retinitis pigmentosa. *Experimental eye research* 113:41–48
- Crossland MD et al (2012) ARVO. E-Abstract 4822. *IOVS* 53
- Rotenstreich Y, Fishman GA, Anderson RJ (2003) Visual acuity loss and clinical observations in a large series of patients with Stargardt disease. *Ophthalmology* 110:1151–1158
- Molday RS (2007) ATP-binding cassette transporter ABCA4: molecular properties and role in vision and macular degeneration. *J Bioenerg Biomembr* 39:507–517
- Cideciyan AV, Aleman TS, Swider M et al (2004) Mutations in ABCA4 result in accumulation of lipofuscin before slowing of the retinoid cycle: a reappraisal of the human disease sequence. *Hum Mol Genet* 13:525–534
- Gomes NL, Greenstein VC, Carlson JN et al (2009) A comparison of fundus autofluorescence and retinal structure in patients with Stargardt disease. *Invest Ophthalmol Vis Sci* 50:3953–3959
- Greenstein VC, Santos RA, Tsang SH, Smith RT, Barile GR, Seiple W (2008) Preferred retinal locus in macular disease: characteristics and clinical implications. *Retina* 28:1234–1240
- Salvatore S, Fishman GA, McAnany JJ, Genead MA (2013) Association of dark-adapted visual function with retinal structural changes in patients with Stargardt disease. *Retina* (in press)
- Jarc-Vidmar M, Popovic P, Hawlina M (2006) Mapping of central visual function by microperimetry and autofluorescence in patients with Best's vitelliform dystrophy. *Eye* 20:688–696
- Bakall B, Marknell T, Ingvas S et al (1999) The mutation spectrum of the bestrophin protein – functional implications. *Hum Genet* 104:383–389
- Stone EM, Nichols BE, Streb LM, Kimura AE, Sheffield VC (1992) Genetic linkage of vitelliform macular degeneration (Best's disease) to chromosome 11q13. *Nat Gen* 1:246–250
- Zhang K, Garibaldi DC, Li Y, Green WR, Zack DJ (2002) Butterfly-shaped pattern dystrophy: a genetic, clinical, and histopathological report. *Arch Ophthalmol* 120:485–490
- van Lith-Verhoeven JJ, Cremers FP, van den Helm B, Hoyng CB, Deutman AF (2003) Genetic heterogeneity of butterfly-shaped pigment dystrophy of the fovea. *Mol Vis* 9:138–143
- Francis PJ, Schultz DW, Gregory AM et al (2005) Genetic and phenotypic heterogeneity in pattern dystrophy. *Br J Ophthalmol* 89:1115–1119
- Sunness JS, Bressler NM, Tian Y, Alexander J, Applegate CA (1999) Measuring geographic atrophy in advanced age-related macular degeneration. *Invest Ophthalmol Vis Sci* 40:1761–1769

22. Sunness JS, Margalit E, Srikumaran D et al (2007) The long-term natural history of geographic atrophy from age-related macular degeneration: enlargement of atrophy and implications for interventional clinical trials. *Ophthalmology* 114:271–277
23. Chen FK, Patel PJ, Webster AR, Coffey PJ, Tufail A, Da Cruz L (2011) Nidek MP1 is able to detect subtle decline in function in inherited and age-related atrophic macular disease with stable visual acuity. *Retina* 31:371–379
24. Popovic P, Jarc-Vidmar M, Hawlina M (2005) Abnormal fundus autofluorescence in relation to retinal function in patients with retinitis pigmentosa. *Graefes Arch Clin Exp Ophthalmol* 243:1018–1027

Monica Varano, Mariacristina Parravano,
and Daniele De Geronimo

15.1 Introduction

Vitreoretinal macular diseases are caused by abnormal cell migration and proliferation into or behind the posterior vitreous cortex or by vitreous traction of the macula. Posterior vitreous detachment (PVD) has an important role in the pathogenesis of vitreoretinal macular diseases. Indeed these disorders may arise from anomalous PVD, as the separation of the posterior vitreous cortex from the internal limiting membrane (ILM) does not occur in a clear fashion. Some remnants of the retina may remain attached to the vitreous cortex, as it will be discussed below for some cases of macular hole. In some instances during PVD, a layer of vitreous may remain attached to the macula, explaining some forms of premacular membrane. Moreover, a split with cavitation of the vitreous cortex (vitreoschisis) may be an important factor in macular hole formation [1].

Vitreoretinal interface syndromes may be divided into three categories:

1. *Maculopathy caused by traction due to incomplete posterior vitreous detachment.* A posterior vitreous detachment, starting in peripheral retinal areas, may cause traction on areas with anomalous vitreoretinal adhesion as well as

many other retinal diseases, such as retinal distortion, tractional retinal detachment, avulsion or rupture of a vessel, or even a macular hole.

2. *Maculopathy caused by spontaneous contraction of the prefoveal vitreous cortex not involving PVD (at least at its initial stages).* This group includes the idiopathic macular hole.
3. *Maculopathy caused by contraction of the residual, adherent vitreous cortex after a posterior vitreous detachment.* After partial or total PVD, a translucent fibrocellular membrane may remain adherent to the internal retinal surface: the contraction of this membrane may cause various degrees of retinal distortion and edema. Such contraction may occur according to tangential centripetal forces, with the formation of cellophane and macular pucker, or centrifugal forces, leading to pseudoholes and full-thickness macular holes [2–4].

Microperimetry with a scanning laser ophthalmoscope (SLO, Rodenstock, Germany), and more recently with MP-1 microperimeter (MP-1, Nidek, Japan), has introduced new and more extensive information in the study of retinal function in a number of macular diseases, mainly of vitreoretinal interface syndromes [5–7].

Microperimeter allows an in-depth evaluation of the relations between anatomical and functional changes of macular-related disorders, through the direct correlation of fundus evaluation to retinal threshold, including retinal fixation parameters [8–16]. This approach allows the

M. Varano, MD (✉) • M. Parravano
D. De Geronimo
GB Bietti Eye Foundation, IRCCS, Via Livenza 3,
00198 Rome, Italy
e-mail: m.varano@mclink.it; criparra@tin.it;
danieledegeronimo@gmail.com

identification of absolute or relative defects in these areas which are full restricted to the central visual field [8, 16–18].

Because of these characteristics, microperimetry has become a relevant diagnostic method for the diagnosis, prognosis, and the follow-up of macular diseases of surgical interest, such as vitreoretinal interface syndromes [11, 13].

15.2 Microperimetry, Epiretinal Membranes (ERM), and Macular Pseudoholes

Epiretinal membranes (ERM) are fibrocellular membranes visible over the inner retinal surface in the macular area after partial or complete posterior vitreous detachment (PVD) [19]. ERM are considered a maculopathy secondary to the contraction of vitreous cortex still adhering to the retina in the macular area [20, 21]. They can be idiopathic or secondary to trauma, surgery, ocular inflammation, and other causes [22]. Mori et al. documented that secondary ERM are more likely to be characterized by focal retinal adhesion than primary ERM. Primary ERM differ because they are mainly globally adherent [23]. The pathogenesis of idiopathic ERM is not fully clarified, although PVD was observed in about 60–90 % of cases [2, 20, 21, 24–27]. After partial or total PVD, the contraction of a fibrocellular membrane still attached to the internal retinal surface may produce various degrees of retinal distortion as well as macular edema [20, 21, 28].

According to Gass, macular ERM develop as a consequence of tractional stimulation in the course of PVD through two mechanisms: (1) when a PVD with transitory vitreomacular traction occurs allowing migration and proliferation of astrocytes on the anterior internal limiting membrane (ILM) interface and (2) during the course of PVD, where separation occurs at the level of the vitreous cortex (vitreoschisis) with cortex residues and hyalocytes adhering to ILM. The proliferation, fibrous metaplasia, and the contraction of hyalocytes may favor the formation of ERM [29].

Gass classified ERM in three forms: cellophane maculopathy, wrinkling maculopathy, and pucker maculopathy [29]. Witkin et al. initially described two types of ERM using ultrahigh-resolution OCT [30]. The first type was ERM described as a thin highly reflective line anteriorly situated but separated from the retinal nerve fiber layer (RNFL), corresponding to previously reported ERM on OCT. The second type was unusual appearing ERM presenting as a highly reflective line with a moderately reflective material filling the space between the inner border of the ERM and the RNFL. This specific epiretinal tissue, removed during vitrectomy, had a yellow dense appearance and a fluffy consistency and could be classified neither as vitreous cortex nor as regular ERM [30]. Parolini et al., in a recent study concerning lamellar macular hole, redefined the two types of ERM as “tractional” (instead of “normal”) and “dense” (instead of “unusual”) [31]. The same authors correlated clinical and tomographic features with morphologic and immunohistochemical findings within these two types of ERM.

Transmission electron microscopy of “dense” membranes showed that native vitreous collagen is the major component of observed collagen. Compact fibrous long-spacing collagen (FLSC) was less frequently seen in “tractional” membranes compared with “dense” membranes, but it was surrounded by native vitreous collagen as well. An important difference between “tractional/normal” and “dense/unusual” membranes was shown by the immunolabeling of alpha-smooth muscle actin (α -SMA), the expression of which was more frequently demonstrated in “tractional” ERM than in “dense” ERM. Since the content of α -SMA in epiretinal membranes was demonstrated to be correlated with clinical contractility, the authors postulated that “tractional” membranes possess more potential to generate tractional forces on the retina than “dense” membranes [32].

OCT is certainly the most used diagnostic technique in ERM management. However, microperimetry provides numerous data which can allow to evaluate the degree of evolution of these diseases in the preoperative stage, to define



Fig. 15.1 Pucker maculopathy showing reduction in retinal sensitivity

operative timing, and to evaluate functional results in the postoperative stage (follow-up).

As general rule, microperimetry shows a preservation of macular sensitivity in initial stages of vitreoretinal interface diseases like macular cellophane (grade 0 ERM), whereas it highlights a quite evident reduction of macular sensitivity in the most advanced ones (pucker) [8, 28] (Fig. 15.1). Individual symptoms may be absent or may consist in visual loss in the initial or advanced stage, with or without metamorphopsia. Visual loss induced by ERM can be due to the presence of fibrous tissue distorting and covering the macula or to the formation of intraretinal macular edema caused by the leakage of fluids from vessels [2, 20, 26]. These conditions show variable reduction of sensitivity within the central visual field, causing different clinical manifestations.

Clinical observation is the correct approach for the majority of ERM of medium degree, without metamorphopsia, with fairly preserved visual acuity, and lacking functional decrease in retinal sensitivity, examined by microperimetry. When macular pucker causes persistent visual impairment or gradual decrease of visual acuity (associated or not to a reduction of macular retinal sensitivity, documented by microperimetry) or metamorphopsia, surgery needs to be considered. The isolated decrease of macular sensitivity,

even in case of preservation of visual acuity, is also indication to surgery [28, 33, 34].

Better baseline retinal sensitivity represents a positive prognostic factor in eyes undergoing surgery and having the same preoperative visual acuity at baseline [8]. Negative predicting factors for postoperative visual prognosis of ERM are cystoid macular edema (CME), tractional retinal detachment, increased thickness of membrane, and long-standing visual dysfunction [35]. Too long observation period associated with the irreversible decay in retinal sensitivity worsens the postoperative prognosis. The presence of absolute scotoma is a fully negative predictive factor [8, 28].

An information of primary interest to any vitreoretinal surgeon is the possibility to identify retinal fixation area inside the macular area/s to protect the first one by intraoperative iatrogenic stress. This area which may not be restricted to fovea is the site of preferred retinal locus (PRL), and this is crucial to leave it unchanged in order to obtain a good postoperative functional result, since often as a consequence of iatrogenic stress, a deep scotoma may develop in areas previously used for reading (PRL) [29, 36–38].

As consequence, microperimetry seems mandatory to evaluate the clinical course of macular retraction syndromes, both before and after surgery, in conjunction with visual acuity assessment and morphological evaluation, provided by OCT.

Cappello et al. studied 41 patients with pucker and 18 patients with macular holes and reported improvement of visual acuity as well as retinal sensitivity and reading ability for up to 12 months after vitrectomy [39]. Instead, Richter-Mueksch et al., studying 19 patients with macular holes and 18 patients with macular pucker undergoing surgery, found that a higher number of patients showed greater improvement of retinal sensitivity than visual acuity. They concluded that visual acuity assessment without information supplied by microperimetry may underestimate functional benefit of surgery [40] (Figs. 15.2 and 15.3).

In eyes with ERM, structural changes in the photoreceptor layer, such as varying degrees of disruption of the photoreceptor inner and outer

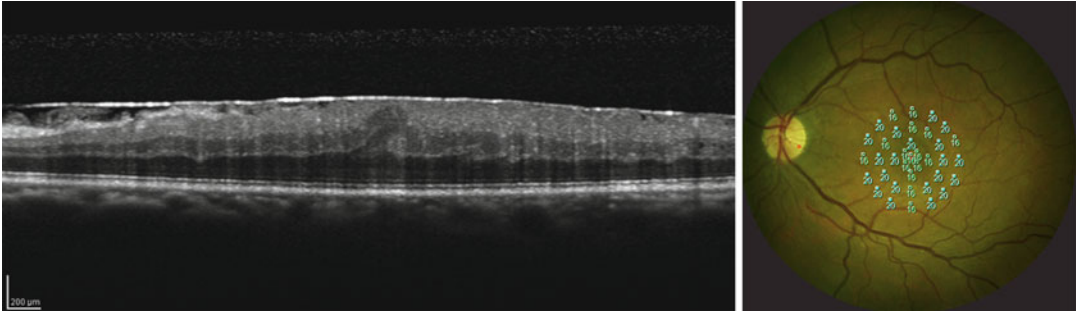


Fig. 15.2 Preoperative spectral domain OCT and microperimetry (MP-1) in a case of pucker maculopathy, with a mild reduction of retinal sensitivity

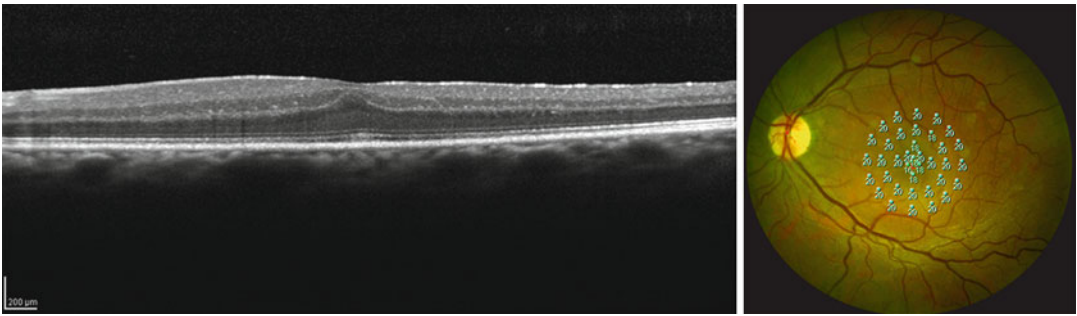


Fig. 15.3 Postoperative spectral domain OCT and microperimetry (MP-1) of the same case in Fig. 15.2 showing normalization of the macular profile with increased retinal sensitivity

segment junction (IS/OS) and increased foveal thickness, have been identified using both time domain and spectral domain OCT [41–44]. However, the studies using time domain or spectral domain OCT have not yet provided sufficiently clear images of individual foveal photoreceptor cells allowing to identify a specific structural abnormality able to explain metamorphopsia in eyes with ERM.

Pilli et al. studied 24 eyes of 19 patients with ERM in order to correlate morphologic changes (both time and spectral domain OCT) with visual function assessed by visual acuity and macular sensitivity. Macular sensitivity was evaluated using microperimetry in 15 eyes of 11 patients. To compare the macular thickness maps with macular sensitivity they overlaid microperimetry data over retinal thickness map, with retinal vessels and foveal center acting as reference points. Only 67 % of the eyes showed some qualitative correlation [45].

These data lead to hypothesize that the functional damage due to ERM could not be related

just to the severity of macular edema, as previously suggested, but also to other morphologic changes in the macula. Electrophysiologic studies have shown both outer and inner retinal layer dysfunction associated with vision loss in eyes with idiopathic ERM [46, 47]. A recent case report showed that an adaptive optics flood illumination retinal camera, in association with spectral domain OCT images, can be used to visualize, in eyes with ERM, subtle changes within single retinal layers. Using adaptive optics system, the authors detected fine microstriae among the macular cone that resolved completely after surgical removal of ERM, with a complete visual recovery even if macular morphology on OCT never normalized [48].

This shows that current OCT and other imaging techniques such as scanning laser ophthalmoscopy fail to provide sufficiently detailed images of photoreceptor microstructure, primarily because of aberrations inside ocular optics. These aberrations can be compensated by using imaging systems that incorporate adaptive optics

consisting in a wavefront sensor to measure aberrations on the eye surface and a deformable mirror or a spatial light modulator to compensate for these aberrations. Ooto et al. used their adaptive optics-SLO system to investigate structural abnormalities in individual photoreceptor cells and changes in visual function, such as metamorphopsia and visual acuity, in patients with idiopathic ERM. On adaptive optics-SLO images, 96 % of eyes with ERM show many thin and straight hyporeflective lines in the cone mosaic. These lines, which they described as “microfolds,” were not seen in any normal eye. In 83 % of the eyes, microfolds were localized in the fovea. These authors also checked metamorphopsia, using the Amsler grid. In all the eyes with metamorphopsia, microfolds were seen in the fovea. No microfolds were seen in 83 % of the eyes without metamorphopsia. Therefore, microfolds seen on adaptive optics-SLO can be directly associated to metamorphopsia. In 60 % of the eyes in which microfolds were visible in the fovea on adaptive optics-SLO images, the IS/OS appeared intact using spectral domain OCT images [49]. These data highlight how OCT alone is insufficient in the ERM management, but, thanks to microperimetry with future new tools using adaptive optics system, we will be able to have a more complete approach in the preoperative stage, to better define the operative timing and to better evaluate final functional results.

Macular pseudoholes (MPH) are macular lesions that have the appearance of macular holes, but without any loss of foveal tissue due to the centripetal contraction of an epiretinal membrane. Vice versa, lamellar holes (LH) are an abortive process to full-thickness macular hole formation characterized by loss of foveal tissue, but without a full-thickness foveal defect with intact foveal photoreceptors. Haouchine et al. identified in 40 patients with MPH a characteristic macular profile: a steepened foveal pit combined with thickened foveal edges and a small foveal pit diameter, a normal or slightly increased ($167 \pm 42 \mu\text{m}$) central foveal thickness, and mean perifoveal thickness greater than normal [50].

Although OCT studies have added valuable information regarding the definition,

pathogenesis, and progression of macular holes, the differential diagnosis between MPH and lamellar macular holes (LMH) is still unclear [51–55]. In particular, when there is residual retinal tissue at the bottom of the foveal defect, as occurs with OCT classification stage 2 according to Azzolini et al., OCT imaging cannot correctly determine whether or not there is loss of retinal tissue [54]. In this case, the diagnosis of MPH or LMH is often a matter of speculation. Bottoni et al. reviewed OCT and autofluorescence images of 50 eyes of 46 patients with stage 2 idiopathic macular hole with residual retinal tissue at the bottom of the foveal defect, classified as MPH or LMH according to OCT profiles established by Haouchine et al. [50, 54, 56]. After OCT image analysis, the corresponding autofluorescence images recorded with a confocal scanning laser ophthalmoscope were evaluated. Considering that foveal autofluorescence usually increases when there is a foveal defect, these authors found that the two groups showed similar foveal autofluorescence, demonstrating a similar loss of foveal tissue. In addition, they also found a lack of correlation between the amount of autofluorescence and the thickness of the residual retinal tissue at the base of both MPH and LMH. The absence of any difference in autofluorescence between the two groups and the lack of correlation between foveal autofluorescence and retinal thickness raises questions about the validity of distinguishing between macular pseudoholes or lamellar macular holes on the basis of OCT data alone.

The application of microperimetry to these disorders gives us a lot of new information to functionally differentiate macular pseudohole, the hole with partial thickness and the impending macular hole from full-thickness macular hole [11]. The full-thickness macular hole always corresponds to an absolute scotoma surrounded by a perilesional ring of relative scotoma, and fixation is located in a retinal area immediately adjacent to the scotoma. In MPH or LMH, we observe the presence of normal or slightly reduced foveal retinal sensitivity (Fig. 15.4). Therefore, the appearance of a central absolute scotoma detectable by means of microperimetry is the sign of a full-thickness macular hole. On the other hand, the

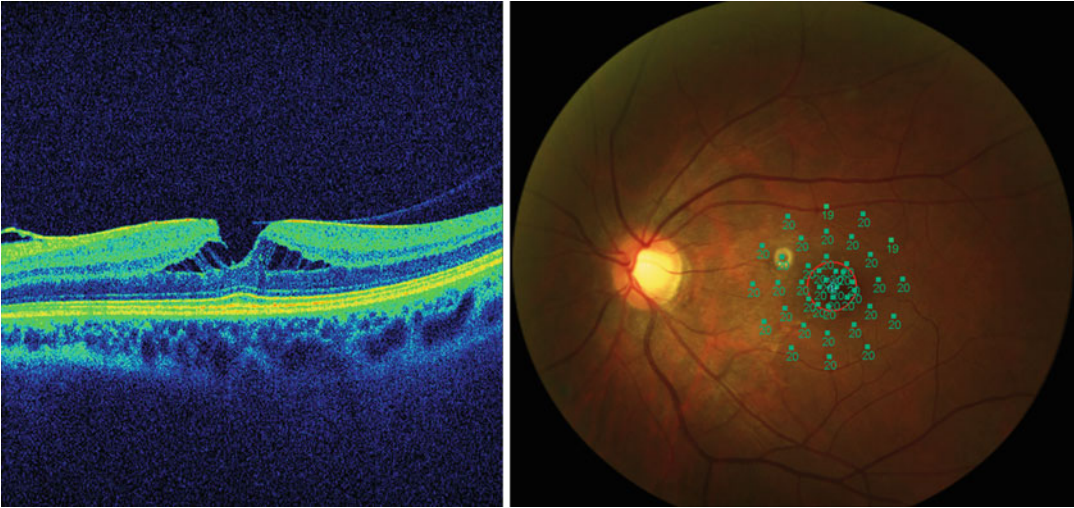


Fig. 15.4 Spectral domain OCT and microperimetry (MP-1) in a case of macular pseudohole with normal retinal sensitivity

presence of a normal or slightly reduced retinal sensitivity in macular pseudoholes and in lamellar holes results from the persistence of more external retinal layers [5, 7, 11, 57, 58]. In some cases a change of the site of fixation (PRL) could occur to better preserve reading function [59].

Macular pseudohole tends to remain stable and visual acuity is usually preserved [60]. Greven et al., in a survey dating back to 1998, observed in macular pseudohole, after 1-year follow-up, the tendency to maintain stable visual acuity [57]. Garcia-Fernandez et al. also recently documented as most idiopathic LMH and MPH do not anatomically progress and do not contribute to a significant loss of visual acuity during follow-up period (12–84 months) [61]. Considering this trend, attention must be paid before proceeding with surgery in patients with MPH.

15.3 Microperimetry and Macular Holes

The term *lamellar macular hole* (LMH) was originally suggested by Gass in 1975, when he identified a macular lesion resulting from cystoid macular edema [62]. Since then, the term lamellar macular hole has been used to describe the abortive process of full-thickness macular hole

formation, in which, clinically, the patient has relatively preserved visual acuity, usually 20/40 or better, and the macula contains a stable, round, and well-circumscribed reddish lesion [50, 52, 53, 55, 63–65]. Witkin and colleagues recently proposed distinct OCT criteria, based on qualitative image analysis without measurement of retinal thickness, according to which the diagnosis of lamellar macular hole (LMH) is based on (1) an irregular foveal contour, (2) a break in the inner fovea, (3) a dehiscence of the inner foveal retina from the outer retina, and (4) an absence of a full-thickness foveal defect with intact foveal photoreceptors [30].

As mentioned above, in LMH microperimetry shows normal or slight reduction in retinal sensitivity as a result of the persistence of more external retinal layers [66–68] (Figs. 15.5 and 15.6).

According to Bottoni et al. LMH monitored with spectral domain OCT and fundus autofluorescence seems to be a stable macular condition, and vitrectomy should be considered only when progressive thinning of foveal tissue and/or decrease of visual acuity is documented [69]. Moreover, microperimetry has become a very important method for the diagnosis, prognosis, and the follow-up of these macular disorders of surgical interest [11, 13]. Recently, several authors have stressed the importance of retinal

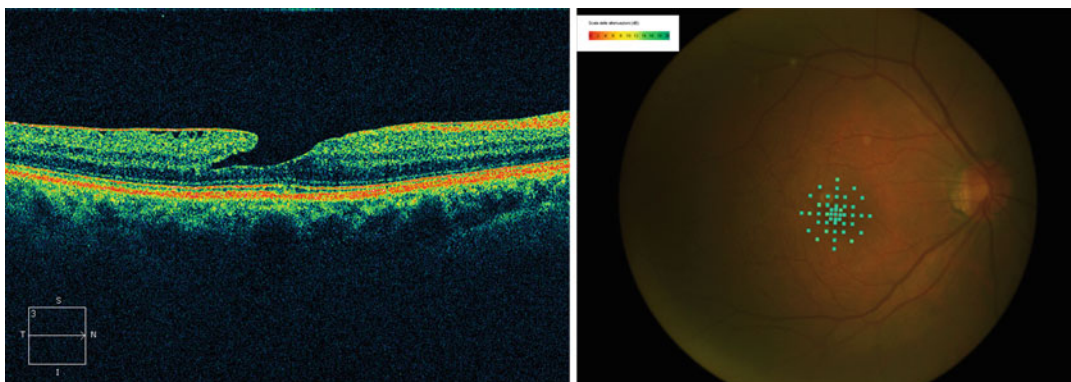


Fig. 15.5 Spectral domain OCT and microperimetry (MP-1) in a case of lamellar macular hole with preserved retinal sensitivity

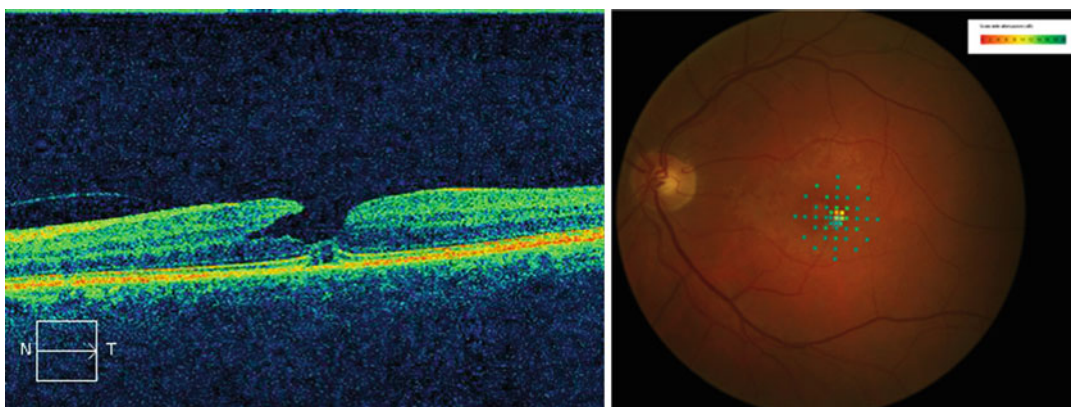


Fig. 15.6 Spectral domain OCT and microperimetry (MP-1) in a case of lamellar macular hole with mild reduction of retinal sensitivity

outer layer integrity for a good visual prognosis. Reibaldi et al. studied with spectral domain OCT and microperimetry 60 eyes of 60 patients with a diagnosis of LMH based on OCT characteristics and divided into three groups according to the integrity of the foveal photoreceptor layer, as proposed by Witkin et al. [30, 70]. The same authors found that integrity of the foveal photoreceptor layer, evaluated by spectral domain OCT, is closely associated with visual acuity and retinal sensitivity [70]. Only central retinal sensitivity was significantly different between the group with preserved inner/outer segment (IS/OS) and external limiting membrane (ELM) defect and the group with only IS/OS defect. This suggests that microperimetry is sensitive enough to identify early morphologic alteration of the photore-

ceptors layer before visual acuity is impaired in LMH patients. Furthermore, visual acuity was lower in eyes with disruption of ELM suggesting that preservation of ELM is mandatory in the potential preservation of visual acuity. In a personal survey concerning the functional and structural characteristics of LMH, we found that visual acuity and retinal sensitivity are reduced in LMH. Visual acuity, different from what was reported by Chen et al., was found to be unrelated to any of the morphological dimensions of LMH [71, 72]. Vice versa LMH depth was associated with macular sensitivity (Table 15.1). According to our results from 14 to 18 % of the variation of macular sensitivity within, the central 8° and 2° can be explained by changes of LMH depth. The discrepancy between visual acuity and mean

Table 15.1 Correlation between functional (BCVA, MTRS, and MCRS) and morphological LMH parameters obtained by optical coherence tomography

Functional parameters	Morphological parameters	R^2	p value
BCVA	Base diameter	0.04	0.3
	Apex diameter	0.002	0.8
	Residual thickness	0.08	0.1
	Depth	0.05	0.2
	Mean nasal perifoveal thickness	0.006	0.62
	Mean temporal perifoveal thickness	0.002	0.76
MTRS	Base diameter	0.007	0.6
	Apex diameter	0.05	0.2
	Residual thickness	0.02	0.3
	Depth	0.18	0.006
	Mean nasal perifoveal thickness	0.056	0.10
	Mean temporal perifoveal thickness	0.09	0.05
MCRS	Base diameter	0.01	0.5
	Apex diameter	0.08	0.08
	Residual thickness	0.04	0.2
	Depth	0.14	0.02
	Mean nasal perifoveal thickness	0.04	0.14
	Mean temporal perifoveal thickness	0.06	0.078

BCVA best corrected visual acuity, LMH lamellar macular hole, MCRS mean central retinal sensitivity, MTRS mean total retinal sensitivity

central retinal sensitivity in relation to the depth could be due to the wider perifoveal area explored by microperimetry that is more likely to involve retinal locations functionally impaired by the presence of LMH and ERM. Moreover, as shown by Reibaldi, the impaired macular function is more pronounced in LMH eyes with outer retinal abnormalities [70].

The major pathogenetic hypotheses concerning the origin of macular holes are trauma, macular cystic degeneration, involutonal macular thinning, and posterior vitreoretinal traction in the course of PVD [63, 73–76]. In 1988, the theory sustained by Gass and Johnson who recognized in the tangential traction the main mechanism for the pathogenesis of MH received large consensus [63, 77]. Johnson and others

reported the presence of a perifoveal vitreous detachment in 96 % of the cases observed as the main pathogenetic factor in the formation of idiopathic macular holes at the initial stage [78].

In 1995, Gass revised his previous classification of idiopathic macular holes in four stages: stage 1, yellowish spot centered on the fovea; stage 2, yellowish foveal ring; stage 3, central full-thickness fault diameter >400 μm without Weiss ring; and stage 4, full-thickness central deficiency with Weiss ring [64]. The eye affected by macular hole (stage 2 and 3) may report visual loss (mainly for near vision), central scotoma, and metamorphopsia [79]. The Watzke-Allen test (interruption of the cleft of the biomicroscope in line within the hole) may be useful for the diagnosis and prognostic evaluation of full-thickness holes, but false-negative and positive results are quite common [80]. If information supplied by microperimetry about macular puckers and pseudoholes are important, this test becomes crucial in order to understand the natural history and surgical approach to macular holes. As regards microperimetry, a full-thickness macular hole always corresponds to an absolute scotoma surrounded by a perilesional ring of relative scotoma, with a secondary change fixation location in a retinal area immediately adjacent to the scotoma [8, 11, 36, 37] (Fig. 15.7).

The factors driving the site of PRL may be different, but the most important is the maintenance of adequate reading ability. According to our observations, the PRL is located, in most of cases, on the left side and immediately close to the scotoma. Such PRL is located in 75 % of right eyes in supratemporal areas from the fovea and in 85 % of left eyes in supranasal areas from the fovea [8, 59] (Figs. 15.8 and 15.9). This obviously occurs spontaneously in order to maintain reading ability. The possibility offered by microperimetry to exactly determine fixation location and to quantify its stability in patients affected by full-thickness macular hole and candidate for surgery is clinically very relevant in order to identify the retinal sites where manipulations should be avoided or performed in a very delicate way [9, 11, 36, 59]. Microperimetry evaluation is also useful in the early evaluation of functional

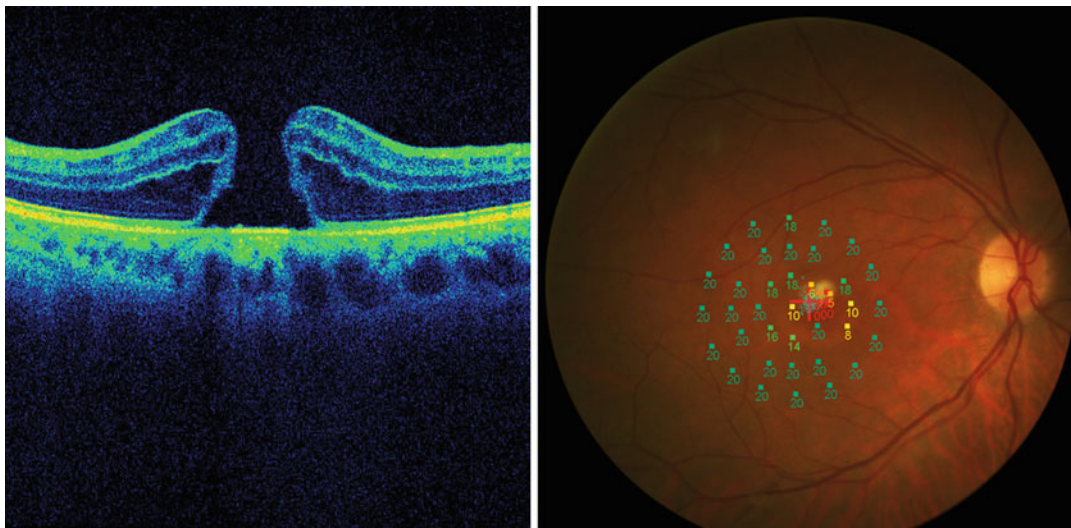


Fig. 15.7 Spectral domain OCT and microperimetry (MP-1) in a case of full-thickness macular hole. The presence of an absolute scotoma is clearly documented



Fig. 15.8 Microperimetry of a macular hole. The PRL is located in the immediate proximity of the scotoma, in a supratemporal area with respect to the fovea (right eye)

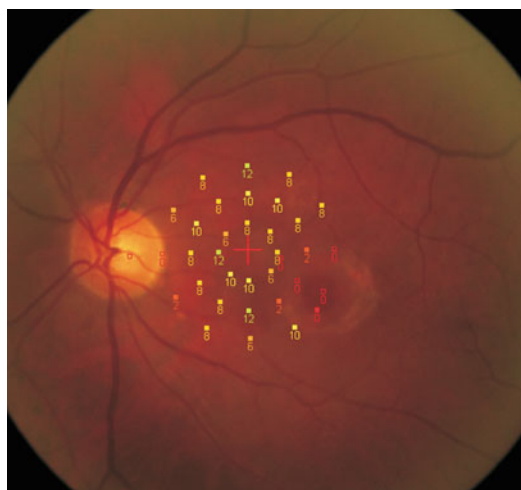


Fig. 15.9 Microperimetry of the other eye of the same patient showing macular hole in which the PRL is situated in a supranasal area with respect to the fovea

damage (absolute or relative scotoma) in the central and perilesional area, in the identification of negative prognostic factors, in establishing the location of the fixation area, and in predicting and monitoring, during the follow-up period, the functional effects of any surgical approach [8, 10, 11, 19, 36, 37, 58, 66, 81].

In a survey carried out in 2001, Amari et al. concluded that a better preoperative retinal (microperimetric) sensitivity is a positive predicting factor for better postoperative functional results [81]. Sjaarda et al., studying 30 eyes affected by full-thickness macular hole, also concluded that better postoperative visual acuity is related to the smaller size of the scotoma and to better perilesional sensitivity observed in preoperative phase, as well as

to the duration of the symptoms [13]. Tsujikawa et al. evaluated (with the old SLO microperimeter) 106 eyes with clinical diagnosis of full-thickness macular hole, macular pseudohole, and impending macular holes in order to qualify the relationship between scotoma characteristics (absolute or relative) and clinical data. In the 57 eyes having full-thickness macular hole, absolute scotomas were always found, while in the 49 eyes diagnosed with early pseudohole and impending macular hole, just relative scotoma but no absolute scotoma were found. They concluded that the presence of an absolute scotoma measured by means of microperimetry is able to detect the presence of full-thickness macular hole with 100 % sensitivity and specificity, while a relative scotoma displays the same level of sensitivity and lower specificity (98 %) [11]. More recently, Sun et al. studied 39 surgically closed idiopathic macular holes with microperimetry and spectral domain OCT (12 months of follow-up) in order to identify a method to foresee the long-term vision recovery of idiopathic macular hole [82]. They also studied the IS/OS junction. Eyes presenting continuous IS/OS junction at the 12-month follow-up were classified as group 1, and those presenting disrupted IS/OS junction were classified as group 2. These authors found that in all 39 patients preoperative mean retinal sensitivity and fixation location percentage were significantly correlated with the 12-month postoperative visual acuity. These results showed a strong relationship between microperimetry data with the visual prognosis, confirming that the value of microperimetry results in quantitatively predicting visual prognosis, just before surgery. Quantitative analysis indicates that the value of preoperative mean retinal sensitivity which prognosticates postoperative 0.50 logMAR visual acuity (Snellen equivalent 20/63) was approximately 12.56 dB. Any 1 dB increment compared to baseline value represents 0.034 logMAR improvement 12 months after surgery. Similarly, the value of preoperative fixation location percentage which predicts postoperative 0.50 logMAR visual acuity was around 29.1 %. Any 10 % increase compared to baseline induces visual acuity increase 0.058 logMAR unit. Evaluating fixation quality score, eyes with stable fixation before surgery had better

visual recovery than those with relatively unstable ($p=0.001$) or unstable ($p=0.003$) fixation. It is interesting to note that preoperative measurements were found to be correlated with the recovery of IS/OS junction: Group 1 patients had better preoperative mean retinal sensitivity ($p=0.003$), better fixation location percentage ($p=0.008$), and higher fixation quality scores than did group 2 patients. Therefore, microperimetry results are useful in quantitatively predicting long-term visual prognosis in eyes with macular hole. Moreover, in this study, neither preoperative visual acuity nor macular hole size was predictive of postoperative visual acuity. Instead, visual prognosis after successful hole closure depends mainly on macular sensitivity, quantified by microperimetry.

Furthermore, evaluating the data of surgery in patients with macular holes Richter-Mueksch et al. found that postoperative visual acuity assessment, without the information supplied by microperimetry, may underestimate functional benefit of surgery [40]. To better understand the reason why microperimetry is so useful to predict final visual prognosis, it must be considered that with the development of the hole, photoreceptors might undergo centrifugal retraction toward the surrounding retina: the hole margin [64, 80]. Subsequently, patients' fixation will gradually shift to the hole margin and paracentral fixation will develop [59]. After tangential traction is removed by vitrectomy, the hole margin moves centripetally back to form a new foveola, along with the centripetal shifting of fixation toward the foveola [59, 63, 83]. This indicates that the hole margin might also affect the postoperative visual function. For this reason the analysis of the hole margin is central in predicting visual prognosis and microperimetry specifically gives fundamental information concerning the macular function, mainly regarding the function of the hole margins. As reported above for MH eyes, the typical microperimetric layouts show a central absolute scotoma representing the full-thickness retinal defect and a pericentral ring-shaped area of decreased sensitivity (relative scotoma) reflecting the dysfunction of hole margins. In addition, fixation stability and fixation location percentage evaluate the capability of gaze control and gaze

selection, respectively. They also evaluate the function of the hole margins where PRL is commonly localized [59, 84]. Another reason for the predictive role of microperimetry data is that they are correlated with IS/OS junction. Two factors determine IS/OS restoration: the diameter of IS/OS defect and the status of photoreceptors along the hole margin. As microperimetry measures both the IS/OS defect (the central absolute scotoma) and the photoreceptors (the pericentral relative scotoma) and fixation exam may be useful to check hole margins, they are effective in predicting the prognosis of IS/OS junction. About IS/OS defect, Chen et al. recently reported that central macular sensitivity, which reflects retinal function just over the area of the MH, correlates with IS/OS defects more closely and for longer duration than mean macular sensitivity [85]. Moreover, they found that IS/OS defect size is a good predictor value for postoperative macular sensitivity and that IS/OS defect area is more correlated to macular sensitivity than IS/OS defect diameter.

Many of the previous studies found a significant correlation between the extent of the foveal IS/OS defect and postsurgical visual outcome. However, this was not confirmed by other studies [86, 87]. Pilli et al. did not find a correlation between the size of the foveal IS/OS defect and visual outcome among the eyes that underwent ILM peeling [88].

Any surgical indication is determined according to anatomic characteristics of the lesion, symptoms, and microperimetry data, as well as to duration, stabilization, or vice versa progression of the retinal changes. As a general rule, when microperimetry indicates decrease in retinal sensitivity, even in case of apparent stability of visual acuity, long-term experience suggests to undergo surgery, in order to avoid any further retinal damage [66, 89]. On the other hand, attention must be paid to choose surgery, particularly vitrectomy with ILM peeling. In fact, some authors recently published data concerning the effects of ILM peeling for MH surgery. They showed that mean retinal sensitivity decreases after ILM peeling with increased rate of microscotomas, detected by microperimetry [90]. Moreover, sometimes

spontaneous resolution of the hole (5–12 %) develops with anatomic closure and increase in central retinal sensitivity [67, 68, 91, 92]. Beutel et al. documented that there is no proof that using dyes may be better than ILM removal without staining [93]. The cause of the development of microscotomas after ILM peeling is still under investigation. The main hypotheses are direct trauma caused by the forceps when gripping the ILM and a toxic effect of dyes (indocyanine green is the only dye that has been demonstrated to have a toxic effect on ganglion cells). But these two hypotheses seem unlikely. Retinal sensitivity deterioration and microscotomas might be due to alterations involving mainly Müller cells, whose end feet are closely connected to the ILM and may be affected by ILM peeling [94]. Deterioration of other cells is also possible, either directly, due to the stretching caused by the peeling, or indirectly, due to Müller cell deterioration.

Conclusions

In conclusion, we highlight the importance of accurate retinal sensitivity checking, by means of microperimetry, in current clinical practice. Microperimetry allows us to better understand several aspects of the clinical behavior of many macular diseases, in particular those related to the vitreoretinal interface changes.

References

1. Sebag J (1992) Anatomy and pathology of the vitreoretinal interface. *Eye (Lond)* 6:541–552
2. Wise GN (1975) Clinical features of idiopathic preretinal macular fibrosis. Schoenberg Lecture. *Am J Ophthalmol* 79:349–357
3. Kenyon KR, Michels RG (1977) Ultrastructure of epiretinal membrane removed by pars plana vitreoretinal surgery. *Am J Ophthalmol* 83:815–823
4. Clarkson SG, Green WR, Massof D (1977) A histopathologic review of 168 cases of preretinal membrane. *Am J Ophthalmol* 84:1–17
5. Fish RH, Anand R, Izbrand DJ (1992) Macular pseudoholes: clinical features and accuracy of diagnosis. *Ophthalmology* 99:1665–1670
6. Varano M, Billi B, Scassa C et al (1997) Scanning laser ophthalmoscopy in the early diagnosis of vitreoretinal interface syndrome. *Retina* 17:300–305

7. Martinez J, Smiddy WE, Kim J et al (1994) Differentiating macular holes from macular pseudo-holes. *Am J Ophthalmol* 117:762–767
8. Varano M, Scassa C (1998) Scanning laser ophthalmoscope microperimetry. *Semin Ophthalmol* 13: 203–209
9. Rohrschneider K, Bultmann S (2001) Fundus-controlled functional evaluation in macular diseases with the scanning laser ophthalmoscope. *Ophthalmologie* 98:3–9
10. Guez JE, Gargasson JF, Massin P et al (1998) Functional assessment of macular hole surgery by scanning laser ophthalmoscopy. *Ophthalmology* 105:694–699
11. Tsujikawa M, Ohji M, Fujikado T et al (1997) Differentiating full thickness macular holes from impending macular holes and macular pseudoholes. *Br J Ophthalmol* 81:117–122
12. Andersen MV (1996) Scanning laser ophthalmoscope microperimetry compared with octopus perimetry in normal subjects. *Acta Ophthalmol Scand* 74:135–139
13. Sjaarda RN, Frank DA, Glaser BM et al (1993) Assessment of vision in idiopathic macular holes with macular microperimetry using the scanning laser ophthalmoscope. *Ophthalmology* 100:1513–1518
14. Rohrschneider K, Fendrich T, Völcker HE et al (1995) Static fundus perimetry using the scanning laser ophthalmoscope with an automated threshold strategy. *Graefes Arch Clin Exp Ophthalmol* 233:743–749
15. Oyagi T, Fujikado T, Hosohata J et al (2004) Foveal sensitivity and fixation stability before and after macular translocation with 360-degree retinotomy. *Retina* 24:548–555
16. Rohrschneider K, Becker M, Fendrich T et al (1995) Kinetic fundus controlled perimetry with the scanning laser ophthalmoscope. *Klin Monatsbl Augenheilkd* 207:102–110
17. Ergun E, Maár N, Radner W et al (2003) Scotoma size and reading speed in patients with subfoveal occult choroidal neovascularization in age-related macular degeneration. *Ophthalmology* 110:65–69
18. Cohen SY, Lamarque F, Saucet JC et al (2003) Filling-in phenomenon in patients with age-related macular degeneration: differences regarding uni- or bilaterality of central scotoma. *Graefes Arch Clin Exp Ophthalmol* 241:785–791
19. Gass JDM (1996) Macular dysfunction caused by vitreous and vitreoretinal interface abnormalities. In: Gass JDM (ed) *Stereoscopic atlas of macular diseases*, 4th edn. CV Mosby, St. Louis, pp 938–951
20. Sidd RJ, Fine SL, Owens SL et al (1982) Idiopathic preretinal gliosis. *Am J Ophthalmol* 94:44–48
21. Hirokawa H, Jalkh AE, Takahashi M et al (1986) Role of the vitreous in idiopathic preretinal macular fibrosis. *Am J Ophthalmol* 101:166–169
22. McDonald HR, Johnson RN, Ai E et al (2006) Macular epiretinal membranes. In: Ryan SJ, Hinton DR, Schachat AP, Wilkinson P (eds) *Retina*, vol 3, 4th edn. Mosby Elsevier Publishers, St. Louis, pp 2509–2525
23. Mori K, Gehlbach PL, Sano A et al (2004) Comparison of epiretinal membranes of differing pathogenesis using optical coherence tomography. *Retina* 24: 57–62
24. Sivalingam A, Eagle RC Jr, Duker JS et al (1990) Visual prognosis correlated with the presence of internal limiting-membrane in histopathologic specimens obtained from epiretinal membrane surgery. *Ophthalmology* 97:1549–1552
25. Wise GN (1972) Preretinal macular fibrosis. (An analysis of 90 cases). *Trans Ophthalmol Soc UK* 92: 131–140
26. Appian AP, Hirose T (1989) Secondary causes of premacular fibrosis. *Ophthalmology* 96:389–392
27. Schubert HD (1989) Cystoid macular edema: the apparent role of mechanical factors. *Prog Clin Biol Res* 312:277–291
28. Goto M, Nishimura A, Shirao Y (2000) Scanning laser ophthalmoscopic microperimetry on idiopathic epiretinal membrane and vitreomacular traction syndrome. *Nihon Ganka Gakkai Zasshi* 104:559–566
29. Gass JDM (1987) Macular dysfunction caused by vitreous and vitreoretinal interface abnormalities. Vitreous traction maculopathies. In: Gass JDM (ed) *Stereoscopic atlas of macular diseases: diagnosis and treatment*, 3rd edn. CV Mosby, St. Louis, pp 676–693
30. Witkin AJ, Ko TH, Fujimoto JG et al (2006) Redefining lamellar holes and the vitreomacular interface: an ultrahigh-resolution optical coherence tomography study. *Ophthalmology* 113:388–397
31. Parolini B, Schumann RG, Cereda MG et al (2011) Lamellar macular hole: a clinicopathologic correlation of surgically excised epiretinal membranes. *Invest Ophthalmol Vis Sci* 52:9074–9083
32. Sramek SJ, Wallow ICH, Stevens TS et al (1989) Immunostaining of preretinal membranes for actin, fibronectin, and glial fibrillary acidic protein. *Ophthalmology* 96:835–841
33. Massin P, Paques M, Masri H et al (1999) Visual outcome of surgery for epiretinal membranes with macular pseudo-holes. *Ophthalmology* 106:580–585
34. Azzolini C, Patelli F, Codenotti M et al (1999) Optical coherence tomography in idiopathic epiretinal macular membrane surgery. *Eur J Ophthalmol* 9:206–211
35. Rice TA, De Bustros S, Michels RG et al (1986) Prognostic factors in vitrectomy for epiretinal membranes of the macula. *Ophthalmology* 93:602–610
36. Guez JE, Le Gargasson JF, Rigaudiere F et al (1993) Is there a systematic location for the pseudo-fovea in patients with central scotoma? *Vision Res* 33:1271–1279
37. Timberlake GT (1986) Reading with a macular scotoma. I. Retinal location of scotoma and fixation area. *Invest Ophthalmol Vis Sci* 27:1137–1147
38. Haritoglou C, Gass CA, Schaumberger M et al (2002) Long-term follow-up after macular hole surgery with internal limiting membrane peeling. *Am J Ophthalmol* 134:661–666

39. Cappello E, Virgili G, Tollot L et al (2009) Reading ability and retinal sensitivity after surgery for macular hole and macular pucker. *Retina* 29:1111–1118
40. Richter-Mueksch S, Vécsei-Marlovits PV, Sacu SG et al (2007) Functional macular mapping in patients with vitreomacular pathologic features before and after surgery. *Am J Ophthalmol* 144:23–31
41. Niwa T, Terasaki H, Kondo M et al (2003) Function and morphology of macula before and after removal of idiopathic epiretinal membrane. *Invest Ophthalmol Vis Sci* 44:1652–1656
42. Watanabe A, Arimoto S, Nishi O (2009) Correlation between metamorphopsia and epiretinal membrane optical coherence tomography findings. *Ophthalmology* 116:1788–1793
43. Wilkins JR, Puliafito CA, Hee MR et al (1996) Characterization of epiretinal membranes using optical coherence tomography. *Ophthalmology* 103:2142–2151
44. Suh MH, Seo JM, Park KH et al (2009) Associations between macular findings by optical coherence tomography and visual outcomes after epiretinal membrane removal. *Am J Ophthalmol* 147:473–480
45. Pilli S, Lim P, Zawadzki RJ et al (2011) Fourier-domain optical coherence tomography of eyes with idiopathic epiretinal membrane: correlation between macular morphology and visual function. *Eye (Lond)* 25:775–783
46. Li D, Horiguchi M, Kishi S (2004) Tomographic and multifocal electroretinographic features of idiopathic epimacular membranes. *Arch Ophthalmol* 122:1462–1467
47. Parisi V, Coppè AM, Gallinaro G et al (2007) Assessment of macular function by focal electroretinogram and pattern electroretinogram before and after epimacular membrane surgery. *Retina* 27:312–320
48. Park SS, Choi SS, Zawadzki RJ et al (2009) Fine retinal striae associated with epiretinal membrane visualized using adaptive optics. *Retin Cases Brief Rep* 3:233–236
49. Ooto S, Hangai M, Takayama K, Sakamoto A, Tsujikawa A, Oshima S, Inoue T, Yoshimura N (2011) High-resolution imaging of the photoreceptor layer in epiretinal membrane using adaptive optics scanning laser ophthalmoscopy. *Ophthalmology* 118:873–881
50. Haouchine B, Massin P, Tadayoni R et al (2004) Diagnosis of macular pseudoholes and lamellar macular holes by optical coherence tomography. *Am J Ophthalmol* 138:732–739
51. Hee MR, Puliafito CA, Wong C et al (1995) Optical coherence tomography of macular holes. *Ophthalmology* 102:748–756
52. Gaudric A, Haouchine B, Massin P et al (1999) Macular hole formation: new data provided by optical coherence tomography. *Arch Ophthalmol* 117:744–751
53. Tanner V, Chauhan DS, Jackson TL et al (2001) Optical coherence tomography of the vitreoretinal interface in macular hole formation. *Br J Ophthalmol* 85:1092–1097
54. Azzolini C, Patelli F, Brancato R (2001) Correlation between optical coherence tomography data and biomicroscopic interpretation of idiopathic macular hole. *Am J Ophthalmol* 132:348–355
55. Haouchine B, Massin P, Gaudric A (2001) Foveal pseudocyst as the first step in macular hole formation: a prospective study by optical coherence tomography. *Ophthalmology* 108:15–22
56. Bottoni F, Carmassi L, Cigada M et al (2008) Diagnosis of macular pseudoholes and lamellar macular holes: is optical coherence tomography the “gold standard”? *Br J Ophthalmol* 92:635–639
57. Greven CM, Slusher MM, Czyn CN et al (1998) The natural history macular pseudoholes. *Am J Ophthalmol* 125:360–366
58. Klein BR, Hiner CJ, Glaser BM, Murphy RP, Sjaarda RN, Thompson JT (1995) Fundus photographic and fluorescein angiographic characteristics of pseudoholes of the macula in eyes with epiretinal membranes. *Ophthalmology* 102:768–774
59. Nakabayashi M, Fujikado T, Ohji M et al (2000) Fixation patterns of idiopathic macular holes after vitreous surgery. *Retina* 20:170–175
60. Allen AW Jr, Gass JD (1976) Contraction of a perifoveal epiretinal membrane simulating a macular hole. *Am J Ophthalmol* 82:684–691
61. García-Fernández M, Navarro JC, Sanz AF et al (2012) Long-term evolution of idiopathic lamellar macular holes and macular pseudoholes. *Can J Ophthalmol* 47:442–447
62. Gass JD (1975) Lamellar macular hole: a complication of cystoid macular edema after cataract extraction: a clinicopathologic case report. *Trans Am Ophthalmol Soc* 73:230–250
63. Gass JD (1988) Idiopathic senile macular hole. Its early stages and pathogenesis. *Arch Ophthalmol* 106:629–639
64. Gass JD (1995) Reappraisal of biomicroscopic classification of stages of development of a macular hole. *Am J Ophthalmol* 119:752–759
65. Smiddy WE, Gass JD (1995) Masquerades of macular holes. *Ophthalmic Surg* 26:16–24
66. Byhr E, Lindblom B (1998) Preoperative measurements of macular hole with scanning laser ophthalmoscope. Correlation with functional outcome. *Acta Ophthalmol Scand* 76:579–583
67. Ebato K, Kishi S (2000) Spontaneous closure of macular hole after posterior vitreous detachment. *Ophthalmic Surg Lasers* 31:245–247
68. Takahashi H, Kishi S (1999) Optical coherence tomography images of spontaneous macular hole closure. *Am J Ophthalmol* 128:519–520
69. Bottoni F, Deiro AP, Giani A et al (2013) The natural history of lamellar macular holes: a spectral domain optical coherence tomography study. *Graefes Arch Clin Exp Ophthalmol* 251:467–475
70. Reibaldi M, Parravano M, Varano M et al (2012) Foveal microstructure and functional parameters in lamellar macular hole. *Am J Ophthalmol* 154:974–980

71. Parravano M, Oddone F, Boccassini B et al (2013) Functional and structural assessment of lamellar macular holes. *Br J Ophthalmol* 97:291–296
72. Chen JC, Lee LR (2008) Clinical spectrum of lamellar macular defects including pseudoholes and pseudocysts defined by optical coherence tomography. *Br J Ophthalmol* 92:1342–1346
73. Morgan CM, Schatz H (1985) Idiopathic macular holes. *Am J Ophthalmol* 99:437–444
74. Morgan CM, Schatz H (1986) Involitional macular thinning: a premacular hole condition. *Ophthalmology* 93:153–161
75. Ho AC, Guyer DL, Fine SL (1998) Macular hole. *Surv Ophthalmol* 42:393–416
76. Gordon LW, Glaser BM, Ie D, Thompson JT et al (1995) Full-thickness macular hole formation with a pre-existing complete posterior vitreous detachment. *Ophthalmology* 102:1702–1705
77. Johnson NS, Gass JDM (1988) Idiopathic macular hole. Observations, stages of formation, and implications for surgical intervention. *Ophthalmology* 95:917–924
78. Johnson MW, Van Newkirk MR, Meyer KA (2001) Perifoveal vitreous detachment is the primary pathogenic event in idiopathic macular hole formation. *Arch Ophthalmol* 119:215–222
79. Saito Y, Hirata Y, Hayashi A et al (2000) The visual performance and metamorphopsia of patients with macular holes. *Arch Ophthalmol* 118:41–46
80. Tanner V, Williamson TH (2000) Watzke-Allen slit beam test in macular holes confirmed by optical coherence tomography. *Arch Ophthalmol* 118:1059–1063
81. Amari F, Ohta K, Kojima H et al (2001) Predicting visual outcome after macular hole surgery using scanning laser ophthalmoscope microperimetry. *Br J Ophthalmol* 85:96–98
82. Sun Z, Gan D, Jiang C et al (2012) Effect of preoperative retinal sensitivity and fixation on long-term prognosis for idiopathic macular holes. *Graefes Arch Clin Exp Ophthalmol* 250:1587–1596
83. McDonnell PJ, Fine SL, Hillis AI (1982) Clinical features of idiopathic macular cysts and holes. *Am J Ophthalmol* 93:777–786
84. Tarita-Nistor L, Gonzalez EG, Mandelcorn MS et al (2009) Fixation stability, fixation location, and visual acuity after successful macular hole surgery. *Invest Ophthalmol Vis Sci* 50:84–89
85. Chen WC, Wang Y, Li XX (2012) Morphologic and functional evaluation before and after successful macular hole surgery using spectral-domain optical coherence tomography combined with microperimetry. *Retina* 32:1733–1742
86. Kitaya N, Hikichi T, Kagokawa H et al (2004) Irregularity of photoreceptor layer after successful macular hole surgery prevents visual acuity improvement. *Am J Ophthalmol* 138:308–310
87. Chung H, Shin CJ, Kim JG et al (2011) Correlation of microperimetry with fundus autofluorescence and spectral-domain optical coherence tomography in repaired macular holes. *Am J Ophthalmol* 151:128–136.e3
88. Pilli S, Zawadzki RJ, Werner JS et al (2012) Visual outcome correlates with inner macular volume in eyes with surgically closed macular hole. *Retina* 32:2085–2095
89. Varano M, Scassa C, Capaldo N et al (2002) Development of macular pseudoholes: a 36-month period of follow-up. *Retina* 22:435–442
90. Tadayoni R, Svorenova I, Erginay A et al (2012) Decreased retinal sensitivity after internal limiting membrane peeling for macular hole surgery. *Br J Ophthalmol* 96:1513–1516
91. Carpineto P, Ciancaglini M, Aharrh-Gnama A et al (2005) Optical coherence tomography and fundus microperimetry imaging of spontaneous closure of traumatic macular hole: a case report. *Eur J Ophthalmol* 15:165–169
92. Milani P, Seidenari P, Carmassi L et al (2007) Spontaneous resolution of a full thickness idiopathic macular hole: fundus autofluorescence and OCT imaging. *Graefes Arch Clin Exp Ophthalmol* 245:1229–1231
93. Beutel J, Dahmen G, Ziegler A et al (2007) Internal limiting membrane peeling with indocyanine green or trypan blue in macular hole surgery: a randomized trial. *Arch Ophthalmol* 125:326–332
94. Haritoglou C, Schumann R, Reiniger I et al (2006) Evaluation of the internal limiting membrane after conventional peeling during macular hole surgery. *Retina* 26:21–24

Ahmed M. Abu El-Asrar, Marwan Abouammoh,
and Hani S. Al-Mezaine

Macular function of patients with inflammatory chorioretinal disorders is usually tested by best-corrected visual acuity (BCVA) assessment as the primary end point to measure the effectiveness of therapies and to identify prognostic factors for final outcome. Although BCVA testing is an established modality to assess functional improvement, it may only represent foveal function and does not reflect structural changes of the neurosensory retina outside the foveal region. In addition, macular involvement in patients with inflammatory chorioretinal disorders extends, in most cases, to the larger macular area. BCVA, therefore, poorly evaluates the functional impact of inflammatory chorioretinal diseases involving the posterior pole. Therefore, evaluation of the topographic sensitivity of the entire central retina is much more informative to better determine the effect of treatment in these patients. The recently developed fundus microperimetry (MP-1; Nidek Technologies, Italy) is able to quantify macular sensitivity and to study the location and the stability of retinal fixation in an exact fundus-related fashion, thus adding detailed information about the degree and pattern of macular function alteration. Decrease in fixation stability and central fixation loss are among the characteristics of cen-

tral visual function deterioration in patients with macular pathologies resulting in the development of eccentric and unstable fixation indicating that an extrafoveal preferred retinal locus is established [1, 2]. MP-1 microperimetry has also the ability to overlay a retinal sensitivity map on color fundus photograph allowing better localization of the pathology. In addition, the tracking software ensures that repeated examinations test the same retinal points tested during baseline examination [3]. The use of microperimetry was first described by Midena et al. as an excellent tool to measure central macular sensitivity, scotoma size, and fixation status in patients with macular pathology [1, 2]. Automated fundus microperimetry therefore facilitates the accurate assessment and reassessment of a patient's central macular sensitivity and provides an objective and quantitative assessment of macular function over time. This may be a more comprehensive approach for quantifying macular function in inflammatory chorioretinal disorders than BCVA measurement alone. Microperimetry, therefore, has been successfully used in the diagnosis and follow-up of inflammatory chorioretinal diseases such as Vogt-Koyanagi-Harada (VKH) disease, presumed tuberculous choroiditis, serpiginous choroiditis, birdshot chorioretinopathy, and uveitic macular edema [5–9].

We longitudinally evaluated the macular function in 14 patients (28 eyes) with VKH disease in the acute uveitic phase (exudative retinal detachment) following immunosuppressive therapy using BCVA and fundus microperimetry

A.M.A. El-Asrar, MD, PhD (✉)
M. Abouammoh • H.S. Al-Mezaine
Department of Ophthalmology,
College of Medicine, King Saud University,
Old Airport Road, 245, Riyadh 11411, Saudi Arabia
e-mail: abuasrar@ksu.edu.sa, abuelasrar@yahoo.com

to assess central retinal sensitivity and fixation stability. The following four findings were demonstrated: (1) Patients displayed a markedly decreased BCVA, fixation stability, and mean retinal sensitivity at baseline, reflecting severely impaired macular function; (2) BCVA, fixation stability, and mean retinal sensitivity significantly increased from baseline after treatment. The beneficial effect was obtained as early as 1 month after treatment; (3) BCVA and fixation stability recovered earlier, faster, and better than mean retinal sensitivity; and (4) at the final follow-up, retinal sensitivity was significantly reduced even in eyes with full recovery of BCVA (Fig. 16.1). Although BCVA and fixation stability seemed to be almost maximum at 3 months after treatment, retinal sensitivity as measured by microperimetry showed progressive improvement till 12 months. However, mean retinal sensitivity was still significantly reduced at 12 months [4].

A recent multicenter study examined 190 healthy subjects with a BCVA of 20/20 or better with the MP-1 microperimeter. In the same age range as in our study, the authors showed that the mean macular sensitivity was 19.6 ± 0.5 dB. Repeatability of the test performed at three separate visits showed consistent values over time [10]. In patients with VKH disease, the mean central retinal sensitivity at 12 months after immunosuppressive therapy was 12.1 ± 2.3 dB. These findings suggest that retinal sensitivity, assessed by the MP-1 microperimeter, even in eyes with full recovery of visual acuity, was reduced in patients with VKH disease [4]. Decreased retinal sensitivity may reflect photoreceptor dysfunction attributable to subretinal fluid or photoreceptor loss itself. When subretinal fluid resolved after treatment, mean macular sensitivity significantly increased. The beneficial effect was obtained as early as 1 month after treatment and continued up to 12 months. Another possibility is that this photoreceptor dysfunction may be secondary to diffuse pathologic changes in the choroid and/or retinal pigment epithelium in VKH. Persistent reduced retinal sensitivity suggests that prolonged photoreceptor dysfunction is a feature of acute uveitis associated with VKH disease. Our

data reveal that distant BCVA alone significantly underestimates the impairment of photoreceptors and that subclinical macular dysfunction is a permanent damage in VKH disease. It is tempting to speculate that functional mapping with microperimetry may therefore give a more accurate representation of perceived visual function after immunosuppressive therapy than BCVA alone. These findings stress the importance of a full assessment of macular function by integrating microperimetry and BCVA in patients with VKH disease.

The efficacy of antituberculous therapy and systemic corticosteroids in a group of patients suffering from active presumed tuberculous choroiditis was investigated by the assessment of central retinal sensitivity and fixation characteristics. Macular sensitivities and fixation characteristics improved significantly after treatment (Figs. 16.2 and 16.3). These findings suggest that MP-1 microperimetric evaluation of macular function is useful in monitoring the efficacy of treatment in patients with presumed tuberculous choroiditis [5].

Pilotto et al. analyzed fixation pattern and retinal sensitivity in a group of 14 consecutive patients (28 eyes) with serpiginous choroiditis [6]. With microperimetry, they demonstrated that atrophic lesions are characterized by dense scotomas in all cases, with relative scotoma bordering the lesions at the margins in 36 % of the cases. Moreover, they documented a dense scotoma topographically related to an active lesion. They detected relative scotomas in unaffected areas both at the posterior pole and in the peripapillary region. These retinal areas appeared normal at fundus examination, but in two cases, the relative scotoma corresponded to a choroidal filling defect detectable in the early indocyanine green angiographic phases. These findings suggest that some cases have a wider functional involvement than expected. Of the 28 eyes, 16 had central, one poor central, and 11 eccentric fixation, and 18 had stable, four relatively unstable, and six unstable fixation. In patients with posterior pole symmetrically involved in both eyes, fixation was central and stable in the best functioning eye (best BCVA) in all cases.

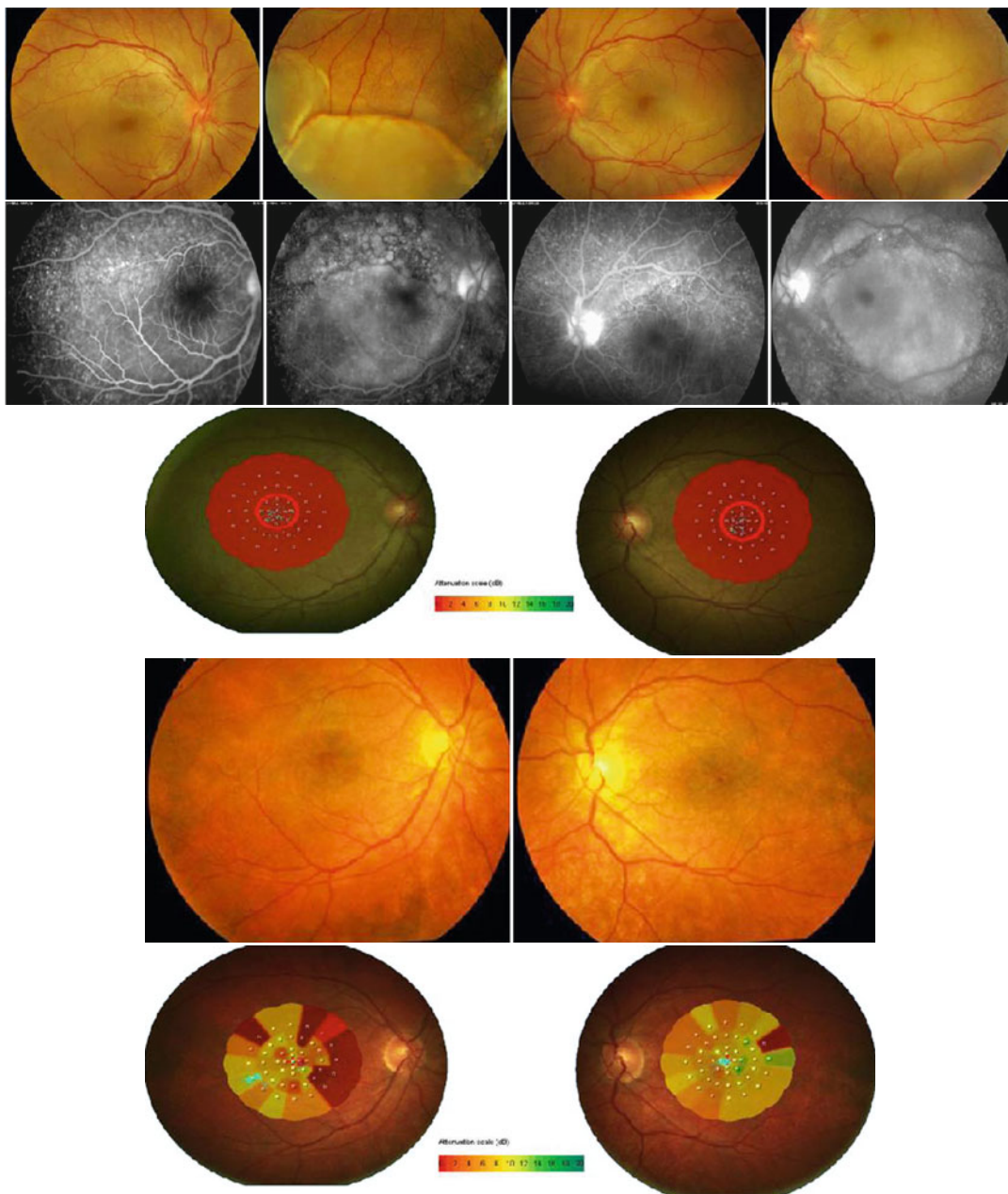


Fig. 16.1 A 28-year-old female with Vogt-Koyanagi-Harada disease in the acute uveitic phase. Note the exudative retinal detachments and the hyperemic optic discs. Visual acuity was counting fingers at 2 ft in both eyes (*top*). Fluorescein angiography shows multiple pinpoint hyperfluorescence at the levels of the retinal pigment epithelium and late pooling of dye in the areas of exudative retinal detachment (*second row*). The mean retinal sensitivity in the central 12° was 0.0 dB in both eyes. Color-coded, numeric scale shows the threshold in 2 dB steps

from 0 to 20 dB. Normal sensitivity is indicated by green color and decreased sensitivity is indicated by red color. The fixation stability inside the 2° was 7 % in the right eye and 11 % in the left eye (*third row*). Three months after treatment, best-corrected visual acuity improved to 20/25 in both eyes (*fourth row*). The mean central retinal sensitivity improved to 1.4 dB in the right eye and to 9.0 dB in the left eye. However, mean central sensitivity was still significantly reduced. Fixation stability improved to 89 % in the right eye and to 87 % in the left eye (*bottom*)

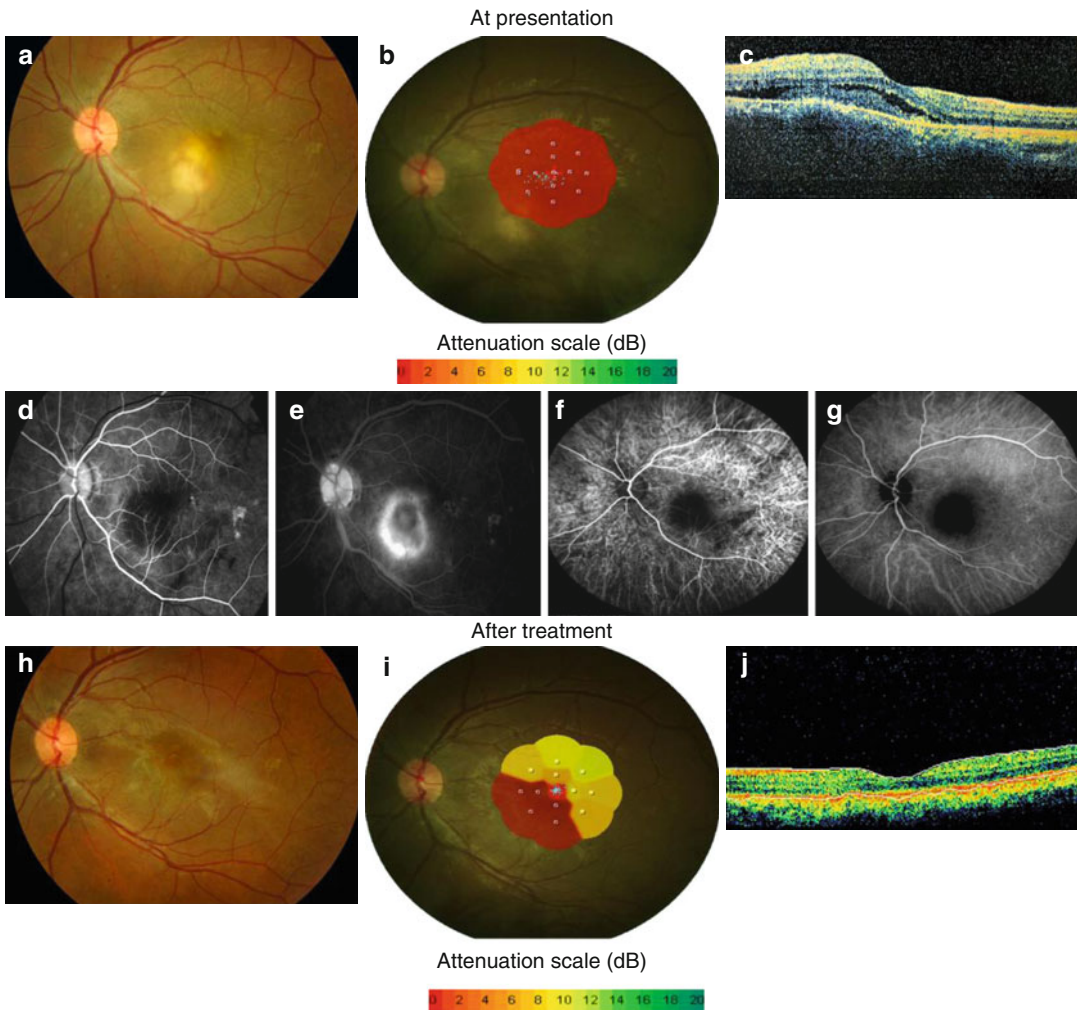


Fig. 16.2 Fundus photograph at presentation showing solitary choroidal granuloma (a). A retinal sensitivity map obtained with MP-1 microperimetry shows reduced sensitivity (0.0 dB) (b). Optical coherence tomography shows overlying exudative retinal detachment and the granuloma under the detached neurosensory retina (c). On fundus fluorescein angiography, the lesion is hypofluorescent in

the early phase (d) and becomes hyperfluorescent in the late phase (e). Indocyanine green angiography shows hypofluorescence throughout, corresponding to the lesion (f, g). Six months after starting antituberculous therapy and systemic corticosteroids. Fundus photography shows resolution of the granuloma (h). MP-1 microperimetry shows improved sensitivity (4.2 dB) (i). Optical detachment (j)

Giuliani et al. evaluated the role of MP-1 microperimetry as an ancillary tool in patients with birdshot chorioretinopathy (BSCR) [7]. In their cohort of patients, they noticed a greater reduction of the macular sensitivities in eyes with active inflammation than in eyes with inactive inflammation and in eyes in the control group. They also noticed a greater reduction of the macular sensitivities in eyes with inactive

inflammation than in eyes in the control group. The authors concluded that microperimetric quantification of macular sensitivity in patients with BSCR may provide an ancillary tool to evaluate activity and may help to assess visual impairment in these patients.

In patients with uveitic macular edema, there was a significant negative correlation between logarithm of the minimum angle of

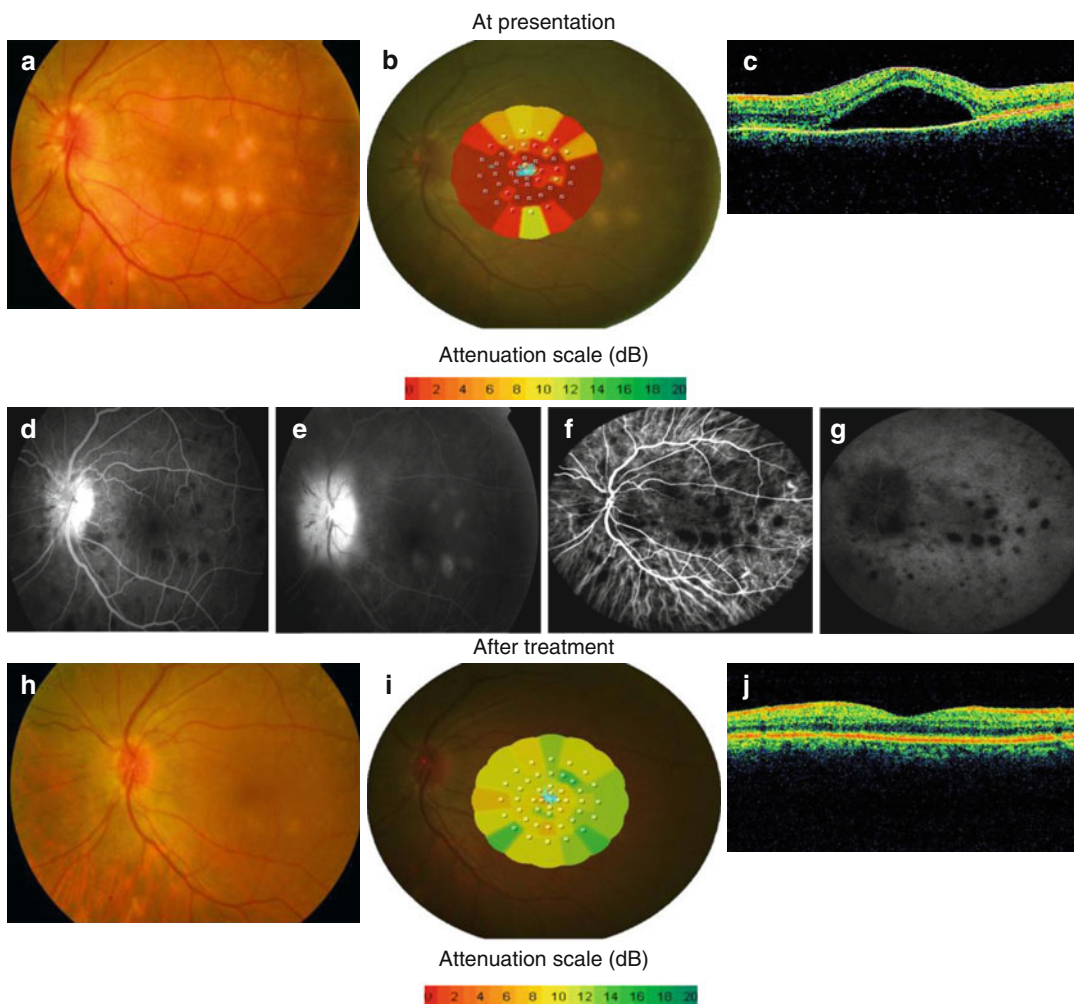


Fig. 16.3 Fundus photograph at presentation showing multifocal choroiditis and optic neuritis (a). MP-1microperimetry shows decreased sensitivity (1.1 dB) (b). Optical coherence tomography shows exudative retinal detachment (c). On fluorescein angiography, the lesions are hypofluorescent in the early phase (d) and hyperfluorescent in the late phase (e). The optic nerve head shows leakage and staining. Indocyanine green angiography shows that the lesions are hypofluorescent throughout

(f, g). Note the lesions on indocyanine green angiography are more numerous than on fluorescein angiography. One month after starting antituberculous therapy and systemic corticosteroids. Fundus photograph shows resolution of choroiditis (h). Microperimetry shows improved sensitivity (11.1 dB) (i). Optical coherence tomography shows resolution of exudative retinal detachment (j). Coherence tomography displays resolution of exudative retinal detachment

resolution and retinal sensitivity as detected by fundus-related microperimetry [8]. Paroli et al. also demonstrated reduced macular sensitivity in eyes with juvenile idiopathic arthritis-related uveitis complicated with macular edema [9]. They suggested that microperimetry might be a reliable tool in the follow-up of macular edema in juvenile idiopathic arthritis-related uveitis.

References

1. Midena E, Radin PP, Pilotto E, Ghirlando A, Convento E, Varano M (2004) Fixation pattern and macular sensitivity in eyes with subfoveal choroidal neovascularization secondary to age-related macular degeneration. A microperimetry study. *Semin Ophthalmol* 19:55–61
2. Midena E, Vujosevic S, Convento E, Manfré A, Cavarzeran F, Pilotto E (2007) Microperimetry and

- fundus autofluorescence in patients with early age-related macular degeneration. *Br J Ophthalmol* 91: 1499–1503
3. Springer C, Bültmann S, Völcker HE, Rohrschneider K (2005) Fundus perimetry with the Micro perimeter 1 in normal individuals: comparison with conventional threshold perimetry. *Ophthalmology* 112:848–854
 4. Abu El-Asrar AM, Al-Mezaine HS, Hemachandran S, Hariz R, Kangave D (2012) Retinal functional changes measured by microperimetry after immunosuppressive therapy in patients with Vogt-Koyanagi-Harada disease. *Eur J Ophthalmol* 22:368–375
 5. Abu El-Asrar AM, Al-Mezaine HS (2010) Anti-tuberculous therapy combined with systemic corticosteroids improves retinal sensitivity in patients with active presumed tuberculous choroiditis. *Int Ophthalmol* 30:567–576
 6. Pilotto E, Vujosevic S, Grgic VA, Sportiello P, Convento E, Secchi AG, Midena E (2010) Retinal function in patients with serpiginous choroiditis: a microperimetry study. *Graefes Arch Clin Exp Ophthalmol* 248:1331–1337
 7. Giuliari GP, Pujari S, Shaikh M, Marvell D, Foster CS (2010) Microperimetry findings in patients with birdshot chorioretinopathy. *Can J Ophthalmol* 45:399–403
 8. Roesel M, Heimes B, Heinz C, Henschel A, Spital G, Heiligenhaus A (2011) A comparison of retinal thickness and fundus-related microperimetry with visual acuity in uveitic macular oedema. *Acta Ophthalmol* 89:533–537
 9. Paroli MP, Spinucci G, Fabiani C, Pivetti-Pezzi P (2010) Retinal complications of juvenile idiopathic arthritis-related uveitis: a microperimetry and optical coherence tomography study. *Ocul Immunol Inflamm* 18:54–59
 10. Midena E, Vujosevic S, Cavarzeran F, Microperimetry Study Group (2010) Normal values for fundus perimetry with the Microperimeter MP1. *Ophthalmology* 117:1571–1576

Raffaele Parrozzani and Silvia Bini

17.1 Introduction

Toxic retinopathies are a group of conditions in which the retina is damaged by substances or medications introduced systemically, topically or through loco-regional ways of administration. Although liver and kidneys are the most common organs involved in drug toxicity if medication is systemically administered, severe insults may occur before any clinical manifestation, causing most often a late diagnosis with irreversible side effect. Conversely, if the retina and/or optic nerve experiences direct or indirect toxicity, a small amount of damage may cause a significant clinically detectable loss of sensitivity, commonly causing visual symptoms and eventually visual loss. There are over 30,000 prescription drugs available in the United States alone and many more available worldwide. Moreover, over-the-counter drugs should be also taken into account, because such drugs are commonly used by patients and can theoretically have adverse ocular side effects. Furthermore, many daily used substances may affect the retina by direct toxicity, such as iron (siderosis) or copper, and systemic deficit of specific substances (i.e. vitamin A defi-

ciency-related retinopathy after bariatric surgery) may also cause retinal toxicity and loss of vision. It would be impractical to try to comprehensively cover every known retinal change reported from every type or class of substances. Therefore, representative medications and substances currently in use that have recent and significant reports of retinal toxicity are included in this chapter (see Table 17.1).

17.2 Clinical Features and Diagnostic Approaches

Toxic retinopathy remains a relatively rare disease, but when signs and symptoms of a patient include decreased visual acuity, abnormalities of colour vision and visual field defects, unexplained by other conditions, a complete history may reveal past or present use of potentially retinotoxic substances. Fundus findings may sometimes suggest the presence of a toxic retinal damage, but most often there are no specific ophthalmoscopic aspects. Fluorescein angiography, fundus autofluorescence and optical coherence tomography are valuable parts of the focused clinical evaluation, mainly when maculopathy is suspected. However, it is primarily important to accurately evaluate the visual function of these patients. Standard perimetry remains an essential diagnostic tool in the clinical diagnosis of toxic retinopathies. This technique continues to be considered the gold standard for detecting and assessing panretinal and optic nerve toxicity, but

R. Parrozzani, MD, PhD (✉)
GB Bietti Foundation, IRCCS, Via Livenza 3,
Rome 00198, Italy
e-mail: oncologia.tossicologia@fondazionebietti.it

S. Bini
Department of Ophthalmology, University of Padova,
Via Giustiniani 2, Padova 35128, Italy

Table 17.1 List of the major drugs and substances causing toxic retinopathies

Retinal toxicity by drugs and substances			
Drug/substance	Administration	Use/category	Main ocular toxicity sites
Canthaxanthin	Oral	Tanning/photosensitivity disorders	Retina
Chlorpromazine	Oral	Antipsychotic	Retina
Chloroquine	Oral	Antimalaria	Retina
Clofazimine	Oral	Antimycobacterial	Retina
Cobalt	Systemic	Implants	Retina
Copper	Intravitreal	Accidental	Anterior segment–retina
Desferrioxamine	Oral	Iron chelating	Retina
Gentamicin	Intravitreal	Antibacterial in endophthalmitis	Retina
Hydroxychloroquine	Oral	Antimalaria	Retina
Indocyanine green dye	Intravitreal	Staining in surgical procedures	Retina
Interferon α	Subcutaneous	Leukaemia, lymphoma, hepatitis C	Retina
Iron	Intravitreal/systemic	Accidental/iron deficiency	Retina
Latanoprost	Topical	Lowering intraocular tension	Retina
Methanol	Oral	Poisoning	Retina–optic nerve
Methoxyflurane	Inhalator	Anaesthesia	Retina
Nicotinic Acid	Oral	Cholesterol lowering	Retina
Nitrofurantoin	Oral	Antibacterial	Retina
Tamoxifen	Oral	Adjuvant therapy in breast cancer	Anterior segment–retina–optic nerve
Thioridazine	Oral	Antipsychotic	Retina
Vigabatrin	Oral	Antiepileptic	Retina–optic nerve

focal macular involvement, initial small scotomas and mild or moderate changes in retinal function may remain fully undetected using standard perimetry.

Visual acuity is a limited measure of visual function because it reflects only the status of the fovea. Conversely, assessment of visual function must take into account at least the function of the entire macular area.

Microperimetry allows to quantitatively assess macular function and/or the visual function of selected retinal areas. It also provides a quantifiable way to measure the changes of retinal function impairment in examined areas. Thus, microperimetry should be theoretically considered a relevant and careful diagnostic procedure to quantitatively assess macular function in the diagnosis and follow-up of toxic retinopathy. Although there are few data on microperimetry in toxic retinopathies, it may easily substitute standard perimetry, because of its higher sensitivity, which allows to detect macular toxicity before irreversible damage to visual function occurs.

Furthermore, the proven reproducibility of this technique allows clinicians to follow the same patients over time. Microperimetry seems to be an ideal tool also for screening patients who are starting a therapy with a potential toxicity to the retina. Visual function information obtained by microperimetry (at baseline and during follow-up) may result in the decision to discontinue the medication before any irreversible damage, thus preserving or restoring, physiological retinal function.

17.3 Retinal Toxicity by Drugs: Systemic Administration

17.3.1 Chloroquine-Hydroxychloroquine

Chloroquine (CQ) was originally used to prevent and treat malaria, and CQ-related retinopathy was first described in the 1950s [1]. Nowadays CQ and its analogue, hydroxychloroquine (HCQ), are

widely used in the treatment of different inflammatory conditions, including rheumatoid arthritis and systemic lupus erythematosus [2]. The mechanism of CQ/HCQ-related retinal toxicity is not completely understood. Both CQ and HCQ bind melanin in the retinal pigment epithelium (RPE), leading to the late characteristic feature of bull's eye maculopathy, where a ring of RPE depigmentation spares the fovea. These drugs have acute effects on the retinal cells metabolism, including photoreceptors, but it is unclear whether these short-term metabolic effects are the cause of the slow and chronic damage characterizing its clinical toxicity [3]. In 2002 the American Academy of Ophthalmology (AAO) reported specific recommendations on screening procedures for CQ and HCQ users, stratifying patients into two risk groups: low-risk patients, receiving less than or equal to 6.5 mg/kg/day of HCQ (less than or equal to 3 mg/kg/day of CQ) for a duration less than 5 years, and high-risk patients (higher dosage, long-term treatment >5 years, concomitant risk factors like high body fat level, kidney or liver disease and age greater than 60). Baseline examination should be done within the first year of administration, and annual screening should begin 5 years later for low-risk patients [4]. However, the criteria for judging the risk of developing retinal toxicity have been amplified in the 2011 revision, introducing the new concept of "cumulative dose". Concomitant medical and ocular conditions must be carefully evaluated by the physician to anticipate annual screening. The baseline visit must include full ophthalmic examination and visual field testing. Suggested additional tests are spectral domain optical coherence tomography, multifocal electroretinogram (mfERG) and fundus autofluorescence. No mention of microperimetry is present [5]. Nevertheless, patients with CQ/HCQ-related maculopathy are commonly asymptomatic or complain for non-specific visual symptoms in the presence of normal visual acuity. At this stage central or paracentral limited scotomas may be theoretically already present. Scotomas often begin within 10° of fixation and are commonly located in the superior part of the macula [6]. Subsequently scotomas may enlarge involving

the fovea with severe visual impairment. Once any scotoma has been demonstrated, the damage is usually irreversible and progresses despite stopping the treatment. The only reversible stage of this disease is the early phase, when the discontinuation of therapy may stop the damage to the macula. Thus, a correct use of screening procedure, including microperimetry, is fundamental to save visual function in these patients. Microperimetry has been used in only two case reports describing retinal sensitivity changes in patients treated by CQ and HCQ. In both cases microperimetry showed reduced macular sensitivity. The areas of decreased sensitivity at microperimetry corresponded in one case to areas of hypopigmentation and inner segment–outer segment (IS–OS) junction discontinuity at spectral domain optical coherence tomography. In the second case, increased autofluorescence and hyperfluorescence at fluorescein angiography were found, confirming the early alteration of the retinal pigment epithelium [7, 8].

17.3.2 Vigabatrin

Vigabatrin is a selective GABA aminotransferase inhibitor used as an antiepileptic drug in seizures and infantile spasms. Vigabatrin has been associated with visual field defects, mainly characterized by peripheral visual field constriction. It has been hypothesized that the defect was predominantly characterized by peripheral cone dysfunction. Several studies have recently shown that there is also a central involvement of cone-mediated vision. Visual function assessment, perimetry, colour vision and multifocal ERG have demonstrated that central cone function is not spared when vigabatrin therapy is administered, and a generalized dysfunction is often induced [9]. Animal studies have not yet clarified where the damage is exactly localized inside the retina, but some authors have hypothesized that both inner and outer retina are equally involved.

Even if patients are usually asymptomatic, visual field defects occur in more than 30 % of patients, and the central involvement may be

associated with a prolonged use or with a cumulative dose of the drug. The discontinuation of vigabatrin seems to be effective in restoring macular function only in the early phases of toxicity, thus making microperimetry an adequate tool to detect initial signs of macular dysfunction.

17.3.3 Tamoxifen

Tamoxifen is a selective oestrogen receptor modulator widely used as adjuvant treatment of breast cancer in women whose tumour is positive for oestrogen receptors. Because the retina physiologically contains oestrogen receptors, vision may be affected, even if rarely. Tamoxifen use may cause retinopathy but also corneal opacities, lens alteration and optic neuritis and increases the risk of developing a macular hole [10, 11]. Tamoxifen maculopathy was first described in 1978 by Kaiser-Kupfer and Lippman in women receiving high doses of tamoxifen (greater than 180 mg/day and up to 320 mg/day). Fundus examination of these patients showed tiny refractile deposits in the inner retina, together with pigmented alteration at the level of retinal pigment epithelium. Fluorescein angiography showed the presence of cystoid macular oedema (CME) [12]. The current dosage of tamoxifen has been reduced to 20–40 mg/day; notwithstanding, this drug continues to be associated with abnormalities in visual function, including colour vision. The incidence of maculopathy at low-dose therapy is not yet defined. Nourreddin et al. and Heier et al. reported an incidence of 4.6 and 1.5 %, respectively, of tamoxifen-related maculopathy, characterized by different clinical patterns [13, 14]. Eisner et al. prospectively investigated a group of women with normal fundus appearance treated by a low dose (20 mg/day) of tamoxifen for 2 years using short-wavelength automated perimetry visual fields. These authors reported that the mean deviation was significantly decreased, suggesting that retinal dysfunction may precede fundus changes [15]. Watanabe et al. and Salomão et al. investigated a similar group of patients by means of focal, full-field and multifocal ERG

showing no alteration. These results have raised some questions about the role of ERG in detecting tamoxifen-related retinopathy, suggesting that ERG (even multifocal) is poorly sensitive to detect early changes in retinal function during tamoxifen therapy [16, 17]. Considering the higher sensitivity of microperimetry, this technique may be useful in detecting tamoxifen maculopathy in an early stage, but a definite role has not yet been proved.

17.3.4 Canthaxanthin

Canthaxanthin is a carotenoid commonly present in nature and used in over-the-counter oral tanning products, in food colouring and as a therapeutic agent for photosensitivity disorders. Cortin et al. in 1982 firstly described canthaxanthin maculopathy as a crystal deposition around the macular region, in the inner retinal layers [18]. This deposition is usually bilateral and is associated with ingestion of high doses of the artificial carotenoid. Patients are usually asymptomatic, but some authors found decreased retinal sensitivity with static perimetry and ERG abnormalities in patients showing clinically evident macular alterations [19]. Hueber et al. suggested that the deposition of these particles may be partially dose dependent and influenced by previous retinal conditions, i.e. pre-existing retinal pigment epithelium changes [20]. If macular deposits are absent, no functional changes have been documented. Crystal deposits disappear over time, with complete restoration of the anatomy and retinal function. The use of microperimetry in canthaxanthin toxicity has not yet been investigated but should be rationally considered an intriguing tool to assess macular function in these subjects.

17.3.5 Nicotinic Acid

Nicotinic acid is a vitamin used for many years in patients with dyslipidemia, especially when characterized by low blood levels of

high-density lipoprotein, because of its lipid-modifying effects. Nicotinic acid administration is associated with several side effects, including flushing and abdominal pain. Ocular involvement is rare [21]. In 1973, Gass firstly described the existence of a nicotinic acid-related maculopathy in patients taking high doses of this drug. Cystoid macula oedema was described as clinically evident only in some of these patients [22]. The intraretinal cysts were subsequently described as predominantly localized in the outer plexiform layer by Spirm et al. using optical coherence tomography [23]. Nicotinic acid-related maculopathy usually affects patients using this drug at a dosage higher than 1.5 mg/day, and it is reversible with discontinuation of the therapy.

17.3.6 Thioridazine–Chlorpromazine

Phenothiazines are used as oral antipsychotic and antihistaminic drugs. Thioridazine maculopathy was described for the first time in 1960s when the dosage of the drug was higher than today [24]. The administration of more than 800 mg/day of thioridazine may cause in a few weeks vision loss and nyctalopia. Fundus changes consist in “salt and pepper” RPE pattern, with progression to focal loss and clumps or the RPE to a diffuse atrophy of both RPE and choriocapillaris [25]. Chlorpromazine is another antipsychotic drug also associated with RPE changes at the fundus. Actual dosage of phenothiazine is considerably lower than in the past, thus toxic maculopathy is now a very rare condition.

17.4 Retinal Toxicity by Drugs: Retrobulbar/Parabulbar/ Intra-arterial Administration

Most of the data on this topic are related to the current use of antineoplastic drugs in the treatment of child with retinoblastoma. Periocular topotecan and carboplatin have been associated to significant retinal toxicity [26]. Also the recent reintroduction of superselective catheterization

of the ophthalmic artery for intra-arterial chemotherapy is associated with significant retinal toxicity [27].

17.5 Retinal Toxicity by Drugs: Topical Administration

Topical administration is the most common way for ophthalmologic treatments. Even if the absorption by this route is limited by many barriers (the cornea, the conjunctiva and sclera and the nasolacrimal drainage of tears, aqueous humour, blood–aqueous barrier and blood–retinal barrier), different side effects have been reported also for topically administered drugs. Eye drops containing epinephrine, dipivefrin, latanoprost and timolol can induce CME in cases of aphakia and pseudophakia [28]. The onset of postoperative CME connected with the use of preoperative or postoperative latanoprost is particularly interesting. Latanoprost increases the disruption of blood–aqueous barrier and induces CME demonstrated with fluorescein angiography. Latanoprost is a prostaglandin (PG) analogue, and PG’s role in inducing CME is already known. Furthermore, mechanical stimulation during surgery may play a cumulative role in inducing the formation of CME. Unfortunately, the pathophysiology of this phenomenon is poorly understood.

17.6 Retinal Toxicity by Drugs: Intravitreal Administration

Intravitreal administration of drugs may cause clinically significant retinal toxicity in a limited number of cases. Intravitreal indocyanine green (ICG) dye is used in vitrectomy (chromovitrectomy) to stain preretinal structures, such as epiretinal membranes and internal limiting membranes. The staining of these structures facilitates their identification and peeling during vitrectomy. There are many concerns about the use of ICG, because of its potential toxicity. The main toxic effects are direct injury to ganglion cells, neuroretinal cells, RPE and superficial retinal

vessels. Moreover osmolarity changes at the vitreoretinal interface due to the ICG solution and light-induced injury must be considered. ICG toxicity seems to be dose dependent; thus, some recommendation can reduce retinal damage. In 2007 Rodrigues et al. proposed specific recommendations to minimize the toxic effects of ICG suggesting to use this dye at the lowest concentration and to practise the injection far from a macular hole, to prevent direct contact of the dye with the bare retina [29].

Intravitreal injection in the treatment of endophthalmitis may also cause retinal toxicity. Gentamicin has been proved since the 1980s to be toxic to the retina. Erroneous intravitreal gentamicin injections have been reported with catastrophic effects on the retina, including intraretinal haemorrhages, cotton-wool spots infarcts, retinal oedema, arteriolar narrowing and venous beading. In the new intravitreal therapy era, macular function is always more frequently documented by means of microperimetry, during treatments with intravitreal anti-VEGF or corticosteroids [30, 31]. This topic is described in detail in the chapters dedicated to AMD and diabetic retinopathy.

17.7 Retinal Toxicity by Other Substances: Systemic Administration

Few very rare cases have been reported in literature about retinal toxicity secondary to systemic elevated concentration of substances different from drugs. We have already mentioned the toxicity by the carotenoid canthaxanthin, used in tanning tablets. Methanol poisoning may be a cause of retinal and optic disc dysfunction. Hyperaemic, swollen optic discs and cystoid macular oedema have been reported in cases of acute intoxication. Automated field analysis usually reveals a generalized depression of retinal sensitivity and an enlargement of the blind spot or paracentral scotomas. Retinal and optic disc dysfunction is usually reversible in acute poisoning [32]. Another cause of retinal toxicity may be altered iron homeostasis. Retinal function is

affected by iron retention as proved in patients affected by hereditary iron homeostasis disorders, like aceruloplasminaemia or Friedreich's ataxia, where retinal degeneration is frequent. Recently Ng et al. reported a case of implant-related cobalt toxicity. In this case the patient underwent slit lamp examination, automated visual field testing, optical coherence tomography, fluorescein angiography and indocyanine green angiography. Optical coherence tomography and indocyanine green angiography were the only exams that revealed abnormalities: lesions at the level of retinal pigment epithelium and photoreceptors and hypofluorescence at the indocyanine green angiography [33]. Cobalt toxicity is rare, but the increasing use of cobalt in prostheses for joint replacement is creating new problems and challenges for systemic and organ's safety, including the eye.

17.8 Retinal Toxicity by Deficiency of Specific Substances

17.8.1 Vitamin A Deficiency

Vitamin A deficiency, defined by serum retinol concentration $<0.7 \mu\text{mol/L}$, can be an acquired condition. Malnutrition, Crohn's disease and other causes of malabsorption, bowel surgery, mutation to the plasma retinol binding protein and pregnancy are some examples. In bariatric surgery a significant postoperative complication is visual impairment [34]. The earliest symptom of vitamin A deficiency is night blindness, followed by peripheral and central visual field constriction, photophobia and reduced visual acuity. The revised WHO clinical classification of xerophthalmia includes night blindness, conjunctival xerosis, Bitot spots, corneal xerosis, corneal ulceration/keratomalacia, corneal scarring and xerophthalmia fundus. Photopic stress to the rods can exacerbate night blindness by up-regulating the rhodopsin turnover. The fundus is normal in early vitamin A deficiency, but later on may show multiple white or grey-white spots in the peripheral retina, which usually disappear

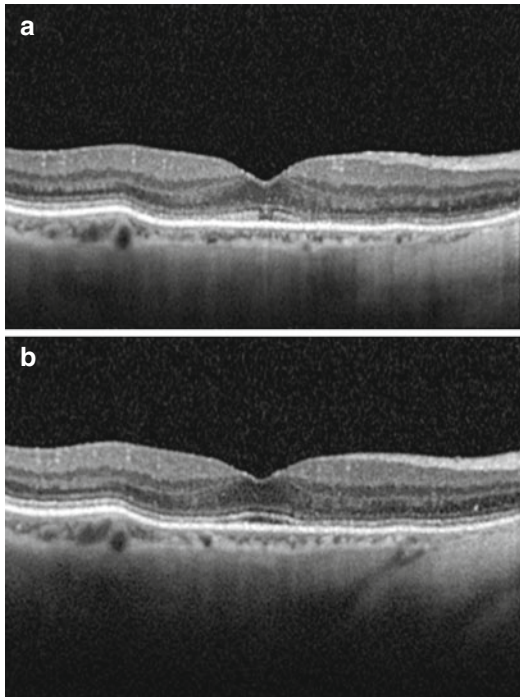


Fig. 17.1 A case of vitamin A deficiency after bariatric surgery. Spectral domain optical coherence tomography 180° scan showing disruption of IS–OS junction in foveal area (RE) (a). Spectral domain optical coherence tomography 180° scan after therapy (vitamin A supplementation) showing normalized IS–OS junction in foveal area (RE) (b)

with vitamin A supplementation. The treatment of vitamin A deficiency is straightforward by supplementing vitamin A. During vitamin A deficiency, spectral domain optical coherence tomography usually shows disruption of IS–OS junction in foveal area, and microperimetry documents reduced retinal sensitivity in the macular area (Figs. 17.1 and 17.2). After vitamin A supplementation, spectral domain optical coherence tomography may document normalized IS–OS junction in foveal area, and microperimetry often reveals improvement of retinal sensitivity (Figs. 17.1 and 17.2).

References

1. Hobbs HE, Sorsby A, Freedman A (1959) Retinopathy following chloroquine therapy. *Lancet* 2:478–480

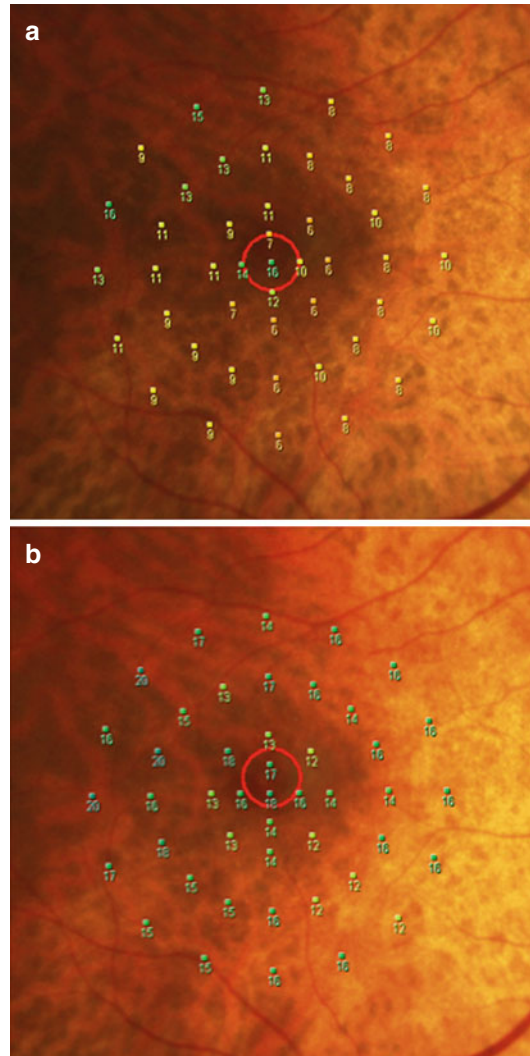


Fig. 17.2 The same case of 18.1. Pretreatment microperimetry of the 12 central degrees showing reduced retinal sensitivity (RE) (a). Microperimetry of the 12 central degrees after therapy showing improvement of retinal sensitivity (RE) (b)

2. Stelton CR, Connors DB, Walia SS et al (2013) Hydrochloroquine retinopathy: characteristic presentation with review of screening. *Clin Rheumatol* 32:895–898
3. Marmor MF, Kellner U, Lai TY et al (2011) Revised recommendation on screening for chloroquine and hydroxychloroquine retinopathy. *Ophthalmology* 118: 415–422
4. Marmor MF, Carr RE, Easterbrook M et al (2002) Recommendations on screening for chloroquine and hydroxychloroquine retinopathy: a report by the American Academy of Ophthalmology. *Ophthalmology* 109:1377–1382

5. Marmor MF (2012) Comparison of screening procedures in hydroxychloroquine toxicity. *Arch Ophthalmol* 130:461–469
6. Hart VM, Burde RM, Johnston GP et al (1984) Static perimetry in chloroquine retinopathy. Perifoveal patterns of visual field depression. *Arch Ophthalmol* 102:377–380
7. Kelmerson AT, Brar VS, Murthy RK et al (2010) Fundus autofluorescence and spectral domain optical coherence tomography in early detection of plaqueniil maculopathy. *Eur J Ophthalmol* 20:785–788
8. Angi M, Romano V, Valldeperas X et al (2010) Macular sensitivity changes for detection of chloroquine toxicity in asymptomatic patient. *Int Ophthalmol* 30:195–197
9. Banin E, Shalev RS, Obolensky A et al (2003) Retinal function abnormalities in patients treated with vigabatrin. *Arch Ophthalmol* 121:811–816
10. Nayfield SG, Gorin MB (1996) Tamoxifen-associated eye disease. A review. *J Clin Oncol* 14:1018–1026
11. Cronin BG, Lekich CK, Bourke RD (2005) Tamoxifen therapy conveys increased risk of developing a macular hole. *Int Ophthalmol* 26:101–105
12. Kaiser-Kupfer MI, Lippman ME (1978) Tamoxifen retinopathy. *Cancer Treat Rep* 62:315–320
13. Noureddin BN, Seoud M, Bashshur Z et al (1999) Ocular toxicity in low-dose tamoxifen: a prospective study. *Eye* 13:729–733
14. Heier JS, Dragoo RA, Enzenauer RW et al (1994) Screening for ocular toxicity in asymptomatic patients treated with tamoxifen. *Am J Ophthalmol* 117:772–775
15. Eisner A, Austin DF, Samples JR (2004) Short wavelength automated perimetry and tamoxifen use. *Br J Ophthalmol* 88:125–130
16. Watanabe SE, Berezovsky A, Motono M et al (2010) Retinal function in patients treated with tamoxifen. *Doc Ophthalmol* 120:137–143
17. Salomão SR, Watanabe SE, Berezovsky A et al (2007) Multifocal electroretinography, color discrimination and ocular toxicity in tamoxifen use. *Curr Eye Res* 32:345–352
18. Cortin P, Corriveau LA, Rousseau AP et al (1982) Maculopathy with golden particles. *Can J Ophthalmol* 17:103–106
19. Harnois C, Samson J, Malenfant M et al (1989) Canthaxanthin retinopathy. Anatomic and functional reversibility. *Arch Ophthalmol* 107:538–540
20. Hueber A, Rosentreter A, Severin M (2011) Canthaxanthin retinopathy: long-term observations. *Ophthalmic Res* 46:103–106
21. Millay RH, Klein ML, Illingsworth DR (1988) Niacin maculopathy. *Ophthalmology* 95:930–936
22. Gass JDM (1973) Nicotinic acid maculopathy. *Am J Ophthalmol* 76:500–510
23. Spinn MJ, Warren FA, Guyer DR et al (2003) Optical coherence tomography findings in nicotinic acid maculopathy. *Am J Ophthalmol* 135(6):913–914
24. Weekley RD, Potts AM, Reboton J et al (1960) Pigmentary retinopathy in patients receiving high doses of a new phenothiazine. *Arch Ophthalmol* 64:65–76
25. Borodoker N, Del Priore LV, De A, Carvalho C et al (2002) Retinopathy as a result of long-term use of thioridazine. *Arch Ophthalmol* 120:994–995
26. Chantada GL, Fandino AC, Carcaboso AM et al (2009) A phase I study of periocular topotecan in children with intraocular retinoblastoma. *Invest Ophthalmol Vis Sci* 50:1492–1496
27. Steinle JJ, Zhang Q, Thompson KE et al (2012) Intra-ocular artery chemotherapy triggers vascular toxicity through endothelial cell inflammation and leukostasis. *Invest Ophthalmol Vis Sci* 53:2439–2445
28. Miyake K, Ibaraki N (2002) Prostaglandins and cystoid macular edema. *Surv Ophthalmol* 47(Suppl 1): S203–S218
29. Rodrigues EB, Meyer CH, Mennel S et al (2007) Mechanisms of intravitreal toxicity of indocyanine green dye: implications for chromovitrectomy. *Retina* 27:958–970
30. Kriechbaum K, Prager F, Geitzenauer W et al (2009) Association of retinal sensitivity and morphology during antiangiogenic treatment of retinal vein occlusion over one year. *Ophthalmology* 116:2415–2421
31. Mylonas G, Sacu S, Dunavoelgyi R et al (2013) Response of retinal sensitivity to ranibizumab treatment of macular edema after acute branch retinal vein occlusion. *Retina* 33:1220–1226
32. Koehrer P, Creuzot-Garcher C, Bron AM (2011) Methanol poisoning: two case studies of blindness in Indonesia. *Int Ophthalmol* 31:517–524
33. Ng SK, Ebnetter A, Gilhotra JS (2013) Hip-implant related chorio-retinal cobalt toxicity. *Indian J Ophthalmol* 61:35–37
34. Petzold A, Plant GT (2006) Clinical disorders affecting mesopic vision. *Ophthalmic Physiol Opt* 26:326–341

Michele Iester

18.1 Introduction

Glaucoma is the second commonest cause of blindness in the West and the commonest cause of blindness worldwide [1]. Early detection of glaucoma forms the basis of effective management. If the disease is detected in its early stages, damage can be minimised and the long-term prognosis for the patient improved. Thus, early detection and prevention of retinal nerve fibre layer (RNFL) glaucomatous damage is mandatory, because injury to the RNFL is largely irreversible [2, 3]. The diagnosis of glaucoma is based on the appearance of the optic nerve head (ONH) and standard achromatic automated perimetry, but damage to the RNFL has been shown to precede visual field loss [1–4]. It has been shown that 30–50 % of retinal ganglion cells may be lost before an abnormality appears on standard automated perimetry [4, 5]. Therefore, morphological and functional evaluation of RNFL is essential in detecting and monitoring glaucoma [6, 7].

ONH and RNFL morphometry is carried out using different approaches, mainly optical coherence tomography [7–11].

Historically, clinical evaluation of patients suspected of having glaucoma has relied on the detection of visual field damage by automated perimetry and the detection of optic nerve damage by subjective retinal examination. Visual field analysis can detect visual field loss with high sensitivity and specificity in patients with moderate to advanced optic nerve damage, but it is less useful for the detection of early damage. Subjective examination of the optic nerve and retinal nerve fibre layer can detect this early damage, but it is limited because of the need for expert evaluation of the optic nerve appearance and the low level of agreement between observers for subjective evaluation of the optic disc.

These limitations have driven the development of digital imaging technologies such as digital fundus photography and scanning laser ophthalmoscopy (SLO) that can provide objective evidence of early optic nerve damage [12–14]. Both these techniques provide high-quality images of the ONH and, in the case of scanning laser ophthalmoscopy, detailed information on the surface topography of the retina. Statistical analysis of these images has been shown to detect early glaucomatous damage with high sensitivity and specificity—in many cases before the development of significant visual field damage [12, 14].

M. Iester, MD, PhD
Laboratorio clinico anatomico-funzionale
per la diagnosi e il trattamento del glaucoma
e della malattie neurooftalmologiche,
Clinica Oculistica, DiNOGMI,
University Eye Clinic of Genoa,
Viale Benedetto XV, 5, Genoa 16132, Italy
e-mail: iester@unige.it

18.2 Imaging in Glaucoma

Although clinical examination still remains the most important method of assessing the ONH for glaucomatous damage, three main ONH/RNFL imaging systems have been studied and used for many years suggesting a good reproducibility and diagnostic precision. None has a 100 % diagnostic capacity to distinguish glaucomatous from normal ONHs; however, the utilities of these systems are to detect glaucomatous changes at baseline and during follow-up [15].

Since glaucoma is a progressive disease, a patient with glaucoma will have ONH/RNFL changes, and hence imaging systems should be able to identify and quantify those changes. The idea to compare an ONH to itself and not to a database in the follow-up seems to be a winning idea. Actually there are four different types of devices:

1. The Heidelberg Retina Tomograph III (Heidelberg Engineering, Germany) is a confocal laser-scanning microscope for the acquisition and analysis of three-dimensional images of the posterior segment of the eye. The major clinical applications of the instrument are the quantitative analysis of the optic nerve head structure in glaucoma. In a confocal laser-scanning system, a focused laser beam scans the retina sequentially, and the amount of light reflected from each scanned point is measured. The acquired image is an optical section through the three-dimensional object at the location of the focal plane. The Moorfields regression analysis, the discriminant formulas and the glaucoma probability score are the main formulas used to distinguish a healthy optic disc from a glaucomatous optic disc.
2. The RNFL exhibits substantial linear birefringence with its slow axis parallel to the direction of nerve fibre bundles. This unique property of the RNFL provides a basis for scanning laser polarimetry (SLP) to assess the RNFL thickness by measuring total retardation in the light reflected from the retina. The current SLP system, the GDx (Zeiss, Germany), is a confocal scanning laser

ophthalmoscope integrated with a polarimeter. Images of the ocular fundus are formed by scanning the beam of a near-infrared laser in a raster pattern. In the GDx VCC, a variable corneal compensator (VCC) is employed to neutralise the anterior segment birefringence which is a confounding factor in SLP RNFL assessments. The new version of the GDx, the GDx ECC (enhance corneal compensator), is able to better analyse the peripapillary area in those patients in whom there was an atypical scan of the peripapillary area.

3. Time Domain Optical Coherence Tomography (TD-OCT) is a laser-based imaging system designed to acquire high-resolution cross-sectional retinal images (5–10 μm). The technique is analogous to ultrasonography, but the tomographic OCT image is an intensity map of light backscattered or reflected from tissue structures. The very high depth resolution is based on a low-coherence light source and interferometry. Differentiation of retinal layers at a near-histological level is possible due to a very high depth resolution and because different tissue structures reflect light with different intensities. The major clinical application of OCT at present is the qualitative and quantitative analyses of retinal pathologies, but the RNFL thickness analysis is of great potential in the glaucoma clinic.
4. Spectral Domain OCT (SD-OCT) has some new detection concepts which have led to an improved light detection efficiency by more than 2 orders of magnitude. This significant advance in OCT technology has enabled video rate imaging of retinal structures at a resolution 1.5–3 times (3–5 μm) better than commercially available instruments, without loss to image quality. The new SD-OCT has enabled three-dimensional imaging of retinal morphology and has made ultra-high-resolution imaging at video rate feasible, visualising even very small blood vessels in the retina. High-speed imaging greatly reduces motion artefacts and allows measurement of true topography and cupping of the optic nerve head. The possibility to measure three-dimensional reconstructions of the retinal

morphology recorded at different time points holds great promise for the detection of retinal changes in longitudinal follow-up of patients.

In spite of these successes, up to 10 % continue to be misclassified, even with optimised statistical algorithms. Since glaucoma affects up to 2 % of the population (and up to 4 % of those over 75 years of age), these errors can generate large numbers of patients with incorrect or late diagnoses. It is important that these techniques are developed to achieve further improvements in diagnostic precision. Preliminary works have shown that when the two diagnostic techniques are used in combination, the sensitivity and specificity for the detection of early damage is further improved to achieve useful clinical reductions in the number of inaccurate diagnoses [16].

18.3 How to Improve Imaging

Form here the two possibilities: one is to add more imaging devices and the other is to add imaging to function results. Since optic disc photographs and scanning laser tomographic analysis provide complimentary data on the appearance of the ONH some researchers have developed techniques for the combination of these images that should further improve the diagnostic precision of optic disc analysis.

The use of these modalities is new. Current techniques for retinal image registration use more similar modalities, e.g., angiograms that involve 2D image data, or registering the same modality over time. The principle of this method is that the images are combined to allow better demarcation of the boundary of the optic disc for topographic analysis of the retinal surface contour and to enable better correlation of topographic and visible optic nerve head damage [15–19].

Recently a new index combining information from structural and functional damage in glaucoma was proposed by Mendeiros et al. [20]. This index can be used to stage and provide diagnostic information on the disease. The index performed significantly better than isolated measures of structure and function for diagnosing preperimetric and perimetric glaucoma [20].

18.4 Unconventional Perimetry

However, many different functional tests (short-wavelength automated perimetry, frequency-doubling technology perimetry) have also been proposed with controversial results to try to improve the glaucoma diagnostic capacity [21, 22]. Microperimetry is a functional test that quantifies differential light threshold (DLT) at selected areas, chosen by the examiner, under real-time fundus control [23, 24]. Microperimetry data are independent of eye movements and exactly related to the stimulated areas [25].

18.5 Microperimetry

The term microperimetry was first used in the peer-reviewed scientific literature by Jean et al. in 1990 when describing a scanning laser ophthalmoscope technique [26]. However, the term microperimetry is slightly misleading: the size of the target is the same as in conventional perimetry, and the extent of the visual field measured can be similar in size to a conventional perimeter. Some authors use the term fundus perimetry or fundus-related perimetry instead, which is probably a more descriptive term.

Microperimetry assesses the visual function of a specific area of the retina and fovea and correlates to function results. The user tests the visual sensitivity in a small area which is visible on the screen of the microperimetry. In this way the user could test always the same points.

Some years ago, microperimetry was performed by scanning laser ophthalmoscope (SLO) which provided functional results by direct visualisation of the macular area. SLO microperimetry permitted an exact, point-to-point correspondence between fundus image and perimetric results, impossible to achieve by projection perimetry, so representing the most suitable device for simultaneous fundus imaging and psychophysical testing.

The first commercially available device for fundus-specific perimetry described in the literature was the SLO-101 (Rodentstock GmbH, Munich, Germany), which permits other

applications. SLO microperimetry allowed the real-time functional study of retinal sensitivity by direct ophthalmoscopic control of the retinal surface. Foveal or excentric fixation could be assessed as well. Instability of fixation during computerised perimetry was a possible misleading factor resulting in unexplainable findings, especially in the eyes with decreased visual acuity. The main characteristic of microperimetry was the ability to see the stimuli presented on the retina in real time: this permitted an accurate monitoring of fixation and correlation of anatomical or pathological features directly with retinal function.

The first next-generation microperimeter was the MP-1 microperimeter, launched in 2002 by Nidek Technologies (Nidek Technologies, Italy). It was determined that a value of 0 dB on the MP-1 is equivalent to 14 dB on the Humphrey and that 0 dB on the MP-1 is equivalent to 34 dB on the Humphrey Field Analyser. The stimulus is relatively dim: maximum target luminance is approximately 130 cd/m².

The OCT-SLO (OPKO, Miami, FL, USA) is a device that combines a spectral optical coherence tomographer (OCT) with a scanning laser ophthalmoscope-based microperimeter. Since the optical pathways of the two imaging modes are coherent, the machine allows precise registration of the SLO fundus image with the OCT structural image. The dynamic range of stimulus presentation is also 2 log units. The nominal intensities of the OCT-SLO perimetry stimuli are 0–20 dB, which is roughly equivalent to 14–34 dB on the Humphrey Field Analyser. The connection between OCT and microperimetry seemed to significantly improve the productivity and enhances diagnosis of retinal diseases and glaucoma and can also correlate to HRT results. In this way, microperimetry monitors retinal visual function against retinal thickness or structure and the condition of the patient's fixation over time. Microperimetry provided a retinal visual function map on a selected, localised fundus location with preset or customised scan patterns. The OCT retinal topography map provides retinal structure details, thickness and a volume map at the same location on the retina; furthermore, the

SLO fundus image used in microperimetry and OCT topographic map to ensure the alignment of the microperimetry with the 3D topography could permit a better analysis of the relationship between changes in retinal structure and function in specific locations on the retina.

Although standard automated perimetry (SAP) is able to show the functioning of individual retinal locations in the macula, reliable test results can be difficult to obtain because of unstable fixation in some cases. A new SLO-MP device (MAIA, CenterVue, Italy) has an electronic eye tracking system for automatic correction of stimulus position as a function of eye movements, and this allows precise automatic follow-up examinations irrespective of baseline fixation. The lack of age-corrected normal threshold values and indices for glaucoma diagnosis and follow-up, however, limits its widespread use at the present time. When using an auto-tracking system, MAIA (Macular Integrity Assessment; CenterVue, Padova, Italy) is able to automatically record the fixation behaviour during the test while the auto-tracking system makes it possible to adjust the stimulus points to predefined retinal positions and perform reliable field testing, even in eyes with unstable fixation. This microperimeter uses a scanning laser to perform retinal imaging and an LED light as a stimulus. As with the OCT/SLO perimeter, the retinal image quality is very high and pupil dilation is rarely required.

Although the usefulness of macular evaluation using microperimetry in retinal diseases, such as age-related macular degeneration, macular dystrophies and diabetic macular oedema has been demonstrated, there is little information regarding its applicability in glaucoma patients. Since the first version of the SLO-MP device used in the previous studies had limitations, such as lack of real-time fundus tracking and narrow field of examination, it was not widely adopted [27].

In the past, relationships between RNFL losses and VF defects have been studied using different theoretical curves to fit the data [28–32]. Results have shown that a complete loss in sensitivity does not result in an RNFL thickness of zero but, instead, is actually associated with a finite RNFL thickness. In the early stage of glaucoma,

the decline in RNFL thickness is rapid, and there is a lag in the visual sensitivity loss. However, as the glaucoma becomes severe, RNFL thicknesses reach a base level beyond which only the visual sensitivity declines. The relationship between structure and function has been shown and is still under evaluation. Garway-Heath et al. and Lemij et al. tried to find a stronger correlation between function and structure [31–33]. The strength of fundus perimetry is to analyse the retinal function in the same retinal area, and this could improve the structure–function relationship. Furthermore, the tested areas are smaller than in standard. Thus, the determination of which region has a stronger structure–function association has clinical implications, as use of the stronger region could provide better detection and follow-up in glaucoma patients who might present with an early stage of macular visual field defects.

18.6 Microperimetry in Glaucoma

Orzalesi et al., Miglior and Rohrschneider et al. previously pointed to the importance of SLO microperimetry (peripapillary and extrapapillary) in glaucomatous eyes to detect early loss of retinal sensitivity [34–36]. In particular, in a study evaluating primary open-angle glaucoma patients with localised RNFL defects, Orzalesi et al. found a good correlation between microperimetry with SLO using a 40° field of view and SAP of the central 30° [34]. Rohrschneider suggested that analysing peripapillary DLT might show morphological changes that precede typical visual field defects [36]. Okada et al. showed that SLO fundus perimetry might be an alternative method of evaluating advanced glaucoma [37].

Unfortunately, the data about microperimetry in glaucomatous eyes were never replicated because the SLO microperimetry technique limited further studies [25]. Microperimetry was developed as a functional clinical application of scanning laser ophthalmoscope [38–41]. Recently, a reliable and simple automatic fundus perimeter was introduced in clinical practice [23, 24]. The MP1 microperimeter and Humphrey perimeter use noncomparable protocols, mainly because

of different background intensity (4 vs 31.5 asb, respectively) and control of stimulus projection. This control is fully reliable in fundus perimetry, where an active eye tracking is used.

A more recent study using a different device, liquid crystal display microperimetry, demonstrated that microperimetry correlated with SAP in detecting glaucomatous visual field defects in the macular area of patients with primary open-angle glaucoma. Finally, microperimetry in eyes with advanced glaucomatous damage (central island of vision) correlated with Goldmann perimetry results and could be useful in detecting retinal sensitivity in the remaining areas of RNFL [42].

Lima et al. found that in glaucomatous eyes with paracentral visual field defects, SLO-MP results not only correlated significantly with those from SAP in all quadrants analysed but also detected abnormal areas of retinal sensitivity in quadrants with normal SAP values [27]. Furthermore, good correlations between SLO-MP and SAP have been shown in some previous studies comparing these two modalities [34, 37, 42]. SLO-MP could detect more subtle glaucoma functional damage than SAP, and those findings were consistent with macular structural injury as determined by OCT. In most cases, a corresponding area of macular thickness reduction was present on OCT, suggesting that microperimetry could be more sensitive than standard achromatic perimetry to detect paracentral visual field loss in glaucoma patients.

Convento et al. confirmed the progressive and specific reduction in thickness of peripapillary RNFL with progressive glaucomatous damage (normal vs ocular hypertensive vs OHT vs glaucoma) documented by peripapillary OCT [43–45]. Their data also documented the loss of peripapillary DLT quantified with peripapillary fundus perimetry in the same eyes. Furthermore, using both techniques, in all peripapillary-examined sectors, glaucomatous eyes showed significantly ($p < 0.05$) lower morphological and functional values. Peripapillary microperimetry data showed that the differences between normal and ocular hypertensive eyes were significant ($p < 0.05$) in sectors 1 (superior region), 7 (inferior

region) and 12 (superotemporal region). A better ability of microperimetry to discriminate ocular hypertensive eyes from normal eyes in retinal sectors 1, 7 and 12 was confirmed by higher values of AROC data. Microperimetry documents glaucomatous damage beginning over the inferior and superior arcuate fibres, where OCT shows a thinning of the RNFL.

In particular, peripapillary microperimetry could be able to detect and topographically document early functional RNFL glaucomatous changes through exact quantification of peripapillary DLT. Analysing the AROC of fundus perimetry and OCT of the superior and inferior arcuate fibres, Convento et al. showed that in ocular hypertensive eyes, the function of the eyes is more altered than morphology, even if the morphological change seemed more diffuse (more sectors affected). Average AROC values were slightly better for OCT versus fundus perimetry.

Furthermore, in glaucomatous eyes, microperimetry data were more sensitive than OCT in identifying changes in the RNFL of sensitivity to specificity ratio. AROC values of microperimetry in the superior and inferior peripapillary retinal areas are higher than those of OCT.

By using this technology, Ozturk et al. showed that perimetric macular changes could occur while macular topographic remains stable in patients with glaucoma [42]. In this study MP-1 correlated to Humphrey Field Analyser in detecting glaucomatous visual field defect in macular area. Furthermore, Shi et al. found that in glaucomatous patients, fixation instability manifested in early and moderate primary open-angle glaucoma eyes, which might be an early sign of primary open-angle glaucoma [46]. Different results were obtained by Klamann et al. which found that blue/yellow perimetry and MP-1 had no ability to discriminate between subjects with early glaucoma and healthy subjects, while RNFL thickness measured with HRT III and OCT showed a significant difference [47]. In early primary open-angle glaucoma, morphological changes like RNFL thickness seemed to occur prior to functional defects in the visual field.

The strength of the structure-function relationship is related to the individual anatomy and

its variation in the subject, the stage of glaucoma present in the study sample, the visual field scale and the regression model used. During the previous examinations of the correlations between the visual field sensitivity and the early glaucomatous stages, healthy individuals and the glaucoma-suspect eyes, the correlations were shown to be weaker than those observed in moderate-to-severe glaucoma [48, 49]. The reason for this is because the range of visual field is narrow in healthy and glaucoma-suspect eyes. Thus, the strength of a structure-function relationship may be dependent upon both the actual retinal and visual field areas in which the association is assessed and the specific imaging device that is used in the study. In addition, histological studies in human and monkey eyes have shown that in the central retina, there are more ganglion cells in the nasal and superior sectors than in the temporal and inferior sectors, respectively [50, 51]. These differences in the distribution of the ganglion cells might affect the strength of the structure-function relationship.

Sato et al. found that macular visual field sensitivity (dB) and ganglion cell layer plus inner plexiform layer (GCA) thickness relationships were statistically significant in each sector ($r=0.365-0.706$, all $p<0.001$) [52]. The highest correlation observed was between the inferotemporal average mean sensitivity and the inferotemporal average GCA thickness ($r=0.706$) with both visual field and OCT in retinal view. Strength of the structure-function relationship for each of the corresponding inferior sectors was higher than those for the corresponding superior sectors. The strength of the structure-function relationship of the temporal sector was higher than that of the nasal sector. Raza et al. recently reported finding that the local GCA thickness correlated well with the local sensitivity loss obtained with the 10–2 SAP setting in the central 7.2° of the 14 patients with glaucoma and in the 19 normal subjects [53]. The difference between the two studies was that the strength of the correlation between the mean sensitivity and the GCA thickness varied within the macular region. In addition, the former study measured

the visual field sensitivity with microperimetry in an attempt to improve the spatial localisation.

Although the GCA thickness measured by Cirrus HD-OCT (Zeiss, Germany) was significantly correlated with the macular retinal sensitivity assessed by MAIA, the strength of the correlation varied from region to region. Combining GCA thickness with macular visual field sensitivity might provide a better understanding of the amount of glaucomatous damage that occurs in the macula region (Figs. 18.1 and 18.2).

18.7 Microperimetry and Peripapillary Atrophy

Interesting results have been shown by Rensch and Jonas, when they tested the beta and alpha peripapillary area [54]. They found an absolute scotoma in the beta zone of parapapillary atrophy, while in the alpha zone, the mean stimulus attenuation values were 6.29 ± 4.82 dB, corresponding to a relative scotoma. The difference in the stimulus attenuation between alpha zone and beta zone was statistically significant ($p=0.028$). The present study was in agreement with a previous

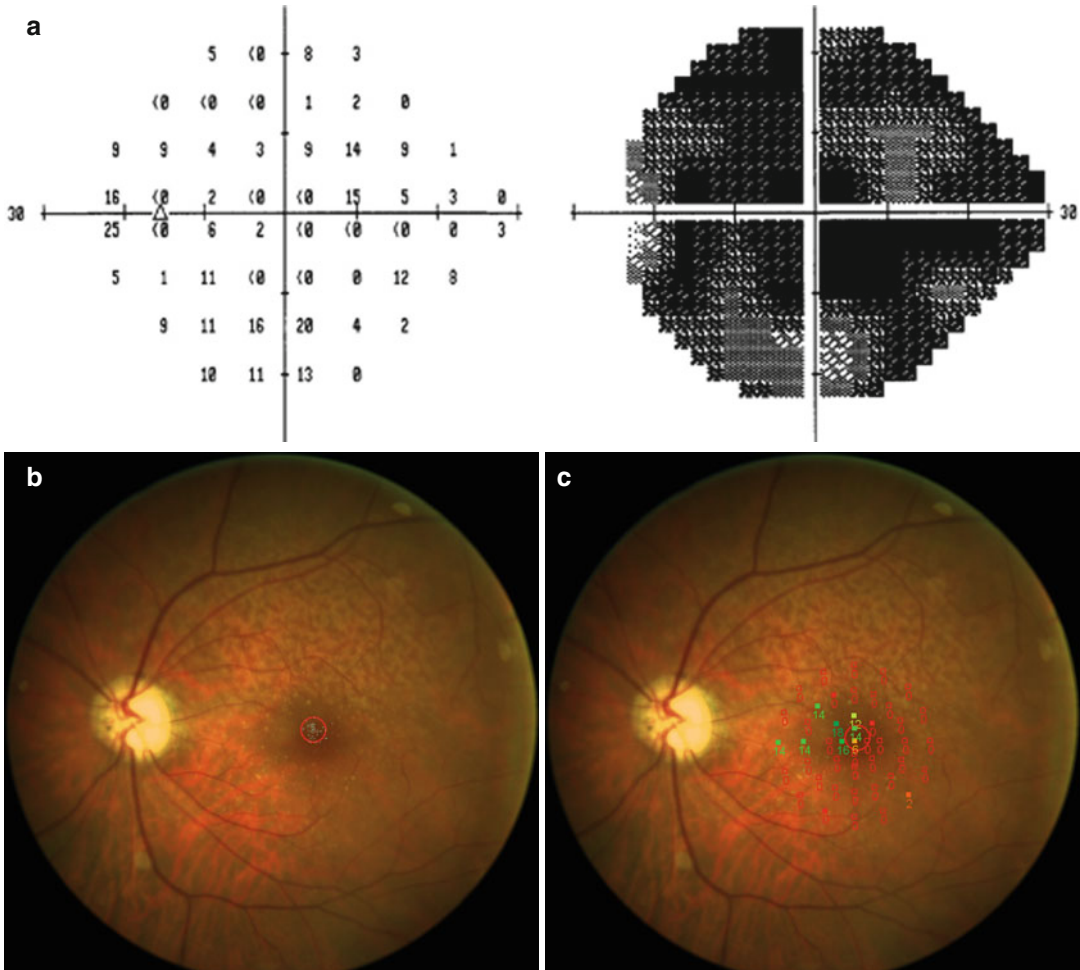


Fig. 18.1 End stage glaucoma. (a) Achromatic perimetry shows diffuse fully scotomatous areas. (b) Microperimetry fixation map (the area of fixation is represented by

the light blue points): fixation is central and stable. (c) Microperimetry sensitivity map (in dB) shows large areas of central full scotoma (red empty squares)

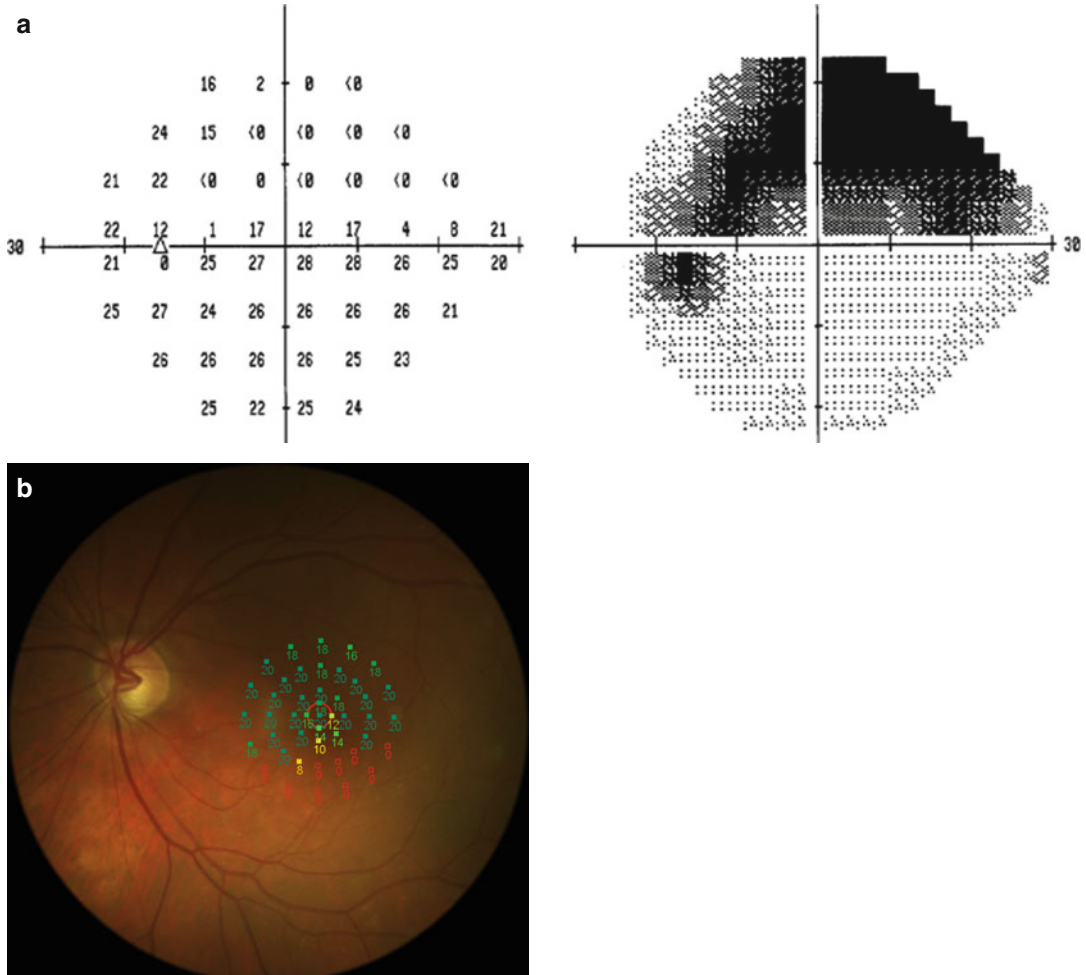


Fig. 18.2 Patients with a superior arcuate absolute scotoma. (a) Achromatic perimetry shows a large fascicular defect. (b) Microperimetry map (in dB) shows that the macular map clearly identifies the full scotomatous area (red empty squares)

investigation in which kinetic Goldmann perimetry was used to measure the psychophysical equivalent of the parapapillary atrophy [55]. These data agree with the histological findings in which beta zone is an area with a complete loss of retinal pigment epithelium cells and photoreceptors (absolute scotoma), while in the alpha zone, there are structural irregularities of the retinal pigment epithelium (relative scotoma).

As in the present study using the more precise direct microperimetry, the previous investigation with kinetic Goldmann perimetry revealed a relative scotoma for alpha zone and an absolute scotoma for beta zone in conjunction with the blind spot of the optic disc itself. Since the former study could not differentiate between the absolute

scotoma representing the optic disc itself and the absolute scotoma in relation to beta zone, our study extends the former observation that beta zone was indeed an absolute scotoma independent of the absolute scotoma caused by the optic disc itself. The present study was also in agreement with another investigation in which scanning laser ophthalmoscopy was applied to assess the differential light threshold in the parapapillary region [56].

Conclusion

Microperimetry, a fundus-related examination, could be a more reliable way to perform visual field assessment because the same area is tested and retested with great precision, even if it is always a psychophysical

test which, in part, depends on the patient. This technique could be useful to assess the visual sensitivity of a chosen area and the data could be easily integrated to structure data. Whereas OCT measurement of RNFL thickness was currently used for the detection of early RNFL morphological damage in ocular hypertensive and glaucomatous eyes, topographically related functional information from the same areas might be useful, particularly in eyes without standard visual field loss. Microperimetry, therefore, might represent a complement to OCT (and standard automated perimetry) for the detection of early stages of glaucoma. In this way new structure-function indices could be introduced in the future. Furthermore, it could be of particular benefit in assessing glaucoma in patients with central field loss, with very poor fixation or in case of unreliable conventional visual fields.

References

- Sommer A (1996) Doyné lecture. Glaucoma: facts and fancies. *Eye* 10:295–301
- Quigley HA, Katz J, Derick RJ et al (1992) An evaluation of optic disc and nerve fiber layer examinations in monitoring progression of early glaucoma damage. *Ophthalmology* 99:19–28
- Quigley HA, Dunkelberger GR, Green WR (1989) Retinal ganglion cell atrophy correlated with automated perimetry in human eyes with glaucoma. *Am J Ophthalmol* 107:453–464
- Quigley HA, Addicks EM, Green WR (1982) Optic nerve damage in human glaucoma. III: quantitative correlation of nerve fiber loss and visual field defect in glaucoma, ischemic neuropathy, papilledema, and toxic neuropathy. *Arch Ophthalmol* 100:135–146
- Mikelberg FS, Yidegiligne HM, Shulzer M (1995) Optic nerve axon count and axon diameter in patients with ocular hypertension and normal visual fields. *Ophthalmology* 102:342–348
- Reus NJ, Lemij HG (2004) Diagnostic accuracy of the GDx VCC for glaucoma. *Ophthalmology* 111:1860–1865
- Medeiros FA, Zangwill LM, Bowd C et al (2005) Evaluation of retinal nerve fiber layer, optic nerve head and macular thickness measurements for glaucoma detection using optical coherence tomography. *Am J Ophthalmol* 139:44–55
- Iester M, Mermoud A (2005) Retinal nerve fiber layer measured by Heidelberg retina tomograph and nerve fiber analyzer. *Eur J Ophthalmol* 15:246–254
- Bagga H, Greenfield DS, Feuer W et al (2003) Scanning laser polarimetry with variable corneal compensation and optical coherence tomography in normal and glaucomatous eyes. *Am J Ophthalmol* 13:5521–5529
- Medeiros FA, Zangwill LM, Bowd C et al (2004) Comparison of the GDx VCC scanning laser polarimeter, HRT II confocal scanning laser ophthalmoscope, and stratus OCT optical coherence tomograph for the detection of glaucoma. *Arch Ophthalmol* 122:827–837
- Miglior S, Guareschi M, Romanazzi F et al (2005) The impact of definition of primary open-angle glaucoma on the cross-sectional assessment of diagnostic validity of Heidelberg retinal tomography. *Am J Ophthalmol* 139:878–887
- Mardin CY, Horn FK, Jonas JB et al (1999) Preperimetric glaucoma diagnosis by confocal scanning laser tomography of the optic disc. *Br J Ophthalmol* 83:299–304
- Azuara-Blanco A, Spaeth GL, Lanzl J et al (1999) Comparison between laser scanning tomography and computerised image analysis of the optic disc. *Br J Ophthalmol* 83:295–298
- Iester M, Mikelberg FS, Drance SM (1997) The effect of optic disc size on diagnostic precision with the Heidelberg retina tomograph. *Ophthalmology* 104:545–548
- Iester M, Garway-Heath D, Lemij H (2005) Optic nerve head and retinal nerve fibre analysis. Dogma, Savona
- Morgan JE, Sheen NJ, North RV et al (2005) Discrimination of glaucomatous optic neuropathy by digital stereoscopic analysis. *Ophthalmology* 112:855–862
- Rolando M, Macrì A, Iester M (1999) Optic disc surface smoothness and visual field. *Graefes Arch Clin Exp Ophthalmol* 237:372–376
- Iester M, De Ferrari R, Zanini M (1999) Topographic analysis to discriminate glaucomatous from normal optic nerve heads with a confocal scanning laser: new optic disk analysis without any observer input. *Surv Ophthalmol* 44:s33–s40
- Reis AS, O'Leary N, Yang H et al (2012) Influence of clinically invisible, but optical coherence tomography detected, optic disc margin anatomy on neuroretinal rim evaluation. *Invest Ophthalmol Vis Sci* 18:1852–1860
- Medeiros FA, Lisboa R, Weinreb RN et al (2012) A combined index of structure and function for staging glaucomatous damage. *Arch Ophthalmol* 130:1107–1116
- Boden C, Pascual J, Medeiros FA et al (2005) Relationship of SITA and full-threshold standard perimetry to frequency-doubling technology perimetry in glaucoma. *Invest Ophthalmol Vis Sci* 46:2433–2439
- Demirel S, Johnson CA (2001) Incidence and prevalence of short wavelength automated perimetry deficits in ocular hypertensive patients. *Am J Ophthalmol* 131:709–715

23. Midena E, Radin PP, Pilotto E et al (2004) Fixation pattern and macular sensitivity in eyes with subfoveal choroidal neovascularization secondary to age-related macular degeneration: a microperimetry study. *Semin Ophthalmol* 19:55–61
24. Rohrschneider K, Springer C, Bultmann S et al (2005) Microperimetry: comparison between the microperimeter 1 and scanning laser ophthalmoscope fundus perimetry. *Am J Ophthalmol* 139:125–134
25. Sunness JS, Schuchard RA, Shen N et al (1995) Landmark-driven fundus perimetry using the scanning laser ophthalmoscope. *Invest Ophthalmol Vis Sci* 36:1863–1874
26. Jean B, Frohn A, Thiel HJ (1990) Laser scanning in ophthalmology. *Fortschr Ophthalmol* 87:158–167
27. Lima VC, Prata TS, De Moraes CGV et al (2010) A comparison between microperimetry and standard achromatic perimetry of the central visual field in eyes with glaucomatous paracentral visual-field defects. *Br J Ophthalmol* 94:64–67
28. Hood DC, Anderson SC, Wall M et al (2007) Structure versus function in glaucoma: an application of a linear model. *Invest Ophthalmol Vis Sci* 48:3662–3668
29. Hood DC, Kardon RH (2007) A framework for comparing structural and functional measures of glaucomatous damage. *Prog Retin Eye Res* 26:688–710
30. Horn FK, Mardin CY, Laemmer R et al (2009) Correlation between local glaucomatous visual field defects and loss of nerve fiber layer thickness measured with polarimetry and spectral domain OCT. *Invest Ophthalmol Vis Sci* 50:1971–1977
31. Garway-Heath DF, Caprioli J, Fitzke FW et al (2000) Scaling the hill of vision: the physiological relationship between light sensitivity and ganglion cell numbers. *Invest Ophthalmol Vis Sci* 41:1774–1782
32. Garway-Heath DF, Holder GE, Fitzke FW et al (2002) Relationship between electrophysiological, psychophysical, and anatomical measurements in glaucoma. *Invest Ophthalmol Vis Sci* 43:2213–2220
33. Reus NJ, Lemij HG (2005) Relationships between standard automated perimetry, HRT confocal scanning laser ophthalmoscopy, and GDx VCC scanning laser polarimetry. *Invest Ophthalmol Vis Sci* 46:4182–4188
34. Orzalesi N, Miglior S, Lonati C et al (1998) Microperimetry of localized retinal nerve fiber layer defects. *Vision Res* 38:763–771
35. Miglior S (2002) Microperimetry and glaucoma. *Acta Ophthalmol Scand Suppl* 23:619
36. Rohrschneider K, Glück R, Kruse FE et al (1998/1999) Automatic static fundus perimetry for precise detection of early glaucomatous function loss. *Perimetry Update* 453–462
37. Okada K, Watanabe W, Koike I et al (2003) Alternative method of evaluating visual field deterioration in very advanced glaucomatous eye by microperimetry. *Jpn J Ophthalmol* 47:178–181
38. Mainster MA, Timberlake GT, Webb RH et al (1982) Scanning laser ophthalmoscopy. Clinical applications. *Ophthalmology* 89:852–857
39. Timberlake GT, Van de Velde FJ, Jalkh AE (1989) Clinical use of scanning laser ophthalmoscope retinal function maps in macular disease. *Laser Light Ophthalmol* 2:211–222
40. Tezel TH, Del Priore LV, Flowers BE et al (1996) Correlation between scanning laser ophthalmoscope microperimetry and anatomic abnormalities in patients with subfoveal neovascularization. *Ophthalmology* 103:1829–1836
41. Rohrschneider K, Fendrich T, Becker M et al (1995) Static fundus perimetry using the scanning laser ophthalmoscope with an automated threshold strategy. *Graefes Arch Clin Exp Ophthalmol* 233:743–749
42. Oztürk F, Yavas GF, Küsbeci T et al (2008) A comparison among Humphrey field analyzer, Microperimetry, and Heidelberg Retina Tomograph in the evaluation of macula in primary open angle glaucoma. *J Glaucoma* 17:118–121
43. Convento E, Midena E, Dorigo MT et al (2006) Peripapillary fundus perimetry in eyes with glaucoma. *Br J Ophthalmol* 90:1398–1403
44. Leung CK, Chan WM, Yung WH et al (2005) Comparison of macular and peripapillary measurements for the detection of glaucoma: an optical coherence tomography study. *Ophthalmology* 112:391–400
45. Jaffe GJ, Caprioli J (2004) Optical coherence tomography to detect and manage retinal disease and glaucoma. *Am J Ophthalmol* 137:156–169
46. Shi Y, Liu M, Wang X et al (2013) Fixation behavior in primary open angle glaucoma at early and moderate stage assessed by the MicroPerimeter MP-1. *J Glaucoma* 22:169–173
47. Klamann MKJ, Grünert A, Maier A-KB et al (2013) Comparison of functional and morphological diagnostics in glaucoma patients and healthy subjects. *Ophthalmic Res* 49:192–198
48. Miglior S, Riva I, Guareschi M et al (2007) Retinal sensitivity and retinal nerve fiber layer thickness measured by optical coherence tomography in glaucoma. *Am J Ophthalmol* 144:733–740
49. Ajtony C, Balla Z, Somoskeoy S et al (2007) Relationship between visual field sensitivity and retinal nerve fiber thickness as measured by optical coherence tomography. *Invest Ophthalmol Vis Sci* 48:258–263
50. Curcio CA, Allen KA (1990) Topography of ganglion cells in human retina. *J Comp Neurol* 300:5–25
51. Curcio CA, Messinger JD, Sloan KR et al (2011) Human chorioretinal layer thickness measured using macula-wide high resolution histological sections. *Invest Ophthalmol Vis Sci* 52:3943–3954
52. Shino S, Kazuyuki H, Tetsuya B et al (2013) Correlation between the ganglion cell-inner plexiform layer thickness measured with cirrus HD-OCT and macular visual field sensitivity measured with microperimetry. *Invest Ophthalmol Vis Sci* 54:3046–3051
53. Raza AS, Cho J, de Moraes CG et al (2011) Retinal ganglion cell layer thickness and local visual field sensitivity in glaucoma. *Arch Ophthalmol* 129:1529–1536

-
54. Rensch F, Jonas JB (2008) Direct microperimetry of alpha and beta zone parapapillary atrophy. *Br J Ophthalmol* 92:1617–1619
55. Jonas JB, Gusek GC, Fernandez MC (1991) Correlation of the blind spot size to the area of the optic disc and parapapillary atrophy. *Am J Ophthalmol* 111:559–565
56. Meyer JH, Guhlmann M, Funk J (1997) Blind spot size depends on the optic disc topography: a study using SLO controlled scotometry and the Heidelberg retina tomograph. *Br J Ophthalmol* 81: 355–359

Part III

The Contribution to Visual Rehabilitation

Samuel N. Markowitz

19.1 Introduction

There are around 285 million people worldwide with visual impairments according to the WHO [1]. Most (90 %) live in developing countries. Most visual impairments (80 %) can be prevented or cured.

Almost two million people in the UK are living with sight loss. That's approximately one person in 30. In 2008 sight loss cost at least £6.5 billion, and this is likely to increase as the number of people with sight loss increases [2]. There were in 2007 an estimated 817,000 Canadians living with visual impairment and passing the million mark by 2032 [3].

In the United States, it is expected that the annual number of new cases of visual impairment will double that of the current rate by 2025 [4].

Low vision as understood in the practice of low vision rehabilitation (LVR) is vision which cannot be improved with either further surgical and/or medical therapy and which is not acceptable to the patient or the significant other.

Among incurable impairments age-related macular degeneration (AMD) is today the leading cause of low vision in the developed countries and worldwide [5]. In younger age groups,

retinitis pigmentosa and Stargardt's disease are quite common in clinical practice as causes responsible for low vision in spite of being less prevalent than AMD. Many other conditions could be added to the list.

LVR offers today a beneficial alternative to those who have irreversible vision loss for which surgical or medical care is not available. LVR is a new subspecialty which emerged from the traditional fields of ophthalmology, optometry, occupational therapy, and sociology. The body of knowledge on LVR available today was created or published primarily within the past three decades [6]. There is a large body of evidence today in the literature which confirms that provision of LVR services results in improved clinical and functional ability outcomes in low vision patients [7].

19.2 Microperimetry and Low Vision

Probably the most significant contribution to recent advancements in LVR in research and clinical practice was the introduction of knowledge acquired with scanning laser ophthalmoscopy (SLO). The modern equivalent of SLO technology is the microperimetry instruments available today quite everywhere.

Current concepts on residual visual functions and functional vision are the direct result of advent of applied newer technologies based on SLO as well as newer computing and eye

S.N. Markowitz, MD
Low Vision Service,
Department of Ophthalmology and Vision Sciences,
University Health Network Hospitals,
University of Toronto, 1225 Davenport Rd.,
Toronto, ON M6H2H1, Canada
e-mail: snm1@rogers.com

tracking devices. Today's instruments commonly known as microperimeters embody the technological abilities required to assess components of residual visual functions and functional vision in any clinical practice, components which previously could be assessed with great difficulty [8]. Most significantly microperimeters also extended our abilities to assess residual visual function in those with poor fixation stability and/or with eccentric fixation patterns.

The diagnostic abilities of microperimetry instruments reside into four areas:

1. Assessment of residual retinal sensitivity with exquisite topographic sensitivity providing hence information on retinal areas with the residual highest retinal sensitivity as well as information on scotomata, relative or absolute.

Microperimetric assessment of retinal sensitivity was found to be at least equivalent to standard automated perimetry (SAP) or superior at detecting early visual function loss [9]. In AMD, reduced retinal sensitivity was positively correlated to areas with pathological changes such as drusen or retinal pigment epithelial layer changes [10]. Also in patients with AMD, there was significant positive relationship between outer segment layer thickness values on OCT and reduced retinal sensitivity [11]. Highest correlations were reported between reduced retinal sensitivity and retinal pigment epithelium and photoreceptor layers disruptions and macular edema in AMD cases [12]. In Stargardt's disease significant relationship between photoreceptor layer thickness values on OCT and reduced retinal sensitivity was reported [13, 14]. Positive correlation between changes in retinal sensitivity and progression of disease was documented in geographic atrophy as it was reported also after treatments for retinal neovascularization [15, 16].

Specifically for microperimetric assessment, one should notice that the decibel scales of various microperimetry instruments available today (Nidek MP-1, MAIA, and Optos OCT SLO) (Optos PLC, Dunfermline, Scotland, UK), and Humphreys SAP are not directly comparable or interchangeable in any way. Baseline values for topographic macular

sensitivity and correlations to age, gender, and ethnicity are needed for establishing degrees of impairment and comparison of progression when using the same instrument. In order to compare decibel scales between instruments, one has to take into account equivalency between threshold sensitivity outputs. It has been suggested that a conversion factor of 15 dB can be used in most cases where equivalency comparison between instruments is considered [17]. Best options with current instruments are to monitor retinal sensitivity change over time with same instrument [8].

Another observation worth noticing and taking into account is that in the presence of macular function loss, SAP produces scotoma records with displaced scotoma location since fixation during testing is performed using the PRL, of which SAP cannot account for. Also scotoma size records produced with the SAP are about half the size of same scotoma recorded with microperimetry instruments [18, 19].

2. Assessment of topographical fixation areas on the retina known as preferred retinal loci (PRLs) which represent fixation attempts, central or eccentric, during viewing of targets.

Development of PRLs occurs naturally in most cases when macular visual function is lost and exhibit dynamic performances. Such PRLs can develop on any part of the residual retina, can be single or multiple, are apparently related to performance of specific tasks, and offer superior visual function unmatched by any other locus on the retina. Multiple PRLs tend to be associated with recent onset of disease and/or with scotomatous defects with relative densities and ring scotomata [20].

In those with macular function loss, like AMD cases, the majority of PRLs detected occur in the upper and the right quadrants of the retina which correspond to the inferior and left parts of the visual field [21]. In Stargardt's disease and other macular dystrophies, most PRLs tend to be localized on the upper retina [22]. In some cases PRLs are bordering on more than one side with the existing scotoma. When scotoma borders the PRL from 3 or 4 directions, usually one refers to this as a

ring scotoma. The prevalence of patients with scotoma on three or four sides of PRL fixation has been shown to be 26.4 % among all low vision patients [21]. In those with peripheral retinal functional loss and some additional macular function loss, PRLs occur in the macular area close to the splitting of fixation locus and in some cases may be located in an area surrounded by a ring scotoma.

3. Assessment of retinal areas representing residual function known as functional retinal loci (FRLs) which represent the retinal area with the residual highest retinal sensitivity and the PRL area associated with it [23].

Later on after the initial adaptation to loss of macular function, it seems that one single functional retinal locus (FRL) is used for eccentric viewing [23]. Such an FRL is quite established on the retina in terms of location and functionality, and the patient summons its services on an ongoing basis. Recent research shows that established PRLs apparently exhibit various overlapping fixation stability patterns for different types of tasks within the area of an FRL [24].

4. Recording of fixation locations during the length of any viewing attempt and creating raw data for calculation of fixation stability estimates.

Accurate estimates of fixation stability could be obtained from raw data provided by microperimeters by calculation of a bivariate contour ellipse area (BCEA) [25]. For normal subjects the mean BCEA was found to measure $0.053 \text{ }^{\circ 2}$ (SD 0.022), and in AMD cases, the mean BCEA was found to measure $6.76 \text{ }^{\circ 2}$ (SD 8.36 with a range from 0.21 to $31.85 \text{ }^{\circ 2}$ [25]. Fixation stability in the poorer eye is significantly less in many cases than in the better eye under conditions where binocular vision is absent. Recent research reveals also that fixation stability estimates in low vision cases are reliable predictors of visual acuity estimates. In a few studies, it was demonstrated that there is a direct relationship between better visual acuity and better fixation stability [25–27].

In addition to diagnostic abilities, the Nidek MP 1 (Nidek Technologies Inc., Padova, Italy) and MAIA (CenterVue SpA,

Padova, Italy) microperimeters offer therapeutic abilities with biofeedback modules aimed at training refixation precision of eye movements.

Ideally a status report on a low vision patient following examination with a microperimeter instrument would include comments on all of the above residual abilities assessed and on suitability for biofeedback therapy. Anything less could be viewed as incomplete.

19.3 Modern Low Vision Rehabilitation

Diagnosis of low vision leading towards rehabilitation interventions usually starts with functional vision deficits noticed either by the patient or by the significant other: spouse, child, caregiver, and doctor. Diagnosis of low vision is based today on definitions which vary among various jurisdictions. In Ontario, Canada, recent changes to health legislation provide probably the most encompassing definitions for low vision. Low vision for the purpose of providing rehabilitation services is defined as any of the following: best corrected visual acuity of 20/50 or less in the better eye and not amenable to further medical and/or surgical treatment; significant oculomotor dysfunction, nerve palsy or nystagmus resulting in low visual acuity or visual field defects as defined and not amenable to further medical and/or surgical treatment; and visual field defect, splitting of fixation, scotomata, and quadrantic or hemianopic field defects not amenable to further medical and/or surgical treatment [28]. In the United States, guidelines for diagnosis and assessment are listed in the SmartSight protocol from the American Academy of Ophthalmology [29].

A practice template for LVR practice is probably the most useful way to practice LVR in order to cover most local LVR guidelines and customary practice of LVR. The Ontario Practice Template (OPT) is a modular format which can be adapted to any jurisdiction accordingly to local standards for practice of LVR. The OPT allows assessment of residual visual functions such as visual acuity, contrast sensitivity, residual

fields, and scotomata as well as on residual oculomotor functions and eccentric viewing. It also allows assessment of residual functional vision such as reading. Interventions are grouped to reflect outcomes aimed at improving vision for near, intermediate, and far distances with options detailing other interventions like vision therapy training [30].

There are many other protocols for LVR practice usually reflecting standards of practice in the jurisdiction they were created in. Such protocols lead to the conclusion of a meaningful LVR assessment and a productive and positive LVR intervention which benefits the patient. It is not the intention of this paper to describe traditional modalities used for LVR. This was done in a previous paper [6]. We definitely use today in many cases plus lenses in glasses and handheld magnifiers in order to create various levels of magnification as needed by the patients. We definitely use today in many cases telescopic devices, monoculars and binoculars, handheld, and head borne. We use prisms and selective transmission lenses. However, today we have at our disposal modern tools for LVR. Ideally today any protocol for LVR practice should include also elements of modern LVR as discussed in this paper.

Besides following the steps of a traditional practice template for LVR, any practitioner wishing to practice modern LVR would also have to address in clinical practice the following modern concepts.

19.3.1 Assessment of Potential Visual Acuity (PVA)

Detection of PVA in patients with low vision is a crucial step in the clinical practice of LVR. The ability to accurately estimate such potential at baseline before vision rehabilitation interventions or surgery and comparing the results to subsequent evaluations may help assess rehabilitation progress.

The tool that helps cataract surgeons determine what the outcome of surgery will be – the potential acuity meter (PAM) – provides esti-

mates of PVA in the macular area. Low vision patients require a different sort of test able to measure PVA on the residual retinal areas outside the macula, specifically at the PRL. For this purpose standard acuity tests currently in use such as the Snellen and ETDRS charts are limited in the sense that they depend on good central macular functions, which are functions lost in patients with low vision. Patients with low vision also have various amounts of fixation instability. They do not have the same ability to move the eyes to a given target and keep it there as people with healthy eyes do. This is because the oculomotor mechanism which moves the eyes to fixate on a given target in normal people is set to land incoming images on the fovea – a mechanism which in low vision patients is lost. If, however, we present simultaneously the same multiple optotypes, in essence flooding the retina with same size optotypes, then one negates the need for eye movements. An image from one of the optotype targets is bound to hit the PRL and provide estimates of vision at the PRL, in essence estimates of PVA (Gonzalez-Markowitz PVA charts, Precision Vision, LaSalle, IL. USA) [31] (Fig. 19.1).

Significance: During regular LVR assessment, one may obtain visual acuity estimates with ETDRS charts showing levels, for example, at 20/200. Same eye tested with PVA charts with reverse polarity with white optotypes on black background will demonstrate a level of 20/80 visual acuity. This means that if one could effectively align the PRL with the visual axis and maintain alignment with optimal fixation stability, one could render twice as good vision to the patient. If this knowledge could be available to the practitioner prior to the LVR process, it could significantly impact on the rehabilitation approach taken and on the final outcome from LVR.

19.3.2 Recovery of Optimal Residual Vision Available at the PRL

Obviously the whole exercise of assessing PVA in a low vision eye is to recover for the patient the vision available at the PRL for daily usage.

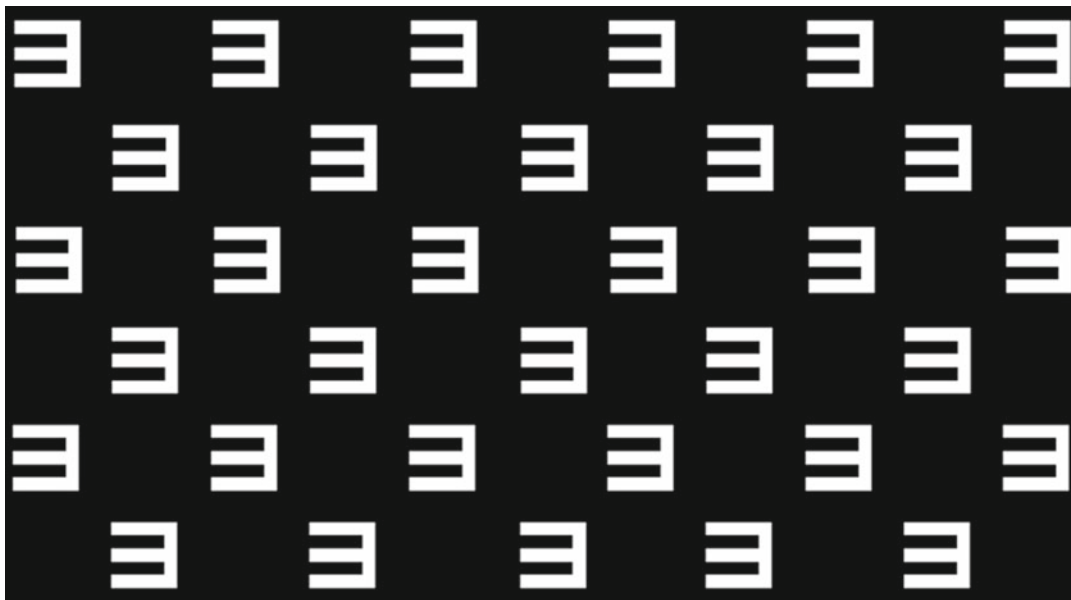


Fig. 19.1 Gonzalez-Markowitz PVA charts

Recent studies may offer also an explanation on the mechanism by which patients may recover PVA available at the PRL. Low vision patients develop functional adaptations aimed at maximizing residual functional vision [32]. One such adaptive strategy attempts to reduce the impact from loss of macular vision by using an eccentric retinal area empowered to assume macular function, areas commonly known in the literature as PRLs. Establishment of PRLs, however, is directly linked to the oculomotor abilities. The nature of oculomotor functions in AMD patients is different than in normal subjects [33]. Following loss of central vision, the oculomotor system recalibrates in a way to enable alignment of the eyeball so that incoming images land on functional eccentric PRLs. Patients adopt compensatory viewing strategies aimed at facilitating on images entering the eye to reach such areas with best vision potential. As expected, such abilities in some may be excellent, in some totally absent, and in most may be present with various degrees of efficiency. Hence, utilization of PRLs is imperfect, mostly because of imperfect oculomotor control [23].

In principle, two modalities are available for rehabilitation of oculomotor control: prisms to assist the eye to redirect incoming images towards the PRL or exercise the new oculomotor skills to do what they intended to do [34, 35]. Improvement in oculomotor control ultimately will result in improvement in visual acuity [34].

A recent meta-analysis study reviewing all studies on the topic to date showed a definite positive benefit to patients using prisms for image relocation of images towards the periphery [34]. The effect size on visual acuity from using prisms was 79 larger than in those where prisms were not used. A main benefit of the prisms method seems to be also nondependence on cognitive skills, whereas the gaze training methods cannot be used in those with immature or poor cognition. Recent data also shows that image relocation with prisms towards the PRL improves fixation stability which eventually translates in better distance visual acuity [36]. Microperimetric technology allows us to visually record the effect of prisms in moving the PRL across the retina towards the closest retinal area with highest retinal sensitivity (HRS) (Fig. 19.2). Directing the incoming image

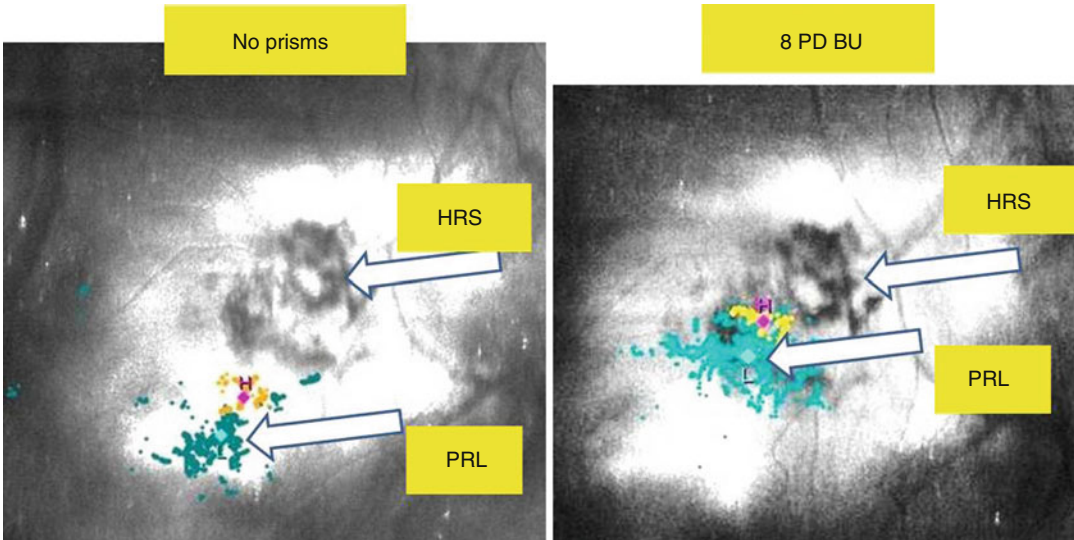


Fig. 19.2 Image relocation with prisms towards retinal area with highest retinal sensitivity

towards the existing PRL with prisms assists the eye to move the PRL closer to the retinal area with the HRS. This will ultimately result in better visual acuity. In a past report, 64 patients who wore distance glasses with prisms for an average of 8 months improved their distance visual acuity from a mean of 20/200 to a mean of 20/100 [37].

Significance: Incorporation of prisms to redirect incoming images towards the PRL in the better-seeing eye is quite simple in clinical practice. It could be incorporated in prescription glasses either for distance or near. First, one determines the directional location of the PRL and its eccentricity in the better eye. One matched the direction of the prism and the power of the prism to match the PRL location (about 1.7 prism diopters for each degree). Image relocation with prisms will not work in cases where residual macular fixation is still strong and also in those exhibiting a ring scotoma around the existing PRL. Using prisms for image relocation can enhance face recognition which is another outcome measure in LVR. The beneficial use of prisms in such cases suffering usually from severe central vision loss is noticed by many practitioners in clinical practice [38]. In such case yoke prisms of 10 prism diopters base up or more usually produce sig-

nificant improvement in face recognition abilities.

To exercise the new oculomotor skills to do what they intended to do is the most prevalent method today in clinical practice aimed at rehabilitation of oculomotor control and subsequently helping recover best residual vision available at the PRL. The methodology is empiric and based on the obvious that the upper and lower retina bordering the macular area have quite a large horizontal visual span which in most cases is not affected by disease. This may be appreciated by the patient or it may be suggested to the patient to use the upper or lower retina. This may be reinforced by specifically training specific eye movements. Variations of this methodology are many; however, all reproduce a methodology commonly known in LVR as “clock face” display [39].

With this method a clock is drawn with hour markings at its periphery and a star at the center and presented to the eye in training. Patients are asked to move the eye along meridians of each hour location until they discover that they can see the star in the center. If best vision resides on the superior retina, the patient is taught to raise the eye until he/she sees the star in the center. Or move the eye along the hourly markings of the clock, again, until the star in the middle of the clock is visible. The patient is asked to remember

the eye maneuver performed in order to see the star in the middle of the clock and apply it in other viewing situations. This method works in cases where the PRL is indeed developed on the upper or lower retina. Other more specific methods aim at training of control eye movements. In one study, a remarkable improvement in reading speed was achieved by using exercises with a series of saccade tasks to nonalphabetical stimuli and then progressed to single letter, letter pairs, and word stimuli [40].

Significance: Training of oculomotor control seems to be efficient if training is aimed at improving saccades implementing fixation accuracy and refixation precision. For this purpose it seems important to follow strict protocols as described in a previous paper [40].

19.3.3 Restoration of Binocularity

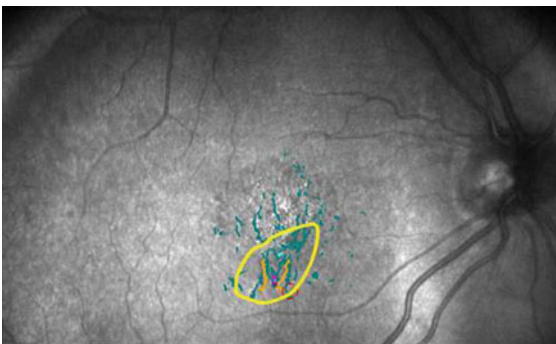
Using microperimetry we could separate between those who have retinal correspondence for the PRL between the 2 eyes and those who do not. After loss of vision in both eyes, PRLs develop in either eye, however in most cases on non-corresponding retinal areas. As a matter of adaptation to the new situation, PRLs in the eye with poorer vision in time will “relocate naturally” on

corresponding retinal areas to match the area of the PRL in the better eye. This is not happening in everybody. In a recent study, we showed that non-correspondence is prevalent in almost half of those who lost vision in both eyes (49 %) [41] (Fig. 19.3).

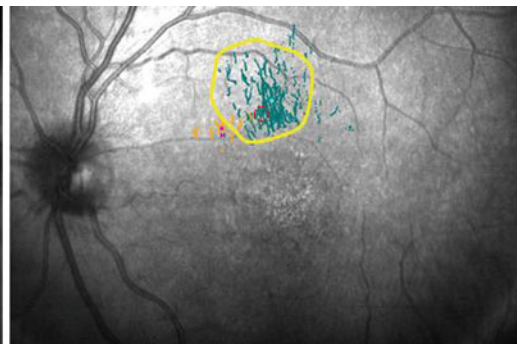
Binocular viewing is the most common viewing condition in daily life for all, either for those who are visually impaired or for those who are not. When binocularity is still preserved, new data shows that the fixation stability in the poorer eye improves and matches measurements for the better eye [42]. Binocular deficiencies will affect fusion of images from both eyes, with an impact on summation, inhibition, and rivalry functions with obvious deficiencies in stereopsis [43]. A recent study indeed confirms that those who retained stereopsis demonstrated overall functional visual abilities (OFVA) scores higher than those who did not. Also stereopsis was correlated with higher abilities scores for reading and visual motor skills [44]. Hence, restoration of binocular vision in LV cases should have a high priority.

Significance: Restoration of binocularity is quite easy to do in clinical practice. After assessing the location of the PRL in the better eye, one could prescribe yoke prisms to match the location of the PRL in the better eye. In the case

34 year old M with Stargardt's
BCVA : 20/252 OD, OS
PRLs on non-corresponding retinal area



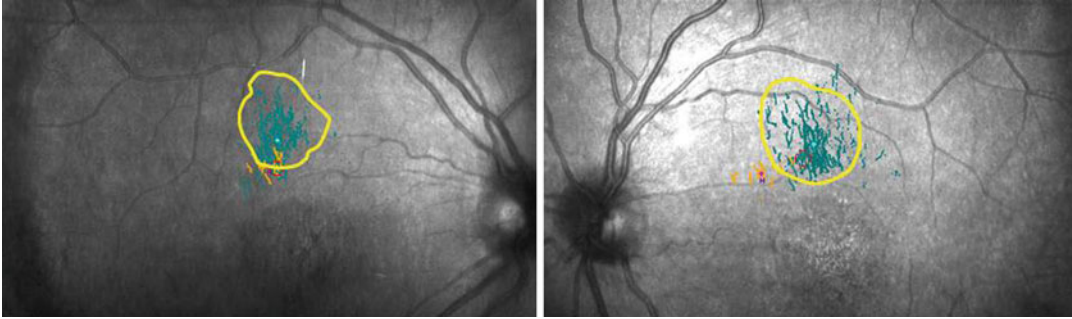
Bivariate contour ellipse area:
63 % BCEA: 1.5° x 1.6°, Area = 7.5°², angle = 60.6°
95 % BCEA: 4.5° x 4.8°, Area = 67.3°², angle = 60.6°



Bivariate contour ellipse area:
63 % BCEA: , Area = 5.1°², angle = 66.2°
95 % BCEA: , Area = 45.6°², angle = 66.2°

Fig. 19.3 PRLs on non-corresponding retinal areas

34 year old M with Stargardt's
BCVA : 20/200 OD, OS
PRLs on corresponding retinal area



Bivariate contour ellipse area:
63 % BCEA: 1.2° x 1.3°, Area = 5.1°², angle = -66.2°
95 % BCEA: 3.7° x 4.0°, Area = 45.6°², angle = -66.2°

Bivariate contour ellipse area:
63 % BCEA: , Area = 5.1°², angle = -66.2°
95 % BCEA: , Area = 45.6°², angle = -66.2°

Fig. 19.4 PRLs on corresponding retinal areas

presented in Fig. 19.3, yoke prisms were prescribed base up to match the location of the PRL in the left eye which was the better eye. This resulted in restoration of binocularity with PRLs located on corresponding retinal areas with better vision in the poorer right eye as well as better fixation stability as expressed by the BCEA value (Fig. 19.4).

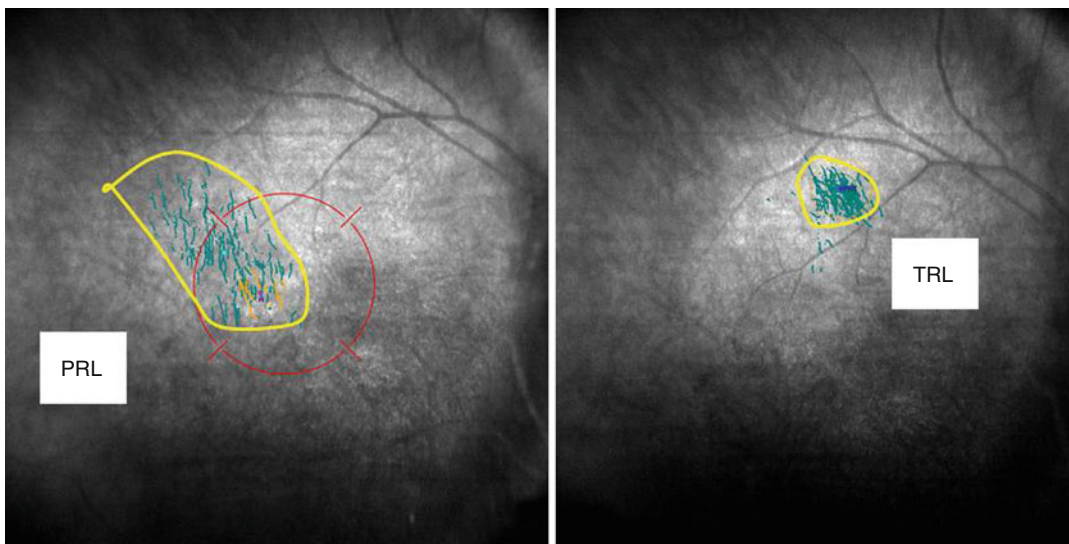
19.3.4 PRL Rehabilitation

In some cases, however, “PRL rehabilitation” is required before proceeding with optimal PRL utilization. The “optimal” location for a PRL is “on top” or in the immediate vicinity of a retinal area with HRS. Yet this may not be enough for producing acceptable reading abilities, the most common visual function sought after macular function loss. The additional requirement for optimal reading abilities with peripheral retina is availability at the PRL of a physical horizontal span to accommodate a minimum number of characters (5 characters at 10° eccentricity) [45]. This may not be the case in about half of those who lost macular function. Those who have developed a PRL on the temporal retina next to a macular scar may suffer from the scotoma limiting the visual span nasally to the PRL. Those who have developed a PRL on the nasal retina

next to a macular scar may suffer from the scotoma limiting the visual span temporally to the PRL and also from span limitations from the natural blind spot produced by the optic nerve head. In those two cases, PRLs are considered to be located on “unfavorable” locations.

A practitioner may recognize this situation and in order to remedy it may have to proceed with PRL rehabilitation. In essence the concept describes production of a new PRL in the vicinity of the old one located on top or near a retinal area with HRS and having a suitable visual span required for reading. In the LVR jargon, this procedure refers to the creation of a trained retinal locus (TRL) in a “favorable” location.

The most modern method for PRL rehabilitation is based on microperimetric instruments offering what is known as biofeedback modules. The method based on biofeedback is staged into two parts. An initial microperimetry examination determines the location of the retinal area with HRS. The retinal area with less eccentricity and closest to the vertical meridian is potentially the best candidate for creating a new TRL on it. The second part of the method consists on training attention, eye movements towards the TRL, and fixation on the TRL by using biofeedback based on auditory stimuli and under direct visual scrutiny by the trainer of the trained retinal fixation locus.



Bivariate contour ellipse area:

63 % BCEA: $1.4^\circ \times 1.5^\circ$, Area = $6.5^{\circ 2}$, angle = -50.4°
 95 % BCEA: $4.3^\circ \times 4.3^\circ$, Area = $58.6^{\circ 2}$, angle = -50.4°

Bivariate contour ellipse area:

63 % BCEA: $1.0^\circ \times 1.0^\circ$, Area = $3.3^{\circ 2}$, angle = -43.3°
 95 % BCEA: $3.1^\circ \times 3.1^\circ$, Area = $29.7^{\circ 2}$, angle = -43.3°

Fig. 19.5 Trained retinal locus created with biofeedback

After fixation with the habitual PRL, the patient is asked verbally by the trainer to move the eye for a certain planned length of time and to a certain direction where the patient would be able to fixate on the TRL selected for development. The eye movement performed is encouraged or discouraged by audio feedback sounds and by verbal direction by the trainer. Once fixation on TRL is attained, the patient is asked to maintain such fixation for certain period of time. The procedure is repeated a few times during a training session, and the patient is required to remember the eye maneuver performed and use it at home during reading sessions [46]. The mechanism behind improvement in visual function when using the biofeedback method is an improvement in fixation stability (Fig. 19.5). As shown in our paper, fixation stability will be better at the TRL but in time will be better also at the old PRL if the patient chooses to use it [46].

Significance: Individuals with a score below 25 with the Mini-Mental Status Exam (MMSE) which indicates cognitive impairment will probably not benefit from this methodology [47]. It will not work in most cases which retain central

fixation as well as in cases with a ring scotoma around the habitual PRL. Benefits from using this method in cases other than those with geographic atrophy or those with severe AMD with macular function loss are still to be proven.

Training sessions could be tedious. In our experience maintaining fixation attempts on TRL for 60–90 s is tolerated well by patients. One could train 4–5 such sessions during an hour training time with the rest of the time used for rest of the eye. We found weekly training sessions most beneficial for 4 weeks. Between training sessions, the patient is given reading homework with material matching the patient's critical print size (smallest print size that can be read with maximum speed).

19.3.5 Perceptual Learning

Perceptual learning is well known in visual sciences as a method for enhancing visual perception. The ability for perceptual learning is retained throughout life. It is achieved with repetitive visual sensorial stimulation and results in

physical changes in neural circuitry. Practically perceptual learning is the scientific expression of what is commonly known as “practice” or “training.”

Perceptual learning was proven to improve visual functions in normal as well as in those with various visual system pathologies, in younger as well as in older [48–51]. In a recent study, perceptual training with images provided by telescopic magnification resulted to better vision in cases with anisometropic amblyopia [52].

In principle there are two ways in devising perceptual learning: one way is by exercising eye movements and the other way is without involvement of eye movements.

All forms of reading exercise could be considered perceptual training. Methods as described above at improving oculomotor control could be viewed also as perceptual training methods [39, 40].

The method used for perceptual training without involvement of oculomotor control is based on serial presentation of stimuli to the center field of vision which is assumed to be the resting position of the eyes. In cases with loss of macular function, it is assumed that the eye fixates at the central field with the PRL without the additional burden of page or screen navigation from tracking stimuli across the page or the screen. The nature of the stimulus presented during serial presentation is the subject of a few studies. In essence the stimuli could be presented at the level of reading acuity or at the level of critical print size, rapidly or with speed adjustment for the specific case. In a recent study, serial presentation of words at the reading acuity limit resulted in better reading speed and better fixation stability [53].

Significance: Perceptual training or “practice” is commonly used in LVR clinical practice. The benefits from “practice” are well known, and scientific evidence is slowly accumulating in favor of this rehabilitation method. It is quite obvious though that optimal use of PRLs and other modern concepts applied to the individual low vision rehabilitation protocol can enhance further outcomes from perceptual training for any skill.

19.3.6 Brain Plasticity

Brain plasticity is believed today to be the underlying mechanism for all other mechanisms described above by which we achieve today better vision following loss of macular function. Brain plasticity is a term used today in neurosciences describing a concept that implies changes throughout life in the brain function and physical structure. It could be expressed as outright neurogenesis, synaptic plasticity, and compensatory functional processing. Published work in ophthalmology attempts also to clarify the role of this mechanism in the restoration of vision after macular function loss.

Activation of the visual cortex representing the fovea was reported in the literature and produced as evidence of large-scale reorganization of visual processing following stimulation directed at loci on the peripheral retina [54]. Furthermore, additional studies linked cortical reorganization in AMD cases to functional adaptation which took place after loss of vision such as PRLs. Specifically, it was shown that when stimulating the PRL area on the retina, one can demonstrate activation of the visual cortex area representing the macula [55]. It seems though that this form of brain plasticity is happening only in cases where there is complete loss of macular function [56].

Significance: Brain plasticity is very welcome news in LVR. It means that all those who can benefit from LVR interventions as described above will enhance further their abilities due to additional structural changes in the visual cortex. It is quite obvious therefore that optimal use of PRLs and other modern concepts applied to the individual low vision rehabilitation protocol can enhance further outcomes for any skill on account of brain plasticity.

Conclusions

There is no greater joy in academic life than being able to teach a student. Sharing your knowledge and stimulating another mind is exciting. Developing an idea and being engaged with another mind in working out the details is exhilarating. Seeing interest and

excitement in the eyes of the student is truly rewarding. This was my experience in my practice of LVR in an academic setting. In fairness and to a large extent, I also owe this joyful academic and experience and rewarding clinical practice to the exciting times we witness in modern LVR. The new ideas detailed above have “opened the eyes” to numerous practitioners of LVR, myself included, and brought significant help to uncountable numbers of patients. To a large extent, microperimeters made this reality possible. Microperimetric instruments make it possible today that any practitioner of LVR can bring into the office the latest modern concepts and apply them in clinical practice. As I am excited from the advancements I witness in LVR, so are the younger generations of practitioners who seem to be “infected” by the same ideas of progress as I am. The opportunities which opened before us are numerous, and new ones waiting to be opened depend only on our imagination.

References

- World Health Organisation (WHO) (2012) Visual impairment and blindness: fact sheet no 282. <http://www.who.int/mediacentre/factsheets/fs282/en/index.html>. Accessed 21 June 2012
- RNIB (Supporting Blind and Partially Sighted People) (2012) Key information and statistics. <http://www.mib.org.uk/aboutus/research/statistics/Pages/statistics.aspx>. Accessed 14 Dec 2012
- Gordon KD, Cruess AF, Bellan L et al (2011) The cost of vision loss in Canada. 1. Methodology. *Can J Ophthalmol* 46:310
- Massof RW (2002) A model of the prevalence and incidence of low vision and blindness among adults in the U.S. *Optom Vis Sci* 79:31–38
- Jager RD, Mieler WF, Miller JW (2008) Age-related macular degeneration. *N Engl J Med* 358:2606–2617
- Markowitz SN (2006) Principles of modern low vision rehabilitation. *Can J Ophthalmol* 41:289–312
- Binns AM, Bunce C, Dickinson C et al (2012) How effective is low vision service provision? A systematic review. *Surv Ophthalmol* 57:34–65
- Markowitz SN, Reyes SV (2013) Microperimetry and clinical practice – an evidence based review. *Can J Ophthalmol* 48(5):350–357
- Lima VC et al (2010) A comparison between microperimetry and standard achromatic of the central visual field in eyes with glaucomatous paracentral visual-field defects. *Br J Ophthalmol* 94:64–67
- Midena E, Vujosevic S, Convento E, Manfre A, Cavarzeran F, Pilotto E (2007) Microperimetry and fundus autofluorescence in patients with early age-related macular degeneration. *Br J Ophthalmol* 91:1499–1503
- Acton JH, Smith RT, Hood DC, Greenstein VC (2012) The relationship between retinal layer thickness and the visual field in early age-related macular degeneration. *Invest Ophthalmol Vis Sci* 53:7618–7624
- Sulzbacher F, Kiss C, Kaider A et al (2012) Correlation of SD-OCT features and retinal sensitivity in neovascular age-related macular degeneration. *Invest Ophthalmol Vis Sci* 53:6448–6455
- Burke TR, Rhee DW, Smith RT et al (2011) Quantification of peripapillary sparing and macular involvement in Stargardt disease (STGD1). *Invest Ophthalmol Vis Sci* 52:8006–8015
- Testa F, Rossi S, Sodi A et al (2012) Correlation between photoreceptor layer integrity and visual function in patients with Stargardt disease: implications for gene therapy. *Invest Ophthalmol Vis Sci* 53:4409–4415
- Meleth AD, Mettu P, Agron E et al (2011) Changes in retinal sensitivity in geographic atrophy progression as measured by microperimetry. *Invest Ophthalmol Vis Sci* 52:1119–1126
- Parravano M, Oddone F, Tedeschi M et al (2010) Retinal functional changes measured by microperimetry in neovascular age-related macular degeneration treated with ranibizumab: 24-month results. *Retina* 30:101710–101724
- Springer C, Bültmann S, Völcker HE et al (2005) Fundus perimetry with the Micro Perimeter 1 in normal individuals: comparison with conventional threshold perimetry. *Ophthalmology* 112:848–858
- Markowitz SN, Aleykina N (2010) The relationship between scotoma displacement and PRLs in low vision patients with AMD. *Can J Ophthalmol* 45:58–61
- Lee K, Markowitz SN (2010) Effective scotoma size in age-related macular degeneration. *Can J Ophthalmol* 45:393–398
- Lei H, Schuchard RA (1997) Using two preferred retinal loci for different lighting conditions in patients with central scotomas. *Invest Ophthalmol Vis Sci* 38:1812–1818
- Fletcher DC, Schuchard RA (1997) Preferred retinal loci relationship to macular scotomas in low-vision population. *Ophthalmology* 104:632–638
- Messias A, Reinhard J, Velasco e Cruz AA et al (2007) Eccentric fixation in Stargardt’s disease assessed by Tübingen perimetry. *Invest Ophthalmol Vis Sci* 48:5815–5822
- Shima N, Markowitz SN, Reyes SV (2010) The concept of a functional retinal locus in age-related macular degeneration. *Can J Ophthalmol* 45:62–66
- Markowitz SN (2011) Functional retinal locus rather than multiple PRLs? – letter to the editor. *Invest Ophthalmol Vis Sci* 52:1191

25. Tarita-Nistor L, González EG, Markowitz SN et al (2008) Fixation characteristics of patients with macular degeneration recorded with the MP-1 microperimeter. *Retina* 28:125–133
26. González EG, Tarita-Nistor L, Mandelcorn ED et al (2011) Fixation control before and after treatment for neovascular age-related macular degeneration. *Invest Ophthalmol Vis Sci* 52:4208–4213
27. Tarita-Nistor L, González EG, Mandelcorn MS et al (2009) Fixation stability, fixation location, and visual acuity after successful macular hole surgery. *Invest Ophthalmol Vis Sci* 50:84–89
28. Markowitz SN (2008) Ontario recognizes low vision rehabilitation, editorial. *Can J Ophthalmol* 43:398–399
29. The SmartSight initiative from the American Academy of Ophthalmology. <http://one.aaopt.org/CE/EducationalContent/Smartsight.aspx>
30. Markowitz SN (2009) A practice template for low vision rehabilitation. *Can J Ophthalmol* 44:610
31. González EG, Tarita-Nistor L, Markowitz SN et al (2007) Computer-based test to measure optimal visual acuity in age-related macular degeneration. *Invest Ophthalmol Vis Sci* 48:4838–4845
32. Cheung SH, Legge GE (2005) Functional and cortical adaptations in central vision loss. *Vis Neurosci* 22:187–201
33. Whittaker SG, Budd JM, Cummings RW (1988) Eccentric fixation with macular scotoma. *Invest Ophthalmol Vis Sci* 988(29):268–278
34. Markowitz SN, Reyes SV, Sheng L (2013) The use of prisms for vision rehabilitation after macular function loss: an evidence based review. *Acta Ophthalmol* 91(3):207–211
35. Seiple W, Szlyk JP, McMahon T et al (2005) Eye movement training for reading in patients with age-related macular degeneration. *Invest Ophthalmol Vis Sci* 46:2886–2896
36. Reyes SV, Silvestri V, Amore F, Markowitz SN et al (2013) Use of prisms for vision rehabilitation after macular function loss may impact oculomotor control. *Can J Ophthalmol* 48(5):427–430
37. Al-Karmi R, Markowitz SN (2006) Rehabilitation with image relocation in patients with age related macular degeneration. *Can J Ophthalmol* 41:313–318
38. Verezen CA, Volker-Dieben HJ, Hoyng CB (1996) Eccentric viewing spectacles in everyday life, for the optimum use of residual functional retinal areas, in patients with age-related macular degeneration. *Optom Vis Sci* 73:413–417
39. Holcomb JG, Goodrich GL (1976) Eccentric viewing training. *J Am Optom Assoc* 47:1438–1443
40. Seiple W, Grant P, Szlyk JP (2011) Reading rehabilitation of individuals with AMD: relative effectiveness of training approaches. *Invest Ophthalmol Vis Sci* 52:2938–2944
41. Podbielski DP, Reyes SV, Markowitz SN (2013) The worse-seeing eye is not as bad as it seems to be. *Can J Ophthalmol* 48(5):381–385
42. Tarita-Nistor L, Brent MH, Steinbach MJ et al (2011) Fixation stability during binocular viewing in patients with age-related macular degeneration. *Invest Ophthalmol Vis Sci* 52:1887–1893
43. Tarita-Nistor L, Gonzales EG, Markowitz SN et al (2006) Binocular interactions in patients with age-related macular degeneration: acuity summation and rivalry. *Vision Res* 46:2487–2498
44. Cao KY, Markowitz SN (2010) Residual stereopsis in age-related macular degeneration patients and its impact on vision related abilities. In: Paper presented at Canadian Ophthalmological Society Congress, Montreal, June 2010
45. Legge GE, Mansfield JS, Chung STL (2001) Psychophysics of reading. XX. Linking letter recognition to reading speed in central and peripheral vision. *Vision Res* 41:725–743
46. Tarita-Nistor L, González EG, Markowitz SN et al (2009) Plasticity of fixation in patients with central vision loss. *Vis Neurosci* 26:487–494
47. Crum R, Anthony J, Bassett S, Folstein M (1993) Population-based norms for the mini-mental state examination by age and educational level. *JAMA* 269:2386–2391
48. Kolb B, Muhammad A, Gibb R (2011) Searching for factors underlying cerebral plasticity in the normal and injured brain. *J Commun Disord* 44:503–514
49. Karni A, Sagi D (1991) Where practice makes perfect in texture discrimination: evidence for primary visual cortex plasticity. *Proc Natl Acad Sci U S A* 88:4966–4970
50. Beard BL, Levi DM, Reich LN (1995) Perceptual learning in parafoveal vision. *Vision Res* 35:1679–1690
51. Levi DM (2005) Perceptual learning in adults with amblyopia: a reevaluation of critical periods in human vision. *Dev Psychobiol* 46:222–232
52. Nazemi F, Markowitz SN, Kraft S (2008) Treatment of anisometropic amblyopia in older children using macular stimulation with telescopic magnification. *Can J Ophthalmol* 43:100–104
53. Tarita-Nistor L, Brent MH, Steinbach MS et al (2008) Perceptual learning with threshold stimuli leads to improvement in visual performance of patients with central vision loss. *Optom & Vis Sci* (in press)
54. Baker CI, Peli E, Knouf N, Kanwisher NG (2005) Reorganization of visual processing in macular degeneration. *J Neurosci* 25:614–618
55. Schumacher EH, Jakob JA, Primo SA et al (2008) Reorganization of visual processing is related to eccentric viewing in patients with macular degeneration. *Restor Neurol Neurosci* 26:391–402
56. Baker CI, Dilks DD, Peli E et al (2008) Reorganization of visual processing in macular degeneration: replication and clues about the role of foveal loss. *Vision Res* 48:1910–1919